TECHNISCHE UNIVERSITÄT
BERGAKADEMIE FREIBERG
The University of Resources. Since 1765.

Risk assessment for integral safety in operational motion planning of automated driving

To the Faculty of Mathematics and Informatics
of the Technische Universität Bergakademie Freiberg

approved

THESIS

to attain the academic degree of

Doktor-Ingenieur
(Dr.-Ing.)

submitted

by Dipl.-Ing. **Clemens Markus Hruschka**

born on the 23 March 1992 in Altdöbern

Reviewers: Prof. Dr.-Ing. Sebastian Zug, TU Bergakademie Freiberg,
Faculty of Mathematics and Informatics, Software technology and Robotics

Prof. Dr.-Ing. Marcus Baum, Georg August University of Göttingen,
Institute of Computer Science, Data Fusion Lab

Date of the award 01 September 2021

Confidentiality

Ergebnisse, Meinungen und Schlüsse dieser Dissertation sind nicht notwendigerweise die der Volkswagen Aktiengesellschaft.

The results, opinions and conclusions expressed in this thesis are not necessarily those of Volkswagen Aktiengesellschaft.

To Aileen and Valerie who have encouraged me with great patience

Abstract

The “Vision Zero“ aims to minimise the number of fatalities and severe injuries in road transport sustainably. Thereby, new automated vehicles have the chance of high improvements to road safety with their intelligent functions as over 90 % of accidents are induced by humans directly. Nevertheless, from today's perspective accidents will always be a part of future mobility due to human mistakes in mixed traffic or malfunctions and thus the major impact to road safety is seen in the combined use of active and passive safety. Therefore, this work contributes to the design of such newly integral safety systems.

Current available safety systems separates into active and passive components with specific use cases and triggering strategies. Therefore, an approach is needed to consider single, passive systems in forward-looking active safety. As answer, this thesis bases the combined deployment of safety actions on a holistic criticality measure which is determined by the application. Uncertainties and demanded real time capability add further requirements to the criticality estimation. As result, a novel risk based criticality measure is used in this thesis and thus the function behaviour is determined by a statistical approach.

The exemplary integral application in this thesis constitutes the trajectory planning in automated driving with focus on critical incidents. However the idea is easily transferable to assisted driving. The combined safety system comprises the steer, brake, and crumple zone. The objective is to prevent critical situations as early as possible and to mitigate the harm in the case of imminent collision. That means to address both, safe regular driving and intelligent crash interaction in one driving function. Thereby, only few research has been done to include crash consequences into the driving and pre-crash decision what is especially required for mitigation manoeuvres, such as impact point localisation. Additionally, uncertainties due to the environment perception and traffic participants' behaviour prediction impedes a clear choice in the trajectory planning, such as the selection between collision avoidance or mitigation by braking and steering. On top of that, the real time requirements of the trajectory planning constitute a challenge and followed approximations in the modelling add further uncertainties to the process.

The basic idea of this thesis is to assess each possible trajectory according to the potential crash severity which is determined by the velocity change during a potential crash Δv. However, as mentioned before, uncertainties impedes these calculations. Therefore, a continuous, real time, risk-based criticality measure weights the technical accident severity Δv with the collision probability. The severity Δv is predicted with an eccentric impact model for the most probable collision configuration. The collision probability and derivation of the most probable collision configuration base on a 3D Minkowski Difference.

The selection of the eccentric impact model bases on an investigation of five different prediction models. It provides the best compromise between accuracy, calculation time, and

transparency in comparison to a centric impact, multi-body system, feed forward neural network, and random forest regression. A database with more than 6000 FEM vehicle crash simulations is used as reference.

The trajectory planning framework itself bases on dynamic programming and uses massive parallelisation to meet real time requirements. The weights of the reward function are tuned in simulation to balance aspects of comfort, progress, and safety. The driving performance is assessed with an individual approval cost function to enable regular driving likewise to an intelligent crash interaction. Thereby, the vehicle dynamic, locomation, and a crash model differentiate multiple test drives. The final driving strategy of the automated vehicle bases on a graceful degradation with a risk threshold.

The evaluation of the risk based trajectory planning is performed in simulation, real world testing, fleet data and accident database analyses. Thereby, it is focused on the integral performance, such as the collision avoidance, collision mitigation with impact point localisation, and uncertainty adaptation. Thereby, a new scenario catalogue for the evaluation is derived from GIDAS accident database, the Shanghai's A Nice City scenario Catalogue, and systematical reasoning. The quantitative results base on relative comparisons between several test drives or in comparison to the driving performance of a vehicle equipped with an automatic emergency braking system.

The results show in posteriori analyses of fleet data that the risk measure is a valid indicator for the situation's criticality. It remains at low level in regular driving and rises imminent before a crash. Aspects of the uncertainty adaptivity are shown in test drives with different sensor configurations. The combination of lidar, radar, and camera results in different perception uncertainty and the vehicle behaviour adopts directly to these uncertainty levels. That is expressed by the begin of braking manoeuvres and strength of deceleration. An other scenario deals with the collision avoidance under uncertainties. The ego vehicle tries to avoid a collision with a vehicle ahead by a swerving manoeuvre. However, that emergency manoeuvre is only performed if the environment perception ensures free driving by a certain environment representation. If the uncertainties are too high and the chance rise to collide with oncoming traffic and thus to obtain high accident severities, a mitigation manoeuvre to the vehicle ahead is performed. The mitigation performance is shown in a similar scenario with constant uncertainty level. If oncoming traffic is present, a severity reducing mitigation manoeuvre is performed. Otherwise, an emergency swerving avoids the collision. Systematic analyses between the risk based planner and the reference planner show an improvement of 20-30 % technical accident severity with respect to the underlying scenarios. That means up to one-third less injury probability for the vehicle occupants. The feasibility in automated driving is shown with currently available test equipment on the testing ground.

In conclusion, the integral functionality is demonstrated with the example application of trajectory planning. The risk based criticality measure enables a smooth transition between preventative driving, collision avoidance, and collision mitigation including impact point localisation. Additionally, the uncertainty consideration improves the performance and robustness of the function deployment. For example, the vehicle would adapt the behaviour

inherently to changing perception and environment prediction performance, e.g., caused by volatile weather conditions, malfunctions, or hardware modifications. Furthermore, in accordance with the statistical approach, no pre-selection of a collision avoidance or collision mitigation stage is necessary and thus a robust decision between these strategies in one approach is enabled. On the other hand, the statistical approach does not ensure to chose the best decision all the time but to have a positive risk balance with improvements on average. Finally, predicting the risk preventively has the chance to increase the road safety and thus take the “Vision Zero“ one step further.

Acknowledgements

At this point, I want to express my gratitude to everyone who has encouraged and motivated me during my research and thus has contributed to the success of this thesis. The dissertation was prepared during my activities in the Group Innovation of the Volkswagen Group.

Many thanks go to Mr. Prof. Dr.-Ing. Sebastian Zug from the TU Bergakademie Freiberg for supervising the preparation of this thesis. I appreciate the exiting discussions and food for thoughts from the beginning. Further, I take a great benefit from emboldening me in participating several international conferences and presenting interim results of my thesis. That and your personal feedback have supported the reflection of my line of argument and thus to increase the comprehensibility and transparency of my findings.

I also thank the examination committee. Especially, I thank Mr. Prof. Dr.-Ing. Sebastian Zug and Mr. Prof. Dr.-Ing. Marcus Baum for preparing the assessment reports.

A big word of thanks goes to my colleagues of the Volkswagen Group. I thank the colleagues of the department of Integral Safety for the frequent discussions, detailed feedback, and continuous support. Particularly, I thank my supervisor from Volkswagen for advising me from industrial point of view and for the assistance to find the main theme of this thesis. Further, I am thankful to my two students for preparing their internships and theses under my supervision. Moreover, I thank all business associates. Especially, I thank you for your assistance with the trajectory planning framework and components for visualisation purpose. I am also grateful to my colleagues of the department of Automated Driving for their support with the trajectory planning framework and maintenance of the test vehicle fleet. Furthermore, I send many thanks to my colleagues from the Audi Group for providing an essential part of the FEM structure simulations.

I thank my family for encouraging and supporting me during all phases of my thesis, from successes to failures, and paving the way for this education and career. Finally, big thanks belongs to two persons who enrich my life with incredible great moments, happiness, and unwavering support. Aileen and Valerie, I thank you both for your understanding and patience. You have given your partner and father, respectively, the necessary free spaces to prepare his research. I am looking forward to continuing the fulfilled life with you.

Contents

Nomenclature

Abbreviations

AACN	Advanced Automatic Crash Notification
ABS	Anti-lock Braking System
ADAS	Advanced Driver Assistance Systems
AEB	Automatic Emergency Braking
AIS	Abbreviated Injury Scale
ATMS	Advanced Traffic Management Systems
CA	Collision avoidance
CDF	Cumulative density function
CIM	Centric impact model
CM	Collision mitigation
COG	Center of Gravity
CS	Concrete scenario
CTR	Constant turn rate
CV	Constant velocity
DMS	Dynamic Message Sign
DOF	Degree of freedom
E911	Enhanced 9-1-1
eCall	Emergency call
Ego	Own (ego) vehicle
EIM	Eccentric impact model
ESC	Electronic Stability Control
FE(M)	Finit Element (Method)
FES	Functional evaluation scenario
FFNN	Feed forward neural network
FRG	Federal Republic of Germany
FS	Functional scenario
GA	Genetic algorithm
GDP	Gross domestic product
GIDAS	German In-Depth Accident Study
GNSS	Global Navigation Satellite System
GPSA	Generalized Pattern Search Algorithm
GPU	Graphics Processing Unit

HIL	Hardware-in-the-loop
HMI	Human Machine Interface
ICS	Inevitable collision state
IIHS	Institute for Highway Safety IIHS
INS	Inertial Navigation System
Kelvin model	Two masses are connect by a parallel spring and damper
LHS	Latin hypercube sampling
LPTB	Last point to brake
LPTS	Last point to steer
LS	Logical scenario
MAIS	Maximal Abbreviated Injury Scale
MDP	Markov Decision Process
MKB	Multi collision brake
MPC	Model Predictive Control
MSE	Mean squared error
NASS-CDS	National Automotive Sampling System – Crashworthiness Data System
NCAP	New Car Assessment Programme
NOC	Number of Conflicts
OEM	Original Equipment Manufacturer
PCA	Principal Component Analysis
PCM	Pre-Crash-Matrix
PDF	Probability density function
RF	Random forest
RK3	Runge-Kutta integrator third order
SAE	Society of Automotive Engineers
SIL	Software in the loop
SUV	Sports utility vehicle
TM	Tunnel Middle
TN / FN	True / false negatives
TP / FP	True / false positives
TPS	Third Party Services
TTB	Time to brake
TTC	Time-To-Collision
TTCCP	Time-to-critical-collision-probability
TTR	Time to react
TTS	Time to steer
TTX	Time to x

UTYP	GIDAS accident type
V2I	Vehicle-to-infrastructure
VRU	Vulnerable Road User

General symbol guidlines

$(\cdot)$	Placeholder for a variable
$(\cdot)$ and $(\cdot)'$	Before and afterwards
$(\cdot)(t)$	Time variant value (e.g., $a(t)$, $v(t)$, $s(t)$)
$(\cdot)^*$	Optimal value
$(\cdot)_\mathrm{E}$, $(\cdot)_\mathrm{K}$, $(\cdot)_\mathrm{EK}$	The bidirectional relation between ego vehicle E and one target object K is emphasised by the identifiers E / K / EK
$(\cdot)_\mathrm{lat}$	Value in lateral direction (e.g., a_lat)
$(\cdot)_\mathrm{long}$	Value in longitudinal direction (e.g., a_long)
$(\cdot)_f$, $(\cdot)_r$	Front and rear axle of the non-linear single track model
$(\cdot)_n$, $(\cdot)_t$	Normal and tangential direction
$\boldsymbol{A}$	A bold, capital letter indicates a matrix, or vector of random variables
$\boldsymbol{A}$, $\boldsymbol{a}$	A bold symbol indicates a vector or matrix
$\boldsymbol{Z} \sim \mathcal{N}(\boldsymbol{\mu}, \boldsymbol{\Sigma})$	The random vector $\boldsymbol{Z}$ is normal distributed with the expected value vector $\boldsymbol{\mu}$ and covariance matrix $\boldsymbol{\Sigma}$
$\Delta(\cdot)$	Relative values (e.g., relative pose such as Δx, Δy, and $\Delta\varphi$)
$\hat{(\cdot)}$, $(\cdot)$	Estimated value $\hat{(\cdot)}$ in relation to the reference value $(\cdot)$
$\mathbb{R}$	Real numbers
$\overline{(\cdot)}$	Indicates an average value; Other marker than $\widetilde{(\cdot)}$
A	A capital letter indicates a single random variable
a	A lower, non-bolded letter indicates a scalar variable; scalar sample from a sample space Ω or distribution
$a_{b,c}$	Notation means: variable a with the properties b AND c (e.g. ego velocity in longitudinal direction: $v_{\mathrm{E,long}}$)
$a_{b/c}$	Notation means: variable a with the property b AND variable a with the property c (e.g., velocity v for the ego vehicle E and velocity for the target vehicle K: $v_{\mathrm{E/K}}$)
$E(\cdot)$	Expected value
$f(\cdot)$	Function in general; External force (e.g. $f(t)$); Features (in a sense a function of action a and states s and s'); Frequency
$P(e)$	Probability of event e
$p_Z(z)$	Probability density function to the random variable Z and sample z

$Z \sim \mathcal{N}(\mu, \sigma)$	The random variable Z is normal distributed with the expected value μ and standard derivation σ
$z : \Omega \rightarrow \mathbb{R}$	The random variable z maps the sample space Ω to a scalar value of a real number
N	Absolute number of a finite set
n	arbitrary counter

Symbols

ΔT	Deformation energy
λ	Eigenvalue; Constraint; Progress on trajectory (e.g., λ_{ego})
φ	Orientation
a	Acceleration; Action in the MDP $a \in \mathcal{A}$
a_{in}	Input acceleration and deceleration due to the engine and brake, respectively, according to the motion planning
d	Distance (e.g. distance between current position of the vehicle and the centerline d_{lat}, distance to potential collision objects at the moment of appearance d_{appear}
E_{kin}	Kinetic energy
F	Force
f_{update}	Update frequency of the planning process
k_{air}	Constant of the flow resistance
k_e	Engine proportion relating to front and rear axle
p	Momentum; Index of time step t_p between different states s of the MDP
x	Position in x direction
y	Position in y direction
t	time
t_0	Time at the moment "0" (begin of a sequence); Moment of impact (fig. 2.1)
t_p, t_i, t_m	Different time t discretisation levels (t_p: between states s, t_i: reward generation, t_m: integration steps dynamic model)
i	Index of time step t_i for the reward generation $Re_{t_i}(s, a, s')$ of the MDP
v	Velocity
v_{rel}	Relative velocity
v_{ego}, v_{E}	Velocity of ego vehicle
v_{target}, v_{K}	Velocity of target vehicle

s	Displacement on a trajectory; State in the MDP $s \in \mathcal{S}$; empirical standard derivation
$\{\mathcal{S}, \mathcal{A}, \mathcal{T}, \mathcal{R}e, \gamma\}$	5-tupel which defines the Markov Decision Process (MDP) with the set of states $\mathcal{S}$, the set of actions $\mathcal{A}$, the set of transitions $\mathcal{T}$, set of rewards $\mathcal{R}e$, and discount factor γ
$\mathcal{A}_s$	Set of available actions a in state s
s'	Future state in the MDP $s' \in \mathcal{S}$ with reference to state s
$T(s,a,s')$	Transition in the MDP between the state s and s' according to the action a
$Re(s,a,s')$	Reward in the MDP between the state s and s' according to the action a
$f(s,a,s')$	Feature in the MDP which is derived between the state s and s' according to the action a
θ	Weight of the reward function
π	Policy (sample of Π)
π^*	Optimal policy
π^s	Selected policy
Π	Set of possible policies
$\Delta t_{\mathrm{E,dyn}}$	Step size to integrate the dynamic model $\tau_{\mathrm{E,dyn}}$ ($\Delta t_{\mathrm{E,dyn}} = t_{m+1} - t_m$)
$V(s)$	Value in the MDP of the state s
TH	Time horizon of the planning process
l	Length of a vehicle
w	Width of a vehicle
$\boldsymbol{M}$	Mass matrix of multi-body system
m	Mass; Index of time step t_m for the integration of a dynamic model
$\boldsymbol{C}$	Damper matrix of multi-body system
c	Damper coefficient of a damper
$\boldsymbol{K}$	Stiffness matrix of multi-body system
k	Stiffness of a spring, Index of objects o_k
ξ	Additional static feature
J	Moment of inertia; Value of cost function
M	Environment model
η	Accident severity prediction function
ω	Label for the instantaneous vehicle object (collision) configuration ($\omega := \boldsymbol{z}_{\mathrm{EK}}$); Yaw rate

ω_{coll}, $\omega_{\overline{\text{coll}}}$	Instantaneous vehicle object configuration which is in collision or not in collision
$\omega_{\text{coll}}^{\text{Pmax}}$	Most probable collision configuration
Ω	Sample space; Random variable to the yaw rate ω
Ω^{dyn}	Sample space of dynamic elements
Ω^{stat}	Sample space of static elements
Ω^{voc}	Sample space of vehicle object constellations
τ	Dynamic model (e.g., $\tau_{\text{E,dyn}}$ represents the ego vehicle dynamic with a non-linear single track model)
$o_k \in \mathcal{O}$	The sample target vehicles o_k are summarised by the set $\mathcal{O}$
$h_k^j \in \mathcal{H}_k$	The sample intentions h_k^j of target vehicle o_k are summarised by the set $\mathcal{H}_k$ of the target vehicle
EK	Bidirectional event between ego vehicle E and one target object $o_{k=\text{K}}$. It relates to the substate z_{EK} of one time step t_i of object o_k with intention h_j and thus is equal to $\text{EK} \hat{=} \text{EK}_{i,k}^j$
C	Event collision
$\boldsymbol{z} \in \boldsymbol{Z}$	State vector as sample vector and random vector(e.g., $\boldsymbol{z}_{\text{E}} \in \boldsymbol{Z}_{\text{E}}$, $\boldsymbol{z}_{\text{K}} \in \boldsymbol{Z}_{\text{K}}$)
$x_c \in X_c$	Object classification as sample and random variable
$\boldsymbol{z}_{\text{EK}} \in \boldsymbol{Z}_{\text{EK}}$	State vector of bidirectional substate between ego E and one target object K as sample vector and random vector with $\text{EK} \hat{=} \text{EK}_{i,k}^j$
$\boldsymbol{z}_{\text{dyn}} \in \boldsymbol{Z}_{\text{dyn}}$	State vector with dynamic, time variant elements of $\boldsymbol{z}$ as sample vector and random vector
$\boldsymbol{z}_{\text{stat}} \in \boldsymbol{Z}_{\text{stat}}$	State vector with static, time invariant elements of $\boldsymbol{z}$ as sample vector and random vector
$\boldsymbol{g} \in \boldsymbol{G}$	State vector with geometric elements of $\boldsymbol{z}$ as sample vector and random vector
$\widetilde{\boldsymbol{g}} \in \widetilde{\boldsymbol{G}}$	Reduced state vector with geometric elements of $\boldsymbol{z}$ as sample vector and random vector
$\boldsymbol{p} \in \boldsymbol{P}$	Reduced state vector excluding geometric elements of $\boldsymbol{z}$ as sample vector and random vector
$\boldsymbol{z}_{\text{input}} \in \boldsymbol{Z}_{\text{input}}$	Reduced state vector with directly and indirectly measureable elements of $\boldsymbol{z}$ as sample vector and random vector
$\boldsymbol{z}_{\text{train}} \in \boldsymbol{Z}_{\text{train}}$	Reduced state vector with non-measureable elements of $\boldsymbol{z}$ as sample vector and random vector
$f_{\text{crit}}(s,a,s')$	Feature for the criticality estimation
$f_{\text{comfort}}(s,a,s')$	Feature for the comfort estimation
$f_{\text{progress}}(s,a,s')$	Feature for the progress estimation
ψ_{Pmax}	Accident severity at the most probable collision configuration $\omega_{\text{coll}}^{\text{Pmax}}$

D, D' etc.	Minkowski Difference. The apostrophe indicates a transformed Minkowski Difference.
δ	Confidence interval for the angle probability; Steering angle
$\mathbf{\Lambda}$	Matrix of eigenvalues
$\boldsymbol{V}$	Matrix of eigenvectors
α	Rotation angle of eigenvectors; Angle to COG line; Accuracy function $\alpha(\cdot)$; Slip angle
$\mathbf{\Sigma}$	Covariance matrix
f_{model}	Established models (e.g., dynamic model τ) to map direct measreable parameters
ρ	Correlation coefficient
q	Weighting factor between self and target protection
S	Momentum (impact drive)
B	Impact point
μ	Friction; Expected value
$\boldsymbol{r}$	Distance vector
$\boldsymbol{r}_F$	Distance vector to force insertion
e	Error (defined as difference between the estimated and reference value such as $e = (\hat{\cdot}) - (\cdot)$; Restitution coefficient
$\phi(\cdot)$	Relevance function
F1-score	harmonic mean (e.g., between precision and recall)
$g(t)$	Execution time value
T-score	harmonic mean (e.g., between F1-score and $g(t)$)
σ	Standard derivation; Mechanical load
ε	Deformation / displacement
z_{cm}	State to the crash motion model τ_{cm}
$\psi \in \Psi$	Accident severity as part of risk R (criticality feature)
R, R_f	Risk (criticality feature) - in general terms and as feature in the motion planning (partly aggregated)
Δv	velocity change during crash / technical acccident severity
ψ_{impact}	Severity in the moment of impact
$P(C)$	Collision probability
R_{thr}	Risk threshold for the graceful degradation

1 Introduction

1.1 Background

The opportunity for individual mobility represents prosperity and comfort to people all around the globe. Thus, the world road traffic have increased continuously over the past decades [1, p. 5]. Accordingly, the amount of traffic accidents have grown as well leading to nearly 1.35 million fatalities per year over the world in 2016 [1, p. 4]. Currently, it is the eighth and first leading cause of death for all generations and humans between 5-29 years, respectively [1, 2].

Related to that amount, the European Union is doing relatively well by reducing their frequencies of accidents by 21 % between 2010 and 2018. Figure 1.1 shows the traffic fatalities and severe injuries over the years for the European Union (28 States and 24 States) as well as for the Federal Republic of Germany (FRG). Germany is presented as one example member of the European Union with long-term, enhanced consistent data sources, such as [3], to emphasize the relevance of relative trends to the road safety, here e.g., according to the yearly driving performance. The impact of other influences such as age, sex, education, population and vehicle fleet conditions are neglected. In short, the total and relative progress of FRG follows the EU's level qualitatively. While the EU's frequency of fatalities declined at the beginning by 43 % between 2001 and 2010, the reduction has stagnated about the last 5 years. That means 25058 dead people and 214940 seriously injured in the year 2018. Therefore, the European Commission states in the working paper "Europe on the Move" that these numbers "represent an unacceptable humanitarian and social cost" [4, p. 2] and propose a strategy for safe mobility to reduce the frequencies in the future. The need of action is also shown in monetary terms. The European Commission estimates the annual cost of road fatalities and serious injuries to be more than 120 billion Euro, equivalent to approximately 1 per cent of GDP [4, p. 2].

As answer, the "Vision Zero" has been established by the European Union meaning zero fatalities and serious injuries in road transport with outlook for 2050 [4]. The term "Vision Zero" emerged firstly in the occupational safety and was transferred by the swedish Road Administration (Vägverket) to road safety. Since 1997, it is the legal basis for the swedish transportation policy [5]. Moreover, it is adopted by many other countries and symbolise now in the European Union and beyond the major effort to avoid deadly and severe accidents in road traffic and other areas (e.g., [1], [4], [6], and [7]). Unfortunately, the actual target of halving the overall frequency of road death in the European Union by 2020 related to 2010 is failed and hence an important milestone to the "Vision Zero" is missed [8, p. 4]. Nonetheless, the long-term goal "Vision Zero" remains and it was added with "new interim targets to reduce the number of road deaths by 50 per cent between 2020 and 2030 as well as to reduce the number of serious injuries by 50 per cent in the same time period" [4, p. 3].

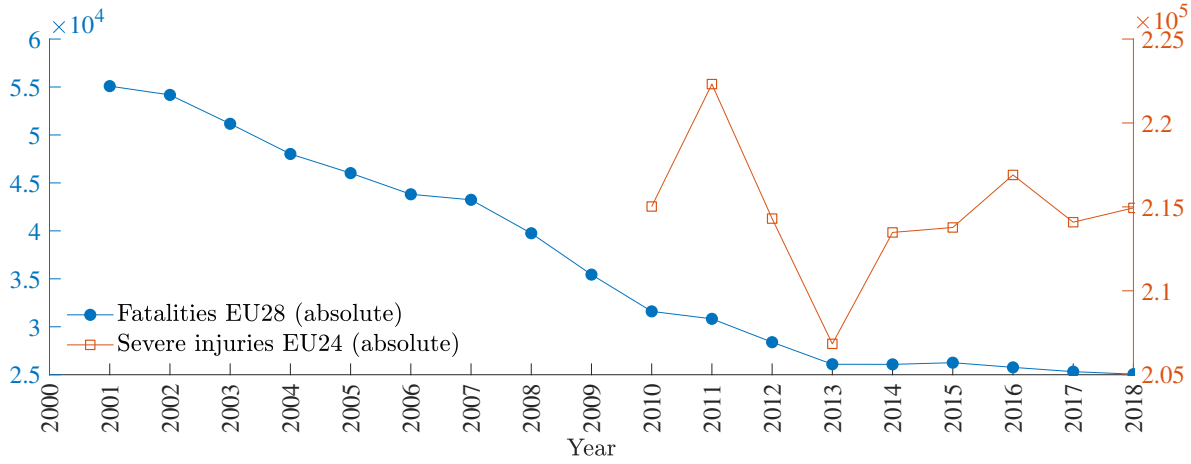

(a) **European Union** - Absolute frequency of fatalities and severe injuried over the years [9]

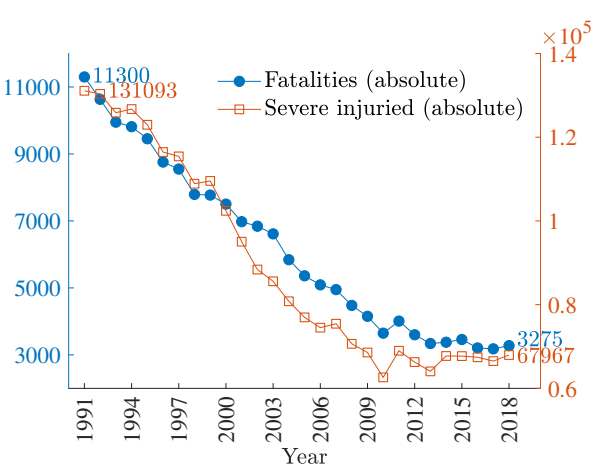

(b) **FRG** - Absolute frequency [3]

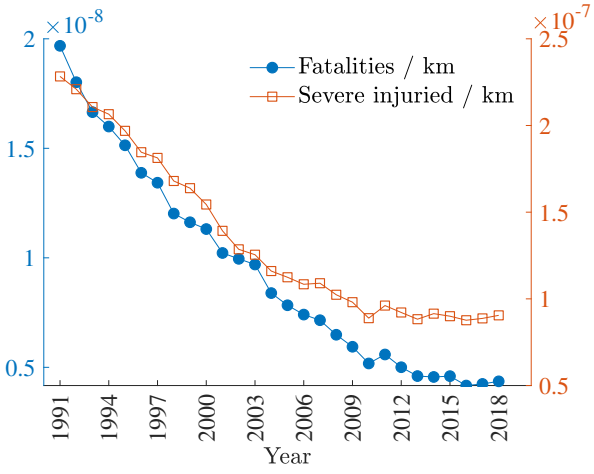

(c) **FRG** - Relative frequency [3], [10]

Figure 1.1: Accident data EU and FRG - Incidences of accident fatalities and severe injuries are shown in (a), (b), and (c) in absolute and relative (related to traffic performance) frequencies over the past years. The graphs decline at the beginning of data recording, yet stagnate in recent years (about 2013-2018). The data source for (a) is [9]. The data on European level are vaguer compared to single countries due to the different understanding of accidents and their diligence in data recording. As for the FRG, the relative accident consequences remain constant lately, showing that at least the side effect of enhanced traffic performance has no impact on the progress. The data refer to [3] and [10].

The current strategy bases on the “Safe System Approach“ from the World Health Organisation [1]. That means road safety on different levels and shared responsibilities. If one level falls, so the idea, there should be the next level forgiving any previous mistake. Thus, [11] discusses main intervention areas, such as safe road use, infrastructure safety, vehicle safety, and emergency response. “While collisions will continue to occur, death and serious injury are largely preventable“ [11, p. 4]. That statement refers at one hand to technical

opportunities and on the other to the conscientious spread of burden or rather responsibility over all safety levels.

This work focus on the part of the vehicle safety. While passive vehicle safety has a long important tradition for vehicle manufactures, new safety benefits are mainly seen in the improvement of active vehicle safety systems [12, chap. 3], [13, sec. 9.9], [14, pp. 55-57], [15, pp. 48-63]. Especially, the passive safety limits are reached by high velocities and heavy masses of the traffic participants [16, p. 53]. Beyond, this work contributes to new safety approaches combining the active and passive part to integral technologies taking the accident outcome by pre-crash actions into account.

Furthermore, seeing that over 90 % of the accidents are induced by humans directly, the crucial potential of automated safety systems is emphasised [17, pp. 49-50]. Consequently, automated driving would gain the most safety benefit, e.g., due to reaction time reduction with no need for the behaviour prediction of the driver, broad environment perception, fast decision making and precise vehicle control. "However, new risks are emerging in the transition phase, some related to the functioning of highly automated vehicles in mixed traffic and the complex interaction between the driver and the vehicle (Human-Machine Interface), as well as cybersecurity issues" [4, p. 3]. Examples are already given by [18], [19, 20] and [21]. In this case, the failure of automated functionalities has increased the frequency of fatalities giving a foresight what it could mean if the "Vision Zero" is neglected in emerging trends. In conclusion, the safety issues are the most important concerns in terms of automated driving and need further development.

However, transferring the idea of the "Safe System Approach" may be an enabler to these new functionalities by distributing the safety responsibility over all safety levels. In other words, collisions would be justifiable if the crash severity remains acceptable low. A tremendous effort to accident free automated driving, likely not reachable, e.g., due to unforeseeable scenario evolving while driving, unpredictable behaviour prediction of traffic participants, third-party negligence, or just system failures, would be evaded. Besides, in the case of [18], a simple automated emergency braking probably had saved the fatality. What is more, the "Safe System Approach" does not undermine the "Vision Zero". For example, [22], [23], and [24] discuss the safety philosophy indicating that accident frequency and road safety are no synonymous, even if they might correlate. Further they state that a crash that does not result in loss of health is a cost rather than a safety problem. In conclusion, passive or rather integral safety is assumed to be required even in full automated vehicles and changed mobility and thus the development of new intelligent safety solutions is motivated.

Currently, the automated driving functions emerge step by step related to the technical opportunities. Accordingly, automation levels to full automated vehicles are proposed by the SAE [25]. The driver is exempted gradually of the driving task. While at level 0 no assistance is available, fully automated vehicles require no driver at all. The biggest gap is between level 2 and 3. Here, the monitoring task passes from the driver to the driving system including the transfer of responsibility.

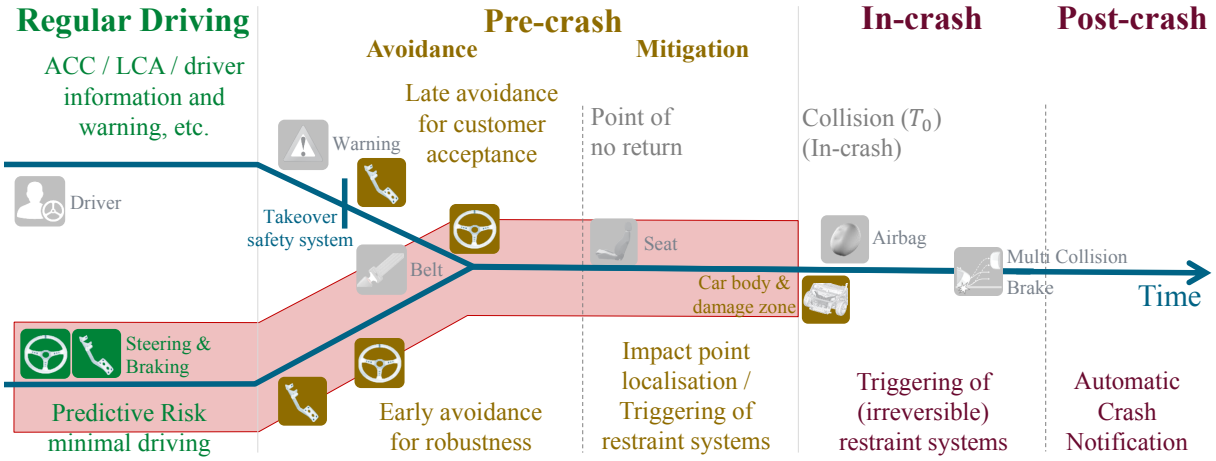

Figure 1.2: Difference assisted and automated driving - The figure shows how assisted and automated driving functions merge in critical situations. In regular driving the driving monitoring and responsibility distinguish. If an imminent collision occurs, only few hundred milliseconds remain to choose an appropriate manoeuvre. Therefore, advanced driver assistant systems (ADAS) protect the traffic participants without any human driver required, similar to automated systems. The same holds for the deployments in the pre-, in-, and post-crash phase. Moreover, the figure shows examples of safety functions highlighting engine, steer, and vehicle structure as considered in this work.

This system view of responsibilities relates to regular driving in general using the engine and steer as driving actor. Besides, when it comes to critical situations, further safety components gain importance. Here, the deployment remains similar whether in assisted or automated driving. Fig. 1.2 exemplifies this statement. Passive elements engage if the collision is likely to occur or already happens. Restraints systems, such as belt tensioners and air bags, work for all automation levels. In other words, the closer the crash, the more merge the functionalities of assisted and automated driving, such as emergency braking and steering, in the pre-crash phase. Only the point of activation may differ. While the automation probably acts more preventively, the driver needs to be overridden by the system considering law and personal sensitivities. That outline is presented, since this thesis contributes to integral safety technologies usable in assisted as well as in automated driving even if the research application is discussed only for full automated vehicles.

1.2 Problem statement and research question

New safety systems aiming to achieve the “Vision Zero“ for current and future mobility. Even if it is accepted that integral safety would gain the most benefit (sec. 1.1), it is common to develop active, including driver assistance, and passive systems separately and moreover for single, specific use cases as shown in section 2.1.1. Consequently, the function deployment is related to isolated phases of preventative driving (comfort and assistance systems), pre-crash, in-crash, and post-cash with each having own activation strategies, e.g., based on

individual triggering metrics, system limits, reaction times, function validations, redundancies, and control units. Therefore, a strategy is needed to consider single, passive systems in forward-looking active safety to derive appropriate vehicle behaviours in critical situations. More detailed, only few research has been done to include crash consequences into the driving and pre-crash decision. That is especially required for trajectory planning with impact point localisation and the pre-crash deployment of restraint systems.

However, the more preventable and pre-crash the vehicle behaviour is derived, the more environment evolvement uncertainties increase due to the additional time interval. By way of example, that includes uncertainties to the environment perception and behaviour prediction. As result, it is difficult to assign the appropriate vehicle answer to each driving state not knowing whether preventative actions, emergency avoidance manoeuvres or mitigation applications with impact point consideration including the triggering of (ir-)reversible restraint systems are reasonable. Therefore, considering uncertainties is a promising way in a reliable function selection, especially for the decision between collision avoidance and mitigation manoeuvres. Moreover, taking passive elements into account means to estimate crash consequences pre-crash and thus in real time. However, crashes are almost chaotic processes and are usually investigated by time-consuming crash tests or FEM simulations. Inferred prediction model approximations add further uncertainties to the process even if the input parameters would be perfectly known, what they are not.

Furthermore, the computation effort grows the more single safety components or rather behaviour opportunities needs to be assessed. Nonetheless, the results need to be available in few hundred milliseconds for pre-crash application. Even if the performance of appropriate control units varies widely, and hence constitutes no focus in this work, it is assumed necessary to find proper approximations in the calculations anyway. More detailed, it is necessary to estimated potential crash consequences as part of the trajectory planning in real time. Exemplary, the function deployment should at least work on current available automotive test hardware what, most probably, exceeds the power of normal series vehicles.

Summarising, the objective of this thesis is an approach for an integral safety technology in automated driving. It should work for preventative driving, collision avoidance in critical situations as well as accident severity mitigation in inevitable collisions. Thereby, uncertainties and real time requirements constitute a major challenge. Exemplary, without the loss of generality, also highlighted in figure 1.2, the engine, steer, and statical passive components, such as car body and damage zone, shall be used to instantiate general integral findings of this thesis.

As result, following main research questions arise:

1) How to combine established active and passive vehicle safety components, such as steer, brake, and car body deformation zone, in one integral safety approach?

2) How to address uncertainties in the function selection, e.g., due to environment perception or behaviour prediction, to enable robust integral safety, such as reliable collision avoidance and mitigation by braking and steering?

3) How to process the required calculations of the integral safety system in real time with currently available test equipment? In other words, related to the instantiation of this thesis, how to process the criticality estimation as part of the trajectory planning in real time?

1.3 Contribution

The assessment and selection of appropriate vehicle behaviours require a quantification of the safety consequences related to integral action alternatives. Reversely, the criticality of the vehicle behaviour needs to be estimated. Characterising and developing of a risk based criticality measure as part of trajectory planning is key of this work. Since the criticality is evaluated pre-crash, with increased time gap to crash, it deals with uncertainties, e.g., due to the environment perception and prediction, and derives vehicle behaviours in real time. The results are obtained from simulations, real word testing, fleet data, and accident database analyses.

The following contributions combine and enhance investigations of previous publications [26–28]. Besides, two supervised student theses [29] and [30], and 7 patents (partly pending) are addressed. Furthermore, the contribution comprise both, general integral findings and their instantiations with the example system of steer, brake, and deformation zone.

1) This thesis presents a new approach to concatenate active and passive components in integral vehicle safety. The combined deployment of safety actions bases on a holistic criticality measure which is determined by the application.

   More detailed, a novel risk based criticality measure is used in the trajectory planning and thus enables a smooth transition between preventative driving, collision avoidance, and collision mitigation including impact point localisation. Thereby, each trajectory is assessed according to the potential crash severity which is determined with the velocity change during a potential crash Δv.

   A new scenario catalogue and test procedure is derived to evaluate the risk assessment in trajectory planning, since legal requirements are currently missing. However, the approach itself works scenario independent. Fleet data of regular driving and the GIDAS accident database show the criticality indication of the risk measure. The uncertainty-adaptivity and mitigation performance are demonstrated by six use cases, on the testing ground and in simulation.

   The results show, that the risk based trajectory planning reduce the technical accident severity compared to established Automatic Emergency Braking (AEB) about 20-30 % in average pursuant to the selected evaluation scenarios. That means up to one-third less injury probability for the vehicle occupants.

2) In contrast to similar approaches, uncertainties, e.g., due to environment perception and traffic participants' behaviour prediction are taken into account. As result, the novel criticality, referred as risk measure, combines the potential, predicted accident

consequences with the probabilities of occurrence, improving the performance and robustness of the function deployment. Therefore, the vehicle behaviour follows the expected value of the crash severity and thus implements a statistical strategy.

More detailed, for the first time, potential crash severities Δv are weighted with the collision probability. That enables a robust decision between collision avoidance and mitigation emergency manoeuvres by braking and swerving in one approach.

Due to the continuous uncertainty consideration, the systems adapts inherently to changing perception and environment prediction performance, e.g., caused by volatile weather conditions, malfunctions, or hardware modifications.

In accordance with the statistical approach, no pre-selection of a collision avoidance or collision mitigation stage is made. However, it is shown and evaluated that a switching of the optimisation problem, at least referring to preventative driving and emergency manoeuvres, is a necessary premise for integral safety.

3) The feasibility of the integral driving function is shown in real test vehicles on the testing ground. The real time requirements are met by the adopted trajectory planning framework, which bases on dynamic programming and massive parallelisation, as well as approximating risk prediction procedures, which scale between computing time and estimation quality.

   The switching of the optimisation problem between preventative driving and emergency manoeuvres is conducted by changed weights of the reward function. Advantageously, that enables to use the same trajectory planning framework and thus to reduces the maintenance effort and time-consuming data transfers.

   Firstly, an eccentric impact model provides approximately the accident severity Δv while driving and thus provides labelled results of FEM simulations in real time. With reference to a database with more than 6000 FEM structure simulations, it is selected as compromise between accuracy, calculation time, and transparency in comparison to a centric impact, multi-body system, feed forward neural network, and random forest regression.

   The estimation of the collision probability and selection of the most probable collision configurations base on a 3D Minkowski Difference.

2 Fundamentals and related Work

The following sections deal with the state of the art with respect to the main contributions of integral safety (sec. 2.1) and related preliminaries of an automated driving function (sec. 2.2). Due to the interdisciplinary theme of this thesis, fundamentals, related work, and concerning discussions are grouped for each different subject instead of sorting all issues by the meta level.

2.1 Integral safety

2.1.1 Integral applications

Integral safety designates the combination of active and passive safety components. So far, it is widely described in the literature, yet the term is not used identically. Even the usage of the terms *active* and *passive safety* differs slightly. The same holds for the crash related formulations. Therefore, definitions are given for the use in this thesis as following and the related work is assigned to these terms.

Fig. 2.1 shows the criticality phases related to the driving process adopting the vocabulary of the standard [31] largely and adds commonly used wordings. The driving process is separated into *criticality phases* of I) *regular driving*, II) *pre-crash*, III) *in-crash*, and IV) *post-crash*, while the number II) and III) define an *accident*. While [12, sec 4.1.1] and [13, sec. 9.9.2] define *pre-crash* between the *point of no return* and the first impact moment at t_0, this thesis specifies the time interval more generous as [31] and [32] from a vehicle function point of view not knowing when the *point of no return* occurs. *Pre-crash* denotes here the time interval before a potential crash, where only a certain *emergency* action may avoid or mitigate the harm of the collision. The *point of no return* indicates the moment when a collision is physically no more avoidable. The *in-crash* phase starts with the collision at the moment t_0. The *pre-crash* and *in-crash phase* repeat in the case of *multi-collisions* until the *rest position* is reached including the *impact phase* and *running out*. Afterwards the *post-crash* phase endures.

The *passive vehicle safety*, also known as *secondary vehicle safety* [31, def. 4.3.8], refers to vehicle systems and features that reduce the crash consequences, once the collision is occured at the moment t_0. Complementary, specialist books, such as [12, p. 3], [13, p. 968], [33, p. 632], and [34, p. 77], determine *active vehicle safety* as systems used before t_0 to avoid collisions. It involves a widely range beginning with common components as light and air-conditioner, followed by vehicle stabilisation as anti-lock braking system (ABS) and electronic stability control (ESC) and the constantly emerging advanced driver assistence systmes (ADAS). Since that systems are not able to guarantee a collision avoidance in every case, this thesis refers to the more precise definition of [31, def. 4.3.8] and [32, p. 9], that *active vehicle safety*, also known as *primary vehicle safety*, avoids collisions *or*

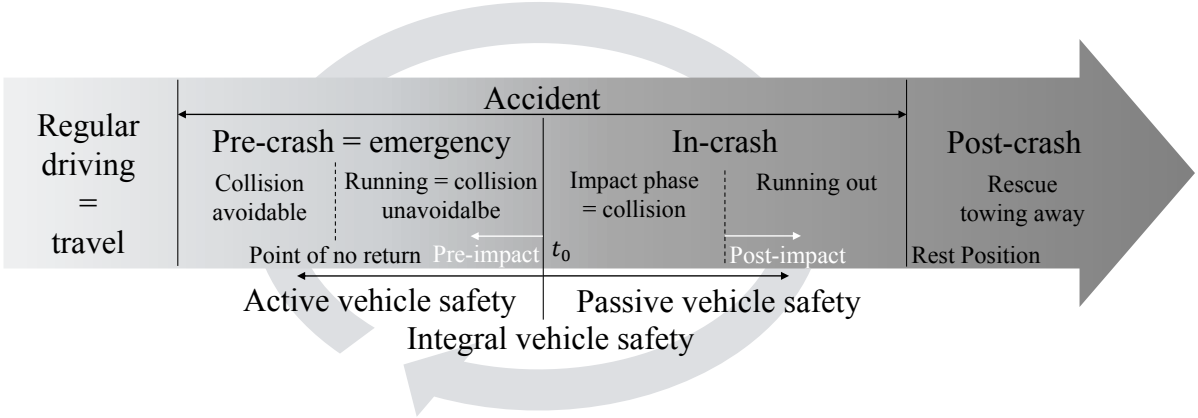

Figure 2.1: Accident-related events - The figure shows the accident-related events according to [31, def. 5.2] enhanced with common wordings as used in this thesis. The arrow with colour gradient indicates the increased criticality.

reduce the occurrence of accidents statistically also inducing less impact severity indirectly in inevitable collisions.

Work as [13, sec. 9.9] and [32, chap. 27] describe the *integral safety* as the "Safe System Approach", introduced in section 1.1, including all efforts to reduce the exposure and crash consequences before, during, and after a possibly collision. However, this work refers to the subfield of *integral vehicle safety* (safety component part of the vehicle) combining *active* and *passive vehicle systems*. In other words, *integral safety* means in the work's context the pre-crash consideration of passive crash protection, such as crumple zone, belt, and airbag, by active trajectory planning and emergency manoeuvres. By way of example, a simple emergency mitigation braking or the integration of multiple active safety functions (e.g., [35] [36]) does not count in contrast to impact point optimisation.

According to that definitions, related work is grouped in table 2.1 and labelled with G1 to G11. The used *safety components*, such as engine, steer, crumple zone and restraint systems, are listed to the criticality phases (columns). Furthermore, it shows the different usage of safety components in the forward-looking and mitigating domains (rows). Additionally to the distinction of the a) integral design (rows), b) criticality phase (columns), and c) safety system usage (body), related work is structured in aspects as d) assisted and automated driving, e) non-probabilistic and probabilistic approaches and f) criticality measures. However, due to the interdisciplinary field, a clear assignment is not always possible, yet tried with maximal purpose. Thereby, each subject might refer as an own research field. Hence, only an overview with focus on integral vehicle safety is given, as far as regarded necessary for this work. For further insights, it is referred to dedicated reviews of ADAS and automated driving, such as [37], dealing with threat assessment, [38], summarising motion prediction techniques, and [39], [40], and [41], concentrating on motion planning. All in all, the strength of the current integral approach is derived by this review.

According to the presented overview, the infrastructure (G1) and the rescue chain (G11) form the margins around the driving process.

Table 2.1: Overview integral safety approaches - Safety systems related to the safety domain (row) and criticality phase (column). Grouped related work (G1 - G11) correlates in the criticality measure, while cyan indicates probabilistic approaches according to table 2.3.

Safety domain	Group description	Uncertainty-adaptive, universal driving Regular driving	Collision Avoidance	Collision Mitigation	In-crash	Post-crash
Infra-structure/ Strategic	**G1)** Advanced Traffic Management Systems ATMS (e.g., [42], [43], [44], [45]), Route planner (e.g., [46], [47], [48])	Routing, DMS etc.	Indirect due to less congestion	-	-	Information prevent secondary accidents
Active vehicle safety	**G2)** ADAS (Emergency brake, ACC, LA etc. [32, sec. 19.8]) TTX [49] [50] [51, 52] [53] [54] [55]; Probabilistic TTX [56, 57] [58] [59, 60]; Advanced criticality assessment in assisted driving [61] [62] [63] [64] [65] [66] [67] [68]	(Driver support)	Brake, steer, warning	(Indirect) if triggered to late for avoidance	-	-
	G3) Automated driving function non-probabilistic (classic) [69–71] [72, 73] probabilistic [74] [75] [76] [77]	Brake, steer	Brake, steer	Brake, often simply not mentioned	out of scope	out of scope
Advanced active vehicle safety	**G4)** Trajectory planning with state and kinetic energy related severity (at least recognition that avoidability cannot be guaranteed) [78–80] [81] [82] [83, 84] [85]	Brake, steer, (HMI)	Brake, steer	Brake, steer	-	-
Integral vehicle safety	**G5)** Trajectory planning with centric impact (vehicle approximated as point mass) [86] [87] [88] [89–91]	Brake, steer, (HMI)	Brake, steer	Brake, steer, car body	-	-
	G6) Trajectory planning with injury risk function (vehicle approximated as point mass) [92] [93] [94]	Brake, steer, (HMI)	Brake, steer	Brake, steer, "restraint system"	-	-
	G7) Trajectory planning with impact point localisation (feedback severity to driving function, vehicle contour extension) [95] [96, 97] [98] [99] [26, 27]	Brake, steer, (HMI)	Brake, steer	Brake, steer, car body	-	-
	G8) Pre-crash triggering of passive restraint systems (no feedback to driving function; nominal operating point for seat, window, sunroof etc., improving crashworthiness; (ir-)reversible internal / external restraint systems, e.g., belt and airbag)	-	-	car body, internal airbag [100–102], [103–105], external airbag [106, 107], vehicle height level adaptation [108], shear thickening [109], safety system in general [110]	once deployed, still active	-
Advanced passive vehicle safety	**G9)** Pre-crashadaptation of passive restraint systems (no feedback to driving function; preferred for irreversible restraint systems) [111–114], [115, 116], [117–119]	-	-	Car body and restraint system, directed linking between active sensing and passive systems	triggering of previous adapted systems (e.g., airbag)	-
Passive vehicle safety	**G10)** Default crash protection (e.g., [32, sec. 27.2], [12, chap. 3], [13, sec. 2.2.4, chap. 9], [120, chap. 4])	-	-	-	Belt, seat, bumper, crumple zone, airbag, MKB [121] [122], etc.	-
Rescue	**G11)** (Advanced) Automatic Crash Notification (A)ACN (eCall [123, 124], E911 [125], TPS, Field Triage [126] [127] [128] [129], etc.)	-	-	-	-	Emergency call
				use case related severity prediction		

Globally, advanced traffic management systems (ATMS, G1) prevents accidents by routing the traffic or at least giving additional information to the traffic participants (e.g., [42], [43], [44], [45]). In order to reduce the accident exposure, they consider knowledge of past accident research. Dynamic, static, traffic- and vehicle-related features, such as street condition, weather, day or night time, road user's type, and traffic congestion, are used to determine the safety level and as result an appropriate reactions are derived and given to the vehicle driver. Thus, they take the accident outcome indirectly for the traffic as whole into account. What is done for all traffic participants by ATMS, can be individualised by personal strategic rout planners (e.g., [46], [47], [48]). By way of example, the number of traffic domain changes, current traffic congestion, time of road use, and weather indicate how dangerous the desired journey or rather route will be.

Anyway, if a collision is already occurred, the rescue of the casualities (G11) has highest priority. However, limited availability of emergency services (amount depending on country and location) leads to a prioritising problem, referred as *field triage* (e.g., [126] [127] [128] [129]). Already few minutes waiting time makes a significant difference by severe injuries. Moreover, seeing that often the traffic accidents result solely in car body damage [129], it seems reasonable to help severe injured first. Improving the decision of the control centre, it is important to transmit the accident consequences as well as the location of the accident site in detail. Advanced automatic crash notifications (AACN), such as eCall [123, 124], E911 [125], or third party service (TPS), transmit these information automatically even if the accident participants are not able to respond. Thereby, it is necessary to take the pre- and in-crash process into account to indicate the accident severity. What is more, it is difficult to judge the internal injuries without detailed investigations. Regarding only the external accident outcome that might lead to missed medical treatments with disadvantageous consequences. Here, AACN help to assess the accident consequences and thus increase the accuracy of accident treatments.

Advanced driver assistant systems (ADAS, G2) support the driver with information, warnings or influence the vehicle guidance directly [32, sec. 19.8]. Thereby, a smooth transition between assistance and safety application can be recognised. When a situation becomes critical, the objective is to avoid collisions pre-crash by braking and swerving interventions. The mitigation of crash consequences is addressed by braking solely when a collision is inevitable. In automated driving (G3) the systems gain the driving responsibility. Related work therefore focus on collision avoidance with no distinction to regular driving. According to the development progress, previous work do not mention any mitigation strategy even if the system capabilities would have high potentials to reduce the crash severity. What is more, they state accident free driving by the formulation of the trajectory planning problem, such as [77], or simple trigger full braking based on the criticality, such as [67]. However, advanced active vehicle safety (G4) is aware of accident possibilities. Therefore, they take state related (e.g., velocities) and kinetic energy related (masses and velocities) accident severities into account. As result, mitigation by braking and the selection of the collision opponent is induced in collision-prone scenarios. While energy reduction is reasonable in the most cases, third party involvement has ethical issues as discussed in section 2.2.3. This group (G4) shows how smooth the transition to integral safety appears. At one hand, these

systems might count to integral safety, yet they consider not really more actors than engine and steer (dashed line).

Passive safety (G10) protects the vehicle occupants in the in-crash phase. Since it is not the focus of this thesis, it is referred to dedicated surveys, such as [32, sec. 27.2], [12, chap. 3], [13, sec. 2.2.4, chap. 9], and [120, chap. 4]), for further information. Improving the benefit, advanced passive vehicle safety (G9) uses the environment sensors to adapt the safety system pre-crash to the expected accident severity. Afterwards, the safety actors are triggered if the collision really occurs after the moment t_0 in the in-crash phase. The in-crash sensors are used as fall-back level since it is difficult to guarantee that a collision is inevitable previously. That strategy is used to prevent false positives, especially in safety critical decisions with irreversible restraint systems such as airbags [111–114] [115, 116]. That leads to a directed linking between active sensors and passive systems, yet is not integral in total. The pre-crash gathered information effect only after t_0 and have no feedback to previous active systems.

The pre-crash triggered passive restraint systems (G8) count as simple integral applications. The active sensors are used to detect an imminent collision and trigger either, adaptive, passive systems or adjust the current occupant situation as far as possible to the operating point of the restraint systems, e.g., by belt pre-tensioning, seat backrest positioning, window and sunroof closing. Since it is difficult to estimate the point of no return, this system activation is used especially by reversible restraint systems. Here, false positives are regarded as customer inconvenience but not as safety issue and therefore are assumed to be accepted more generous. Besides, crash compatibility actions, such as active structures [109], vehicle height level [108] or external airbags [106, 107] need to be triggered pre-crash for their use. Moreover, approaches exist to trigger irreversible restraint systems pre-crash [100–102] [103, 105]. Thereby, the crash inevitability is determined roughly. For example [103] uses a collision unavoidable detector based on the intentions of the own vehicle and other road users. Apart from the pre-crash adaptation and triggering, no further feedback to the driving function is given.

In contrast, approaches exist (G5) which consider the potential crash severity by centric impact models. Thus, the collision opponents, the transformed energy and the collision angle are differentiated and thus targeted by braking and steering. Thereby, the expected or rather modelled car body restitution level is considered. However, the vehicle is modelled as point mass not able to distinguish a special impact point. The same holds for [92], [93] and [94]. Here, injury risk functions (G6) regard the crash knowledge in a general manner, yet distinguish only between multiple objects or increase the robustness of avoidance manoeuvres.

Summarising, the ideal integral safety system would consider subsequent available safety components in decisions of previous criticality phases. In other words, each cell of table 2.1 would be filled with as many available safety systems as possible. However, currently only few systems are combined. If any, single solutions are concatenated rather than forming an holistic approach. Moreover, a big gap exists between the trajectory planning in collision avoidance and the triggering of restraint systems in the mitigation and in-crash phase. First

investigations of the active vehicle safety try to break this gap by including rough severity measures into the trajectory planning. Nevertheless, it is not enough to improve the driving decision with the knowledge about the crash consequence due to the use of advanced restraint systems. Neither, a pre-crash activation of these restraint systems is enabled. Only a simple triggering of fail-safe irreversible restraint systems seems reasonable. On the other hand, improvements on intelligent passive safety have currently no feedback to the driving function.

Therefore, this thesis presents an approach to combine the active trajectory planning with passive occupant protection as proposed in previous publications [26, 27]. In order to find the best linkage between different systems, their combined consequences need to be ranked on one unified scale. Accordingly, a general quantification of the action's safety benefit or vice versa of the criticality is needed. Thereby, the desired application determines the criticality type. That is also emphasised by the structure of table 2.1. The groups G1 to G11, ordered according to the integral evolution, correlate with the use of the criticality measure (sec. 2.1.3.3). In this thesis, the objective includes collision avoidance if possible and else collision mitigation, both by braking, steering and considering of the crumple zone. Thereby, the criticality needs to regard the road infrastructure, to differentiate multiple other road users and their current and future motion state, to distinguish collision configurations given one opponent, and to work situational universally. Furthermore, [130] formulates requirements on the transparency of safety systems. If harm occurs, the accident behaviour needs to be understandable. Meeting that criteria, this work bases the planning of the optimal trajectory on the protecting crumple zone and assesses each potential trajectory with a technical accident severity. Additional challenges to the trajectory's criticality assessment are discussed in the following.

Exemplary for integral applications, this work combines the engine, steer, and crumple zone. That example deals especially with the gap between collision avoidance and collision mitigation by trajectory planning with impact point optimisation in critical situations. Few related work could be found that addresses the same subject (G7). [98] implements an emergency planner parallel to the normal driving function which leads, as told by them, to the least harm in inevitable collisions. Thereby, the criticality assessment is described as data driven based on accident statistics. However, they simplify the trajectory evaluation roughly by the sole consideration of collision types side, rear, or front, favouring the front front impacts compared with side impacts. This simple rule limits the application enormously. Similarly, [96, 97] restricts the use case directly on crossing traffic and having the role of the impacting vehicle. Based on GIDAS accident data, they state that a sole, full reduction of the impact velocity might result in more severe accidents than taking the impact configuration, resulting from the braking sequence, into account. Therefore, the vehicle is decelerated in a way that avoids to impact the compartment. Swerving interventions and other accident types are not considered and therefore the approach is not usable without restrictions in a general manner for automated driving. In contrast, [99] use an eccentric impact model combined with accident type related injury risk functions to assess manoeuvres consequences situational independent. The combined braking and steering interventions are applied by inevitable collisions. However, the work lack of detailed description how the point of no return is

determined taking the driver's and opponent's intentions into account. Furthermore, due to real time challenges, entire intervention simulations are stored in a database for onboard usage. However, the structure of the database is not explained and hence rough approximations have to be assumed. Otherwise, the size of the database would increase tremendously due to the *curse of dimensionality* [131], [132]. Contrary to the estimation of the velocity change Δv, [95] builds crash severity maps based on the vehicle's intrusion and structural rating of the Insurance Institute for Highway Safety (IIHS). When a collision becomes inevitable, referring to the intersection of all ego and opponent intentions, the accident severity for all occupants is minimised. Even if the approach seems to be promising due to the systematic analyses based on FEM simulations in the offline investigations, they simplify the trajectory planning to steering manoeuvres in front front collisions. As result, only the impact angle and offset are considered in the crash severity. Other important parameters, such as vehicle type, masses, and velocities, are neglected. An other advanced approach is presented in [104]. Here, a random jungle is used to estimate the crash severity pre-crash and thus to derive appropriate vehicles behaviours, such as combined braking and steering or the triggering of restraint systems. However, the approach bases the system activation on an unavoidable detector and, in the case of emergency manoeuvres, only a limited number of pre-defined manoeuvres are investigated.

In contrast, this work does not restricts the motion planning in regular driving, collision avoidance or collision mitigation to any pre-defined scenario. Therefore, due to the curse of dimensionality, a database creation for online investigation of potential accident severity is currently not regarded as feasible or rather useful in such general approaches. Thus, the crash severity is calculated in real-time while driving. Nevertheless, the use case related severity estimation of passive-related work is a useful preliminary for pursuing investigations as done in this thesis.

What is more, the safety benefit lies especially in the increased prediction horizons of integral approaches. Unfortunately, if the prediction horizon is increased, the uncertainty to the scenario evolvement rises as well. That refers for example to the prediction of the object behaviours. While related work of the active safety tries to consider such uncertainties, the severity estimation in passive safety of related work often neglects these uncertainties. The same holds for the determination of the point of no return. In conclusion, a major contribution of this thesis lies in the combination of the use case related accident severity prediction of passive safety (sec. 2.1.2) with the uncertainty-adaptive situational-independent trajectory planning of active safety (sec. 2.1.3).

2.1.2 Accident Severity

2.1.2.1 Severity measures

Various measures are defined to quantify the severity level of crash consequences [133, sec. 3.5] [120, sec. 2.2.2, sec. 3.2]. The characteristic values vary related to the field of research and specific area of interest. Figure 2.2 shows an overview of common accident severities for the scope of this thesis. Generally, an accident happens when unintended

forces are exerted to the vehicle body with effect to health impairment or damage. Moreover, a wide range of influences effect the crash outcome what makes it difficult to quantify the accident severity in an objective manner, especially by few single values [134]. By way of example, the same technical crash procedure may result in complete different short-term consequences for vital and non-vital traffic participants with even more uncertainties to long-term implications [135]. Therefore, the field of accident severity is separated into four groups in the following section, also highlighted in figure 2.2: (1) vehicle and occupant load, (2) technical severity, (3) injury severity, and (4) long-term consequences. Owing to pros and cons, the particular application and requirements determine the suitable severity measure. Furthermore, the availability of data leads to necessary approximations.

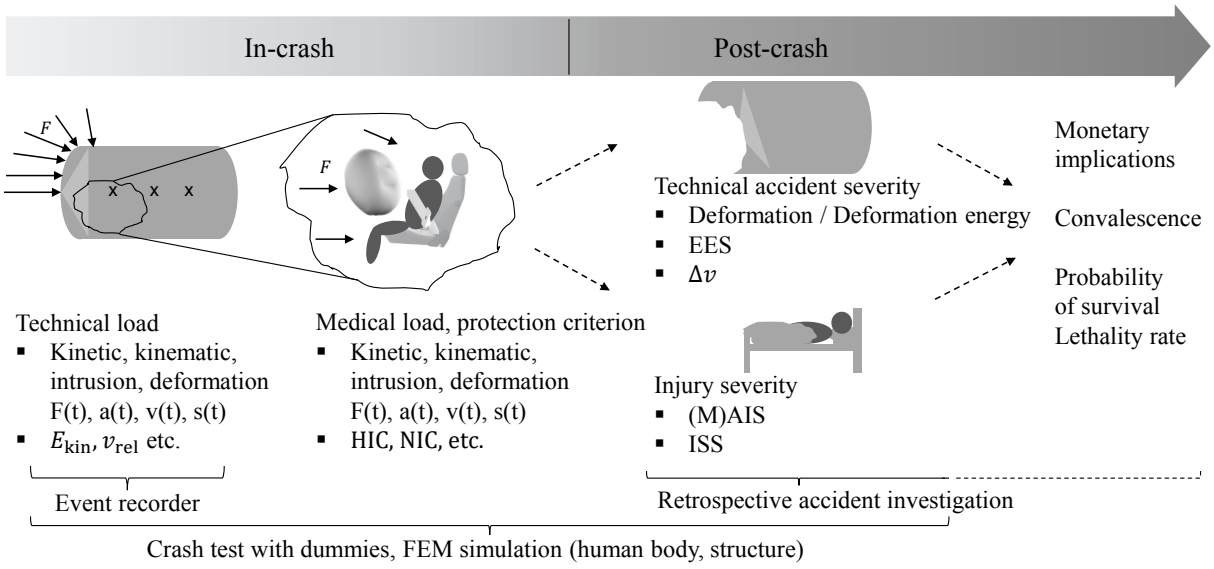

Figure 2.2: Overview accident severity - Examples for vehicle and occupant load, technical severity, injury severity, and long-term consequences are related to the crash sequence and data acquisition.

The technical accident severity quantifies the mechanical vehicle load due to force exertions resulting in acceleration $a(t)$, velocity $v(t)$ and deformation $s(t)$ course of time. Among others, the technical severity depends on the type of collision objects (masses, shapes, compatibility, etc.), velocity and impact position [136, p. 60] [137]. Characteristic values of the kinematics are used to indicate the severity by single values. Thereby, it depends where and how the data are obtained. While FEM simulations followed by crash tests and event recorders provide detailed information about the crash sequences (e.g., $a(t)$, $v(t)$, and $s(t)$), the police and accident investigators take down the incident retrospective finding the vehicle only in the rest position. Nevertheless, several measures have been established over the years [133, sec. 3.5]. For example, the deformation energy ΔT is obtained by reconstructing the force over the intrusion. Since the intrusion is measured post-crash, it indicates only the plastic exchange of energy. The Equivalent Energy Speed (EES) relates the deformation energy ΔT as kinetic energy to the vehicle mass m: $\Delta T = 0.5\,m\,\mathrm{EES}^2$. Reconstructing the accident includes to determine the velocities at impact, referred as $\boldsymbol{v}_{\mathrm{rel}}$, as well as the velocity change during the crash Δv.

Regarding the own vehicle, the external force exertion stresses the vehicle body and thus indirectly the occupants. Consequently, the crash pulse $a(t)$ and intrusion $s(t)$ are the major causalities for injuries. Mitigating the harm, the vehicle deformation takes energy from the compartment. Additionally, the restraint systems is constructed to distribute stress on the occupants over the crash time according to human load limits. Even though, the individual passenger might receive strong impacts. These are measured for example by the Head Injury Criterion (HIC) or Neck Injury Criterion (NIC) indicating the acceleration of the specific body region over a certain time interval. The same holds for other traffic participants, such as vulnerable road users (VRU). The only difference is most probably in the lack of proper crash protection. Further information on the human load limits need a deeper understanding in the field of biomechanics, e.g., presented in [138, sec. A19], [13, sec. 9.5], and [120, chap. 3].

The injury severity depends, additionally to force exertion and the restraint system, on the occupant related features, such as vitality, size, or gender, and the inner vehicle occupant position [137, p. 330]. The Abbreviated Injury Scale (AIS) is a commonly used measure to indicate and compare the medical severity level in the field of accident research [133, sec. 3.5] [138, chap. A19]. The AIS assesses the lethality of single injuries. The Maximum AIS (MAIS) represents these individual injuries of body regions or the person entire by their maximum value. Alternatively, the Injury Severity Score (ISS) aggregates the most severe traumas of three body regions quadratically.

Beyond, the long-term consequences might be expressed in monetary terms, such as vehicle damage cost and medical expenses, or human related characteristics, such as convalescence, probability of survival or lethality rate.

Summarising, there exist no all-in-one solution to express the harm of a collision. In fact, the application needs to determine the suitable severity measure. Due to automated driving with human traffic participants, the road user protection is the objective in this thesis following ethical guidelines (sec. 2.2.3). Therefore, it seems appropriate to take the injury severity as measure into account. However, the injury severities are very individual impeding an objective crash assessment and are very difficult, if possible at all, to predict with enough accuracy in real time. Furthermore, the chosen example application of this thesis base on the impact of the vehicle structure. It does not necessarily require any injury severity and can be expressed by the vehicle crash dynamics. Therefore, the technical accident severity is chosen in this thesis to represent the crash harm.

Exemplary, figure 2.3 shows the acceleration $a_{\mathrm{long}}(t)$ and velocity $v_{\mathrm{long}}(t)$ time course of a frontal vehicle-vehicle-crash in driving (longitudinal) direction and depicts common characteristic values with different biomechanic impact to the injury severity [13, sec. 9.5]. Here again, multiple characteristic values are possible to indicate the severity. Besides, the single vehicle dynamics $a(t)$, $v(t)$, and $s(t)$, are convertible or rather redundant and hence it seems reasonable to reduce the considerations. The restraint systems depends mainly on the deceleration and velocity. The deformation does not indicate the running out and possible multiple collisions. Hence, the intrusion is neglected with foresight to future developments. Furthermore, the acceleration signals will be noisy in the most cases. Therefore, the ego

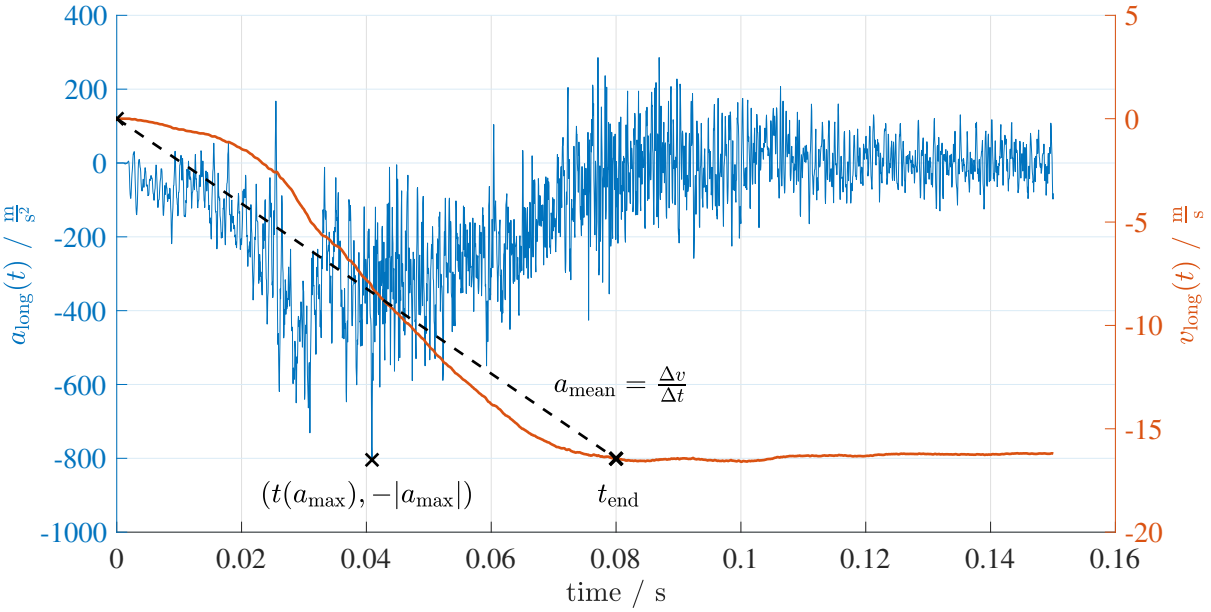

Figure 2.3: Crash kinematics - The figure shows the time course of example crash kinematics supplemented with common characteristic values, such as a_{max}, the maximum absolute acceleration, $t(a_{\text{max}})$, the time when the maximum acceleration occurs, a_{mean}, the average deceleration in $t \in [0, t_{\text{end}}]$ and the crash duration t_{end}. The ego vehicle with velocity $v_{\text{ego}} = 49\,\frac{\text{km}}{\text{h}}$ encounters a target vehicle with velocity $v_{\text{target}} = 53\,\frac{\text{km}}{\text{h}}$.

vehicle velocity change during the crash Δv_{ego}, indicating the crash as a whole and derived from the smoothing velocity curve, is chosen as characteristic value to quantify the technical accident severity ψ in this thesis. In general, it depicts the 2D instantaneous vectorial difference before and after impact [139]:

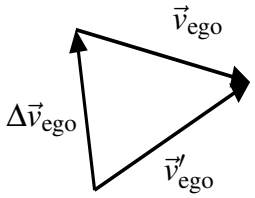

$$\psi = |\Delta\vec{v}_{\text{ego}}| = |\vec{v}'_{\text{ego}} - \vec{v}_{\text{ego}}| \tag{2.1}$$

In the case of rigid bodies, it should be noticed that the value of the velocity change Δv varies over the vehicle shape and thus a reference point or accumulating strategy needs to be specified. That has ethical issues as discussed in section 2.2.3. The final instantiation of the severity measure (equ. 2.1) is presented in section 4.1.2 and 4.1.3 for vehicle-pedestrian and vehicle-vehicle crashes, respectively.

Nevertheless, it needs to be mentioned that one single value is an rough approximation and in this case neglects important temporal features, such as maximum or mean deceleration [140]. On the other hand, this value has a long tradition with deep investigations and it has a strong correlation to injury probabilities [141]. Figure 2.4 shows injury risk functions based on the GIDAS database [142]. The probability of a certain MAIS level is related to

the recorded Δv by logistic regression. What is more, the Δv value is fast to predict due to the state transition and negligence of the time course (sec. 2.1.2.3).

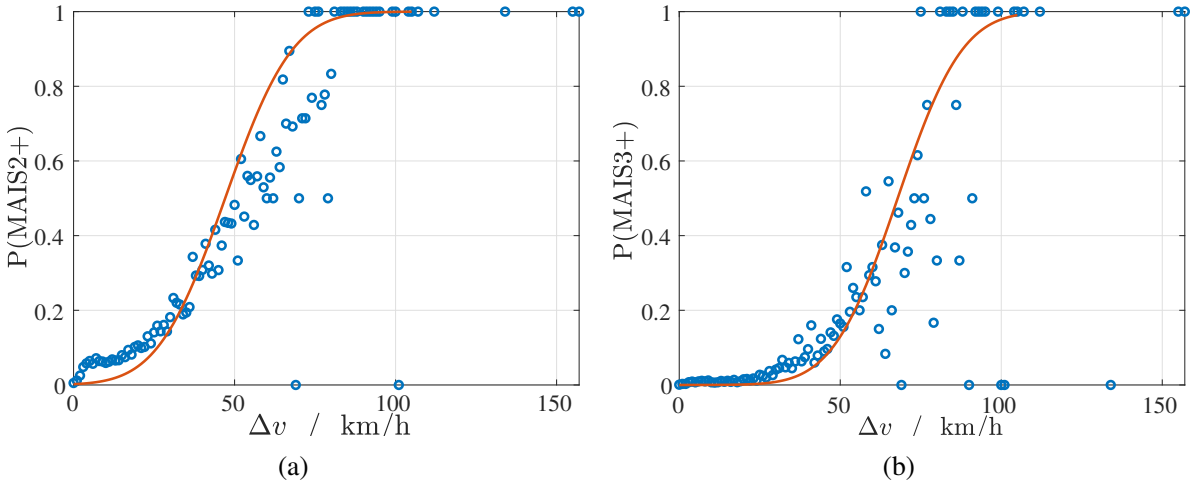

Figure 2.4: Injury risk function - The injury risk function correlates the probability of the MAIS-level to Δv. (a) correlates the probability of MAIS2 and higher and (b) correlates the probability of MAIS3 and higher. The logistic regression bases on data of [142].

2.1.2.2 Severity data bases

The technical accident severity is derived by models with partly rough approximations for real time applications (chap. 4). These simplifications needs to be verified by reference data. Fig. 2.2 sorts temporally the data collection by event recorders, retrospective accident investigation, crash tests with dummies and FEM simulations, both for vehicle structure and human injuries. Additionally, figure 2.5 gives an overview by example images. Each data collection method has a different scope of application.

The longest tradition has the retrospective accident investigation [133, chap. 3]. If an accident happens, the police records the accident due to legal issues. Depending on the country, the data are stored in national databases such as [3]. More detailed, dedicated investigators collect data, such as wheel traces, deformation or injury properties, up to several 100 parameters. These information are afterwards enhanced by reconstructing methods for deeper understandings and stored in in-depth accident databases, such as GIDAS [142] or NASS-CDS [145]. Besides, few approaches try to monitor the long-term consequences of accidents [146]. Finally, it is possible to correlate the parameters, derive relationships between impact severity and injury, as well as to assess the occupant protection. However, due to the retrospective data collection, the databases lack of detailed kinematic data. Moreover, inconsistencies appear due to the manual recordings and made assumptions, what requires a careful use of datasets [147].

Event recorders provide technical information related to the crash. However, due to the evolution of these systems, the obtained data vary over the years [148]. In early developments

(a) Picture bases on [143]

(b) Picture: [142]

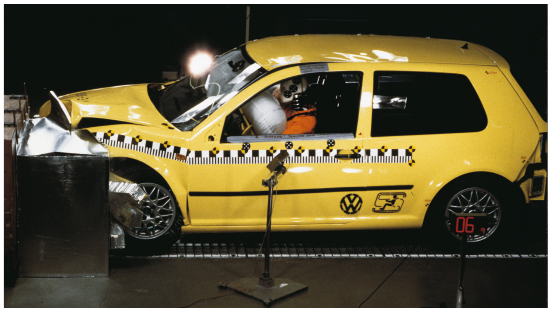

(c) Picture: [144]

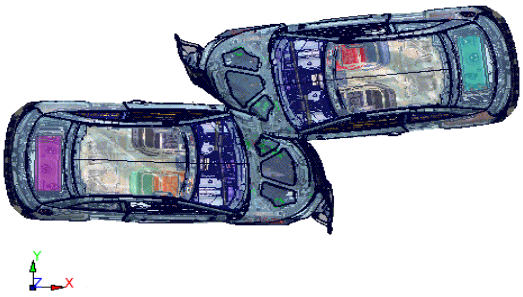

(d)

Figure 2.5: Overview reference databases - The figure shows exemplary the data collection for different reference databases, which might be used to evaluate the accident severity prediction. The subplots show a) the data transmitting of an event recorder crash-posteriori, b) a posteriori accident investigation, c) a crash test, and d) a FEM crash simulation in top view.

only binary signals are present, such as belt use or airbag deployment. Newer vehicles may provide more information, yet the market penetration and thus the occurrence in the accident data is limited. Besides, the most strength is seen in the combined automatic and manual recording, also enhancing the dataset with occupant related parameters.

Crash tests are used to gain detailed information to the crash behaviour. However, due to the massive costs only selected use cases are tested. Besides, the occupant load is measured with crash dummies being a model itself.

In contrast, FEM simulations provide detailed information about the technical crash sequence and, if considered mutually, detailed information about the occupant [149]. Moreover, the information are available for every knot of the vehicle without reconstructions giving a deep insight in deformation, kinematics and force exertions. On the other hand, also FEM models needs to be verified on real counterpart measures [150]. The structure and occupant simulation are often separated due to the field of application and available computation power. Detailed injury severities are obtained by simulations of FE human body models or FE dummy models and constitutes an own field of research out of scope for this thesis.

Summarising, FEM simulation results are regarded as ground truth in this thesis. That choice bases on the detailed time-based acceleration and velocity curves, data consistency,

availability, and variant diversity. Compared to the severity prediction models in sec. 4.2, FEM simulations are much more precise. Moreover, the used reference database include parameters, such as impact velocity, object types, impact position, which are varied systematically giving a deep insight without cross-influences as occurring in real world data. Section 4.3.1 presents further information to the used reference database.

2.1.2.3 Severity estimation

Accident severity calculations are investigated in several research areas. Thereby, the field of application is not necessarily the pre-crash severity prediction for integral safety functions as part of this thesis. Nevertheless, findings may be transferred to the current work and thus an overview of the major related research is given in the following. The main differences consist in the available input parameters, used models, and desired target values.

In the field of *accident reconstruction*, the detailed understanding of the accident sequence is important. Specialist books, such as [138] and [133], summarises the experience of the last decades. In general, the accident investigators inspect the accident scene post-crash and thus the available information are limited to the accident outcome, such as rest positions, wheel traces, deformations, and injuries. Optionally, further information are provided by witnesses or event recorders. However, if available at all, they are neither sufficient due to the lack of detailed information about the full accident process. Therefore, multiple reconstruction methods and practices have been established to derive the accident emergence and detailed crash sequence from the posteriori data. Thereby, physical models have a long tradition and thus great popularity [133, chap. 5]. Among others, the results are used to assign responsibilities of the accident event and thus clarify legal or actuarial issues. An other important application constitute the improvement of the traffic safety in general.

An other field for severity calculation is the *vehicle construction*. It reduces the costs and development time as well as increase the safety benefit generally if the vehicle crashworthiness is considered early in the development process [13, chap. 11]. Thereby, simulations are an important alternative to expensive crash tests. Contrary to the accident research, detailed information about the input parameters and the material characteristics are here available. Therefore, complex models, such as FEM, can be used to investigate the modules in detail [13, sec. 9.10]. However, the execution is in general very time-consuming and thus out of scope for the integral application of this work. Nevertheless, as mentioned in section 2.1.2.2, such detailed calculations are used as reference for more approximating severity estimations.

In the area of *integral vehicle safety*, the pre-crash estimation of the accident severity is used to enable an intelligent crash interaction (sec. 2.1.1). Thereby, the available time window amounts only few hundred milliseconds and thus demands for fast severity predictions most probably implying rough estimations. Furthermore, vehicles are nowadays only equipped with exteroceptive sensors to percept other road users. As result, input parameters for the crash prediction are limited or needs to be estimated from the available exteroceptive data

[100]. Among others, that includes the masses and material characteristics like stiffness of the accident opponent.

All in all, the crash severity calculations lead back to classical mechanics independent of the research area. Thereby, physical models and fundamentals are used to explain the object interactions. Consequently, such models are transparent and provide and high interpretability. Alternatively, approaches exit which represent previously calculated or measured input-output-relations by sole mathematical functions. Here, the physical transparency is not the most important objective. That data driven, mostly black box models base on statistical learning and test procedures. In a sense, the simplifying logistic regression used in injury risk functions is one example. However, also more detailed approaches exist to map various crash information. What is more, it needs to be distinguished between the opponent's object classification. For example, [133, sec. 3.7] and [138, chap. A10] evaluate throwing distances in pedestrian collisions. However, due to the vulnerability, this work focus solely on collision avoidance or mitigation by braking if pedestrians are involved. In other words, impact point localisations and corresponding severity estimations are only regarded in vehicle-vehicle crashes, as discussed in the remaining section and main part of chapter 4. Therefore, the selection of the related work focus in the following on the mapping (η) between the vehicle accident configuration ω_{coll} (*input*) and technical accident severity ψ (*output*): $\eta : \omega_{\text{coll}} \rightarrow \psi$. Thereby, this work separates with reference to the available test equipment (sec. 6.3) *input*, which is directly (sensors) or indirectly (established models, such as dynamic model) measureable while driving (e.g., pose $[x, y, \varphi]^{\text{T}}$, velocity v, yaw rate ω and vehicle dimensions $[l, w]$), and *paramters*, which are not measurealbe (e.g., restitution coefficient e, stiffness k) and thus require an independent determination strategy. According to the modelling of section 3.1 and section 4.1, the *input* in this work refers for the most part to the time-variant, dynamic vehicle states and the *parameters* comprise all other influences. Further explanations are presented in section 4.1.1. What is more, table 2.2 gives a summary to the presented approaches.

Impact models constitute a frequently used mechanical approach and have a long tradition due to the simplicity. Details on the impact theory, mechanical background and common used impact models in the field of crash severity estimation may be taken directly from dedicated specialist books or dedicated reviews, such as [133, chap. 4], [138, chap. A9], [151], and [152, sec. 30.2]. Therefore, only a short overview is given in the following. The underlying theory bases on the conservation of momentum. The discontinuous process represents a differential equation first order neglecting complex material laws of the continuous crash process. That loss of information needs to be filled with additional assumptions. This work follows the impact theory of Galilei, Huygens and Newton which focus on a state transitions as discussed in [133, sec. 4.4]. The main assumptions include an infinity small impact time, the domination of the impact forces to all other forces, the finiteness of the momentum, and the remaining of the kinematic as well as geometric configuration during the impact phase. Besides, the impact types are divided into straight and oblique impact, as well as centric and eccentric impact [133, sec. 4.4.1]. In general, the impact models are underdetermined and thus require further assumptions to solve the mathematical equations. According to [133, sec. 4.4.3], these hypotheses refer to the material elasticity, position and direction of the im-

Table 2.2: Overview severity prediction - The table summarises the severity prediction approaches of related work. On that basis, severity estimation methods (turquoise cell colour) are selected for further investigations in this thesis.

	Impact Model	**Multi-Body System**	**FEM Simulations**	**Mathematical predictors**
Description	Conservation of momentum; State transition: impact theory of Galilei, Huygens and Newton	Time continuous modelling; The circuit depends on multiple masses, their connectivity and connectivity type	In a sense, a very accurate multi-body system	Black box models, mathematical, statistical tuning (artificial intelligence)
Related work	[100] [133, chap. 4] [138, chap. A9] [151] [152, sec. 30.2] [153] [154] [155]	[100] [133, sec. 4.3, sec. 4.6] [138, sec. A9-7] [156] [157–159] [160] [161] [162][163]	[95]; general information for example in [13, sec. 9.10]	Feed forward neural network: [164, 165] [111–113] Recurrent neural network: [166] Random forest regression: [103–105] [111–113] Symbolic regression: [111, 112, 114]
Model complexity	State transition; Straight, oblique, centric and eccentric impact; Differential equation first order	Complexity depends on substructures; Multiple differential equations second order (force balance); Multidimensional interaction / connectivity increase complexity; Parameter resolution (lumped vs. depending parameter)	Many knots and connectivity properties leads to complex modelling	Scales with the model structure
Input (measureable)	Direct and indirect measureable values with reference to the available test equipment (sec. 6.3) and established models			
Parameter (non-measureable)	Elasticity, friction	Connectivity parameters of substructures (stiffnesses, damper coefficients etc.)	Detailed modelling requires special knowledge about the vehicle design	No physical parameters
Computing time	Assumed low due to state transition (no time course)	Depends on substructures; Assumed high	No real-time application (e.g., the used database in sec. 4.3.1 is generated by simulations with several hours computing time per accident case)	Scales with the model structure; Assumed low
Main disadvantages in application of related work	Small reference database (few data, few vehicle types); Focus on front-front crashes	Small reference database (few data, few vehicle types); Dedicated accident types (one dimensional, front crash)	*Curse of the dimensionality* when storing pre-calculated data due to the multi-dimensional *input* vector	Small reference database (few data, few vehicle types); Focus on front-front crashes; clinical reference database [105]
	↓	↓	↓	↓
Adoption in this thesis	Centric (sec. 4.2.2) and eccentric (sec. 4.2.1) impact model	Mass damper spring system in two directions combined with a dynamic model (sec. 4.2.3) according to [105]	Reference database with more than 6000 FEM simulations (sec. 4.3.1)	Feed forward neural network (sec. 4.2.4) and random forest regression model (sec. 4.2.5)

pact, and the sliding or non-sliding conditions including the friction parameter. Moreover, the problem formulation in the related work focus on planar objects.

This thesis adopts the centric and eccentric impact models. The centric impact model is used due to the overall simplicity and assumed real-time capability. However, it is not able to distinguish different collision configurations based on the impact position [153]. Therefore, the eccentric impact model is taken additionally into account. A main challenge in the application for the integral safety lies in the parameter identification, such as the determination of the restitution coefficient and the friction coefficient. Related work, such as [154], [155] or [100], tries to find quantitative values and parameter correlations data driven. For example, they found basic correlations between the restitution coefficient and the impact velocity as well as impact position. However, they focus solely on front-front crashes and it is not ensured that the results generalise. Rather it is expected that the usage in other collision types is not suitable. Similarly, this work adjusts the coefficient of restitution and friction data driven. Contrary to the related work, the FEM reference database (sec. 2.1.2.2, sec. 4.3.1) consists of various vehicle-vehicle-crashes with all accident types and multiple collision opponents. The final instantiations of the models are explained in section 4.2.1 and 4.2.2.

More detailed, multi-body systems display the accident sequence continuously. Here again, dedicated specialist books, such as [133, sec. 4.3, sec. 4.6] and [138, sec. A9-7], provide detailed information to the underlying mechanical theories. Basically, multiple differential equations second order express the force balance including reactive forces due to inertia, stiffness, and damping as well as external, active forces. Thereby, the modelling opportunities are tremendous. First of all, the number of bodies or rather masses, their connectivity and their connectivity type (spring, damper etc.) differ. Furthermore, the material characteristics leads to nonlinear parameters of stiffnesses and dampers in general what impedes analytical solutions of the differential equations in the most cases. However, simplifications, such as lumped parameters, might enable analytical solutions but restrict the models elsewhere. For example, [133, sec. 4.6] defines the ending point of the simulation t_{end} between one quarter and the halve of the first time period T by $t_{\text{end}} \in [\frac{T}{4}, \frac{T}{2}]$ to cut of the continuous oscillation of the model. The limits refer to the inelastic and elastic crash behaviour, respectively. Furthermore, related work, such as [156] and [100], indicate parameter dependencies on different crash configurations, such as impact velocity, impact point, or vehicle type. Therefore, analytical solutions with lumped parameters seem only suitable to represent the current investigated crash case without capability of generalisation. Thus, they are not investigated in this thesis. What is more, the modelling of the entire crash course include the free choice of technical severity measures posteriori.

Related work, such as [157–159] and [160], show that already simple circuits are able to map important crash characteristics. However, it should be noticed that these works focus on dedicated accident types. They focus mainly on one dimensional front-vehicle crashes. Moreover, the model parametrisation bases only on one or two real cash tests, respectively. At one hand, they use at least realistic reference values. On the other hand, as mentioned earlier, related work indicate the parameter dependencies on the crash configuration. Seeing

that, one or two crash tests seem not sufficient to cover the necessary parameter permutation and thus the application of the derived models is limited. The previous limitations hold for related work with deeper crash modelling as well. For example, [161], [162], and [163] use multi mass system, yet focus on front crashes and the reference data does not exceed three real crash tests.

Additionally, the one dimensional modelling neglects the other degrees of freedom which are also important in the most accident cases. Therefore, [105] presents an approach where a mass damper spring system is used in two directions and the resulting forces leads back to the vehicle motion based on a nonlinear double-track model. Since it is important to find a severity prediction function for all accident types including offsets, angles and side crashes, the last approach is adopted in this work. Further details on the instantiation are presented in section 4.2.3. Here again, the FEM database (sec. 2.1.2.2 and sec. 4.3.1) is used to derive the model parameters. What is more, also FEM simulations may count as very accurate multi-body system [138, sec. A9-8]. Due to the massive knots and connections almost arbitrary interactions are mapped and thus it is used as reference for all other approximating severity prediction functions in this work. However, it should be noticed, that also the FE models need to be validated by significant real crash tests.

Independent of any physical modelling, [164, 165] and [166] use neural networks to display the crash kinematics of front crashes. Unfortunately, only few data are used for the training and thus it is expected that the results hold only in these dedicated cases. By way of example, [164] use only one real reference crash test. Contrary, [165] and [166] enlarge the training database by FEM simulations but still the number lies below ten references. In conclusion, these results are seen more as an feasibility study rather than an usable severity predictor for integral safety applications.

In general, the usability of such statistical approaches bases crucially on the underlying reference data. Seeing that, [103, 104] generate large virtual databases, e.g., using the combination of a spring-mass-model and double-track-model. Afterwards they train a random forest regression model to provide the crash severity and its uncertainty in real-time. Even if the database is large and the approach seems promising, the results need to be questioned due to the quality of the references based on a one-dimensional, manual tuned spring-mass-model. Therefore, the approach is improved in [105] by generating the reference data with a complex two-dimensional mass-spring-damper system in combination with an double-track-model which parameters are tuned on the basis of about 1500 FEM simulations.

Similarly, [111–114] base the training on more than thousand FEM simulations with multiple crash opponents, relative velocities, impact positions, and impact angles. However, here again, the focus lies solely on vehicle front-front crashes what impedes the general integral approach. At one hand, a classifier is developed which assigns the accident constellation or rather expected technical accident severity to established crash tests. As result, safety measures can be chosen in accordance to the laboratory data. Furthermore, the points of a B-spline curve representing the crash velocity time course are learned and thus it is open to evaluate multiple severity measures posteriori. Thereby, [111] investigates differ-

ent classifiers and regression approaches. As result, random forests, neural networks, and symbol regression models are used as the most promising techniques.

Inspired by the previous works, this thesis investigates the usability of feedforward neural networks (sec. 4.2.4) and random forest regression models (sec. 4.2.5) for the integral approach. Thereby, more than 6000 thousand FEM simulations of vehicle-vehicle crashes with various different accident configurations are used as reference (sec. 4.3.1). Furthermore, the models are trained directly on the reference database to ensure the highest quality of the underlying crash process.

In conclusion, with respect to the various promising related work, it seems not necessary to develop new severity estimation methods. The objective implies rather the evaluation of the existing approaches related to the usability in the integral safety. Nevertheless, they needs to be instantiated and parametrised as explained in section 4.2. Besides, the reference database contains many more FEM simulations than used in the publications of related works. The final severity prediction function needs to transfer arbitrary accident configurations perceived by exteroceptive sensors to the Δv severity measure in real time. That contrasts to the most related work which focus solely on dedicated accident types without high requirements on the computation time. In other words, the prediction function used in this thesis needs to generalise widely, e.g., over multiple vehicle types and accident configurations, with reasonable quality, rather than to express the time-based crash sequence of dedicated accident cases in detail.

2.1.3 Risk assessment in the driving process

2.1.3.1 Uncertainty consideration

A major challenge in automated driving is the behaviour planning on uncertain information. The uncertainties are mainly obtained due to error prone environment perception, unknown motion of other road users, ego vehicle control performance and unknown static vehicle parameter [167, sec. 1.1] [168] [169, chap. 20]. Increasing the robustness of the driving function, they needs to be quantified and regarded appropriately. Table 2.3 presents an overview to the uncertainty sources and implications.

The performance of the environment perception depends on the used sensor equipment. Lidar, radar, and camera are widely used to detect other dynamic and static objects. Thereby, the perception uncertainty is divided in existence, object type classification and state uncertainty [169, chap. 20], while the focus in this work lies on the latter. That includes at one hand the state of movement, and on the other hand, parameters for the prediction of potential accident severity (sec. 4.2). The confidentiality on the object state varies, e.g., due to volatile weather conditions, light conditions, or malfunction of single sensors. Thereby, each sensor has its own operating point providing the information for sensor fusion, typically implemented by Bayes filters, such as the Kalman filter [169, chap. 20]. As result, the strengths of single sensors are combined. Additionally, the prediction of dynamic road users will always depend on a certain finite confidential level. The motion intention of other road

users is composed by the physic-based short-term prediction and the long-term prediction, which regards the infrastructure and assumes a certain degree to regulation conformance. Secondly, the forecast bases on uncertain initial states implying at least the same for future states or rather increased uncertainty due to prediction model inaccuracies. Furthermore, performing the planned trajectory is accompanied by certain control error. The consideration has particular importance in precarious emergency evasive manoeuvres driving up to the vehicle dynamic limits. Hence, [170] suggests to model this error stochastically. It may be added to the ego localisation uncertainty over the planning horizon.

What is more, while it is assumed that the new development, e.g., on sensors, on prediction algorithms or V2X-communication, will increase the performance dramatically, other objectives such as cost reduction might dominate, most probably having an opposite effect. Summarising, it is expected that also in the future uncertainties will be an important part of automated driving. Therefore, a robust driving function needs to be aware of such changing influences as discussed in previous publications, such as [171] and [26–28].

If uncertainties are considered, they are often modelled stochastically and considered either discrete (overapproximating bound as special case, used for example in [64] and [69]) or continuously. Exemplary, figure 2.7 sets discrete object intentions against the entire reachable set or an upper bound for the vehicles poses against a continuous, fading footprint. Thereby, it depends on the sensitivity and quantity to chose the appropriate modeling for each type (fig. 2.6). Only if the uncertainty has a high quantity and sensitivity, it is seems worth to regard it particularly. Otherwise, bounding according to enough confidentiality (continuous values) or the most likelihood (discrete values) seems a suitable approximation. In other words, the strategy related to each value depends on the significance. In addition, the sensitivity changes with the driving state or rather criticality phase and depends on the particular use case. Differences are especially obtained between regular driving and the emergency motion planning.

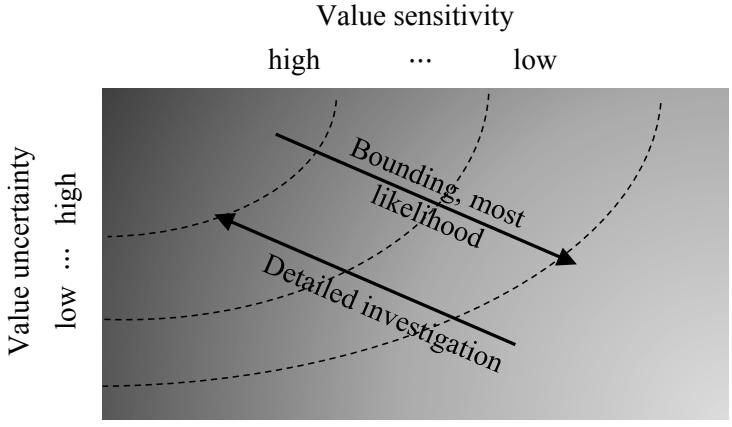

Figure 2.6: Uncertainty influence - The appropriate uncertainty modelling is found by ranking their quantity versus sensitivity.

By way of example, [172] suggests to react on the worst case scenario, referring to traffic motion prediction. However, figure 2.7(a) illustrates that such assumptions are not useful and prevent normal driving on common roads. It is traffic inherent, that due to crowded

roads and cramped infrastructure accidents are physically possible all the time. The example shows, if two cars encounter, each in the own dedicated lane, and one vehicle makes a mistake, an accident is unavoidable almost instantaneously. However, the worst case approximation seems in that example more justifiable for other uncertainty types. For instance, the measurement uncertainties are less significant compared to those of the prediction. While such rough approximations seems suitable in regular driving for the initial object states, detailed uncertainty consideration gain importance in sharp emergency manoeuvres (fig. 2.7(b)). Mainly the non-probabilistic motion planning uses the most likelihood indirectly (table 2.1). In contrast, other work as emphasised in table 2.1, consider uncertainties with continuous influence by probabilistic measures similar to this thesis. The detailed environment model considering uncertainties is derived in section 3.1.

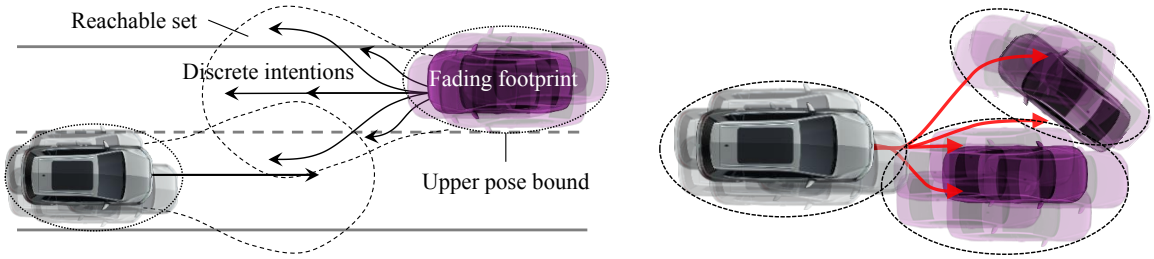

(a) Regular driving (b) Emergency manoeuvre

Figure 2.7: Uncertainty consideration - It shows exemplary the effect of worst case bounding of uncertainties.

Furthermore, uncertainties prevent a clear assignment of safety systems (sec. 2.1.1) to the criticality phase. That is crucial in emergency manoeuvres deciding between collision avoidance and collision mitigation not knowing the point of no return. At one hand, collision avoidance is preferred but may result in hazardous small overlap collisions. On the other hand, optimising the impact point accepts a crash from the beginning but comprises the chance of reduced severity. Related work approximates the point of no return by hard boundaries either in the positive or negative direction (fig. 2.8). For example, [51] calculates the time to react (TTR) denoting the remaining time according to the current trajectory until a collision free emergency manoeuvre can be guaranteed. In point of fact, all approaches calculating a *time to action* (TTX), such as time to brake (TTB) or time to steer (TTS) (e.g., [52], [53], [173]), try to find the last moment for collision avoidance, over-approximating the point of no return. In contrast, [54, 174] estimates explicit the moment which guarantees inevitable collision to trigger appropriate mitigation systems. Similar, the borders between regular driving and the necessity of emergency activities blur. Even though, the conflict of objective lies here between driving progress or rather driving comfort, and safety. Also the time horizon is much bigger compared to the emergency manoeuvres. In other words, over-approximations are widely accepted and are adjusted weighting false positives and false negatives. Here, an under-approximation would undermine the efforts to safety by aggressive driving and hence seems not suitable.

Table 2.3: Uncertainty sources - Overview of different uncertainty sources and their implications. The related work focus on regular driving, collision avoidance and collision mitigation. Besides, the sorting is not always straightforward and unambiguous, even though, it is tried to assign the related work with maximum purpose.

Uncertainty	Description	Source	Related Work
Localisation	Pose uncertainty of ego vehicle	Sensors, map, perception algorithms	[59, 60] [61] [64] [67] [74] [76] [82]
Existence	Uncertainty, if the sensor detected object really exist (tracking existence)	Sensors, perception and tracking algorithms	
	Possibility that dynamic objects appear from blind spots (occlusion)	Limited sensor performance	[87]
Object Classification	Uncertainty on the class assignment on dynamic objects (car, pedestrian, animal, etc.)	Sensors, perception algorithms	
State	Uncertain state of dynamics (pose, velocity, acceleration etc.)	Sensors, perception algorithms	[56, 57] [58] [59, 60] [61] [64] [66] [67] [74] [75] [76] [82] [83, 84] [85] [87]
	Uncertain sate of static parameters (length, width, etc.)	Sensors, perception algorithms	[103–105] [100–102] [96, 97]
Prediction	Behaviour intention of objects (constant velocity, deceleration, turn etc.)	General uncertain environement envolvement, arbitrary behaviour of objects, prediction algorithms	[59, 60] [68] [103–105] [74] [84] [87][88] [89]
	Uncertain future object states (giving one intention) due to propagation of initial uncertain states	General uncertain environement envolvement, arbitrary behaviour of objects, prediction algorithms, propagation model	[58] [59, 60] [61] [64] [66] [67] [82] [83] [87]
Control error	Uncertainty on the trajectory execution	Parameter uncertainty (friction, masses etc.), model inaccuracies	[74] [170]

This thesis models uncertainties explicit enabling a smooth transition between regular driving, collision avoidance and collision mitigation. Since the optimisation problem changes from regular driving to the pre-crash phase, a threshold based switching is used for safe driving (sec. 5.3). Besides, the emergency trajectories are not pre-selected and assessed mutually by one criticality measure to gain the greatest safety benefit in integral motion planning (chap. 3). Figure 2.8 illustrates the approach.

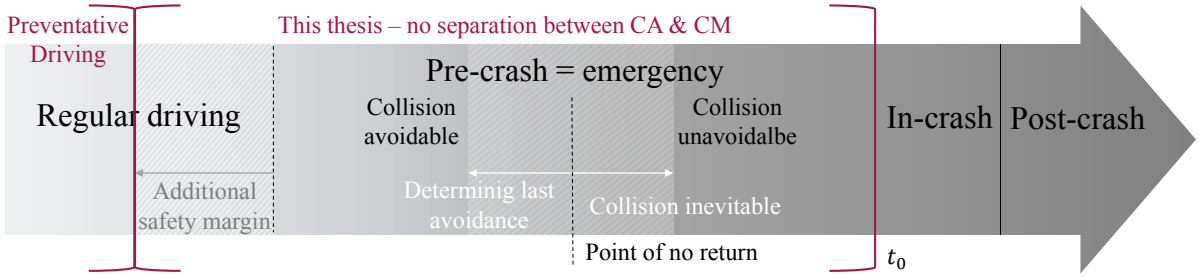

Figure 2.8: Uncertain point of no return - Related work over- and under-approximates the uncertain point of no return contrary to this thesis. The figure is a modification of figure 2.1.

2.1.3.2 Risk as a measure

Section 2.1.1 derives that the integral approach requires an overall measure for different systems. However, uncertainties (sec. 2.1.3.1) impede the correct calculation of the technical accident severity $\psi = \Delta v$ (sec. 2.1.2.1). Even though, well founded decisions are desired in safety critical applications. Confronted with the same challenge, other safety domains have established the risk measure to deal with that issue. By way of example, the risk is estimated in management processes [175], in the field of process control [176], (atomic) power plant technology [177], or other transportation systems such as railway or aerial vehicles [169, sec. 23.3]. Thereby, *risk* has a negative connotation related to uncertain harmful events. The opposite is referred as *chance* constituting a positive outcome, e.g., in the field of gambling. Mathematically, the risk complies to the expected value of the severity. That idea is further developed in section 3.2. Theoretically, the expected values can be calculated to every uncertain event and thus has infinity applications. Therefore, only important related topics are mentioned in the following.

In the automotive context, the ISO 26262 [178] customises the basic norm DIN EN 61508 [179] for functional safety. It defines *risk* as as the "combination of the probability of occurrence of harm and the severity of that harm" [178, def. 1.99]. Figure 2.9 illustrates the risk related terms. The objective is to identify potential risk by hazard analyses, to reduce the determined risk according to legal requirements by appropriate safety measures, and afterwards operating only a safe system. The term *safety* describes a state without unreasonable risk. Important to notice, most probably *residual risk* remains after applying the *safety measures*. It is system inherent to accept a certain level of risk. Thereby, single thresholds are solely definitions, representing the risk averseness of the society. That has ethical implications as discussed in section 2.2.3. Furthermore, that risk measure discipline bases on tremendous investigations and procedures, often specialised to dedicated subjects, to manage the risk appropriately. Therefore, the focus in the following lies on the risk based trajectory planning.

The ideas of the norms are adopted and transferred to the safety of automated driving in this thesis. The specific risk value of a vehicle behaviour related to the current traffic scene is regarded as safety measure. In other words, the potential harm or rather severity $\psi = \Delta v$ of

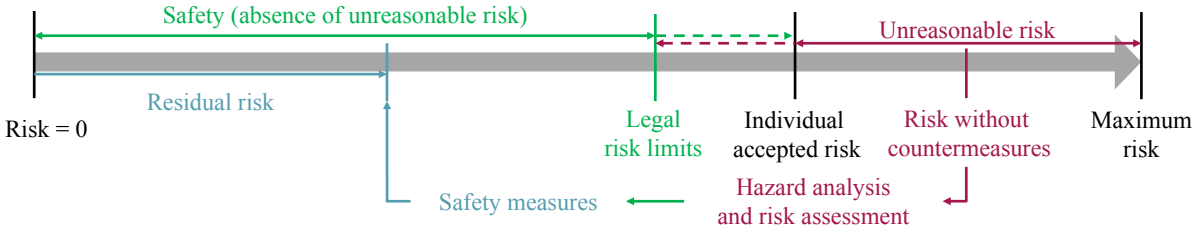

Figure 2.9: Safety terms - Illustration of safety terms according to ISO 26262 [178].

each trajectory is estimated and combined with the probability of occurrence to derive the optimal driving strategy. The probability regards the uncertainties presented in sec. 2.1.3.1. Besides, risk assessment and handling is an established procedure in administrative approval of technical applications. Consequently, the risk calculations to the driving function could prove the safety forward-looking due to *safety by design*. The idea implies that the severity is interpretable and thresholds could be defined by the legislature, such as maximal causalities and deadly injuries on driven distances. As result, major efforts to the vehicle release could be evaded (sec. 2.2.1). However, approximations, at least made in this thesis, impede this ideal deductive logic.

Furthermore, the risk term is widely used to indicate a certain criticality in the motion planning, i.e., how endangered the traffic participants are. However, previous definitions are not always clearly satisfied, also noted by [38] and [139]. By way of example, related work use the terms of *risk assessment*, *threat assessment*, and *hazard assessment* as synonyms for the *criticality assessment*. In this thesis, *criticality* denotes the general term, while *risk* indicates a probabilistic approach. Accordingly, table 2.4 sorts different narrower terms. For example, the *collision probability* denotes a *collision risk*, where the probability is indicated in relation to the *event "collision"*.

Table 2.4: Criticality terms - Frequent criticality terms of the literature in relation.

		Group	Probability	Severity
Criticality	**Classic**	Collision detection	Binary signal / non-probabilistic	Event "collision"
		Severity estimation	Binary signal / non-probabilistic	Crash severity, conflict severity
	Risk assessment	Colllision risk	Collision probability, collision likelihood, probability of conflict	Event "collision"
		Injury risk	Probability of injury	Injury
		Risk	Probability of occurrence (e.g., collision probability)	Accident severity

Safe trajectory planning and risk assessment is also required in other transportation domains. By way of example, the railway need one-dimensional and aerial vehicles three-dimensional directives [169, sec. 21.4.2]. Since these sectors provide more developments to automation, the question arise if strategies could be transferred. For example, similar to the automated

driving, certain approaches for collision avoidance are required. However, closer examinations show that the transport areas are designed very differently. Railways have separated sections to drive on solely. Collision avoidance between multiple trains is more or less a logistic problem [169, sec. 23.3]. Furthermore, due to the one-dimensional movement, if necessary, only deceleration seems to be an appropriate strategy to avoid or mitigate harm. The transport area for aerial vehicles is limited as well. It is built to avoid collisions largely, since every collision will result in fatalities. Besides, the transport area is not only organised to share the space with well known, limited object types, but also has large space compared to the automotive application. Thus, the risk minimisation in trajectory planning refers to the intention uncertainty of other traffic participants [180]. Additionally, remaining time to collision enables redundant control strategies with humans in the loops, such as triggering of emergency manoeuvres only with acknowledgements [181]. Summarising, the approaches of these transport sectors are hardly to transfer. The automotive context is one of the most complex domains due to the shared, crowded transport area, short time horizons to potential collisions and detailed intervention strategies including collision mitigation.

Related to safe driving, ATMS (e.g., [42], [43], [44], [45]) and strategic route planners (e.g., [46], [47], [48]), classified in table 2.1, derive the inherent risk of the traffic domain usage. The underlying idea is here the same. The harm, expressed by the event collision or causalities, is uncertain and therefore modelled stochastically by risk measures. In a sense, it refers to the residual risk of the traffic system as shown in figure 2.9. It is always present, also after applying certain safety measures, yet is tried to reduce to minimum. Contrary to the operational driving, environment features, such as daytime or light conditions, are regarded in a general manner for multiple traffic participants mutually. Even if changing weather conditions influence the perception performance and therefore are considered in the risk assessment of this thesis indirectly as well, the ATMS does not refer to individual quantities. Risk assessment or rather risk analyses in the field of accident research yields to similar objectives. Giving one example, the WHO [1, chap. 4] and European Union [11, sec. 4.1] demand for risk maps ranking the road infrastructure. Here, streets are assessed offline regarding the traffic as a whole. What is more, CN (table 2.1) estimate technical accident severities or injury risks for optimal rescue, yet use features available only after the accident occurrence. As result, the related investigations support the severity estimation but not the operational trajectory planning.

2.1.3.3 Criticality measures in automated driving functions

Well founded driving decisions require the quantification of safety consequences caused by single driving actions in relation to the current traffic scene. Vice versa, the criticality of single driving actions needs to be calculated. That way, each presented approach of table 2.1 estimates a criticality to deploy the assigned safety functions. An overview of these criticality measures is presented in the following with focus on automated driving. The evolutional order correlates with the structure of table 2.1 (rows) due to the fact, that the application determines the criticality measure. Thereby, *criticality* constitutes the general term to non-probabilistic (*classic*) and probabilistic (*risk based*) approaches as discussed

in section 2.1.3.2 and recapped in table 2.4. Related surveys are presented in [37] and [38]. While they focus on collision avoidance, this work emphasise the part of collision mitigation as [26]. Finally, requirements on the risk criticality measure for this thesis are derived.

Time-to-X-Metrics (TTX) are probably one of the best known criticality measures. Examples are given by the Time-to-collision (TTC) [49], Time-to-brake [52], Time-to-steer [51], and Time-to-react (TTR) [51]. Due to the time reference, they are often used in the assisted driving relating the outcome direct to human's reaction time. Calculating the potential collision in the future, the motion behaviour of other road participants are predicted. That is often done by rough simplifications, such as motion with constant velocity, yet is no prerequisite. At one hand, instances, such as the TTC, can be used in the trajectory planning by the understanding that the maximal TTC would gain the most safety when ranking different manoeuvres. On the other hand, they indicate only the time to the event but gives no further information about the severity and do not adapt to uncertainties.

A non-probabilistic collision check (*classic collision check*) is also usual in reward based approaches, which are often describing the usage of cost functions. By way of example, [69] and [72, 73] derive the driving decision in complex scenarios use case independent. Thereby, different aspects are considered as soft constraints and adjusted mutually. The optimal decision bases on the minimal cost, i.e. maximal reward. Other static and dynamic road users effect repulsively, contrary to the demands on locomotion and travel comfort.

The next evolution step is seen by TTX metrics, which consider uncertainties. For example, [56, 57] regards measurement uncertainties of dynamic obstacles' current state. [58] investigates the effect of measurement uncertainties in relation to the significance of TTX-metrics and propagates these uncertainties with a motion model. References such as [59, 60], [66], [67], and [74] take current and predicted state uncertainties into account and evaluate them in collision probabilities. Additionally, [59] links that probability to the time horizon by the Time-to-critical-collision-probability (TTCCP). As result, in addition to the time, a confidence is adjustable when tuning thresholds. What is more, according to table 2.4, the collision probability refers to the event "collision" and is designed for collision avoidance solely. It does not distinguish different collision configurations and thus is modelled too short for mitigation applications.

Advanced active vehicle safety (table 2.1 - G4) is aware of the possibility that collisions occur. In that case, it is tried to reduce the collision energy, either by deceleration or choosing of an appropriate collision opponent. Therefore, [82] and [83, 84] combine the collision probability with either the kinetic energy $E_{\text{kin}} = 0.5\,m\,v^2$, state related severity such as the relative velocity $v_{\text{rel}} = v_{\text{target}} - v_{\text{ego}}$, or momentum $p = m \cdot v$, in a risk based criticality measure. While it enables to differentiate multiple objects and favours deceleration in precarious scenarios, the impact point and collision angle is further on not resolved. With similar drawbacks, [93] and [94] map that rough technical severity to the probability of injury. Thus, the injury risk function weights the technical outcome on the injury significance in pedestrian protection scenarios.

Enhancing the previous properties, the collision angle is included by centric impact models, such as presented in [87], [88], and [89–91]. Assuming plastic impacts, the deformation

energy ΔT constitutes the severity. Nevertheless, the ego and objects are modelled as point mass and no impact position is distinguished by that risk measure.

The most advanced severity measure provide [95] and [99]. Reference [95] estimates the optimal point of impact based on intrusion maps according to FEM simulations. Thereby, the performance of that approach depends on the data points or rather crash resolution of the database. For example, multiple object types (size, masses etc.), crash constellations (side, rear collision etc.) and velocities needs to be considered in realistic automated driving, yet are currently neglected. In consequence, that would demand for tremendous FEM simulations and huge databases. Similarly, [99] uses a database for decision making due to the real-time challenge. Contrary to [95], it pre-calculates the severity Δv (velocity change during crash) with eccentric impact models. What is more, contrary to this thesis, both works do not consider any uncertainties in the trajectory planning. In addition, due to the high dimensionality of input parameters (sec. 2.1.2.3), the technical accident severity (sec. 2.1.2.1) is estimated while driving in this thesis. As result, a risk based criticality measure combines the severity Δv with the occurrence probability.

The criticality measure used in this thesis comprise features of the related work and thus has following requirements. The road infrastructure and other multiple road users' states needs to be considered. Apart from the obviously necessary relative distance, the dynamic is regarded to prevent Inevitable Collision States (ICS) [182, 183]. Even if in the current moment no collision occurs, the motion prediction may indicate conflicts. Related to other concepts, it describes the detecting and exceeding of the point of no return. Furthermore, it needs to regard the crash energy as well as the impact point and force direction. Especially, the collision angle and offset contribute to the accident severity. Besides, the criticality measure needs to work situational independent. Moreover, uncertainties (sec. 2.1.3.1, table 2.3) need to be taken into account for robust decision making. For example, collision avoidance and collision mitigation manoeuvres differ slightly when facing an imminent crash. On top of that, the criticality measure is especially important in critical scenarios. If collisions occur, it is very likely, that the adequate behaviour needs to be proven [130]. Consequently, its transparency, reproducibility and interpretability has high priority.

2.2 Operational motion planning

2.2.1 Performance of a driving function

2.2.1.1 Terms related to scenarios

Terms related to the scenario are not used unambiguous in the literature. Therefore, [184] presents an overview of related work and derives own definitions as a basis to stimulate further discussions. These definitions are adopted in this thesis with the objective to avoid confusing nomenclatures. The focus lies here on the vocabulary for the driving function evaluation.

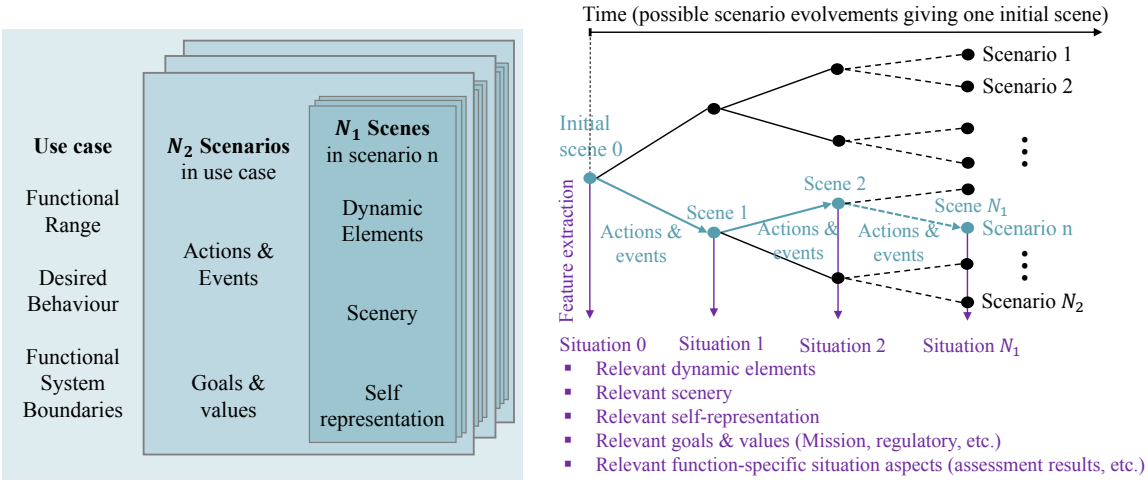

(a) Scenario terms (b) Scenario evolvement

Figure 2.10: Overview of scenario related terms - The illustration relates the terms *scene*, *situation*, *scenario*, and *use case* according to [184]. Subfigure (a) shows the aggregating components. Subfigure (b) emphasises the time relation between *scenes* (nodes), and *actions and events* (edges) as part of a *scenario*. The *situation* is illustrated as an extraction from the *scene*.

According to figure 2.10(a), *scene* describes the smallest entity. This snapshot (one moment) includes the scenery (e.g., environment setup, road graph, static objects), dynamic objects (e.g., states, parameters), and self representation of all actors and observers (e.g., states, attributes, field of view). Thereby only a scene from a simulation contains all information (objective scene, ground truth). In the real world a scene depends on the observers' points of view (subjective scene) and hence on reduced, incomplete information. A sequence of scenes (temporal evolvement) and their transitions due to *actions and events* designates a *scenario* (Fig. 2.10(a) and 2.10(b)). Additionally, *goals and values* (e.g., collision free driving) characterise the temporal evolvement. The *situation* refers to relevant features of a *scene* for the functional assessments and to specific aspects resulting from this assessment (e.g., results, derived vehicle reaction) as well as relevant *goals and values*. Furthermore, it indicates a particular point of time. Due to the process of extraction and augmentation, the *situation* is always a subjective pattern of the *scene* representing the view of dedicated functions.

The declarations are used in the performance evaluation of the automated vehicle. That involves the functional description of the system in *use cases* including the *functional range*, *desired behaviour*, *system boundaries* and several *scenarios*. Thereby, different test levels are distinguished. The *unit test* examines single components. The situation assessment is referred as *open-loop* test due to the disengagement from the *scenario*. It evaluates the driving function without feeding the derived vehicle response back for future *situations*. That procedure is for example used in section 6.4. The time-based interaction and thus *closed-loop* influence on future *scenes* as well as on future *situations* by the driving function is investigated in *scenario*-based testing (sec. 6.5 and 6.6)

Moreover, this work differentiates between *functional*, *logical* an *concrete scenarios* in the evaluation, as proposed by [185]. A *functional scenario* (FS) constitutes the most abstract scenario level. It describes a semantic formulation of a *scenario*, such as "overtaking in a congestion on a three lane highway". More detailed, *logical scenarios* (LS) provide information formally described to the physical state space range. Thereby, distributions and correlations may be assigned to these parameter ranges. Certain instances of the *logical scenarios* are designated as *concrete scenarios* (CS).

2.2.1.2 Evaluation and approval of an automated driving function

The administrative approval of automated driving functions has great challenges and hence is subject of current research. The main cause is seen in the shift of driving responsibility from the driver to the automated vehicle or rather to the provider of such systems [169, chap. 21] [186]. Due to the lack of recognised approval procedures and standards, the regulations vary widely from place to place. Moreover, the degree of accepted residual risk depends on the certain society as this includes ethical considerations (sec. 2.2.3). By way of example, [186] provides an overview of the Californian development on regulations. California, being one of the first places dealing with the issue of automated vehicles, has based the function release most importantly on individual permissions, selected and trained test drivers, and a large reporting system. What is more, the test procedure can be subdivided into system and component tests according to the V-model. Thereby, the following discussion refers to the final system release, additionally to previous component tests.

Two safety domains are most important. Firstly, the *functional safety* needs to ensure the correct system execution. Typically, the failure rates of single components are estimated, aggregated and afterwards the system is released with appropriate safety measures. Here, the procedure principles of the nowadays vehicle release seem also suitable for automated vehicles, even if they are expected to have significant more technology and connected equipment. Secondly, it is important to prove the *driving competency* of the automated system. The driving system needs to handle all possible scenarios, since no longer a driver fall back is available. Current ADAS are proven to be safe in specific test scenarios by trained test drivers [169, chap. 21.2]. In real driving environments, since every driver needs a driving licence, similar skills are assumed to users of ADAS and thus the ADAS is released. Besides, the driving responsibility remains at the driver all the time including the final vehicle control. In every driving stage, it is possible to overrule the ADAS. That procedure works no longer for automated systems due to the full-time driving responsibility. Consequently, a holistic approval procedure is required. Moreover, new drivers receive the license at a certain degree of skills assuming a continuous improvement by further driving experience [169, sec. 22.2]. In contrast, the performance of the automated vehicle remains constant. That holds at least for the basic functionality neglecting the part of "self-learning components" [169, sec. 22].

This thesis focus on the second part, the competency evaluation. It is obvious that not all possible, infinite scenarios can be tested. Therefore, the question arise which mileage is required to prove safety. The exact number varies in the literature, but simple estimations

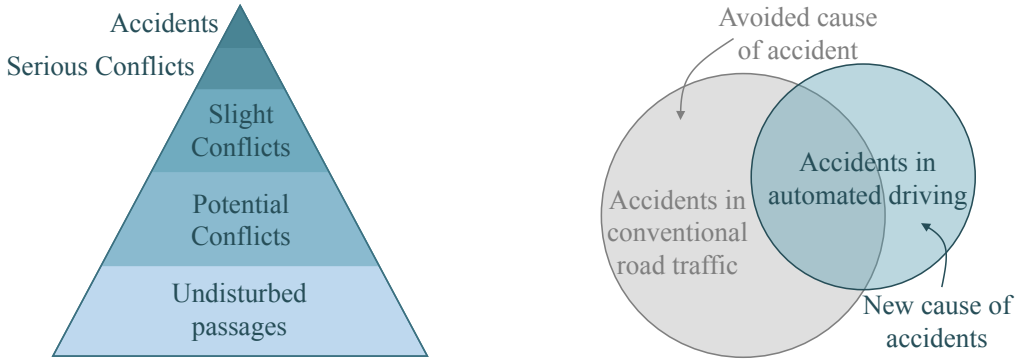

(a) Conflict pyramid [187] (b) Shift of accident causes

Figure 2.11: Dilemma on automated driving approval - The figure visualises qualitatively the massive mileage between two accidents (a) and the shift and rescale of accident causes due to the automation (b).

show that the distance would be huge. Figure 2.11(a) visualises the issue according to [187]. Due to the rare accident frequents, massive regular driving would be part of the approval. By way of example, [169, chap. 21.5.2] assumes that an automated vehicle should at least have the capability of human drivers. Due to approximately 3000 fatalities on 700 billion km driving distance in current German road traffic per year, and a 50 % confidentiality of all relevant scenarios, it concludes 2.1 billion test kilometres for automated vehicles. [186] calculates 380 test years based on USA databases. Moreover, [130] demands for 100 to 1000 times more capabilities of automated vehicles in relation to human drivers what increase the driving distance once again. It demands 10^9 driving hours or thirty billion miles. On top of that, every software update or change would need a repetition of the system release procedure. Besides, also virtual testing is not seen as solution due to the approval of the test environments itself. Summarising, safety proving by mileage seems not feasible.

An other, more promising approach is the scenario based testing. Thereby, it is assumed that the capability of a driving function may be proven by a finite, aggregated subset of driving scenarios. However, the selection of suitable scenarios and the proof for its significance is challenging as well. For example, previous accident databases are of limited use. Figure 2.11(b) shows the shift of scenario occurrence. Even if the automated systems will avoid many well-known accident causes, new incidents may occur, also referred as *automation risk*. On the other hand, some intersections will remain, e.g., due to the fault of third parties. Furthermore, the arising scenarios are currently not known due to the low mileage of automated driving systems. As result, the scenario mining in relation to the field of application of the automated function constitutes an own research area. For example, [188] propose an approach to generate lane change manoeuvres by a neural network trained on drone video data of German highways. More general, [189] investigates risk inducing attributes by odds ratio analyses based on accident data. These attributes are then used for scenario descriptions. [190] evaluates vehicle measured data by self-defined criticality measures to extract critical scenarios. Summarising, the approaches follow the idea to generalise the scenario description data driven to extend the available data with custom virtual enrichments. Con-

trary to the presented related work, the functionality proposed in this thesis focus on emergency manoeuvres including mitigation applications. Therefore, an own scenario set (sec. 6.2) is derived from GIDAS accident database [142], the Shanghai's *A Nice City* scenario catalogue [191], and systematical reasoning similar to [130]. They are used to evaluate the performance of the risk based trajectory planning.

What is more, the evaluation metric is an other impediment [169, chap. 21.7]. On one hand, in regular driving no accidents occur. As result other indicators are necessary to measure safety or criticality related to a certain driving behaviour. On the other hand, the risk based trajectory planning with impact point localisation results in conscious accidents. Due to the lack of absolute regulations, this thesis evaluates the integral approach relative to the state of the art. Exemplary, a reference planner is defined in section 2.2.2.3. Thereby, accident-related assessment criteria are used to rank both planning behaviours.

2.2.2 Driving function architecture

2.2.2.1 Architecture

Previous research has established a hierarchical planning approach, and hence hierarchical control loops, e.g., used in [192], [169, chap. 21.4.1], [69], [193], and [194]. The designation and functionality assignment is not used standardised, yet follows the overview of figure 2.12 largely. In comparison, the human driver performs all levels inherently. The highest level indicates the *strategical* planning. It transfers the user's driving request to a specific route or mission. Afterwards, the *tactical* behaviour planning segments the path and derives manoeuvres, such as "car following", "lane change", "stop at intersection", including traffic rules and preventative driving such as lane selection. The trajectory generation and optimisation is done in the *operational* planning. It derives the desired input values for the actuators. Finally, the *stabilisation* controls the vehicle to these input values. This work refers mainly to the third part, the *operational* trajectory planning, while the used planning approach, presented detailed in section 2.2.2.2, merges the two latter levels partly. At one hand, it seems suitable to simplify the trajectory optimisation by restriction to a certain manoeuvre category. On the other hand, a manoeuvre pre-selection impedes the search for holistic, optimal, smooth trajectory solutions.

The control loop of the driving function is presented in figure 2.13. It illustrates the *operational* level neglecting the cascading structure due to the focus of this thesis. Thereby, the order of single modules follows a general system view of automated driving. Hence, it is referred to specialised books as [32, chap. 50] or reviews as [194] for further information. Besides, the design and basic functionality of single modules have been condition to this thesis and are therefore out of scope to the contributions (sec. 1.3). However, they influence the obtained data in the evaluation part (chap. 6) quantitatively. It may be seen as one driving function example to illustrate the integral safety approach. Even if the modules partly condition each other, the basic idea of the risk based trajectory planning may be transferred to other driving function instances. Furthermore, clear interfaces abstract single modules.

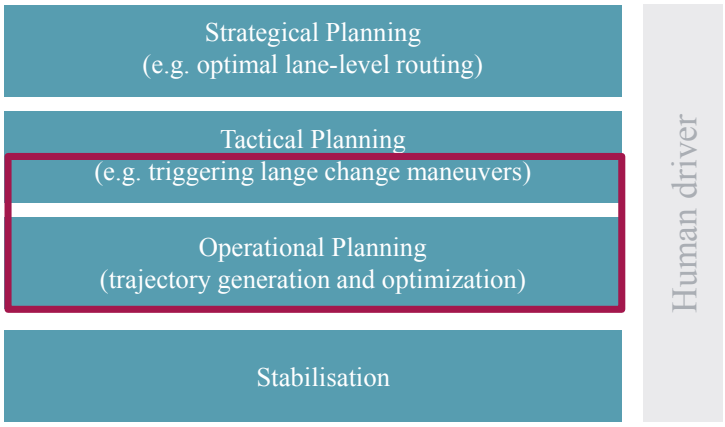

Figure 2.12: Hierarchical behaviour planning - This thesis focus on the operational motion planning (red frame). Thereby, the planning framework, presented in section 2.2.2.2, overlaps partly to the tactical level.

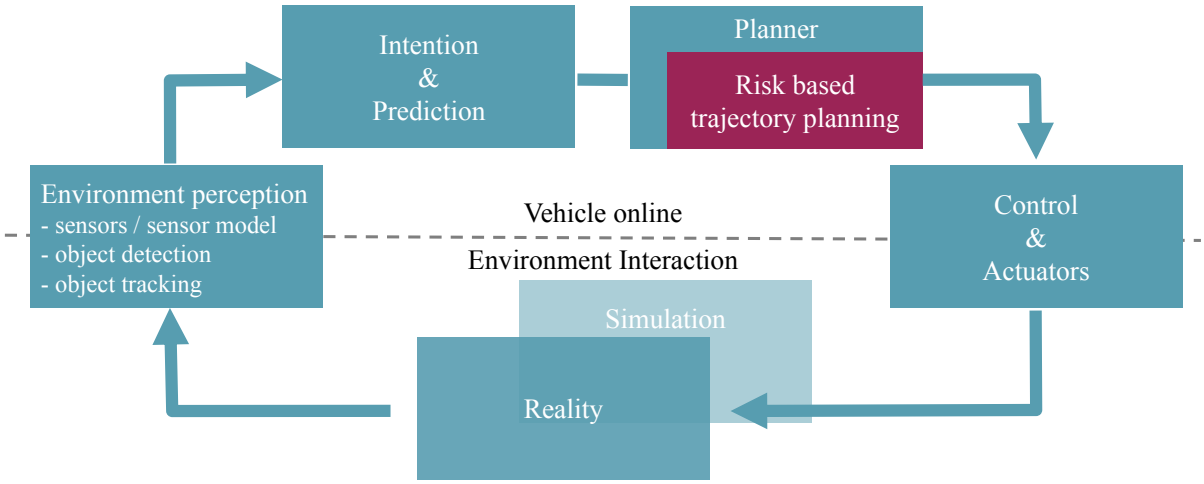

Figure 2.13: Driving function architecture - This thesis focus on the risk based trajectory planning (red) as part of the driving function.

The sensors percept the environment and provide its initial state for further processings. Multi-sensor fusion combines strength of different sensor types, such as lidar, radar, and camera. The object detection, classification, and tracking focus on dynamical obstacles (obstacles with the ability to move). Static obstacles are regarded by a grid representation due to a performance decision. It bases on the assumption that static objects are detected with high confidence due to multiple measures in time of stationary elements as well as the comparison with the deposited map representing the environment.

Due to the movement of dynamic objects, the future states needs to be predicted avoiding ICS [182, 183] when planning the vehicle behaviour. Thereby, the short-term prediction bases on the physical possible movements given the initial state, while long-term the infrastructure and object intention gain importance. Furthermore, the motion behaviour depends on the object type. As result, the current and future states are provided to derive the optimal

vehicle behaviour. Further information on motion prediction are gathered for example in the review [38].

The behaviour planning describes an optimisation process given all collected features about the environment (sec. 2.2.2.2). Thereby, the optimisation strategy bases on the environment representation and decisive use case. Due to situational independent automated driving, a global optimisation is favoured. The physical plausibility of trajectories is ensured by a vehicle model following the idea of model predictive control (MPC).

The behaviour of the ego vehicle and other road users interact in the reality. Therefore, the procedure is repeated periodically to react on unforeseeable incidents. As result, it seems appropriate to restrict the prediction length by a finite *moving horizon*. Optionally, the *reality* is simulated and exchanged by a *simulation environment*. That demands for modification of the perception and actuator module. Due to the perfect scenario understanding in simulation, the environment uncertainties and vehicle dynamic need to be emulated.

2.2.2.2 Planner

The desired trajectory is a solution of an optimisation problem. The combinations of problem formulation with objectives and constraints as well as the solving strategy are manifold. Finding the best optimisation method that fits to automated driving is an own research field. Hence, the overview about related planning approaches and the deployment to the automated driving is out of scope of this thesis. For further information it is referred to specialist books, such as [32], [167], and dedicated reviews, such as [40], [39], [41].

The following planning algorithm bases on [195] and [196]. It is also described with modifications in [197] using similar notations. The basic trajectory planning framework is seen as state of the art and thus is out of the scope to the contributions (sec. 1.3). Additionally to the basis version, this work implements the risk based motion planning illustrating the integral safety approach (fig. 2.13).

The modelling of the agent interaction with the environment bases on a Markov Decision Process (MDP) [167, part IV]. The algorithm contains of a 5-tupel $\{\mathcal{S}, \mathcal{A}, \mathcal{T}, \mathcal{R}e, \gamma\}$, where $\mathcal{S}$ indicates a finite set of states and $\mathcal{A}$ designates a finite amount of possible actions. A continuous action $a \in \mathcal{A}$ is integrated over the time t with the transition function $T(s,a,s') \in \mathcal{T}$ for all states $s, s' \in \mathcal{S}$, whereby s indicates the current state and s' indicates the subsequent, future state. The subset $\mathcal{A}_s$ indicates the set of actions possible in state s. The reward $Re(s,a,s') \in \mathcal{R}e$ is obtained immediate for the transitioning from s to s' with the action a. The linear combination of N_f features $f_n(s,a,s')$ and weights θ_n yields the reward $Re(s,a,s') = \sum_{n=1}^{N_f} -\theta_n f_n(s,a,s')$. The discount factor γ reduces the reward in time, yet is neglected in this work by $\gamma = 1$.

The main problem is to find a policy $\pi \in \Pi$ for the decision maker (trajectory planner). The desired solution constitutes the policy π^* with the optimal value:

$$\pi^* = \arg\max_{\pi} V^{\pi} \tag{2.2}$$

The function $\pi(s)$ specifics the action a in state s and hence derives a sequence of time-continuous transitions $\mathcal{T}(s,a,s')$. The value V^{π} of the policy π is obtained in the continuous form with:

$$V^{\pi} = \int_t \gamma_t Re^{\pi}(s_t, a_t, s'_{t+\mathrm{d}t})\,\mathrm{d}t \tag{2.3}$$

Due to the investigation of a finite set of actions a and discretisation of the time horizon TH, the selected policy π^s is an approximation to π^*. Thereby, three time discretisation levels (indices p, i, m) are used to reduce the computation effort as shown in figure 2.14. The generated actions $\mathcal{A}_s$ spans between s_{t_p} and $s_{t_{p+1}}$. The reward $Re(s,a,s')$ is evaluated once between s_{t_i} and $s_{t_{i+1}}$, and the motion of the ego vehicle as part of the transition $T(s,a,s')$ uses the time steps t_m.

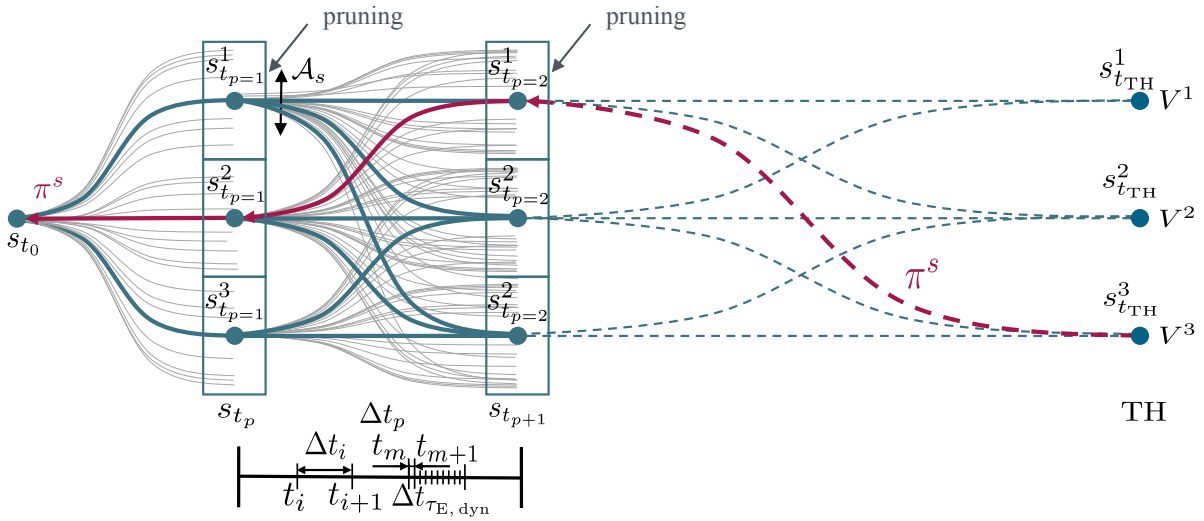

Figure 2.14: Trajectory planning framework - It shows the forward value iteration to find appropriate policies Π. The final trajectory π^s (red) is selected by backward stepping depending on the maximal reward indicated by the final value V.

More detailed, the algorithm 1 in pseudo code and figure 2.14 illustrate the planning process. The solution of the MDP is found in a way similar to *parallel breadth first search* and *forward value iteration*. Among others, [198] explains the procedure of *dynamic programming* detailed. The periodic replanning, as discussed in section 2.2.2.1 and visualised in figure 2.13, is divided into two steps, the *building of the graph* and *search of the graph*.

Firstly, the graph is build to compare different policies π based on the actions a. The planning starts at the current state, the initial state $s_{t_{p=0}}$. An exhaustive forward search of actions

Algorithm 1: Trajectory planner

Input: planning horizon TH, environment model M, reward $\mathcal{R}e$
Output: policies Π, selected trajectory π^s

function *generateTrajectory* $(\mathrm{TH}, M, \mathcal{R}e)$
  for t_p *in* TH **do**
    $\mathcal{S}_{t_p} \leftarrow$ get set of states
    forall $s \in \mathcal{S}_{t_p}$ **do**
      $\mathcal{A}_s \leftarrow$ sample set of actions
      forall $a \in \mathcal{A}_s$ **do**
        forward integration of action a
        observe resultant state s'
        observe resultant features $f(s,a,s')$
        $Re_p(s,a,s') \leftarrow \sum_{i=1\,|\,t_i \in [t_p, t_{p+1}]}^{N_i} \Delta t_i \sum_{n=1}^{N_f} -\theta_n f_{n,i}(s,a,s')$
        $V(s') \leftarrow V(s) + Re_p(s,a,s')$
    $\mathcal{S}_{t_{p+1}} \leftarrow$ prune $\mathcal{S}_{t_p}$
  $\Pi \leftarrow$ get policies in $\mathcal{S}, \mathcal{A}$
  $\pi^s \leftarrow$ select policy from Π according to $\pi^s = \arg\max_{\pi} V^{\pi}$
  return π^s

$a \in \mathcal{A}_s$ in each state s yields a set of policies Π. It describes indirectly certain vehicle behaviours, such as lane change, car following, or stopping. According to the MPC approach, the ego vehicle dynamic $\tau_{\mathrm{E,dyn}}$ and dynamic $\tau_{k,\mathrm{dyn}}$ of other objects o_k constrain the transition $T(s,a,s')$ to future states s'. The ego vehicle dynamic is integrated with the step size $\Delta t_{\tau_{\mathrm{E,dyn}}} = t_{m+1} - t_m$. Due to the use of a graphic processing unit (GPU) massive actions $a \in \mathcal{A}_s$ are evaluated parallely in one step between $s = s_{t_p}$ and $s' = s_{t_{p+1}}$. Nevertheless, a pruning is needed to limit the states $s_{t_{p+1}}$ for the next exhaustive forward search of actions a to $s_{t_{p+2}}$. Thereby, the actions $a \in \mathcal{A}_s$ are chosen according to a *dynamic window* due to the vehicle constraints based on the *circle of friction* [199, sec. 7.3.8]. Furthermore, they constitute a continuous function of fifth and third order for the longitudinal velocity profiles and lateral wheel angles, respectively. The environment model M is used to derive $N_{\mathrm{inst}} = \sum_{p=1}^{N_p} N_{i,p}$ sets of instantaneous features $f_{t_i}(s,a,s')$ to calculate the instantaneous reward $Re_{t_i}(s,a,s')$ and value $V(s)$. The reward $Re_{t_i}(s,a,s')$ is scaled with the time interval $\Delta t_i = t_i - t_{i-1}$. The pruning bases on the current value $V(s)$ avoiding redundant states s_{t_p} and increasing the diversity of policies $\pi \in \Pi$. That procedure is repeated until the planning horizon $\mathrm{TH} = \sum_{p=1}^{N_p} \Delta t_p$ with $\Delta t_p = t_{p+1} - t_p$ is reached.

Secondly, the graph is evaluated. The maximal cumulative reward $V^{\pi^s} = \max\{V^{\pi}(s_{t=\mathrm{TH}})\}$ with $V^{\pi}(s_{t=\mathrm{TH}}) = \sum_{p=1}^{N_p} Re_p^{\pi}(s,a,s')$ determines the driving policy π^s. Thereby, the sequence of actions a are derived by backstepping the directed connected graph of optimal

sub-solutions. The underlying, theoretical background bases on the Bellman's principle of optimality [131, 200].

While physical feasibility of the trajectory is obtained by *hard constraints* (e.g., motion model $\tau_{\mathrm{E,dyn}}$) to the transition functions $\mathcal{T}(s,a,s')$ (sec. 5.1), the risk assessment (chap. 3) is integrated by a repulsive feature R_f working as *soft constraint* in the reward functions $\mathcal{R}e$ (sec. 5.2).

2.2.2.3 Reference planner

The driving performance of the risk based trajectory planner is evaluated relatively to related work. Thereby, an Automatic Emergency Braking (AEB) is chosen as reference, based on a TTC criticality measure (sec. 2.1.1 and 2.1.3.3). The basic planning approach follows the framework presented in section 2.2.2.2. In contrast, the procedure is extended by an extra examination of the selected policy π^s. The modified algorithm is presented in algorithm 2.

Algorithm 2: Reference trajectory planner

Input: planning horizon TH, environment model M, reward $\mathcal{R}e$
Output: policies Π, selected trajectory π^s

function *generateTrajectory* $(\mathrm{TH}, M, \mathcal{R}e)$
  for t_p *in* TH **do**
    $\mathcal{S}_{t_p} \leftarrow$ get set of states
    forall $s \in \mathcal{S}_{t_p}$ **do**
      $\mathcal{A}_s \leftarrow$ sample set of actions
      forall $a \in \mathcal{A}_s$ **do**
        forward integration of action a
        observe resultant state s'
        observe resultant features $f(s,a,s')$
        $Re_p(s,a,s') \leftarrow \sum_{i=1\,|\,t_i\in[t_p,t_{p+1}]}^{N_i} \Delta t_i \sum_{n=1}^{N_f} -\theta_n f_{n,i}(s,a,s')$
        $V(s') \leftarrow V(s) + Re_p(s,a,s')$
    $\mathcal{S}_{t_{p+1}} \leftarrow$ prune $\mathcal{S}_{t_p}$
  $\Pi \leftarrow$ get policies in $\mathcal{S}, \mathcal{A}$
  $\pi^s \leftarrow$ select policy from Π according to $\pi^s = \arg\max_{\pi} V^{\pi}$
  if $\mathrm{TTC}(\pi^s) < t_{\mathrm{threshold}}$ **then**
    $\pi^s \leftarrow$ emergency brake
  return π^s

What is more, the risk assessment is already applied in the reference planner for regular driving. That decision bases on the following circumstances. In a simplified manner, the risk is referenced as state of the art (sec. 2.1.3.3). Approaches exist which deal with risk

measures even if they consider only rough severity measures and predictions. Following these examples, the relative velocity $\psi = v_{\text{rel}}$ before the impact is chosen as severity measure. However, the severity measure is expected to have a minor impact due to the AEB. In other words, the risk measure is only required in regular driving while here the severity has a minor impact compared to the collision probability. When the severity gains importance in critical situations, the AEB overrules the driving process. As result, the collision probability dominates the process with slight influences of a severity measure.

2.2.3 Ethical issues

In automated driving the monitoring task and thus the driving responsibility is transferred to the automated vehicle. Therefore, it is necessary to ensure a reasonable vehicle behaviour in all driving stages. The properties of the driving functions are directly adjusted by the development engineers. That leads necessarily to the discussion in the development process what a reasonable vehicle behaviour means and how the systems should be designed [169, chap. 4]. Hence, this topic is addressed briefly as preliminary for mitigation applications while deeper analyses are out of scope of this thesis. The manifold opportunities to act imply different consequences to human traffic participants, animals and material goods. Moreover, the outcome differs especially in critical scenarios. Thereby, the answer to appropriate vehicle behaviour is not given easily due to the ethical repercussions. The opinions vary, e.g., on the cultural background, context, and individual emotions [201]. As result, societies are encouraged to find acceptable answers to the automated driving as it is done for every new emerging technology in general. Consequently, the regulations may differ around the globe.

In the FRG an ethic commission was summoned to find recommendations for the automated driving and for the responsible legislator [202]. The derived, overall message includes that the focus lies on increased safety including the prioritisation of human road users protection to all other utilitarian considerations. Even if it seems to be a simple maxim, dilemma scenarios might occur with unclear requirements. For example, the question arise whether it is suitable to weight the number of injuries and fatalities, to involve third-parties to accidents, or to be obligated to mitigate the consequences of others misbehave. In conclusion, this work applies the recommendations of the ethics commission as far as possible. Besides, the driving function is customised mainly by the reward function. Hence, the final parametrisation may be adjusted on changing ethical principles and regulations at a later time [169, chap. 5].

Seeing that also automated vehicles will encounter accidents, the ethics commission requests a positive balance of risks in total. These part is directly addressed by the risk based trajectory planning in this thesis. However, even if the risk assessment has a long tradition related to safety issues in general (sec. 2.1.3.2), the relying on the expected value has ethical impacts itself. For example, it is often questioned if upper limits to the severity are necessary even if the risk is low due to the probability of occurrence, as well as how the legal risk limit (fig. 2.9) should be determined. A positive risk balance includes that certain vehicle interventions may increase the negative consequences in singular cases. However,

(a) (b)

Figure 2.15: Ethical impact on severity measure - The subfigures show the definitions used in this work: (a) ego vehicle protection in vehicle-vehicle crashes (b) occupant protection represented by the point *tunnel middle* TM.

it may be noticed that automated vehicles are acting all the time, also in critical scenarios. Consequently, triggering an emergency braking might also be seen as a conscious decision. In a sense, it means targeting with a particular braking trajectory even if uncertainties most probably would impede a clear crash severity prediction and selection of impact point. In other words, partly increased accident severity in individual cases is opposed to neglecting the safety benefit of impact point optimisation in general. In the end, the risk balance has to ensure that the advantages dominates. Similar argumentation is applied to dilemma scenarios when choosing between multiple targets, such as in the trolley example [169, sec. 4.2.4]. What is more, the "Safe System Approach" and related considerations as presented in section 1.1 unfold its potential only by intelligent safety measures on all stages.

Encountering or rather committing an accident with other road users leads to the weighting of the ego vehicle's occupant safety and target protection. Exemplary, this work priorities the ego vehicle in vehicle-vehicle-crashes. Hence, the driving function bases its decision on the ego vehicle accident severity (fig. 2.15(a)) except for crashes with vulnerable road users (VRU). Here, the target protection is prioritised. What is more, also the severity aggregation causes ethical discussions. The severity distribution varies on different positions in the vehicle. By way of example, the force exertion to the driver and passengers diverges. Therefore, this work defines the point *tunnel middle* TM as reference (fig. 2.15(b)).

The definitions are applied without the loss of generality. They are seen as one example implementation. Changing regulations and maxims can easily be applied since the severities of all collision opponents are calculated and weighted afterwards. Besides, that strategy of exemplary implementation is required due to the lack of regulations correlating with the unspecified administrative approval strategy (sec. 2.2.1.2).

3 Risk assessment

3.1 Environment model

The following descriptions refer directly to section 2.2.1.1 and 2.2.2.2, and extends the modelling with focus on the risk assessment. Figure 3.3 summarises the decomposition of the environment model M showing the linkage between different sections. Figure 3.1 illustrates the modelling for the criticality estimation according to equation 3.2 including the issues of normal distributions, instantaneous time steps t_i, multiple objects o_k, multiple object intentions h_k^j, classification x_c, existence, and the substate model. It refers to one planning procedure according to section 2.2.2. The detailed explanations are presented in the following. Besides, following notation should be noticed to understand the modelling correctly. A parallel evolvement of equations and nomenclatures is indicated by a slash "/". For example, $a_{b/c}$ indicates two terms a_b and a_c. Contrary, intersecting properties are emphasised by a comma. Giving an example, $a_{b,c}$ describes variable a with intersecting properties b and c.

The environment model M includes the features $f_{\text{crit}}(s,a,s')$ stochastically. The features $f_{\text{crit}}(s,a,s')$ are a subset of all features $f(s,a,s')$ required for the criticality estimation. Thereby, the regarded uncertainties base on the listing presented in section 2.1.3.1. The features $f_{\text{crit}}(s,a,s')$ are modelled jointly normal distributed according to previous modules dealing with that uncertainty representation (sec. 2.2.2.1). Apart from the specification due to the architecture, established calculation methods for normal distributions enable a fast criticality estimation for real time applications (sec. 3.3). By way of example, related approaches dealing with grid-based or sample-based representations of the dynamic environment are not regarded suitable. At one hand, the accuracy depends directly on the discretisation or number of samples leading to high computation time consumption for appropriate resolutions. On the other hand, the severity prediction requires the object assignment at all stages, what is lost by the grid and sample representation.

The initial dynamic state $\boldsymbol{z}_{\text{E,dyn}}$ of the ego vehicle E and the initial dynamic states $\boldsymbol{z}_{k,\text{dyn}}$ of the objects $o_k \in \mathcal{O}$ with count $N_O = |\mathcal{O}|$ are described by the normal distributed random vectors $\boldsymbol{Z}_{\text{E}/k,\text{dyn}} : \Omega^{\text{dyn}} \rightarrow \mathbb{R}^{n_{\text{E}/k,\text{dyn}}}$ with $\boldsymbol{Z}_{\text{E}/k,\text{dyn}} \sim \mathcal{N}\left(\boldsymbol{\mu}_{\text{E}/k,\text{dyn}}, \boldsymbol{\Sigma}_{\text{E}/k,\text{dyn}}\right)$ and their sample space Ω^{dyn}. The state $\boldsymbol{z}_{\text{E,dyn}}$ of the ego vehicle correlates with the used dynamic model $\tau_{\text{E,dyn}}$ for MPC calculations (sec. 5.1). The state $\boldsymbol{z}_{\text{E,dyn}} = [x_{\text{E}}, y_{\text{E}}, \varphi_{\text{E}}, v_{\text{E,long}}, v_{\text{E,lat}}, \omega_{\text{E}}]^{\text{T}}$ includes the position in x_{E} and y_{E} direction, yaw angle φ_{E}, longitudinal $v_{\text{E,long}}$ and lateral velocity $v_{\text{E,lat}}$, as well as the yaw rate ω_{E}. Without the loss of generality, independent of the criticality estimation procedure, the dynamic model $\tau_{\text{E,dyn}}$ is allowed to vary between simple (e.g., kinematic models) or more precise models (e.g., nonlinear double-track model) as long as the state $\boldsymbol{z}_{\text{E,dyn}}$ provides the required features for criticality estimation or rather motion planning in general. Model examples are presented in [199, chap. 10, 11]. The state $\boldsymbol{z}_{k,\text{dyn}}$ of other objects o_k correlates with the dynamic model $\tau_{k,\text{dyn}}$. Here again, without the

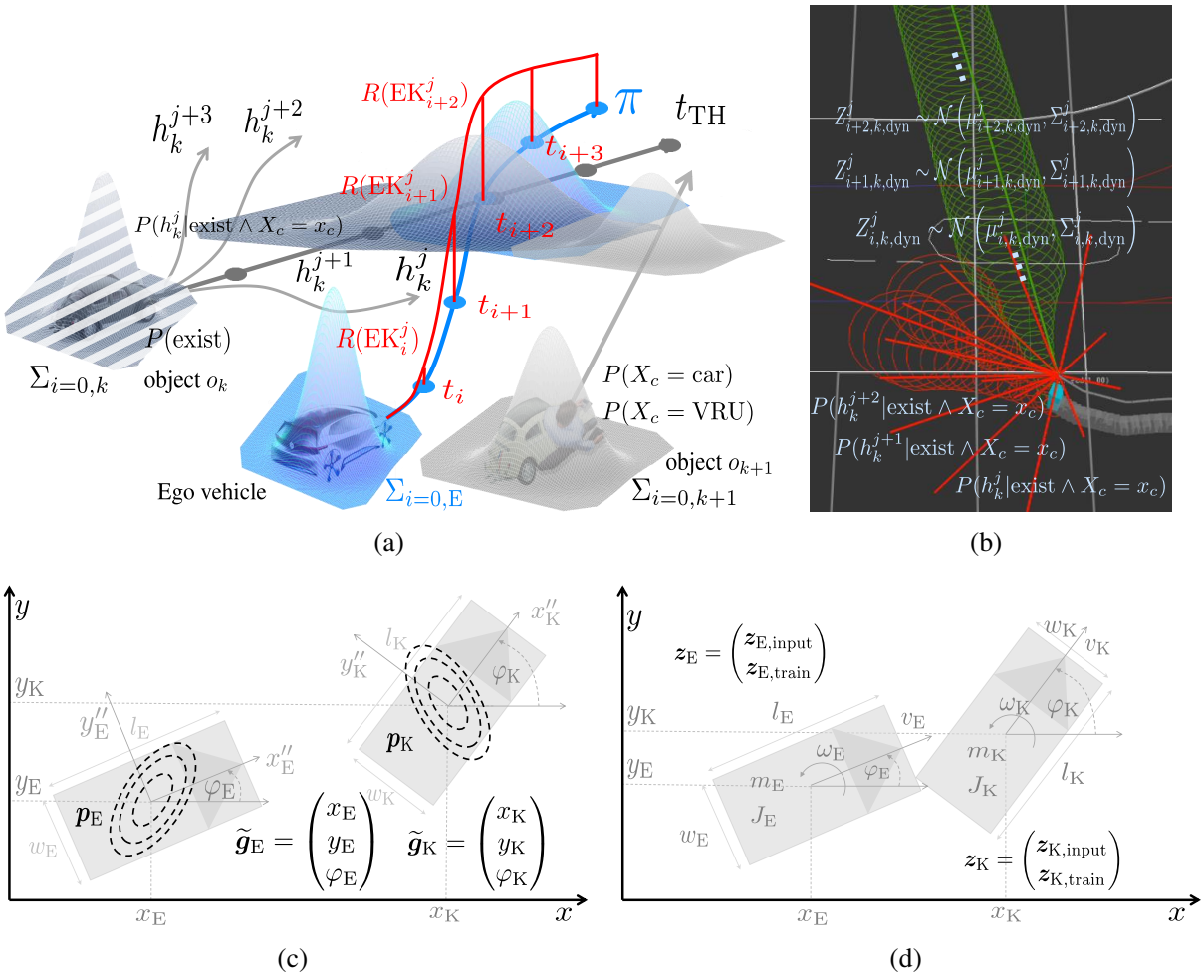

Figure 3.1: Modelling for the criticality estimation - (a) illustrates the modelling for the criticality estimation over the planning horizon TH with focus on the discrete variables, such as instantaneous time steps t_i, multiple objects o_k, multiple object intentions h_k^j, classification x_c, and event of existence. It refers to equation 3.2. Furthermore, the initial pose uncertainties $\boldsymbol{\Sigma}_{i=0}$ (Gaussians) are propagated to future time steps. (b) shows a pedestrian crossing a road in the simulation environment introduced in section 6.3. It shows the intentions h_k as solid line with increasing covariance ellipses due to the uncertainty propagation. Every covariance ellipse belongs to a substate $\boldsymbol{Z}_{i,k}^j$. The color gradient indicates the probability of occurrence on the presumed intentions (green = most likely, red = unlikely). (c) The environment model M is divided into multiple substates $\boldsymbol{Z}_{\mathrm{EK}}$. A substate $\boldsymbol{Z}_{\mathrm{EK}}$ consists of the ego vehicle and one object o_k and their random vectors $\boldsymbol{Z}_{\mathrm{E}}$ and $\boldsymbol{Z}_{\mathrm{K}}$, respectively. Besides, it refers to one single marker of subfigure (a). (d) shows an sample $\boldsymbol{z}_{\mathrm{EK}} \in \boldsymbol{Z}_{\mathrm{EK}}$ of the normal distributed substate $\boldsymbol{Z}_{\mathrm{EK}}$. It is an accident configuration ω_{coll} with a selection of features for the severity prediction η.

loss of generality, the state $\boldsymbol{z}_{k,\mathrm{dyn}} = [x_k, y_k, \varphi_k, v_k, \omega_k]^{\mathrm{T}}$ includes exemplary the position x_k and y_k, yaw angle φ_k, velocity v_k, and yaw rate ω_k as required for the criticality estimation. As the label suggests, the quantitative values of the states $\boldsymbol{Z}_{\mathrm{E}/k,\mathrm{dyn}}$ are time variant (dynamic) over the prediction horizon TH.

The reachable set $\mathcal{H}_k$ of object o_k is discretised in N_H finite exclusive intentions $h_k^j \in \mathcal{H}_k$ with the probability of occurrence $p(h_k^j)$ and the relationship $\sum_{j=1}^{N_H} p(h_k^j) = 1$. Thereby, the resulting mixture of gaussians is able to represent an arbitrary multimodal environment evolvement (fig. 3.1(b)). Apart from the most likely intention, the multiple-intention approach considers also less probable intentions, but in this case with possibly enhanced harm and therefore important criticality influences. Each intention h_k^j contains $N_{\text{inst}} = \sum_{p=1}^{N_p} N_{i,p}$ instantaneous states $\boldsymbol{z}_{i,k,\text{dyn}}^j$ according to the MDP (sec. 2.2.2.2).

The dynamic model $\tau_{k,\text{dyn}}$ depends on the detected object class x_c. Therefore, the discrete random variable X_c maps the example classifications $x_c \in \{\text{vehilce, bicycle, pedestrian, animal}\}$ with count N_C to the classification probability $P(X_c = x_c)$. Additionally, the probability of existence $P(\text{exist})$ indicates if a detected object really exists. Both, the classification and perception existence probability is provided by the perception module and its algorithms. Contrary, the probability of existence related to occlusions is based on the scene understanding. It might be addressed by virtual objects according to not observable areas as presented for example in [203–205].

A detailed description of the object prediction is out of scope of this thesis. The inputs for the motion planning are given via interfaces from previous modules (sec. 2.2.2.1). Nevertheless, giving a short overview, a gaussian uncertainty propagation through an object class inherent motion model $\tau_{k,\text{dyn}}$ processes the initial uncertainty $\boldsymbol{\Sigma}_{i=0,k,\text{dyn}}$ to future time steps t_i while the probability $p(h_k^j)$ is estimated by a Bayes filter according to the object's current behaviour. Similar, the prediction of the ego vehicle control error bases on linear uncertainty propagation through the feedback loop [170]. The localisation uncertainty is simply duplicated to future states $\boldsymbol{z}_{i+1,\text{E,dyn}}$.

Moreover, static ego vehicle features $\boldsymbol{z}_{\text{E,stat}}$ and static object features $\boldsymbol{z}_{k,\text{stat}}$ are modelled normal distributed as well: $\boldsymbol{Z}_{k,\text{stat}} : \Omega^{\text{stat}} \rightarrow \mathbb{R}^n$ with $\boldsymbol{Z}_{k,\text{stat}} \sim \mathcal{N}\left(\boldsymbol{\mu}_{\boldsymbol{Z}_{k,\text{stat}}}, \boldsymbol{\Sigma}_{\boldsymbol{Z}_{k,\text{stat}}}\right)$. Thereby, the parameter set depends on the used severity prediction model η. In general it follows the form $\boldsymbol{z}_{\text{E/k,stat}} = [l_{\text{E}/k}, w_{\text{E}/k}, \boldsymbol{M}_{\text{E}/k}, \xi_{\text{E}/k}^1, ..., \xi_{\text{E}/k}^n]^{\text{T}}$. By way of example, that includes the ego vehicle length l_{E}, width w_{E}, and masses $\boldsymbol{M}_{\text{E}}$. The vector $\boldsymbol{\xi}_{\text{E}/k}$ contains the additional features required by the prediction model η. In contrast to the dynamic features, as the designation indicates, the quantitative values are time invariant (static) over the prediction horizon TH.

The criticality estimation relies on geometric features, such as $\boldsymbol{g}_{\text{E}/k} = [x_{\text{E}/k}, y_{\text{E}/k}, \varphi_{\text{E}/k}, l_{\text{E}/k}, w_{\text{E}/k}]^{\text{T}}$ indicating the accident occurrence purely, and additional features $\boldsymbol{p}_{\text{E}/k}$ used by the severity prediction model η (sec. 4.2). In point of fact, all uncertainty sources can be considered in the criticality assessment of section 3.2 as long as their quantitatives contribute to the previous two categories. The final uncertainty $\boldsymbol{\Sigma}_{i,\text{E}/k}$ is obtained by superimposition. Furthermore, due to the uncertainty propagation, uncertainties of the dynamics are considered

indirectly in the pose. Equation 3.1 summarises the groups of random vectors for one time step t_i:

$$\boldsymbol{Z} = \left[\boldsymbol{Z}_{\mathrm{E}}, \boldsymbol{Z}_{k=1}, ..., \boldsymbol{Z}_{k=N_O}\right]^{\mathrm{T}} \sim \mathcal{N}\left(\boldsymbol{\mu}_z, \boldsymbol{\Sigma}_z\right) \tag{3.1}$$

$$\text{with} \quad \boldsymbol{Z}_{\mathrm{E}} = [\overbrace{\underbrace{X_{\mathrm{E}}, Y_{\mathrm{E}}, \Phi_{\mathrm{E}}}_{\boldsymbol{G}_{\mathrm{E}}}, \underbrace{V_{\mathrm{E,long}}, V_{\mathrm{E,lat}}, \Omega_{\mathrm{E}}}_{\boldsymbol{P}_{\mathrm{E}}}}^{\boldsymbol{Z}_{\mathrm{E,dyn}}}, \overbrace{\underbrace{L_{\mathrm{E}}, W_{\mathrm{E}}}_{\boldsymbol{G}_{\mathrm{E}}}, \underbrace{M_{\mathrm{E}}, E_{\mathrm{E}}, \Xi_{\mathrm{E}}}_{\boldsymbol{P}_{\mathrm{E}}}}^{\boldsymbol{Z}_{\mathrm{E,stat}}}]^{\mathrm{T}}$$

$$\boldsymbol{Z}_k = [\overbrace{\underbrace{X_k, Y_k, \Phi_k}_{\boldsymbol{G}_k}, \underbrace{V_k, \Omega_k}_{\boldsymbol{P}_k}}^{\boldsymbol{Z}_{k,\mathrm{dyn}}}, \overbrace{\underbrace{L_k, W_k}_{\boldsymbol{G}_k}, \underbrace{M_k, E_k, \Xi_k}_{\boldsymbol{P}_k}}^{\boldsymbol{Z}_{k,\mathrm{stat}}}]^{\mathrm{T}}$$

The environment model M bases on the discretisation in time N_{inst}, objects N_O, classification N_C and intentions N_H. For each instance of the combination, the continuous random vector $\boldsymbol{Z}_{\mathrm{EK}} := \boldsymbol{Z}_{i,k}^{j} = [\boldsymbol{Z}_{i,\mathrm{E,dyn}}, \boldsymbol{Z}_{\mathrm{E,stat}}, \boldsymbol{Z}_{i,\mathrm{K}=k,\mathrm{dyn}}^{j}, \boldsymbol{Z}_{\mathrm{K}=k,\mathrm{stat}}]^{\mathrm{T}}$ models the features $f_{\mathrm{EK}}(s,a,s')$ for the criticality $R(\mathrm{EK})$ of the substate $\boldsymbol{z}_{\mathrm{EK}} \in \boldsymbol{Z}_{\mathrm{EK}}$ between the ego vehicle E and one specific target object K at one time step t_i of intention h_k^j according to figure 3.1(c). The event EK is defined to emphasise the bidirectional relation between the ego E and one target object K. Theoretically, the criticality $R(\pi)$ of a trajectory π is obtained by the sum of all permutations of the criticality $R(\mathrm{EK}) \hat{=} R(\mathrm{EK}_{i,k}^{j})$:

$$\begin{aligned} R(\pi) = \sum_{i=1}^{N_{\mathrm{inst}}} \sum_{k=1}^{N_O} P(\mathrm{exist}) \sum_{c=1}^{N_C} P(X_c = x_c | \mathrm{exist}) \cdot \\ \sum_{j=1}^{N_H} p(h_k^j | \mathrm{exist} \wedge X_c = x_c) \cdot R(\mathrm{EK}_{i,k}^{j} \,|\, \mathrm{exist} \wedge X_c = x_c) \end{aligned} \tag{3.2}$$

Figure 3.1(a) refers to that equation 3.2. However, it should be noticed that the reward $Re_{t_i}(s,a,s')$ is calculated iterative over the planning horizon TH and superimposed with other influences, such as the pruning step. While figure 3.1 and equation 3.2 illustrates the complete criticality modelling, the existence and classification uncertainties are regarded by the most likelihood in the following. In other words, an object o_k exists or not and in the case of existence only one object class is assigned. Therefore, equation 3.2 simplifies to:

$$R(\pi) = \sum_{i=1}^{N_{\mathrm{inst}}} \underbrace{\sum_{k=1}^{N_O} \sum_{j=1}^{N_H} p(h_k^j) \cdot R(\mathrm{EK}_{i,k}^{j})}_{:= R_{f,t_i} \text{ (sec. 5.2)}} \tag{3.3}$$

Moreover, the uncertainties of the length $l_{\mathrm{E},k}$ and width $w_{\mathrm{E},k}$ are neglected. Related to the object o_k, that bases on the assumption that the geometric impact is superimposed with the object pose $\boldsymbol{z}_{k,\mathrm{dyn}}$. The ego vehicle length l_{E} and width w_{E} are presumed known due to construction information independent of the planning process. As result, the random vectors $\boldsymbol{G}_{\mathrm{E/k}}$ simplify to $\widetilde{\boldsymbol{G}}_{\mathrm{E/k}} = [x_{\mathrm{E}/k}, y_{\mathrm{E}/k}, \varphi_{\mathrm{E}/k},]^{\mathrm{T}}$.

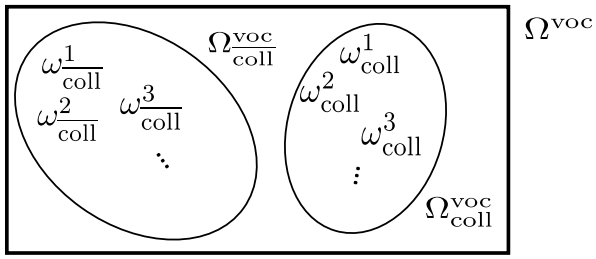

Figure 3.2: Venn diagram vehicle object constellations - The figure shows a Venn diagram of the vehicle object constellations Ω^{voc} and the subsets of collision configurations $\Omega^{\mathrm{voc}}_{\mathrm{coll}}$ and collision free constellations $\Omega^{\mathrm{voc}}_{\overline{\mathrm{coll}}}$.

Figure 3.1(d) visualises a sample $\boldsymbol{z}_{\mathrm{EK}}$ of the normal distributed substate $\boldsymbol{Z}_{\mathrm{EK}}$. With reference to following explanations, the sample $\boldsymbol{z}_{\mathrm{EK}}$ is substituted by the vehicle object constellation $\omega \in \Omega^{\mathrm{voc}}$ with $\omega := \boldsymbol{z}_{\mathrm{EK}}$. Thereby, Ω^{voc} constitutes the sample space to all vehicle object constellations and is subdivided by two disjunct subsets $\Omega^{\mathrm{voc}}_{\mathrm{coll}}$ and $\Omega^{\mathrm{voc}}_{\overline{\mathrm{coll}}}$ with $\Omega^{\mathrm{voc}} = [\Omega^{\mathrm{voc}}_{\mathrm{coll}}, \Omega^{\mathrm{voc}}_{\overline{\mathrm{coll}}}]$ as shown by figure 3.2. The accident configuration ω_{coll} indicates a constellation at the crash beginning between the ego vehicle E and one target object K, and constitutes an instance of all possible collision configurations $\omega_{\mathrm{coll}} \in \Omega^{\mathrm{voc}}_{\mathrm{coll}}$. Contrary, the vehicle object constellation $\omega_{\overline{\mathrm{coll}}} \in \Omega^{\mathrm{voc}}_{\overline{\mathrm{coll}}}$ indicates a collision free configuration.

In preparation of the accident severity prediction η presented in chapter 4, the elements of substate $\boldsymbol{Z}_{\mathrm{EK}}$ are subdivided into (directly or indirectly) measureable *input* and non-measureable *parameters*. In other words, the substate $\boldsymbol{Z}_{\mathrm{EK}}$ comprises independent *input* $\boldsymbol{z}_{\mathrm{input}}$ and static training *parameters* $\boldsymbol{z}_{\mathrm{train}}$. Further explanations are already presented in section 2.1.2.3 and follow in section 4.1.1.

Summarising, it should be noticed that multiple subdivisions of the substate $\boldsymbol{Z}_{\mathrm{EK}}$ are used to explain different aspects of the driving process and criticality estimation:

$$\boldsymbol{Z}_{\mathrm{EK}} \overset{\text{resort}}{\hat{=}} \begin{pmatrix} \boldsymbol{Z}_{\mathrm{E,dyn}} \\ \boldsymbol{Z}_{\mathrm{E,stat}} \\ \boldsymbol{Z}_{\mathrm{K,dyn}} \\ \boldsymbol{Z}_{\mathrm{K,stat}} \end{pmatrix} \overset{\text{resort}}{\hat{=}} \begin{pmatrix} \boldsymbol{G}_{\mathrm{E}} \\ \boldsymbol{P}_{\mathrm{E}} \\ \boldsymbol{G}_{\mathrm{K}} \\ \boldsymbol{P}_{\mathrm{K}} \end{pmatrix} \overset{\text{resort}}{\hat{=}} \begin{pmatrix} \boldsymbol{Z}_{\mathrm{input}} \\ \boldsymbol{Z}_{\mathrm{train}} \end{pmatrix} \tag{3.4}$$

The separation in dynamic ($\boldsymbol{Z}_{\mathrm{E/K,dyn}}$) and static ($\boldsymbol{Z}_{\mathrm{E/K,stat}}$) subvectors is used for the motion prediction and relating state space of the motion model $\tau_{\mathrm{E}/k,\mathrm{dyn}}$ (sec. 5.1). The calculation of the risk R, collision probability $P(C)$ and most probable collision configuration $\omega^{\mathrm{Pmax}}_{\mathrm{coll}}$ excludes the geometric parameters $\boldsymbol{G}_{\mathrm{E/K}}$ from all others $\boldsymbol{P}_{\mathrm{E/K}}$ (sec. 3.2 and 3.3). The accident severity prediction (chap. 4) divides *input* $\boldsymbol{Z}_{\mathrm{input}}$ and *training parameters* $\boldsymbol{Z}_{\mathrm{train}}$.

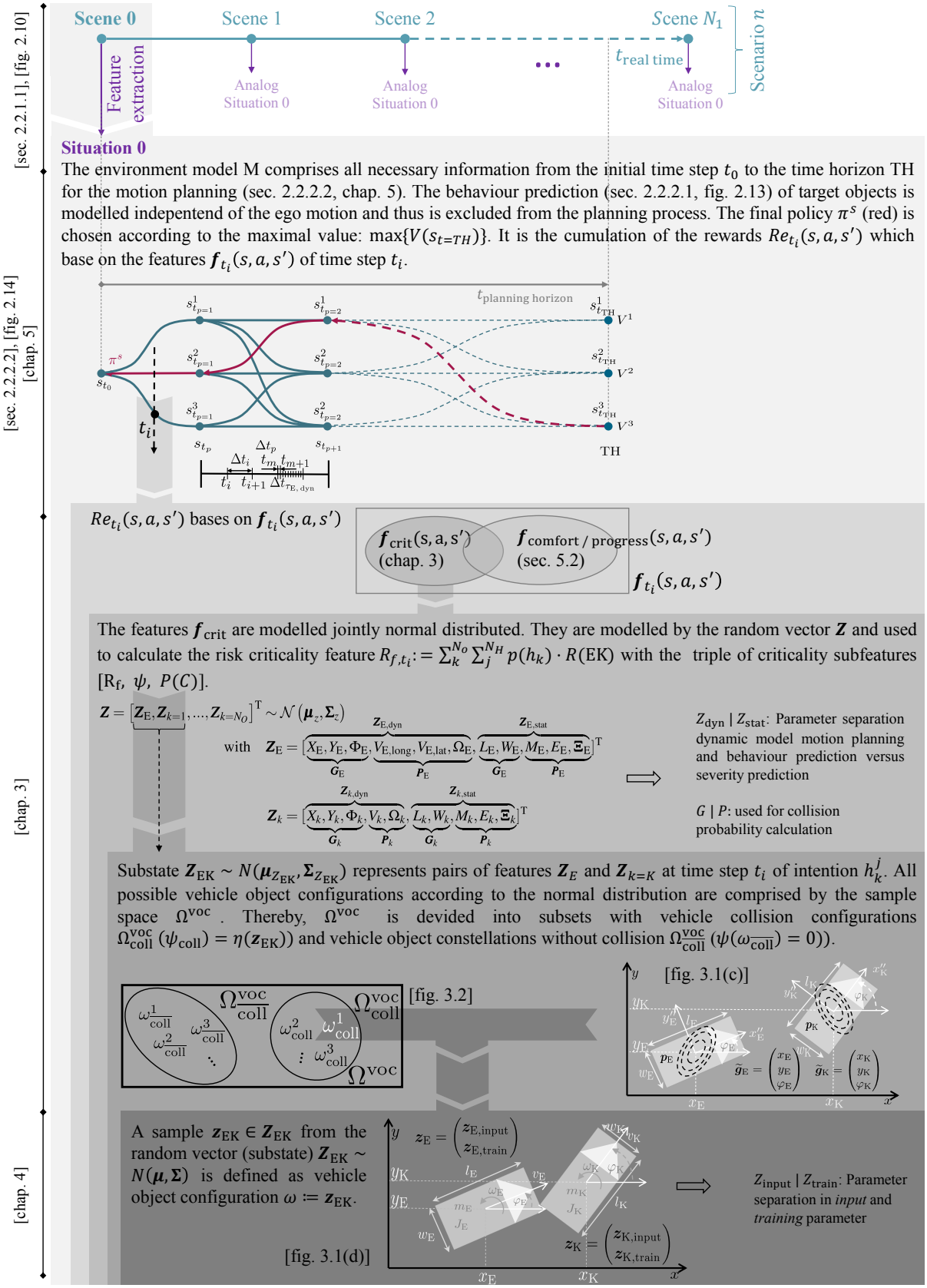

Figure 3.3: Decomposition of the environment model - It is an overview and summary of the environment model M. All further information are presented in the dedicated sections.

3.2 Risk as expected value

The accident severity ψ of a substate z_{EK} is modelled as random variable $\Psi : \Omega^{\mathrm{voc}} \rightarrow \mathbb{R}$. Thereby, Ω^{voc} represents the sample space indicating all possible object constellations $\omega \in \Omega^{\mathrm{voc}}$ between the ego vehicle and one target object o_k (accident free, accident constellation, etc.) with the probability $\mathrm{d}P(\omega)$ and probability density function $p_{\Omega^{\mathrm{voc}}}(\omega)$. Accordingly, the expected value R is calculated by:

$$R(\mathrm{EK}) = E(\Psi) = \int_{\Omega^{\mathrm{voc}}} \Psi(\omega) \cdot \mathrm{d}P(\omega) \qquad \overset{discretisation}{\Longrightarrow} \qquad E(\Psi) = \sum_n \psi_n \cdot p_n \tag{3.5}$$
$$= \int_{\omega \in \Omega^{\mathrm{voc}}} \psi(\omega) p_{\Omega^{\mathrm{voc}}}(\omega) \mathrm{d}\omega$$

That way, the severity of harm $\Psi(\omega)$ and its probability of occurrence $\mathrm{d}P(\omega)$ is combined, namely the *risk* $R(\mathrm{EK})$ of the substate according to the definitions of section 2.1.3.2. The severity Ψ is calculated according to the prediction models η (sec. 4.2) with the input vector $z_{\mathrm{EK}} \in \boldsymbol{Z}_{\mathrm{EK}}$ pursuant to the environment model M (sec. 3.1):

$$\Psi(\Omega^{\mathrm{voc}}) = \eta(\boldsymbol{Z}) \hat{=} \eta(\boldsymbol{Z}_{\mathrm{EK}}) = \eta\left((\boldsymbol{Z}_{\mathrm{E}}, \boldsymbol{Z}_{\mathrm{K}})^{\mathrm{T}}\right) \tag{3.6}$$

Accordingly, the risk $R(\mathrm{EK})$ of equation 3.6 is calculated with the joint probability density function (PDF) $p_{\boldsymbol{Z}}(\boldsymbol{z})$ by

$$R(\mathrm{EK}) = E\left(\Psi = \eta\left(\boldsymbol{Z}\right)\right) = \int_Z \eta(\boldsymbol{z})\, p_{\boldsymbol{Z}}(\boldsymbol{z})\, \mathrm{d}\boldsymbol{z}\,, \tag{3.7}$$

while the ego's and target's geometric state $\widetilde{\boldsymbol{G}}_{\mathrm{E/T}} = (X_{\mathrm{E/T}}, Y_{\mathrm{E/T}}, \Phi_{\mathrm{E/T}})^T$, and the parameter vector $\boldsymbol{P}_{\mathrm{E/T}}$ are modelled mutually stochastic independent:

$$R(\mathrm{EK}) = E(\Psi) = \int_{\widetilde{\boldsymbol{g}}_{\mathrm{E}}} \int_{\widetilde{\boldsymbol{g}}_{\mathrm{K}}} \int_{\boldsymbol{p}_{\mathrm{E}}} \int_{\boldsymbol{p}_{\mathrm{K}}} \eta(\boldsymbol{z})\; p_{X_{\mathrm{E}}, Y_{\mathrm{E}}, \Phi_{\mathrm{E}}}(x_{\mathrm{E}}, y_{\mathrm{E}}, \varphi_{\mathrm{E}})\; p_{X_{\mathrm{K}}, Y_{\mathrm{K}}, \Phi_{\mathrm{K}}}(x_{\mathrm{K}}, y_{\mathrm{K}}, \varphi_{\mathrm{K}}) \cdot$$
$$p_{\boldsymbol{P}_{\mathrm{E}}}(\boldsymbol{p}_{\mathrm{E}})\; p_{\boldsymbol{P}_{\mathrm{K}}}(\boldsymbol{p}_{\mathrm{K}})\; \mathrm{d}\widetilde{\boldsymbol{g}}_{\mathrm{E}}\, \mathrm{d}\widetilde{\boldsymbol{g}}_{\mathrm{K}}\, \mathrm{d}\boldsymbol{p}_{\mathrm{E}}\, \mathrm{d}\boldsymbol{p}_{\mathrm{K}} \tag{3.8}$$

Assuming an cooperative behaviour between average road users, the independence between the ego and target vehicle overestimates the risk $R(\mathrm{EK})$ and hence is a conservative approximation. Equation 3.8 shows the complete risk formulation. However, due to the normal distributions of $\boldsymbol{Z}$, an analytical solution does not exist. Besides, sampling based calculations or numerical integrations are not suitable due to the calculation time consumption (sec. 3.1). Hence, the following section deals with the appropriate approximations of equation 3.8.

A severity $\Psi > 0$ occurs only if an accident happens. Therefore, equation 3.8 is splited on the geometric variables $\widetilde{\boldsymbol{g}}_{\mathrm{E/K}}$ regarding the probability of collision occurrence (I) and harm (II) separately:

$$R(\mathrm{EK}) = E(\Psi) = \int_{\widetilde{\boldsymbol{g}}_\mathrm{E}} \int_{\widetilde{\boldsymbol{g}}_\mathrm{K}} \eta_\mathrm{ind}(\boldsymbol{z})\; p_{X_\mathrm{E},Y_\mathrm{E},\Phi_\mathrm{E}}(x_\mathrm{E}, y_\mathrm{E}, \varphi_\mathrm{E})\; p_{X_\mathrm{K},Y_\mathrm{K},\Phi_\mathrm{K}}(x_\mathrm{K}, y_\mathrm{K}, \varphi_\mathrm{K}) \cdot \quad \text{(I)}$$

$$\Bigg[\int_{\widetilde{\boldsymbol{g}}_\mathrm{E}|\mathrm{coll}} \int_{\widetilde{\boldsymbol{g}}_\mathrm{K}|\mathrm{coll}} \int_{\boldsymbol{p}_\mathrm{E}} \int_{\boldsymbol{p}_\mathrm{K}} \quad \eta(\boldsymbol{z}) \cdot$$

$$p_{\widetilde{\boldsymbol{G}}_\mathrm{E}|\mathrm{coll}}(\widetilde{\boldsymbol{g}}_\mathrm{E}|\mathrm{coll})\; p_{\widetilde{\boldsymbol{G}}_\mathrm{K}|\mathrm{coll}}(\widetilde{\boldsymbol{g}}_\mathrm{K}|\mathrm{coll}) \cdot \quad \text{(II)}$$

$$p_{\boldsymbol{P}_\mathrm{E}}(\boldsymbol{p}_\mathrm{E})\; p_{\boldsymbol{P}_\mathrm{K}}(\boldsymbol{p}_\mathrm{K})\; \mathrm{d}\widetilde{\boldsymbol{g}}_\mathrm{E}\; \mathrm{d}\widetilde{\boldsymbol{g}}_\mathrm{K}\; \mathrm{d}\boldsymbol{p}_\mathrm{E}\; \mathrm{d}\boldsymbol{p}_\mathrm{K} \Bigg] \; \mathrm{d}\widetilde{\boldsymbol{g}}_\mathrm{E}\; \mathrm{d}\widetilde{\boldsymbol{g}}_\mathrm{K} \tag{3.9}$$

The indicator function

$$\eta_\mathrm{ind}(\boldsymbol{z}) = \begin{cases} 1 & \vartheta(x_\mathrm{E}, y_\mathrm{E}, \varphi_\mathrm{E}, l_\mathrm{E}, w_\mathrm{E}) \wedge \vartheta(x_\mathrm{K}, y_\mathrm{K}, \varphi_\mathrm{K}, l_\mathrm{K}, w_\mathrm{K}) \neq \varnothing \\ 0 & \vartheta(x_\mathrm{E}, y_\mathrm{E}, \varphi_\mathrm{E}, l_\mathrm{E}, w_\mathrm{E}) \wedge \vartheta(x_\mathrm{K}, y_\mathrm{K}, \varphi_\mathrm{K}, l_\mathrm{K}, w_\mathrm{K}) = \varnothing \end{cases} \tag{3.10}$$

notifies a collision when the vehicle contour areas ϑ overlap depending on the geometric states $\widetilde{\boldsymbol{g}}_{\mathrm{E/K}}$.

Showing the linkage to the collision probability, the severity $\Psi = \eta(\boldsymbol{Z})$ is described through the binary event "collision". In other words, the severity Ψ depends solely on the geometric states $\boldsymbol{g}_{\mathrm{E/K}}$ independent of further parameters $\boldsymbol{p}_{\mathrm{E/K}}$, since the severity of the collision risk does not distinguish different collision configurations. Using the indicator function 3.10 as well, and having already the precondition "collision", the collision risk is obtained by marginalisation of part II)

$$\int_{\widetilde{\boldsymbol{g}}_\mathrm{E}|\mathrm{coll}} \int_{\widetilde{\boldsymbol{g}}_\mathrm{K}|\mathrm{coll}} \int_{\boldsymbol{p}_\mathrm{E}} \int_{\boldsymbol{p}_\mathrm{K}} 1 \cdot\; p_{\widetilde{\boldsymbol{G}}_\mathrm{E}|\mathrm{coll}}(\widetilde{\boldsymbol{g}}_\mathrm{E}|\mathrm{coll})\; p_{\widetilde{\boldsymbol{G}}_\mathrm{K}|\mathrm{coll}}(\widetilde{\boldsymbol{g}}_\mathrm{T}|\mathrm{coll})$$

$$p_{\boldsymbol{P}_\mathrm{E}}(\boldsymbol{p}_\mathrm{E})\; p_{\boldsymbol{P}_\mathrm{T}}(\boldsymbol{p}_\mathrm{T})\; \mathrm{d}\widetilde{\boldsymbol{g}}_\mathrm{E}\; \mathrm{d}\widetilde{\boldsymbol{g}}_\mathrm{K}\; \mathrm{d}\boldsymbol{p}_\mathrm{E}\; \mathrm{d}\boldsymbol{p}_\mathrm{K} = 1 \tag{3.11}$$

through:

$$R(\mathrm{EK})_\mathrm{coll} = P(C) = \underbrace{\int_{\widetilde{\boldsymbol{g}}_\mathrm{E}} \int_{\widetilde{\boldsymbol{g}}_\mathrm{K}} \eta_\mathrm{ind}(\mathbf{z})\; p_{X_\mathrm{E},Y_\mathrm{E},\Phi_\mathrm{E}}(x_\mathrm{E}, y_\mathrm{E}, \varphi_\mathrm{E})\; p_{X_\mathrm{K},Y_\mathrm{K},\Phi_\mathrm{K}}(x_\mathrm{K}, y_\mathrm{K}, \varphi_\mathrm{K})\; \mathrm{d}\widetilde{\boldsymbol{g}}_\mathrm{E}\; \mathrm{d}\widetilde{\boldsymbol{g}}_\mathrm{K}}_{I)} \tag{3.12}$$

The formulation of equation 3.12 is similar to the first part I) of equation 3.9. By way of illustration, figure 3.4(a) shows the collision risk $R(\mathrm{EK})_\mathrm{col}$ for an arbitrary PDF.

Distinguishing different collision configurations, the second part II) of equation 3.9 indicates the accident severity for each accident constellation (fig. 3.4(b)). Here again, no closed solution exists due to the modelling with normal distributions. Furthermore, the severity

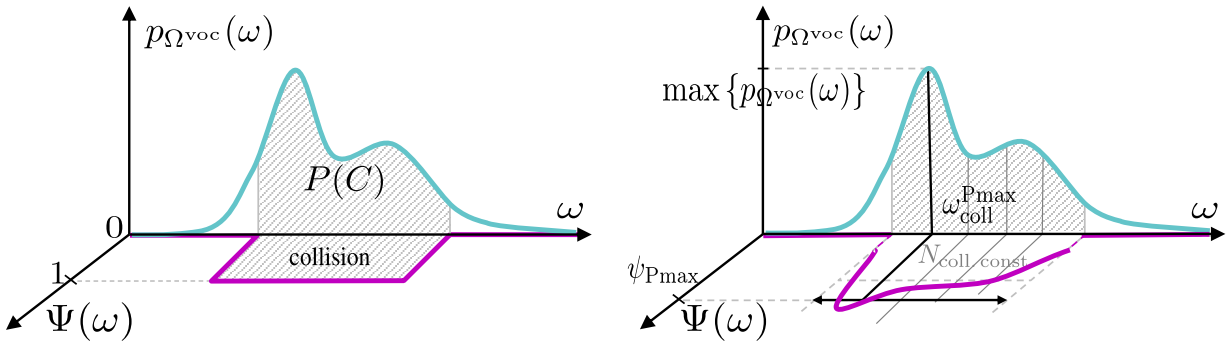

(a) **Collision risk** (b) **Risk in general**

Figure 3.4: Relation risk probability severity - (a) It shows the severity ψ and PDF $p_{\Omega^{\text{voc}}}(\omega)$ over all vehicle object configurations ω with reference to the collision risk R_{coll}. The collision is indicated by a binary event "collision". (b) Different vehicle object configurations are distinguished by the severity ψ. Approximatively, the most probable accident constellation determines the accident severity ψ_{Pmax}.

prediction model $\eta(\boldsymbol{Z})$ is non-linear deforming the shape of the normal distribution. At one hand, the integral II) could be solved by the permutation over the collision configurations $N_{\text{coll.const}}$ with $\psi > 0$ similar to numerical integration as presented in [26]. As result, equation 3.9 changes to:

$$R(\text{EK}) = E(\Psi) = \underbrace{P(C)}_{I)} \cdot \underbrace{\sum_{n=1}^{N_{\text{coll.const.}}} P(z_n \mid \text{coll}) \cdot \eta(\boldsymbol{z}_n)}_{II)} \tag{3.13}$$

The accuracy depends here on the discretisation directly. Theoretically, with an infinite small step size or rather infinity collision constellations $N_{\text{coll.const.}} \to \infty$ the expected values of the severity $E(\Psi)$ and hence risk $R(\text{EK})$ can be calculated exactly. However, even smaller numbers $N_{\text{coll.const.}}$ require a high computation time which is not suitable for real time applications (chap. 6). Alternatively, the uncertainty propagation through the severity model η provides a distribution of the severity Ψ_{coll} with PDF $p_{\Psi_{\text{coll}}} = p_{\Psi|\text{coll}}(\psi \mid \text{coll})$ independent of any discretisations. Moreover, apart from the expected value $E(\Psi_{\text{coll}}) = E(\Psi \mid \text{coll})$, it enables to evaluate different quantiles $\psi_{p-\text{quantile}}$ of the severity Ψ_{coll}:

$$R(\text{EK})_{\text{quantile}} = \underbrace{P(C)}_{I)} \cdot \underbrace{\psi_{p-\text{quantile}}}_{II)} \quad \text{with} \quad \int_{-\infty}^{\psi_{p-\text{quantile}}} p_{\Psi|\text{coll}}(\psi|\text{coll})\, \mathrm{d}\psi = p \tag{3.14}$$

That approximation could be used for additional safety margins.

Since sampling based approaches are not suitable for real time applications (chap. 6), the shape of a normal distribution requires linear uncertainty propagation to not deform the distribution:

$$\begin{aligned} \Psi_{\text{coll}} = \eta(\boldsymbol{Z} \mid \text{coll}) \quad &\overset{\textit{linearisation}}{\Longrightarrow} \quad \widetilde{\Psi}_{\text{coll}} \sim \mathcal{N}\left(\mu_{\widetilde{\Psi}}, \Sigma_{\widetilde{\Psi}}\right) \qquad \text{with} \\ \mu_{\widetilde{\Psi}} &= \eta(\boldsymbol{\mu}_{Z\mid\text{coll}}) \\ \Sigma_{\widetilde{\Psi}} &= \nabla\eta|_{\boldsymbol{\mu}_{Z\mid\text{coll}}} \ \boldsymbol{\Sigma}_Z \ \nabla\eta|^{\mathrm{T}}_{\boldsymbol{\mu}_{Z\mid\text{coll}}} \end{aligned} \tag{3.15}$$

Here, $\nabla(\eta)$ indicates the Jacobi matrix of the severity prediction model evaluated at the point $\boldsymbol{\mu}_Z$.

The major objective is to estimate the risk or rather expected value. Therefore, equation 3.9 changes to:

$$R(\text{EK}) = E(\Psi) = \underbrace{P(C)}_{I)} \cdot \underbrace{E(\Psi_{\text{coll}})}_{II)} \tag{3.16}$$

Assuming symmetric flattening input distributions, such as the normal distribution, the expected value $E(\Psi_{\text{coll}})$ is equally to the severity $\psi_{\text{Pmax}} = \eta(\omega_{\text{coll}}^{\text{Pmax}})$ of the most probable collision configuration $\omega_{\text{coll}}^{\text{Pmax}}$ with $\omega_{\text{coll}}^{\text{Pmax}} = \omega \,|\, \max\{p_{\Omega^{\text{voc}}}(\omega \,|\, \text{coll})\}$. That leads to the risk estimation:

$$R(\text{EK}) = E(\Psi) = \underbrace{P(C)}_{I)} \cdot \underbrace{\psi_{\text{Pmax}}}_{II)} \tag{3.17}$$

Summarising, the risk assessment 3.17 is used for every instantaneous substate z_{EK} in the evaluation of this work (chap. 6). The separation in collision probability $P(C)$ and accident severity ψ_{Pmax} takes care of the segregation between preventative driving and emergency manoeuvres. In regular driving, the accident severity is less important compared to the collision probability. Here, the collision probabilities ensure safe driving. In contrast, the severity distinguish different collision configurations in emergency manoeuvres. What is more, a short distance to the potential collision yields a high resolution of the MDP related to the collision configurations. The most probable accident configuration determines the accident severity. Here, an assumption is made on the shape of the distribution. The input shape needs to be symmetric flattening to hold for exact calculations. Otherwise, it is a slight approximation compared to the severity prediction model inaccuracies enabling real time applications due to the reduced number of computations. The used normal distributions of the inputs constitute a special case of a symmetric flattening distribution. Besides, the most probable collision configuration with respect to the geometric states $\boldsymbol{g}_{\text{E/K}}$ is obtained inherently calculating the collision probability and hence is derived with low computational effort. All other parameters $\boldsymbol{p}_{\text{E/K}}$ are not conditioned and thus their expected values are determined directly pursuant to the belonging distributions. Furthermore, the separation in collision probability I) and accident severity II) enables the usage of established non-linear procedures to estimate the collision probability efficiently (sec. 3.3). Moreover, the severity distribution could be derived by the Gaussian uncertainty propagation. As result, detailed safety requirements becomes adjustable and hence it is open to future standards.

3.3 Collision probability and most probable collision configuration

The calculation of the collision probability $P(C)$ and most probable collision configuration $\omega_{\text{coll}}^{\text{Pmax}}$ of a substate $\boldsymbol{z}_{\text{EK}}$ bases on the combination of approaches presented in [77], [206], and [207] and used in previous publications [26] and [28].

According to equation 3.9 and 3.12, the calculation has a degree of freedom DOF = 6:

$$\widetilde{\boldsymbol{G}}^{6\times1} = \begin{pmatrix} \widetilde{\boldsymbol{G}}_{\text{E}}^{3\times1} \\ \widetilde{\boldsymbol{G}}_{\text{K}}^{3\times1} \end{pmatrix} = (X_{\text{E}}, Y_{\text{E}}, \Phi_{\text{E}}, X_{\text{K}}, Y_{\text{K}}, \Phi_{\text{K}})^{\text{T}} : \Omega^{\tilde{G}} \rightarrow \mathbb{R}^6 \tag{3.18}$$

with

$$\widetilde{\boldsymbol{G}}^{6\times1} \sim \mathcal{N}\left(\begin{pmatrix} \boldsymbol{\mu}_{\text{E}}^{3\times1} \\ \boldsymbol{\mu}_{\text{K}}^{3\times1} \end{pmatrix}, \begin{pmatrix} \boldsymbol{\Sigma}_{\text{E}}^{3\times3} & * \\ * & \boldsymbol{\Sigma}_{\text{K}}^{3\times3} \end{pmatrix} \right) \tag{3.19}$$

References [77] and [207] transfer the indicator function $\eta_{\text{ind}}(\boldsymbol{Z})$ of equation 3.12 to the collision area D or rather integral limits:

$$P(C) = \int\int\int\int\int\int_{D} p_{\widetilde{\boldsymbol{G}}_{\text{E}}}(\widetilde{\boldsymbol{g}}_{\text{E}})\; p_{\widetilde{\boldsymbol{G}}_{\text{T}}}(\widetilde{\boldsymbol{g}}_{\text{K}})\; \mathrm{d}\widetilde{\boldsymbol{g}}_{\text{E}}\; \mathrm{d}\widetilde{\boldsymbol{g}}_{\text{T}} \tag{3.20}$$

Halving the count of DOF, a 3D Minkowski Difference D' (e.g., [208] and [209]) expresses the collision area D in relative coordinates:

$$\begin{aligned} \Delta\widetilde{\boldsymbol{G}} \quad &= \widetilde{\boldsymbol{G}}_{\text{K}} - \widetilde{\boldsymbol{G}}_{\text{E}} \qquad \text{with} \\ \Delta\widetilde{\boldsymbol{G}}^{3\times1} \quad &\sim \mathcal{N}\left(\boldsymbol{\mu}_{\text{K}}^{3\times1} - \boldsymbol{\mu}_{\text{E}}^{3\times1}, \boldsymbol{\Sigma}_{\text{E}}^{3\times3} + \boldsymbol{\Sigma}_{\text{K}}^{3\times3}\right) \end{aligned} \tag{3.21}$$

$$D' \quad = M_{\text{E}} \ominus M_{\text{K}} \; = \; \{m_{\text{E}} - m_{\text{K}} \mid m_{\text{E}} \in M_{\text{E}}, m_{\text{K}} \in M_{\text{K}}\} \tag{3.22}$$

Here, M_{E} and M_{K} denotes the set of all tupels (x, y, φ) according to the vehicle contours $\vartheta(\boldsymbol{g}_{\text{E}})$ and $\vartheta(\boldsymbol{g}_{\text{K}})$, respectively. The mathematical background on the convolution can be taken from [210, sec. 8.1.4]. Figure 3.5 visualises a twisted 3D Minkowski Difference for two example polygons, a rectangle A and rectangle B. Using the relation 3.21 and 3.22, equation 3.20 changes to:

$$P(C) = \int\int\int_{D'} p_{\Delta\widetilde{\boldsymbol{G}}}\left(\Delta\widetilde{\boldsymbol{g}}\right) \mathrm{d}\Delta\widetilde{\boldsymbol{g}} \tag{3.23}$$

Resolving the trivariante normal distribution $\Delta\widetilde{\boldsymbol{G}}$ over the 3D Minkowski Difference D', [77] suggests to extract a finite number of orientation ranges, to enlarge the object contours accordingly to its 2D projection, and then to evaluate the obtained bivariate normal distributions over the 2D Minkowski Differences iteratively. As result, a small upper bound for the real collision probability $P(C)$ is found. The overestimation is a conservative approximation

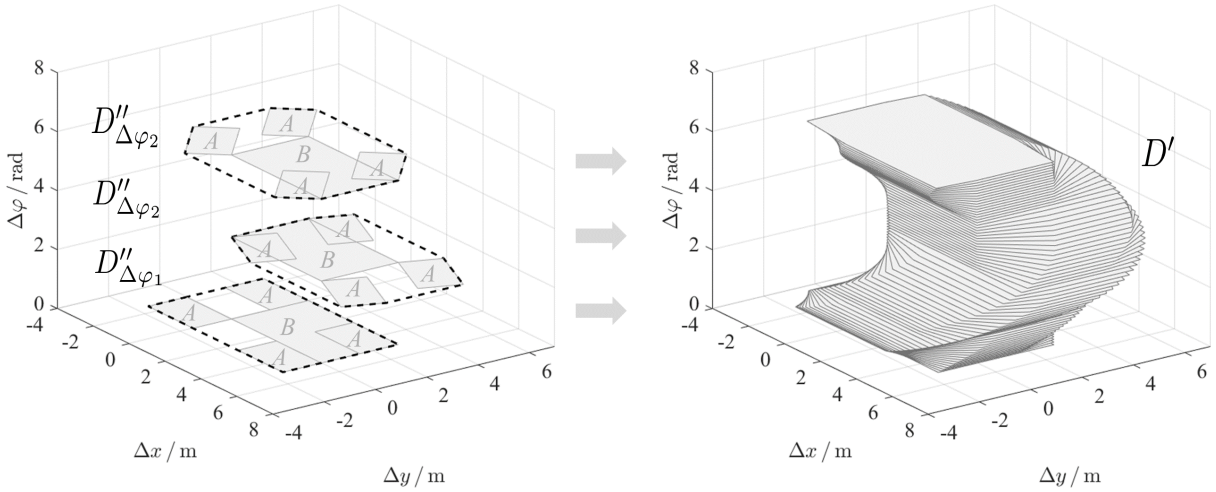

Figure 3.5: 3D Minkowski Difference - The 3D Minkowski Difference D' (right) is obtained by stacking 2D Minkowski Differences D'' (left) with fixed orientations. The numeric values are chosen exemplary.

with an additional safety margin. Figure 3.8 summarises the algorithm. Contrary to [77], both, the ego and the object have an uncertain orientation $\varphi_{\mathrm{E/K}}$ in this work.

The procedure is described mathematically in the following. At first, the collision probability $P(C)$ is conditioned by the orientations $\varphi_{\mathrm{E,K}}$:

$$P(C) = \int_{\varphi_\mathrm{E}} \int_{\varphi_\mathrm{K}} p_{\Phi_\mathrm{E}}(\varphi_\mathrm{E})\, p_{\Phi_\mathrm{K}}(\varphi_\mathrm{K}) \cdot \underbrace{P(C \mid \varphi_\mathrm{E}, \varphi_\mathrm{K})}_{\substack{\text{bivariate} \\ \text{collision probability}}} \, \mathrm{d}\varphi_\mathrm{E}\, \mathrm{d}\varphi_\mathrm{K} \tag{3.24}$$

Here, $P(C \mid \varphi_\mathrm{E}, \varphi_\mathrm{K})$ describes a bivariate collision probability. It depends on the relative coordinates $\Delta\overline{x}$ and $\Delta\overline{y}$ considering the correlations according to equation 3.19 and the transformed collision area D'':

$$P(C \mid \varphi_\mathrm{E}, \varphi_\mathrm{K}) = \int \int_{D''} p_{\Delta\overline{X}}(\Delta\overline{x})\, p_{\Delta\overline{Y}}(\Delta\overline{y}) \mathrm{d}\Delta\overline{x} \mathrm{d}\Delta\overline{y} \tag{3.25}$$

with

$$D'' \quad = D' | \varphi_\mathrm{E}, \varphi_\mathrm{K} \tag{3.26}$$

$$\Delta\overline{G}^{2\times1} = \begin{pmatrix} \Delta\overline{X} \\ \Delta\overline{Y} \end{pmatrix} \sim \mathcal{N}\left(\overline{\boldsymbol{\mu}}_K^{2\times1} - \overline{\boldsymbol{\mu}}_\mathrm{E}^{2\times1}, \overline{\boldsymbol{\Sigma}}_E^{2\times2} + \overline{\boldsymbol{\Sigma}}_\mathrm{K}^{2\times2} \right) \tag{3.27}$$

$$\boldsymbol{Z}_\mathrm{E,K}^{3\times1} \sim \mathcal{N}\left(\boldsymbol{\mu}_\mathrm{E,K}^{3\times1}, \begin{pmatrix} \boldsymbol{\Sigma}_{11}^{2\times2} & \boldsymbol{\Sigma}_{12}^{2\times1} \\ \boldsymbol{\Sigma}_{21}^{1\times2} & \Sigma_{22}^{1\times1} \end{pmatrix} \right) \tag{3.28}$$

$$\begin{pmatrix} \overline{\mu}_{x_\mathrm{E/K}} \\ \overline{\mu}_{y_\mathrm{E/K}} \end{pmatrix} = \begin{pmatrix} \mu_{x_\mathrm{E/K}} \\ \mu_{y_\mathrm{E/K}} \end{pmatrix}^{2\times1} + \boldsymbol{\Sigma}_{12} \Sigma_{22}^{-1} (\varphi_\mathrm{E/K} - \mu_{\varphi_\mathrm{E/K}}) \tag{3.29}$$

$$\overline{\Sigma}_{\mathrm{E,K}}^{2\times 2} = \boldsymbol{\Sigma}_{11} - \boldsymbol{\Sigma}_{12}\Sigma_{22}^{-1}\boldsymbol{\Sigma}_{21} \tag{3.30}$$

The mathematical laws are for example described in [210, sec. 8.1.3]. It should be noticed that here the yaw angles $\varphi_{\mathrm{E/K}}$ are not in relative coordinates contrary to equation 3.23. That takes care of the non-linear relationship of the rotation.

Then, the integrals of equation 3.24 are discretisied through $N_{\mathrm{E,K}}$ angle ranges with $\sum_{n_{\mathrm{E,K}}=1}^{N_{\mathrm{E,K}}} P([\varphi_{\mathrm{E/K}}^{n_{\mathrm{E/K}}-1}, \varphi_{\mathrm{E/K}}^{n_{\mathrm{E/K}}}]) = 1$:

$$P(C) \approx \sum_{n_{\mathrm{E}}=1}^{N_{\mathrm{E}}} P([\varphi_{\mathrm{E}}^{n_{\mathrm{E}}-1}, \varphi_{\mathrm{E}}^{n_{\mathrm{E}}}]) \Bigg(\sum_{n_{\mathrm{K}}=1}^{N_{\mathrm{K}}} P([\varphi_{\mathrm{K}}^{n_{\mathrm{K}}-1}, \varphi_{\mathrm{K}}^{n_{\mathrm{K}}}]) \cdot \underbrace{P(C \mid \varphi_E \in [\varphi_{\mathrm{E}}^{n_{\mathrm{E}}-1}, \varphi_{\mathrm{E}}^{n_{\mathrm{E}}}],\ \varphi_{\mathrm{K}} \in [\varphi_{\mathrm{K}}^{n_{\mathrm{K}}-1}, \varphi_{\mathrm{K}}^{n_{\mathrm{K}}}])}_{P(C|\varphi_{\mathrm{E}},\varphi_{\mathrm{K}}) = f(\Delta\bar{x},\Delta\bar{y},D'')} \Bigg) \tag{3.31}$$

In other words, the 3D Minkowski Difference D' (fig. 3.5) is divided into slices. Afterwards, the resulting prisms are projected on the x-y-plane and enveloped by a convex polygon. According to the angle ranges $(N_{\mathrm{E}}, N_{\mathrm{K}})$, each polygon combination is concatenated to the 2D Minkowski Difference $\overline{D}''$ accompanied by the bivariate normal distribution pursuant to equation 3.27. Figure 3.6 illustrates the transformed collision area D'' and bivariate normal distribution $\Delta\overline{G}$. Simplifying, the average angle of the interval $[\varphi_{\mathrm{E/K}}^{N_{\mathrm{E/K}}-1}, \varphi_{\mathrm{E/K}}^{\mathrm{E/K}}]$ is used as condition in equation 3.31.

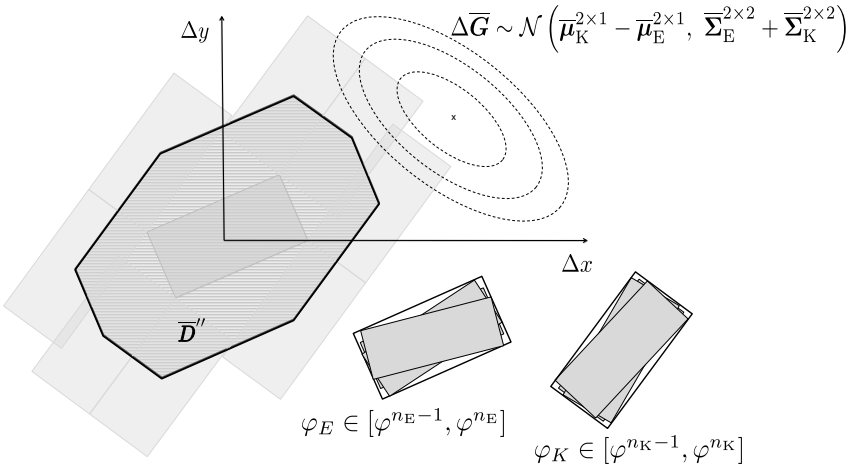

Figure 3.6: 2D Minkowski Difference - The 2D Minkowski Difference $\overline{D}''$ is obtained from two polygonally enveloped slice projections pursuant to the angle ranges of the certain slice.

A high number of discretisations N_{E} and N_{K} obtains accurate results, but takes more computation time. Besides, seeing that the margins of the orientation uncertainty have a low probability of occurrence (fig. 3.7), [77] suggests to consider only a finite confidence interval

with $\sum_{n_{\mathrm{E,K}}=1}^{N_{\mathrm{E,K}}} P([\varphi_{\mathrm{E/K}}^{n_{\mathrm{E/K}}-1}, \varphi_{\mathrm{E/K}}^{n_{\mathrm{E/K}}}]) = \delta$. The share of the collision probability $P(C|\varphi_{\mathrm{E/K,res}})$ for the residual orientations $\varphi_{\mathrm{E/K,res}}$ with $P(\varphi_{\mathrm{E/K,res}}) = (1-\delta_{\mathrm{E/K}})$ is then estimated without angle information by a circular object overapproximation or simply assumed as collision $P(C|\varphi_{\mathrm{E/K,res}}) = 1$:

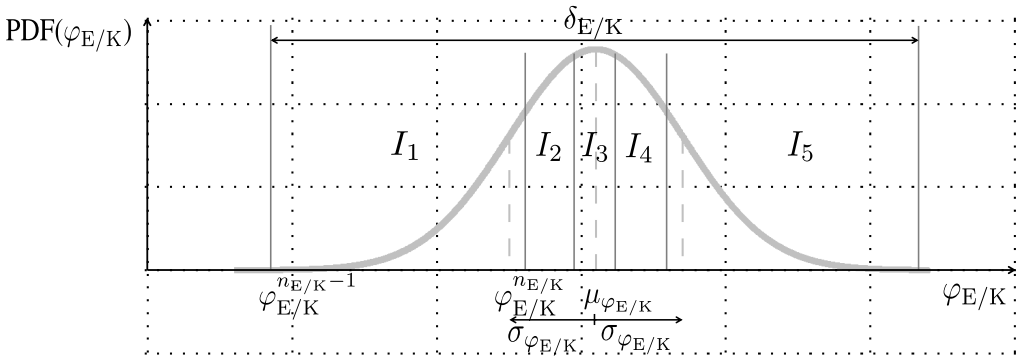

Figure 3.7: Angle discretisation - The distribution of the yaw angle is divided into $N_{\mathrm{E,K}}$ finite intervals.

$$
\begin{aligned}
P(C) \approx \sum_{n_{\mathrm{E}}=1}^{N_{\mathrm{E}}} P([\varphi_{\mathrm{E}}^{n_{\mathrm{E}}-1}, \varphi_{\mathrm{E}}^{n_{\mathrm{E}}}]) \cdot \qquad (3.32)\\
\Bigg(\sum_{n_{\mathrm{K}}=1}^{N_{\mathrm{K}}} P\Big([\varphi_{\mathrm{K}}^{n_{\mathrm{K}}-1}, \varphi_{\mathrm{K}}^{n_{\mathrm{K}}}]\Big) \cdot P\Big(C \mid \varphi_{\mathrm{E}} \in [\varphi_{\mathrm{E}}^{n_{\mathrm{E}}-1}, \varphi_{\mathrm{E}}^{n_{\mathrm{E}}}],\ \varphi_{\mathrm{K}} \in [\varphi_{\mathrm{K}}^{n_{\mathrm{K}}-1}, \varphi_{\mathrm{K}}^{n_{\mathrm{K}}}]\Big)\\
+ \underbrace{\Big(1-\delta_{\mathrm{K}}\Big)}_{<<1} \cdot \underbrace{P\Big(C \mid \varphi_E \in [\varphi_{\mathrm{E}}^{n_{\mathrm{E}}-1}, \varphi_{\mathrm{E}}^{n_{\mathrm{E}}}], \varphi_{\mathrm{K}} = \varphi_{\mathrm{K,res}}\Big)}_{\text{rough estimation}} \Bigg)\\
+ \underbrace{\Big(1-\delta_{\mathrm{E}}\Big)}_{<<1} \cdot \underbrace{P\Big(C \mid \varphi_{\mathrm{E,res}}\Big)}_{\text{rough estimation}}
\end{aligned}
$$

These simplifications decrease the computation time consumption with almost remaining accuracy. Furthermore, [77] investigates the impact of the interval numbers. The strength of high numbers is mainly obtained by increased yaw angle uncertainties with $\sigma_{\varphi_{E/K}} > 15°$. Since the risk assessment is used on a structured road environment, a maximum orientation uncertainty of $\sigma_{\varphi_{E,K},\max} = 15°$ seems reasonable. In other words, taking for example the 6-σ-bound into account, the perception needs to distinguish at least orientations such as straight, diagonal, or crossing. Furthermore, it is expected to obtain even lower uncertainty

values. Therefore, only one interval $N_\mathrm{E} = 1$ and $N_\mathrm{K} = 1$ is chosen for each angle $\varphi_{\mathrm{E/K}}$. As result, equation 3.32 simplifies to:

$$P(C) \approx \delta_\mathrm{E} \Bigg(\delta_\mathrm{K} \cdot \underbrace{P\Big(C \mid \varphi_\mathrm{E} \in [\varphi_\mathrm{E}^1, \varphi_\mathrm{E}^2], \varphi_\mathrm{K} \in [\varphi_\mathrm{K}^1, \varphi_\mathrm{K}^2]\Big)}_{\text{bivariate collision probability } P(C_\mathrm{poly})} \tag{3.33}$$

$$+ \Big(1 - \delta_\mathrm{K}\Big) \cdot \underbrace{P\Big(C \mid \varphi_\mathrm{E} \in [\varphi_\mathrm{E}^1, \varphi_\mathrm{E}^2], \varphi_\mathrm{E,res}\Big)}_{\substack{\text{circular approximation} \\ P(C_\mathrm{circ})}} \Bigg) + \Big(1 - \delta_\mathrm{E}\Big) \cdot \underbrace{P\Big(C \mid \varphi_\mathrm{E,res}\Big)}_{\substack{\text{circular approximation} \\ P(C_\mathrm{circ})}}$$

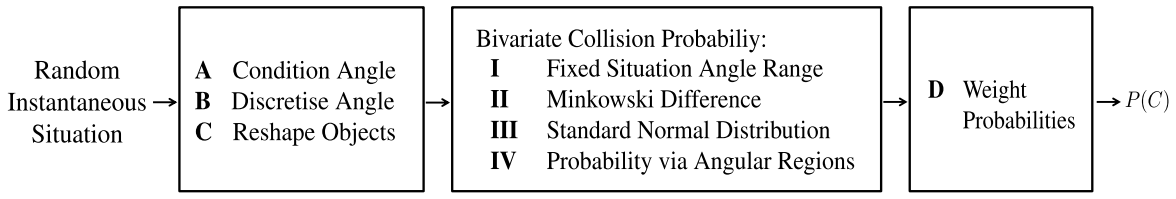

Figure 3.8: Procedure trivariate collision probability - The algorithm derives the collision probability $P(C)$ of two planar objects with each DOF = 3 according to the object pose $\widetilde{\boldsymbol{g}} = (x, y, \varphi)^\mathrm{T}$.

The procedure to solve the bivariate collision probability $P(C \mid \varphi_\mathrm{E}, \varphi_\mathrm{K})$ is summarised in figure 3.9. Firstly, the bivariate normal distribution $\Delta\overline{G}$ is standardised. The used transformation is likewise applied to the 2D Minkowski Difference $\overline{D}''$. The diagonalisation and scaling is either obtained by the Principal Component Analysis (PCA) (e.g., [211]) or by the geometric interpretation of the equipotentials of the normal distribution as ellipses (e.g., [212]):

$$\begin{aligned} \Delta\overline{G}''' &= \frac{\Delta\overline{G} - \boldsymbol{\mu}_{\Delta\overline{G}}}{\sqrt{\boldsymbol{\Sigma}_{\Delta\overline{G}}}} \quad \sim \mathcal{N}\left(\begin{pmatrix} 0 \\ 0 \end{pmatrix}, \begin{pmatrix} 1 & 0 \\ 0 & 1 \end{pmatrix} \right) \\ &= \sqrt{\boldsymbol{\Lambda}}^{-1} \boldsymbol{V}^{-1} (\Delta\overline{G} - \boldsymbol{\mu}_{\Delta\overline{G}}) \end{aligned} \tag{3.34}$$

$$\begin{aligned} \overline{D}''' &= \sqrt{\boldsymbol{\Lambda}}^{-1} \boldsymbol{V}^{-1} (\overline{D}'' - \boldsymbol{\mu}_{\Delta\overline{G}}) \\ &= \begin{pmatrix} \frac{1}{\sigma_{x,\Delta\overline{G}}} & 0 \\ 0 & \frac{1}{\sigma_{y,\Delta\overline{G}}} \end{pmatrix} \begin{pmatrix} \cos\alpha & \sin\alpha \\ -\sin\alpha & \cos\alpha \end{pmatrix} \left(\overline{D}'' - \begin{pmatrix} \mu_{x,\Delta\overline{G}} \\ \mu_{y,\Delta\overline{G}} \end{pmatrix} \right) \end{aligned} \tag{3.35}$$

Here, $\boldsymbol{\Lambda}$ contains the eigenvalues $\lambda_1 = \sigma^2_{x,\Delta\overline{G}}$ and $\lambda_2 = \sigma^2_{y,\Delta\overline{G}}$ in Jordan normal form and $\boldsymbol{V}$ the accompanying eigenvectors with the rotation angle α. Figure 3.9I shows the geometric interpretation.

Secondly, the standardised normal distribution is evaluated over the transformed collision area $\overline{D}'''$. According to [213], the polygon $\overline{D}'''$ is reconstructed by the outer area consisting of angular regions with the probability $P(A_n)$, designing the complementary event:

$$P(C_\mathrm{poly}) = 1 - \sum P(A_n) \tag{3.36}$$

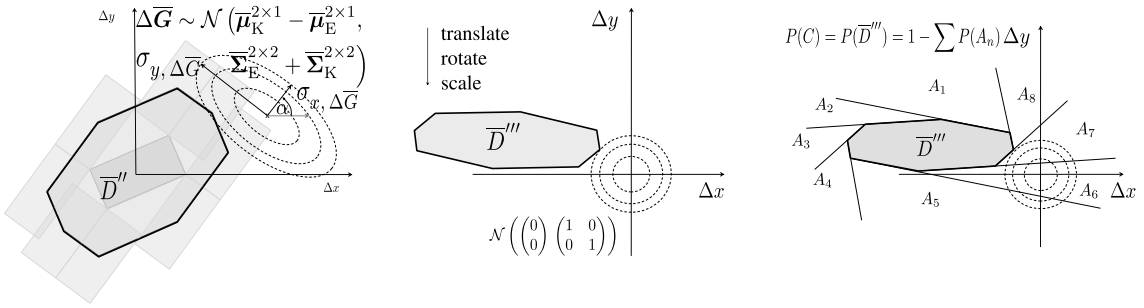

I Minkowski Difference II Standard normal Distribution III Angular regions

Figure 3.9: Procedure bivariate collision probability - The initial set (I) is identically to figure 3.6. The bivariate normal distribution $\Delta\overline{G}$ is standardised (II) and accordingly the Minkowski Difference $\overline{D}''$. (III) The transformed collision area $\overline{D}'''$ is evaluated by angular regions.

Figure 3.9III shows the geometric relations. The probability $P(A_n)$ is either obtained by an approximation of the cumulative density function (CDF), as presented in [213], or simply by using a database of numerically pre-calculated angular region probabilities. Advantageous, the necessary entries of the database are relatively low due to the standardisation, finite angle range $[0, 2\pi]$, and object distance relations. That is an important property for real time applications. The circular collision probability $P(C_{\text{circ}})$ is evaluated by a tight axially parallel bounding box with the Gaussian CDF:

$$P(C_{\text{circ}}) = \left[\text{cdf}\left(\max_x(D'''_{\text{circ}})\right) - \text{cdf}\left(\min_x(D'''_{\text{circ}})\right)\right] \cdot \left[\text{cdf}\left(\max_y(D'''_{\text{circ}})\right) - \text{cdf}\left(\min_y(D'''_{\text{circ}})\right)\right] \tag{3.37}$$

According to the procedure of the bivariate collision probability, the geometric parameters $\boldsymbol{g}_{\text{E/K}}$ of the most probable collision configuration $\omega_{\text{coll}}^{\text{Pmax}}$ are directly identifiable. The equipotentials of the standardised normal distribution are concentric circles around the point of origin. Therefore, the shortest distance to the collision area $\overline{D}'''$ indicates the geometric parameters $\boldsymbol{g}_{\text{E/K}}$ of the most probable collision configuration $\omega_{\text{coll}}^{\text{Pmax}}$. It is either a vertex directly or a point between the two shortest vertexes. Besides, showing the linkage to equation 3.13, the Minkwoski Difference could be divided into subareas with representing collision configurations permuting the geometric features of the severity prediction model η. Finally, due to the linear relationship, the assignment correlates with the untransformed collision area $\overline{D}''$ and hence the geometric input for the severity prediction is derived as figure 3.10 illustrates. All other input parameters $\boldsymbol{p}_{\text{E/K}}$ are not conditioned and thus are determined directly pursuant to the belonging distributions.

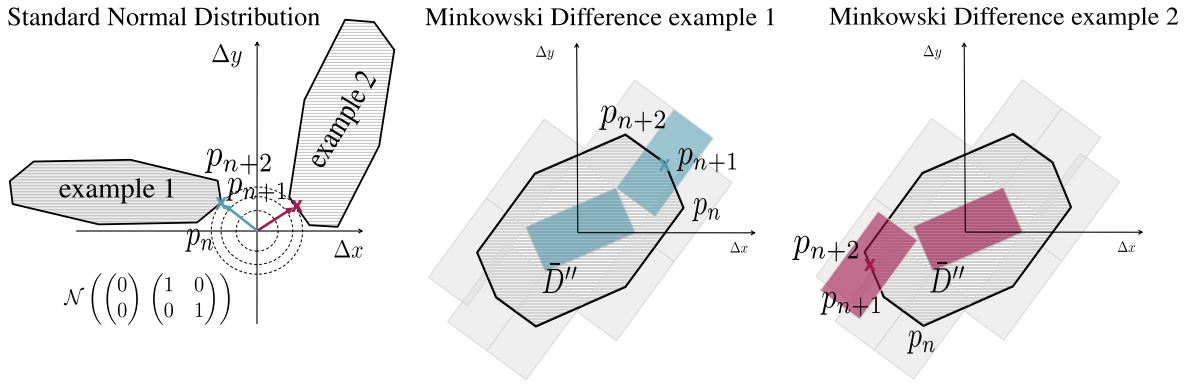

Figure 3.10: Most probable collision configuration - The (transformed) most probable collision configuration is derived in the standardised form. The input constellation for the severity prediction η is then obtained by linear relation to the Minkowski Difference.

4 Accident severity prediction

4.1 Mathematical preliminaries

4.1.1 Methodical approach

The mathematical problem formulation for the accident severity prediction $\eta(\omega)$ and the derived data driven approach is presented in the following. It refers to the environment model M of section 3.1 and hence adopts its nomenclature (overview in fig. 3.3). Moreover, with reference to the state of the art of section 2.1.2.3, it is focused on a driving function point of view. The estimated severity $\psi = \eta(\omega_{\text{coll}})$ is used in the risk assessment as described in section 3.2.

According to section 3.1, the vehicle configuration ω is specified by the state vector (sample) $z_{\text{EK}} = (z_{\text{E}}, z_{\text{K}})^{\text{T}}$. The main problem of this chapter is to find appropriate severity prediction functions η which

The severity prediction function η maps that state z_{EK} to the desired value, the accident severity ψ:

$$\eta : \underbrace{z_{\text{EK}}}_{:=\omega} \rightarrow \psi \tag{4.1}$$

Further details on the output ψ are given in section 4.1.2 and 4.1.3. The collision free vehicle object constellations $\omega_{\overline{\text{coll}}}$ result in a trivial severity outcome $\psi = \eta(\omega_{\overline{\text{coll}}}) = 0\,\frac{\text{m}}{\text{s}}$. Therefore, these cases are not regarded further in this chapter and the focus lies on the collision configurations ω_{coll}.

From output point of view, the state z_{EK} needs to contain the most sensitive dependencies of the accident severity ψ. According to [111], that includes the impact point, vehicle dimensions, velocities and masses for front-front crashes. In other accident constellations, especially when rotations with big levers are involved, the yaw rates and moments of inertia gain importance.

From a severity prediction point of view, the predictors η have different modelled dependencies, which are discussed in detail in the dedicated sections (sec. 4.2.1 to 4.2.3) and need to be covered by the state z_{EK}. The pre-selection of promising prediction functions η is already explained in section 2.1.2.3 and summarised with table 2.2.

From the driving function point of view, and with reference to the used test equipment (sec. 6.3), the elements of the state z_{EK} are sorted to the two categories of (directly or indirectly) *measureable* and *non-measurable* parameters. The assignment of potential input parameters (dependencies) to these two categories restricts the independent variables. In other words, the execution of the prediction function η is only allowed to depend on variables z_{input}

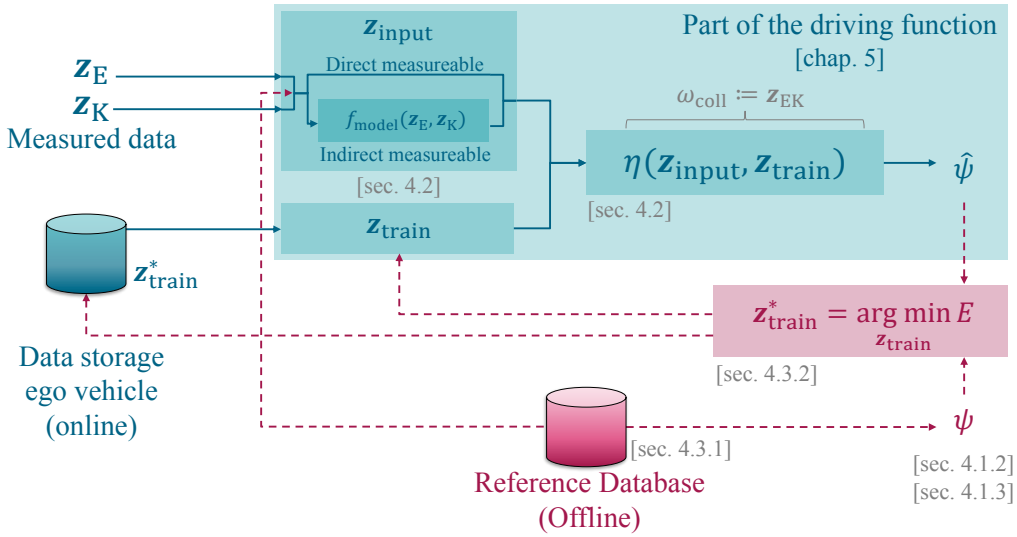

Figure 4.1: Training and execution procedure - It shows a block diagram for the training (dashed red line) and execution (solid turquoise line) of the accident severity prediction. The final driving function is only allowed to depend on measureable z_{input} or previously stored parameters z_{train}. The optimal non-measureable parameters z^*_{train} are obtained data driven as explained in section 4.3.

which are (directly or indirectly) measurable while driving. More detailed, *directly measureable* means that sensors are able to percept the values directly. *Indirectly measureable* means that established models f_{model} exist, such as dynamic models τ_{dyn}, to estimate further values with appropriate uncertainty from the direct measureable values. All other influences (non-measureable) need to be either determined previously or excluded from the modelling. The latter would change the prediction model indirectly and thus this thesis bases on the former. In other words, the reference database 4.3.1 is used to identify the parameters z_{train} statistically. Thereby, the focus lies on an overall accident severity prediction for the risk assessment rather than on the representation of detailed crash sequences for single crash types. Figure 4.1 presents an overview of the training and execution of the data driven prediction functions η. Further explanations to the training strategy are presented in section 4.3.2.

With foresight to the following sections, the measurable input is more or less summarised by

$$z_{input} = [\Delta x, \Delta y, \Delta\varphi, v_{E/K}, \omega_{E/K}, l_{E/K}, w_{E/K}, m_{E/K}, J_{E/K}]^T, \tag{4.2}$$

which includes the relative pose $[\Delta x, \Delta y, \Delta\varphi]$, velocities $v_{E/K}$, yaw rates $\omega_{E/K}$, vehicle dimensions $[l_{E/K}, w_{E/K}]$, masses $m_{E/K}$, and moments of inertia $J_{E/K}$.

The parameter identification of the ego vehicle constitutes a minor challenge. The ego vehicle dynamic state $z_{E,dyn}$ is measured by internal sensors and predicted by a dynamic model to future time steps. The length l_E and width w_E are static over the entire driving process and thus are determined previously. The mass m_E and moment of inertia J_E are either measured by intern sensors to cover the load or approximated by the nominal vehicle data. Similarly, the internal material characteristics need to be determined before departure. In

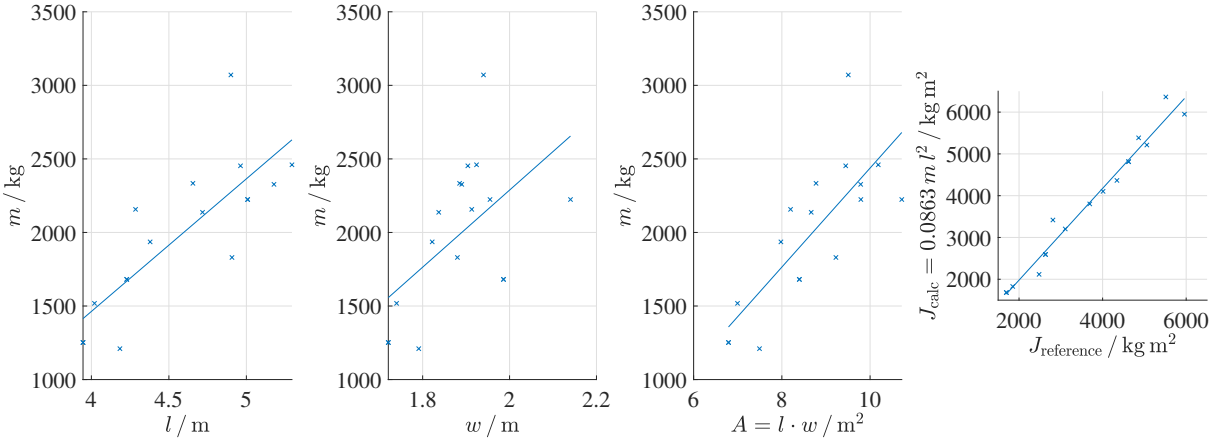

Figure 4.2: Indirectly measureable parameters - The first three subfigures show the correlation between vehicle mass and vehicle footprint. The fourth subfigure shows the correlation between the calculated moments of inertia and the values from the database. The correlation coefficients amount $\boldsymbol{\rho} = [0.8, 0.55, 0.78, 0.98]$ in the order of the given subfigures. The reference moment of inertia $J_{\mathrm{reference}}$ is solely used to show the correlation between the reference database (sec. 4.3.1) and used formula. Further on, the calculated value $J_{\mathrm{K}} = J_{\mathrm{calc}}$ is applied.

contrast to the ego vehicle, the parameters of the object are only obtained by exteroceptive sensors. Due to the low market penetration, emerging technologies, such as V2X communication, are not regarded. As result, only the dynamic state $\boldsymbol{z}_{\mathrm{K,dyn}}$ (instantaneous and future time steps due to dynamic model) and object shape l_{K}, w_{K} are obtained. All other influences needs to be determined in another way.

An exception constitute the mass m_{K} and moment of inertia J_{K}. Reference [100] shows a strong correlation of these parameters with the object shape. Thus, they are regarded as indirectly measurable in this thesis and determined independent of the tuning process of section 4.3. While the reference database (sec. 4.3.1) contains only 17 different vehicle types, related works have investigated much bigger databases with static parameters and thus it is assumed that their results are more precise compared to any potential fitting of section 4.3. The formula for the moment of inertia leads back to the findings of [214]. It is calculated by: $J_{\mathrm{K}} = 0.0863\, m\, l^2$. Moreover, [215] evaluates different inertia estimation methods and attests [214] to be a suitable approach. The mass m_{K} bases on a least squares fitting of a linear function. Figure 4.2 illustrates how the relationship fits to the used reference database (sec. 4.3.1).

Furthermore, the vehicle shape or rather shape representation constitute an other important aspect. Even if the footprint effects the geometrical accident constellation crucially and thus important input parameters such as the impact point, it is often simplified by a rectangle with length l and width w. This thesis uses a stadium area for the eccentric impact model (sec. 4.2.1) and multi-body system (sec. 4.2.3) with following advantages. At one hand, the stadium covers the vehicle front and rear shape more realistic than a rectangle. Nevertheless, also the stadium is an approximation of the vehicle contour and most probably cuts the vehicle corners slightly. Additionally, it should be noticed that the vehicle shapes

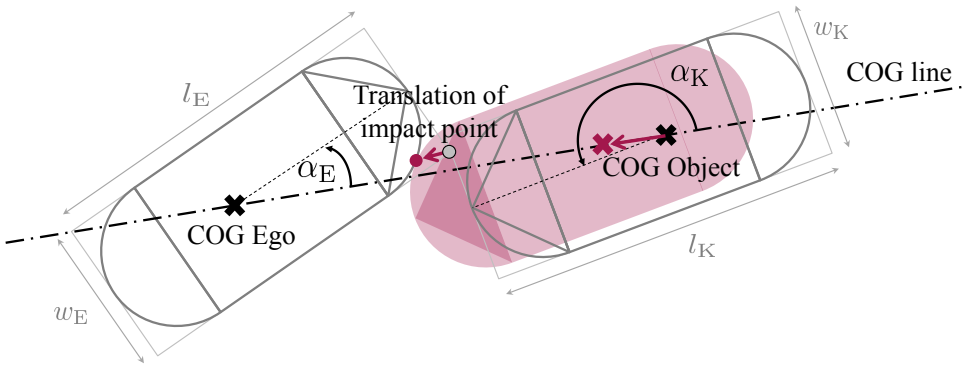

Figure 4.3: Vehicle shape representation - The figure shows a stadium ground area for both vehicles which results from a rectangular footprint. Changing the vehicle representation, it might occur that the vehicle no longer touch each other and thus they are translated along the COG line. As result, a new impact point is obtained.

can be determined independent of the vehicle contour for the calculation of the collision probability $P(C)$, which uses an overapproximating rectangle (sec. 3.1). Seeing that, arbitrary footprints seem possible. However, at the other hand, neglecting unrealistic side-side crashes due to holonomic constraints, an initial collision configuration of stadiums contains only one collision point rather than a collision line. Besides, that enables to formulate an unique tangential and normal coordinate system in the point of contact for the force insertion. In conclusion, the stadium provides an appropriate compromise between the vehicle contour and force insertion property. The mathematical models (sec. 4.2.4 and 4.2.5) uses the length l and width w as input while the centric impact is applied with a point mass (sec. 4.2.2). Besides, all prediction function η of section 4.2 focus on planar bodies what leads to a force exertion only in two dimensions.

What is more, changing the vehicle contour from one representation to an other (e.g., rectangle to stadium, rectangle to circle) following issue should be noticed. Starting with a crash constellation ω_{coll}, it may happen that the vehicles do not touch anymore when changing the footprint centered on the COG. Since it still constitutes an instantaneous substate, the vehicle shapes should not moved according the underlying dynamic but rather just shifted along the connecting line between the centers of gravity (COG line). That is assumed to suitably represent the force insertion. Figure 4.3 illustrates the procedure.

4.1.2 Output definition for pedestrian collisions

According to section 2.1.2.1, Δv constitutes the severity measure in this thesis. However, dealing with pedestrians as crash opponents a slightly modified strategy is pursued and thus further remarks are given in this section to the severity measure Δv_{ped}.

A collision with pedestrians is often modelled with an impact model and resulting throwing distance as shown for example in [133, sec. 4.7.5]. Thereby, it is assumed that a centric, head on collision is experienced by the pedestrian in the longitudinal vehicle direction due

to the small size and low mass compared to the vehicle. As result, the velocity changes during the crash $\Delta v_{\mathrm{E/K}}$ are obtained by:

$$\Delta v_{\mathrm{E}} = \frac{m_{\mathrm{K}}}{m_{\mathrm{K}} + m_{\mathrm{E}}}(v_{\mathrm{E}} - v_{\mathrm{K}})(e+1) \tag{4.3}$$

$$\Delta v_{\mathrm{K}} = \frac{m_{\mathrm{E}}}{m_{\mathrm{K}} + m_{\mathrm{E}}}(v_{\mathrm{K}} - v_{\mathrm{E}})(e+1) \tag{4.4}$$

$$\begin{aligned} \widetilde{\Delta v} &= q\,|\Delta v_{\mathrm{E}}| + |\Delta v_{\mathrm{K}}| \\ &= \frac{q\,m_{\mathrm{K}} + m_{\mathrm{E}}}{m_{\mathrm{K}} + m_{\mathrm{E}}}\,|v_{\mathrm{E}} - v_{\mathrm{K}}|\,(e+1) \end{aligned} \tag{4.5}$$

In general, the velocity change $\Delta v_{\mathrm{E/K}}$ depends on the masses $m_{\mathrm{E/K}}$, elasticity e and initial velocities $v_{\mathrm{E/K}}$. Contrary to the postulation of section 2.2.3, it is not suitable to prioritise the ego vehicle safety. Often, an emergency manoeuvre is especially conducted to protect the pedestrian. Therefore, a scaling factor q is defined to adjust the safety shares.

Assuming a factor $q = 0$, a fully elastic impact $e = 1$, and a much higher mass of the vehicle m_{E} compared to the mass of the pedestrian m_{K} the severity estimation simplifies to:

$$\psi_{\mathrm{ped}} = \Delta v_{\mathrm{ped}} \approx 2\,|\underbrace{v_{\mathrm{E}} - v_{\mathrm{K}}}_{v_{\mathrm{rel}}}| \quad \text{with} \quad m_{\mathrm{E}} \gg m_{\mathrm{K}},\ e = 1 \text{ and } q = 0 \tag{4.6}$$

Seeing that, the severity measure for pedestrians depends mainly on the relative velocity v_{rel}.

What is more, as mentioned earlier, the application determines the severity measure. In other words, the event "collision" is only appropriate to aim collision free driving due to the binary signal. Improving, the relative velocity v_{rel} enables to differentiate multiple objects but designates each object only with one severity value. Therefore, a more detailed Δv measure is used to differentiate multiple collision configurations in section 4.1.3. However, if pedestrians are involved, the safety strategy is restricted to either collision avoidance or sole collision mitigation by braking. Therefore, no detailed impact point needs to be differentiated and thus v_{rel} is regarded to be sufficient in that case.

4.1.3 Output definition for vehicle collisions

Section 2.1.2.1 introduces the severity measure as the absolute value of the vectorised change of velocity obtained by $\psi = \Delta v = |\Delta\vec{v}|$. In the case of rigid bodies, translation and rotation superimpose in a vehicle crash and thus the severity value is subdivided into two components:

$$\begin{aligned} \psi = \Delta v := |\Delta\vec{v}_{\mathrm{E,TM}}| &= |\vec{v}'_{\mathrm{E,TM}} - \vec{v}_{\mathrm{E,TM}}| \\ &= \Delta v_{\mathrm{E,trans}} + \Delta v_{\mathrm{E,rot,TM}} \\ &= \Delta v_{\mathrm{COG}} + r_{\mathrm{TM}}\,\Delta\omega_{\mathrm{COG}} \end{aligned} \tag{4.7}$$

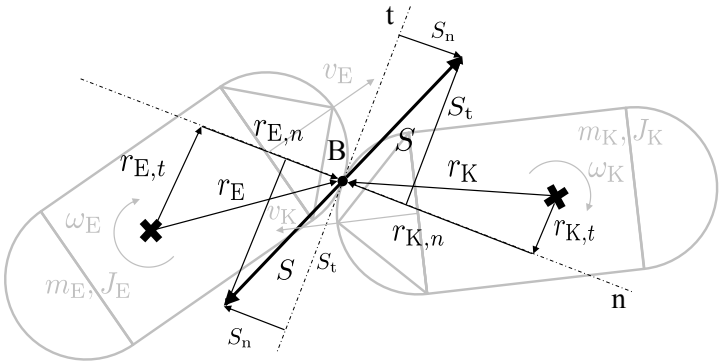

Figure 4.4: Eccentric impact model - It visualises the states $\boldsymbol{z}_{\mathrm{E/K}}$ and momentums occurring in an eccentric impact.

The translation of individual points of the rigid body is equal to the movement of the COG. The rotation bases on the change of the yaw rate $\Delta\omega$ weighted with the distance r from the COG. Due to section 2.2.3, the tunnel middle TM is chosen as reference point and thus the distance $r = r_{\mathrm{TM}}$ is determined accordingly. Disadvantageous in terms of normalisation, the severity measure $\psi = \Delta v$ does not saturate. In other words, the more kinetic energy is involved in the crash, the more the severity ψ increases. On the other hand, it is approximately limited due to the possible driving velocities. Nonetheless, the scalcar value Δv could be transferred with injury risk functions (fig. 2.4) to a probability value known limits.

4.2 Prediction models

The following prediction models base directly on the discussion presented in section 2.1.2.3 and its summary of table 2.2.

4.2.1 Eccentric impact model

The eccentric impact model superimpose the conservation of momentum (translation) and principle of angular momentum (rotation). The forces or rather momentums are applied in the point of contact B. Due to the stadium shape of the objects and holonomic constraints of the vehicles, the direction of the momentum $\boldsymbol{S}$ is deterministic defined. The shapes separate a tangential S_t and normal S_n component which touch or intersect vertically, respectively, the two rigid bodies at the contact point B. Thereby, the state vectors $\boldsymbol{z}_{\mathrm{E/K}}$ include the velocities $v_{\mathrm{E/K}}$, the yaw rate ω, masses $m_{\mathrm{E/K}}$, moment of inertias $J_{\mathrm{E/K}}$ and distances $r_{\mathrm{t/n}}$ between the COG and contact point B. The velocities and yaw rates after the crash are marked with a "'" sign. Figure 4.4 illustrates the impact of the two rigid bodies.

As result, following equations describe the impact:

$$\begin{pmatrix} m_{\mathrm{E}}(v_{\mathrm{E,n}} - v'_{\mathrm{E,n}}) \\ m_{\mathrm{E}}(v_{\mathrm{E,t}} - v'_{\mathrm{E,t}}) \\ 0 \end{pmatrix} = \begin{pmatrix} S_{\mathrm{n}} \\ S_{\mathrm{t}} \\ 0 \end{pmatrix} \tag{4.8}$$

$$\begin{pmatrix} m_{\mathrm{K}}(v_{\mathrm{K,n}} - v'_{\mathrm{K,n}}) \\ m_{\mathrm{K}}(v_{\mathrm{K,t}} - v'_{\mathrm{K,t}}) \\ 0 \end{pmatrix} = \begin{pmatrix} -S_{\mathrm{n}} \\ -S_{\mathrm{t}} \\ 0 \end{pmatrix} \tag{4.9}$$

$$\begin{pmatrix} 0 \\ 0 \\ J(\omega'_{\mathrm{E}} - \omega_{\mathrm{E}}) \end{pmatrix} = \begin{pmatrix} r_{\mathrm{E,n}} \\ r_{\mathrm{E,t}} \\ 0 \end{pmatrix} \times \begin{pmatrix} S_{\mathrm{n}} \\ S_{\mathrm{t}} \\ 0 \end{pmatrix} = \begin{pmatrix} 0 \\ 0 \\ r_{\mathrm{E,n}} S_{\mathrm{t}} - r_{\mathrm{E,t}} S_{\mathrm{n}} \end{pmatrix} \tag{4.10}$$

$$\begin{pmatrix} 0 \\ 0 \\ J(\omega'_{\mathrm{K}} - \omega_{\mathrm{K}}) \end{pmatrix} = \begin{pmatrix} r_{\mathrm{n}} \\ r_{\mathrm{t}} \\ 0 \end{pmatrix} \times \begin{pmatrix} S_{\mathrm{K,n}} \\ S_{\mathrm{K,t}} \\ 0 \end{pmatrix} = \begin{pmatrix} 0 \\ 0 \\ r_{\mathrm{E,n}} S_{\mathrm{t}} - r_{\mathrm{E,t}} S_{\mathrm{n}} \end{pmatrix} \tag{4.11}$$

Owing to 6 equations but 8 unknowns, the system is underdetermined and thus further hypotheses are required to derive the posteriori velocities. Therefore, assumptions on the elasticity and friction are made according to [133, sec. 4.4.3]. It is assumed that the crash opponents do not remain stucked after the crash and thus the elasticity works solely in the normal direction. The coefficient of restitution $e \in [0,1]$ describes the relation between the phase of compression with the change of momentum ΔS_{com} and the phase of restitution with the change of momentum ΔS_{res}:

$$e = \frac{\Delta S_{\mathrm{res}}}{\Delta S_{\mathrm{com}}} = \frac{\int_{t^*}^{t'} F_B \mathrm{d}t}{\int_{t}^{t^*} F_B \mathrm{d}t} \tag{4.12}$$

Detailed information about the impact process are for example presented in [138, sec. 5.3]. In the compression phase, the two velocities $v_{\mathrm{E/K,B}}$ at the point B converges. Afterwards, the energy in the material tries to restore the initial situation. If no kinetic energy is lost, the restitution coefficient amounts to $e = 1$, also called a perfectly elastic collision. In other words, the momentum of the compression is similar to the momentum of the restitution: $\Delta S_{\mathrm{com}} = \Delta S_{\mathrm{res}}$. If parts of the kinetic energy are changed to some other forms of energy, such as deformation energy, the coefficient of restitution is $e < 1$. In a perfectly inealstic collision, the two objects are stucked after the collision and no restitution is happened: $\Delta S_{\mathrm{res}} = 0$. Thus, the coefficient of collision is $e = 0$. According to [133, sec. 4.4.6], equation 4.12 is equivalently expressed by the relative velocities in the contact point B before and after the collision:

$$e = -\frac{v'_{\mathrm{rel,n},B}}{v_{\mathrm{rel,n},B}} = -\frac{v'_{\mathrm{K,n,B}} + r_{\mathrm{t}}\omega'_{\mathrm{K}} - v'_{\mathrm{E,n,B}} - r_{\mathrm{t}}\omega'_{\mathrm{K}}}{v_{\mathrm{K,n,B}} + r_{\mathrm{t}}\omega_{\mathrm{K}} - v_{\mathrm{E,n,B}} - r_{\mathrm{t}}\omega_{\mathrm{K}}} \tag{4.13}$$

The second hypothesis relates to the friction during the collision phase. The coefficient of friction μ relates the momentum in normal and tagential direction at the impact Point B:

$$\mu = \frac{S_{\mathrm{t}}}{S_{\mathrm{n}}} \tag{4.14}$$

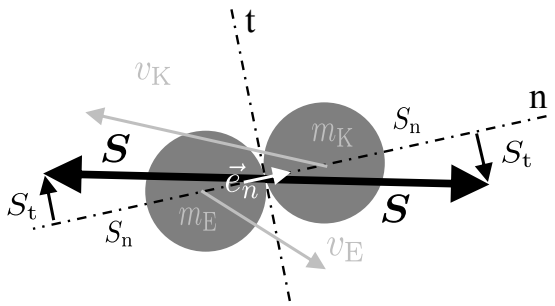

Figure 4.5: Centric impact model - It visualises the states $\boldsymbol{z}_{\mathrm{E/K}}$ occurring in a centric impact.

With reference to section 4.1.1, all input parameters are measurable apart from the coefficient of restitution e and the coefficient of friction μ. Therefore, they are determined data driven and hence constitute the training parameters $\boldsymbol{z}_{\mathrm{train}} = (e, \mu)^{\mathrm{T}}$ in section 4.3.

4.2.2 Centric impact model

The centric impact model simplifies the eccentric impact presented in section 4.2.1. A centric impact means that the centers of gravity $\mathrm{COG}_{\mathrm{E/K}}$ of both vehicles need to lie on a line relating to the normal impact vector $\vec{e}_n = \frac{\vec{S}_n}{|S_n|}$. In this thesis that is enforced by reducing the crash opponents to point mass and thus the shape to points with $\boldsymbol{r}_{\mathrm{E}} = \boldsymbol{0}$ and $\boldsymbol{r}_{\mathrm{K}} = \boldsymbol{0}$. Consequently, there exists no longer a distance between the COG and the impact point B and thus the impact vectors $\boldsymbol{S}$ yields no torque. Therefore, the principle of angular momentum can be neglected. As result, the equations 4.8 to 4.11 reduce to the number 4 with 6 unknowns:

$$\begin{pmatrix} m_{\mathrm{E}}(v_{\mathrm{E,n}} - v'_{\mathrm{E,n}}) \\ m_{\mathrm{E}}(v_{\mathrm{E,t}} - v'_{\mathrm{E,t}}) \\ 0 \end{pmatrix} = \begin{pmatrix} S_{\mathrm{n}} \\ S_{\mathrm{t}} \\ 0 \end{pmatrix} \tag{4.15}$$

$$\begin{pmatrix} m_{\mathrm{K}}(v_{\mathrm{K,n}} - v'_{\mathrm{K,n}}) \\ m_{\mathrm{K}}(v_{\mathrm{K,t}} - v'_{\mathrm{K,t}}) \\ 0 \end{pmatrix} = \begin{pmatrix} -S_{\mathrm{n}} \\ -S_{\mathrm{t}} \\ 0 \end{pmatrix} \tag{4.16}$$

The remaining two conditions are determined by the restitution coefficient e and the friction coefficient μ similar to the eccentric impact model. Both parameters are the training parameters $\boldsymbol{z}_{\mathrm{train}} = (e, \mu)^{\mathrm{T}}$ in the data driven approach.

4.2.3 Multi-body system

Modelling multi-body systems, the elastoplastic behaviour of the vehicle in a crash is represented by a system of nonlinear differential equations second order. Thereby, each equation

describes the movement of one partial mass. Using a matrix of masses $\boldsymbol{M}$, dampers $\boldsymbol{C}$, and stiffnesses $\boldsymbol{K}$, a vector of external forces $\boldsymbol{f}(t)$, and the vector of displacements $\boldsymbol{\varepsilon}$, the interaction in one dimension (e.g., x) is described by:

$$\boldsymbol{M}(t,\boldsymbol{\varepsilon}_x)\ddot{\boldsymbol{\varepsilon}}_x + \boldsymbol{C}(t,\boldsymbol{\varepsilon}_x)\dot{\boldsymbol{\varepsilon}}_x + \boldsymbol{K}(t,\boldsymbol{\varepsilon}_x)\boldsymbol{\varepsilon}_x = \boldsymbol{f}(t) \tag{4.17}$$

However, the geometrical crash constellation has a degree of freedom DOF = 3 with regard to $\Delta\tilde{g} = [\Delta x, \Delta y, \Delta\varphi]^{\mathrm{T}}$ and thus the equation 4.17 needs to be tripled for the translation in the second direction and the rotation to cover the general case. In this thesis, the approach of [105] is adopted which considers the translational forces in two dimensions and the rotation by the feedback of the crash forces to a motion model. That enables a smooth transition between the pre-, in- and post-crash phase. Thereby, the approach of [105] bases on several assumptions without further explanations. Therefore, the process steps are generalised as presented in detail in the previous publication [29]. As result, it is possible to derive multiple instances and thus to select the most promising for further investigations. What is more, it is referred to [105] for the general understanding or rather further information of the approach. This section focus solely on the adaptation.

The crash interaction is divided into three main components as expressed by the following equations, which are applied to the ego vehicle as well as to the object likewise:

$$\sigma = f_{\text{material}}(\varepsilon, \dot{\varepsilon}, \boldsymbol{\xi}_m) \tag{4.18}$$

$$\begin{pmatrix} \boldsymbol{F} \\ \boldsymbol{r}_F \end{pmatrix} = \boldsymbol{f}_{\text{force}}(\varepsilon, \boldsymbol{\xi}_{\text{g}}, \sigma) \tag{4.19}$$

$$\dot{\boldsymbol{z}}_{\text{cm}} = \tau_{\text{cm}}(\boldsymbol{z}_{\text{cm}}, \boldsymbol{F}, \boldsymbol{r}_F, \boldsymbol{\xi}_g) \tag{4.20}$$

First of all, the structure of the mechanical basic circuit (equ. 4.18) needs to be defined representing the material characteristics of the colliding objects. According to [216, sec. 1.3 and 1.4], these include properties of the of elasticity, viscosity, and plasticity which are represented by springs (Hooke element), dampers (Newton element), and coulomb elements, respectively. As result, the mechanical load σ is derived in dependence on the mechanical parameters $\boldsymbol{\xi}_m$ and the deformation ε. Thereby, it is possible to represent the basic elements by constant values $\boldsymbol{\xi}_m = \text{const}$ or, more general, by an arbitrary function of the deformation ε or its change rate $\dot{\varepsilon}$. A complex function provides more tuning parameters and thus the chance of a more individual representations of the crash kinetic. On the other hand, the execution time rises due to the increased number of calculations.

Secondly, multiple basic circuits with the mathematical representation of the load σ are connected in series or parallel accordingly to the geometrical parameters $\boldsymbol{\xi}_g$ of the vehicles (equ. 4.19). For example, [105] defines segments on the body footprint each including a basic circuit (equ. 4.18) of a Kelvin model $\sigma = k\,\varepsilon + c\,\dot{\varepsilon}$ with the stiffness k and the damping coefficient c as mechanical parameters $\boldsymbol{\xi}_m = (k, c)^{\mathrm{T}}$. Thereby, the level of overlap in the dedicated segment scales the properties of the mechanical basic circuit and thus defines the mechanical structure for the current time step of the accident process. As result, the collision force $\boldsymbol{F}$ and vector of force insertion $\boldsymbol{r}_F$ are obtained in dependence on that mechanical circuit and the deformation ε which itself depends on the current state $\boldsymbol{z}_{\text{cm}}$ of the

crash motion. As result, the calculations depend on the geometrical properties $\boldsymbol{\xi}_g$ which include the vehicle representation (rectangle, stadium etc.), the number of segments, and the alignment (series, parallel) of the basic circuits. Furthermore, it is possible to reduce the dimensionality to one dimensional circuits neglecting the second direction and rotations in the crash mechanics.

Finally, the motions of the vehicles are calculated (equ. 4.20) regarding the collision forces $\boldsymbol{F}$. They are inserted at the collision point $\boldsymbol{r}_F$ to the dynamic model $\dot{\boldsymbol{z}}_{\mathrm{cm}} = \tau_{\mathrm{cm}}(\boldsymbol{z}_{\mathrm{cm}}, \boldsymbol{F}, \boldsymbol{r}_F, \boldsymbol{\xi}_g)$ with the state $\boldsymbol{z}_{\mathrm{cm}}$. Thereby, it is free to chose the complexity of the crash motion modelling. By way of example, the dynamic models may range between pure kinematic and advanced two-track-models as presented in [105].

All in all, the presented approach based on [105] combines the the modelling of the crash mechanics by multi-body systems with the motion behaviour due to a crash dynamic model. Thereby, each calculation step (equ. 4.18 to 4.20) needs further specifications to derive the final modelling instance. Therefore, a set of promising combinations is investigated in a hyper parametrisation as presented in the previous publication [29] with the objective to derive the most promising representative for the multi-body systems. As basic circuit the spring, Kelvin, and Prandtl circuit are taken into account. While the spring and Kelvin model are often used in related work, the Prandtl circuit (spring and coloumb elment in series) provides the chance to map the elastoplastic crash behaviour more detailed. The single elements are regarded either with constant parameters or by a cubic spline with 5 supporting points. The number of segments along the footprint is simplified to one big area. Moreover, the influence of one or two dimensional calculations are investigated. The dynamic model is represented by a rigid body and a point mass due to the assumed reduction of the computation time consumption.

A 2D Kelvin model with constant parameters over one geometrical segment, which applies the collision force F to a kinematic point mass model, obtains the best results, as discussed in detail in the previous publication [29], and hence is compared to the other prediction approaches in section 4.3.3. Figure 4.6 visualises the selected multi-body system.

4.2.4 Feedforward neural network

A feedforward neural network is used to propagate the input accident constellation $\boldsymbol{z}_{\mathrm{input}}$ to the severity output Δv.

The input $\boldsymbol{z}_{\mathrm{input}}$ needs to contain the most sensitive dependencies of the accident severity. According to [111], that includes the impact point, velocities and masses. Further it states that all other characteristics are either not important or are indirectly covered by the statistically trained function. Therefore, the input layer bases on measurable data from the accident constellation (sec. 4.1.1): $\boldsymbol{z}_{\mathrm{input}} = [\alpha_{\mathrm{E}}, \alpha_{\mathrm{K}}, v_{\mathrm{E}}, v_{\mathrm{K}}, \omega_{\mathrm{E}}, \omega_{\mathrm{K}}, l_{\mathrm{E}}, l_{\mathrm{K}}, w_{\mathrm{E}}, w_{\mathrm{K}}, m_{\mathrm{E}}, m_{\mathrm{K}}, J_{\mathrm{E}}, J_{\mathrm{K}}]^{\mathrm{T}}$. That includes the angles to the line between the COGs $\alpha_{\mathrm{E/K}}$, the velocities $v_{\mathrm{E/K}}$, the yaw rates $\omega_{\mathrm{E/K}}$, the dimensions $l_{\mathrm{E/K}}$ and $w_{\mathrm{E/K}}$, masses $m_{\mathrm{E/K}}$, and moment of inertias $J_{\mathrm{E/K}}$. Thereby, it is noticeable that the geometric constellation of the two objects $\tilde{g}_{\mathrm{E/K}} = [x_{\mathrm{E/K}}, y_{\mathrm{E/K}}, \varphi_{\mathrm{E/K}}]^{\mathrm{T}}$

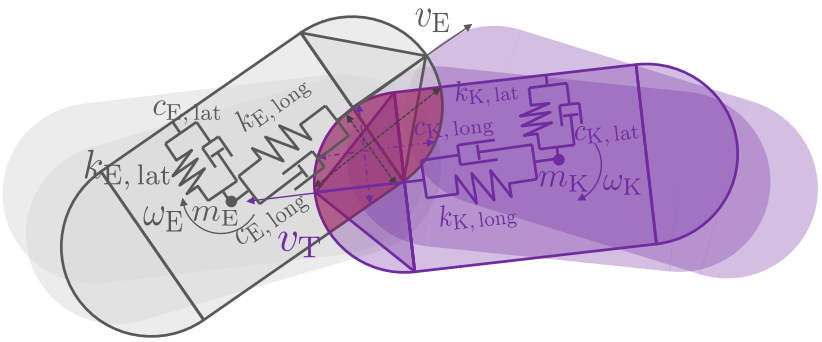

Figure 4.6: Multi-body system - The figure illustrates the procedure of the selected multi-body system. According to the level of overlap (red highlighted) the basic elements $\boldsymbol{\xi}_m = (k,c)^\mathrm{T}$ are linearly scaled. The resulting mechanical circuit in longitudinal and lateral direction of the ego and object vehicle is used to calculate the collision forces. These influence the crash motion and thus the level of overlap for the next iteration step. The procedure is repeated until the end of the collision.

is aggregated to two angles $\alpha_\mathrm{E/K}$. The COG line is visualised in figure 4.3 as well as the position of the corresponding angles. At one hand, that reduces the number of independent variables and thus the complexity of the net topology. On the other hand, that describes the object position independent of vehicle shapes what makes it compatible to other representations. Nevertheless, the impact point is indirectly included. It can be reconstructed using the two angles, a vehicle shape and the definition that the ego vehicle always remains on the left side compared to the object vehicle.

The number of layers and neurons is determined by a hyper parametrisation as described in section 4.3.2. At first, only one hidden layer is defined to keep the net topology simple with respect to the real time application. On the other hand, related work, such as [217], state that also one hidden layer is sufficient for arbitrary representations depending on the number of neurons. Therefore various topologies with different count of neurons are investigated with a cross validation on the test data. Thereby, the search is limited to 250 neurones due to the computation time consumption. As result, the optimal solution of 36 neurons is chosen for the training with all test data. The neurons of the hidden and output layer use a “tanh“ and linear activation functions, respectively. More details about the hyper parametrisation are contained in the previous publication [29].

4.2.5 Random forest regression

The random forest regression uses the method of *ensemble learning* to combine multiple decision trees. The final output bases on the average of these multiple trees, whereby each tree is trained only with a random subset of the training data preventing overfitting. Furthermore, the amount of training data decrease for deeper nodes and the split on every node depends on a random subset of features. The selection of input features follows the discussion of section 4.2.4 with $\boldsymbol{z}_\mathrm{input} = [\alpha_\mathrm{E}, \alpha_\mathrm{K}, v_\mathrm{E}, v_\mathrm{K}, \omega_\mathrm{E}, \omega_\mathrm{K}, l_\mathrm{E}, l_\mathrm{K}, w_\mathrm{E}, w_\mathrm{K}, m_\mathrm{E}, m_\mathrm{K}, J_\mathrm{E}, J_\mathrm{K}]^\mathrm{T}$.

According to [218], the number of trees N_t, features per nodes N_v, data split for each tree N_{ds}, and data assignment for each node N_{da} need to be determined in the hyper parametrisation (sec. 4.3.2). Moreover, [219] shows in empirical studies that the performance of the random forest does not increase significantly with lager forests than $N_t > 100$ trees for the most problems. Therefore, a tree number of $N_t = 100$ and $N_t = 2000$ is investigated exemplary. The depth of the trees is specified indirectly with numbers of features per nodes N_v and the minimum datasets N_{da} per node. The optimal number of input nodes is searched between $N_v \in [1:1:|\boldsymbol{z}_{\text{input}}| = 14]$. According to [218], one third of the input values is a most common standard value: $N_v = \frac{|\boldsymbol{z}_{\text{input}}|}{3}$. The data amount for each specific decision tree is varied between $N_{ds} \in [10:1:100]\%$. However, often all available date are used in each decision tree [218]. The size of the data subsets is determined between $N_{da} \in [1,50]$.

The results of the hyper parametrisation show that the random forest with $N_t = 2000$ decision trees performs slightly better compared to the smaller random forest with $N_t = 100$. However, the bigger instance exceeds the available computation time. Seeing that, and referring to the recommendation of [219], the number of decision trees is set to $N_t = 100$. The systematic search for the other hyper parameters obtains the full input features per node $N_v = 14$, almost all data in each decision tree $N_{ds} = 0.99$ and a node size of $N_{da} \geq 2$. Further details on the hyper parametrisation are presented in the previous publication [29].

4.3 Parameterisation

4.3.1 Reference database

FEM simulations are regarded as ground truth to evaluate the performance of the severity prediction models. At one hand, they could count as very accurate prediction model itself. On the other hand, they have a special status due to the degree of modelling, calculation accuracy, and the validation with real crash data.

The database include a detailed description of the accident configuration ω_{coll} immediate before the crash as well as the simulation results (acceleration courses) for dedicated nodes of the FE model. Among others, all measurable input parameters of equation 4.2 are available. The reference severity ψ for each crash is obtained from the acceleration course of the reference point (sec. 2.2.3) by time integration. Typically, a crash course takes about $150-300\,\text{ms}$ simulation time. The reference database contains 6219 samples. Even if that number is huge compared to the databases used in the related work (sec. 2.1.2.3), it should be noticed that it still constitutes a sparse coverage referring to the 15 input features $\boldsymbol{z}_{\text{input}}$ of equation 4.2. That refers to the *curse of dimensionality*. A fleet of 17 different vehicles of the Volkswagen Group is used in the FEM crash simulations and thus ensures the diversity of the vehicle structures including static parameters, such as $\boldsymbol{\xi}_{\text{static}} = [l,b,m,J]^{\text{T}}$. The models range between small cars, heavy sports utility vehicles (SUV), and one truck. Table 4.1 gives a short overview about important parameter ranges of the underlying fleet. What is more, the database does not contain the full permutation of the vehicle types. Rather 51 different combinations are covered and thus about 122 elements remain in average for the

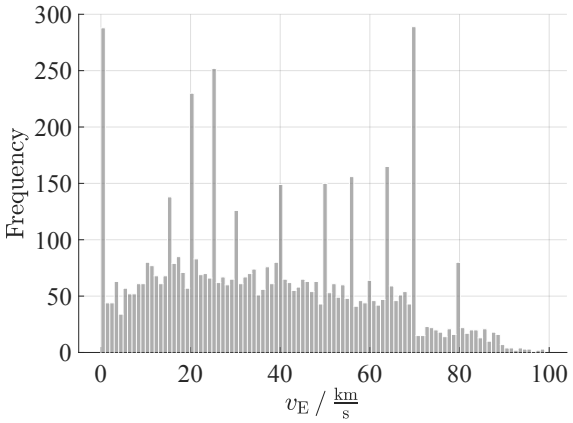

(a) Frequency of samples with ego velocity v_E

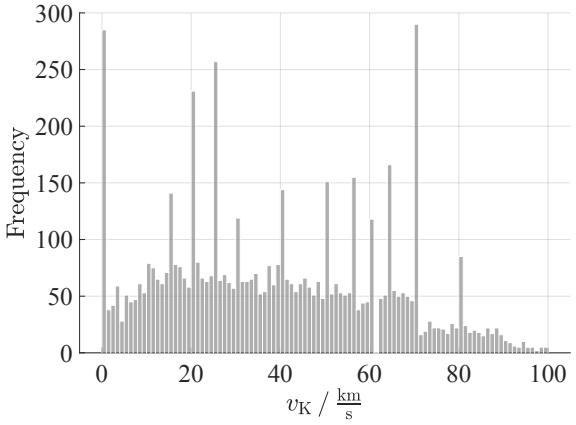

(b) Frequency of samples with object velocity v_K

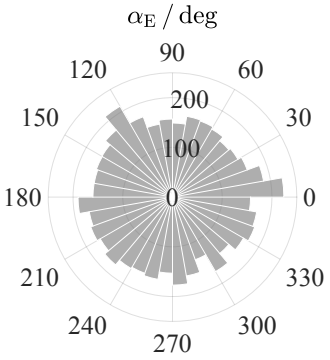

(c) Frequency of samples with ego angle α_E

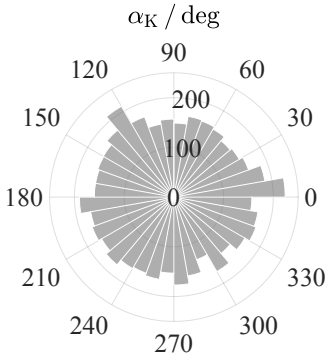

(d) Frequency of samples with object angle α_K

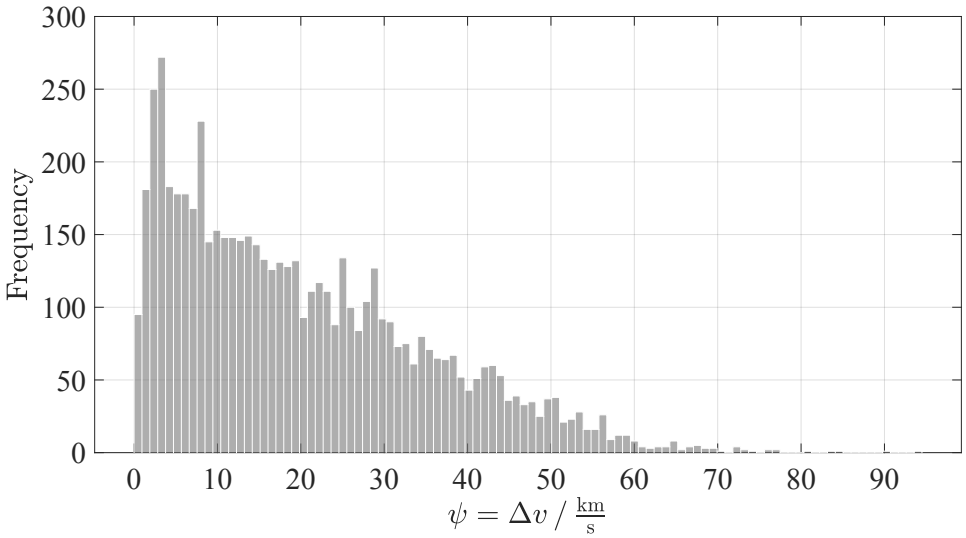

(e) Frequency of samples with reference severity ψ

Figure 4.7: FEM reference database (histograms) - Subfigures (a)-(d) refer to measureable input. They show histograms with reference to important geometric and dynamic features of an accident configuration ω_coll at the crash beginning at time t_0 according to the samples of the FEM reference database. Subfigure (e) visualises the related reference output ψ. Besides, the linkage to figure 4.1 should be noticed in this context.

geometrical accident constellations and initial velocities for each case. These input feature are distributed more or less systematically over the available elements. Only the yaw rates $\omega_{\mathrm{E/K}}$ constitutes an exception and are neglected by $\omega_{\mathrm{E/K}} = 0$. Figure 4.7 shows histograms of important geometric $[\alpha_{\mathrm{E}}, \alpha_{\mathrm{K}}]$ and dynamic $[v_{\mathrm{E}}, v_{\mathrm{K}}]$ features of an accident configuration ω_{coll} at the crash beginning at time t_0. Moreover, it visualises the related reference output ψ. Thereby, the vehicles have in general still a velocity when running out of the collision and thus higher frequencies of lower severities occur.

Table 4.1: FEM reference database (characteristics) - It gives an overview to characteristic values and ranges of the FEM reference database according to the measureable input $\boldsymbol{z}_{\mathrm{input}}$ (equ. 4.2).

	Model type	Vehicle twosome	Length l / m	Width w / m	Mass m / kg	Moment of inertia J / kg m^2
Number / range	17	51	3.9 - 7.7	1.7 - 3.0	1210 - 19073	1697 - 67752

4.3.2 Training strategy

The parametrisation or training of the prediction models (sec. 4.2) constitutes an optimisation problem. The objective is to find the optimal parameters $\boldsymbol{z}^*_{\mathrm{train}}$ for each model which minimise the cost value E:

$$\boldsymbol{z}^*_{\mathrm{train}} = \arg\min_{\boldsymbol{z}_{\mathrm{train}}} E(\boldsymbol{z}_{\mathrm{train}}) \tag{4.21}$$

This thesis use the mean squared error (MSE) between the predicted accident severity $\hat{\psi}$ and the related reference values ψ as cost function:

$$E = \mathrm{MSE} = \frac{1}{n}\sum_{i=1}^{n}\Big(\underbrace{\hat{\psi}_i - \psi_i}_{e_{\psi,i}}\Big)^2 \tag{4.22}$$

The square ensures that the errors do not eliminate each other and weights outliers more compared to related, well fitting values.

Theoretically, it does not matter which numerical values the parameters $\boldsymbol{z}^*_{\mathrm{train}}$ have as long as the models predict the accident severity $\hat{\psi}$ with sufficient accuracy. On the other hand, the prediction models presented in section 4.2.1 to 4.2.3 have a mechanical background and thus constraints are defined with reference to the physical plausibility. That is supposed to enhance the interpretability of the calculations. In the field of vehicle safety that might be an important property as discussed in section 2.1.3.3. Table 4.2 shows an overview of the chosen constraints. According to the modelling, the restitution and friction coefficient of the impact models are restricted between 0 and 1. The limits of the basic elements for the multi-body systems are obtained experimentally according to the reference data. The neural

Table 4.2: Model constraints - The physical models are constrained due to the interpretability. Besides, it summaries the training parameters $\boldsymbol{z}_{\text{train}}$ (sec. 4.2.1 to 4.2.3). The mathematical predictors have no physical parameters and thus are here out of scope.

Model	Parameter	Range
Impact model	Coefficient of elasticity e	[0, 1]
	Coefficient of friction μ	[0, 1]
Multi-body system	Elasticity k	[0, 20] kNm^{-1}
	Damping c	[0, 20] kNsm^{-1}
	Yield stress f_y	[0, 100] kNm

network and random forest are regarded as black box models and thus no further constrains are specified.

The optimisation solver needs to be chosen according to the form of the underlying mathematical problem. A screening for the impact models has derived that a gradient based optimisation is enough to find the optimal solution. Therefore, the *trust-region-reflective* method [220] is used to obtain the training parameter $\boldsymbol{z}^*_{\text{train}}$. Contrary, the multi-body systems have a highly nonlinear structure and the calculation time is assumed much higher. Therefore, a *surrogate* optimisation algorithm is applied [221]. The parameters of the neural network and random forest are obtained with the Matlab toolboxes [222] and [223], respectively.

The reference database constitute only a sparse representation of possible accident configurations. Thus, procedures of the statistical learning are used to optimise the model accuracy as well as to evaluate the generalisation capabilities. The problem statement refers to supervised learning where the input and output relation is contained in the reference database. The database is randomly splitted into a portion for the training and testing with a relation of 80 % to 20 %. The training data are used to obtain the optimal parameters $\boldsymbol{z}^*_{\text{train}}$ according to the available data and the testing data are used to evaluate the generalisation. Additionally, the prediction models of section 4.2.3 to 4.2.5 have hyper parameters which need to be pre-determined. Therefore, a hyper parametrisation is conducted by systematic variations of these parameters. Thereby, the investigation refers solely to the training data to avoid crossinfluences with the following optimisation. Due to a sparse reference database, a *cross validation* on the training data is applied whereby the dataset is divided into $n = 5$ equal sized parts. The model tuning is repeated n-times for each model instance with changing $n-1$ portions for the training and the residual dataset for the validation. The results of the hyper parametrisation have been already discussed in the dedicated section of the prediction models. Finally, the most promising model instances with the optimal hyper parameters are tuned with all available training data.

Apart from the pure data representation, further investigations on the prediction performance are conducted. Thereby, it is focused on the accuracy of the most relevant data points as well as on the execution time. The following discussion refers to the test dataset.

Figure 2.4 visualises the relation between the accident severity $\psi = \Delta v$ and the probability of injury. It shows that a severity of $\psi < 8\,\frac{m}{s}$ implies a low injury probability and a severity of

$\psi > 20\,\frac{m}{s}$ indicates a severe injury in almost every case. Seeing that, it might be reasonable to demand for different accuracy levels depending on the current accident case or rather severity outcome. Therefore, the approach of [224] is adopted. It transfers the idea of *precision* and *recall*, which is originally intended for classification problems, to the function approximation.

The evaluation of a binary classifier refers often to the permutation of the vectors (true T, false F) and (positive P, negative N). Accordingly, precision and recall are defined by the relation between true positives TP and all positive classified values, and the relation between the true positives TP and the combined group of true positives TP and false negatives FN, respectively. More general, according to [224], the precision measures the relation of effective events to all events retrieved by the model while recall depicts the ratio of relevant events to all events retrieved by the model:

$$\text{precision} = \frac{\text{TP}}{\text{TP}+\text{FP}} \quad \rightarrow \quad \text{precision} = \frac{\sum \alpha(\hat{\psi}_i, \psi_i) \cdot \phi(\hat{\psi}_i)}{\sum \phi(\hat{\psi}_i)} \tag{4.23}$$

$$\text{recall} = \frac{\text{TP}}{\text{TP}+\text{FN}} \quad \rightarrow \quad \text{recall} \quad = \frac{\sum \alpha(\hat{\psi}_i, \psi_i) \cdot \phi(\psi_i)}{\sum \phi(\psi_i)} \tag{4.24}$$

Thereby, the accuracy function $\alpha(\hat{\psi}_i, \psi_i)$ indicates the quality of a prediction while the relevance function ϕ indicates the importance of a sample. In other words, both functions provide binary classes and thus a binary output on the continuous regression function is applied.

Figure 4.7 shows a misalignment to lower severity values ψ. However, these values have no significant impact on the injury severity pursuant to figure 2.4. Therefore, the relevance function ϕ is defined as a step function which filters relevant samples by $\psi \geq 8\,\frac{m}{s}$. The injury risk function starts to increase from about 1 % at that threshold. For the accuracy function α, two thresholds are defined which indicate the allowed under- and overestimation. With reference to the probability of injuries (fig. 2.4), a maximal allowed underestimation error $\Delta P_{\text{neg}} = 10\,\%$ and a maximal allowed overestimation error $\Delta P_{\text{pos}} = 15\,\%$ determines the interval of accuracy $e_\psi \in [e_{\psi,\text{neg}}, e_{\psi,\text{pos}}]$, in which the function α has the value 1. The value ΔP_{pos} is chosen greater than the value ΔP_{neg} due to the safety impact. A overestimation is regarded less harmful compared to an underestimation. The accuracy function α refers to the previously defined error value: $\alpha(\hat{\psi}_i, \psi_i) = e_{\psi,i}$.

Furthermore, the precision and recall are aggregated to one value by the F1-score:

$$\text{F1} = 2 \cdot \frac{\text{precision} \cdot \text{recall}}{\text{precision} + \text{recall}} \tag{4.25}$$

The execution times of the prediction functions are evaluated to assess the real time application. Since the final product hardware is not known, the benchmark is seen more as a relative comparison rather than an absolute feasibility study. Moreover, a function $g(t)$ is defined to scale the execution time between 0 and 1. That enables to relate the efficiency results to the prediction quality in a similar value range. Assuming a driving planning step of 200 ms (sec. 6.3) and at least 10 model executions, the maximum execution time for the prediction

models is defined by $t_{\max} = 20\,\text{ms}$. A lower boundary is assumed by $t_{\text{opt}} = 2\,\mu\text{s}$ which is supposed to indicate a carefree real time application. Since the measurement is conducted with Matlab, an experience scaling value of 100 is added due to the expected speed-up on optimised programming as discussed by [105]. The execution time values are obtained with an Intel i7-8850H CPU.

Finally, the F1-score and execution time $g(t)$ are aggregated by the harmonic mean:

$$\text{T} = 2 \cdot \frac{\text{F1} \cdot g(t)}{\text{F1} + g(t)} \tag{4.26}$$

4.3.3 Model evaluation

This section evaluates the most promising instance of each model type presented in section 4.2. Further information on the model selection are presented in the dedicated subsections.

Figure 4.8 visualises the training and test errors e_ψ by the quantiles, ranges for the outliers, as well as the mean value. It is plainly seen, that the centric impact model simplifies the collision mechanics much stronger compared to all other prediction models. The mean errors for both, the training and test phase, amount $\bar{e}_{\psi,\text{train,test}} \approx 6.5\,\frac{m}{s}$. Contrary, the neural network and random forest models obtain the best results. Moreover, the neural network with a mean testing error of $\bar{e}_{\psi,\text{test}} \approx 1.0\,\frac{m}{s}$ outperforms the random forest with a mean testing error of $\bar{e}_\psi \approx 1.5\,\frac{m}{s}$ a bit. The eccentric impact model and the Kelvin model yield a mean testing error with $\bar{e}_{\psi,\text{test}} \approx 1.7\,\frac{m}{s}$ and thus are a little worse compared to the mathematical models. On the other hand, the physical modelling leads to a small difference between the training and test phase. In other words, these models seems to have a much higher generalisation capability compared to the neural network and random forest. In the case of the random forest, the error rises $\Delta e_\psi \approx 230\,\%$ between the training and test phase. The difference related to the neural network amounts $\Delta e_\psi \approx 150\,\%$. However, the mean testing errors are still lower compared to the mean errors of the physical models.

Figure 4.9 contrasts the posteriori investigations for the selected prediction models. Apart from the multi-body system, all prediction models seems suitable for real time applications pursuant to the value $g(t)$. According to the prediction accuracy, the neural network has the highest F1-score (87 %) followed by the Kelvin model (81.5 %). The eccentric impact model (69 %) and random forest (68 %) have a small gap in the negative direction compared to the other both predictors. Aggregating the execution time $g(t)$ and F1-score in the T-value, the eccentric impact model provides a better balance between calculation time consumption and accuracy compared to the Kelvin model and random forest.

Summarising, the neural network obtains the best results in almost every category. Only the generalisation performance lags behind the physical models. Since the random forest is similar in the underlying properties of a black box model to the neural network, it is not regarded further on seeing the poorer results. Besides, the random forest is outperformed slightly by the eccentric impact model which takes the second place according to the T-value.

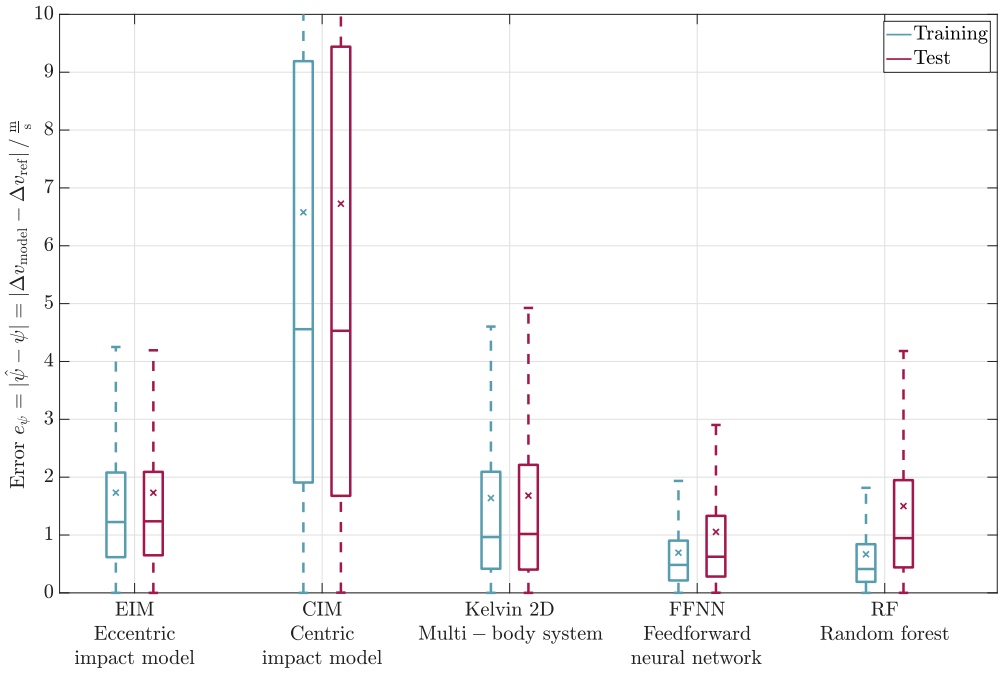

Figure 4.8: Training and test error prediction models - It shows the training ($e_{\psi,\text{train}}$) and test ($e_{\psi,\text{test}}$) errors for the eccentric impact model (EIM), centric impact model (CIM), Multi-body system (Kelvin 2D), feedforward neural network (FFNN), and random forest (RF). Furthermore, quantiles with a step size of 25 % are displayed as well as the mean value by a the small cross.

The centric impact model and the Kelvin model are out of scope to further considerations in the driving function due to the bad prediction accuracy and real time capability, respectively. In other words, the neural network and eccentric impact model remain for the application in the driving function. Even if the neural network yields some better values, the eccentric impact model is chosen in this thesis for the severity prediction in the driving function. That decision bases on the secondary attributes of the eccentric impact model. Related to the safety application, it might be advantageous to base the functionality on plausible physics rather than on black box models. That is supposed to explain the vehicle behaviour more transparently. Especially in critical events, it might be necessary to prove a correct driving function. Furthermore, the eccentric impact model generalises better and thus it is assumed to obtain less drawbacks due to the sparse reference database when it comes to real world driving. Besides, giving an outlook to real world testing and available test vehicles (sec. 6.3), the massive parallelism of the trajectory exploration in the planning framework requires to execute the severity predictors serially on single hardware threads. Here, the execution time of the eccentric impact model is a little bit faster compared to the neural network since no Matlab hardware acceleration is available for the network. Moreover, the eccentric impact model takes the second place according to the T-value and the numerical results seem still sufficient for the driving function. What is more, the presented models have different advantages and disadvantages in general. Therefore, the selection may vary depending on changing requirements.

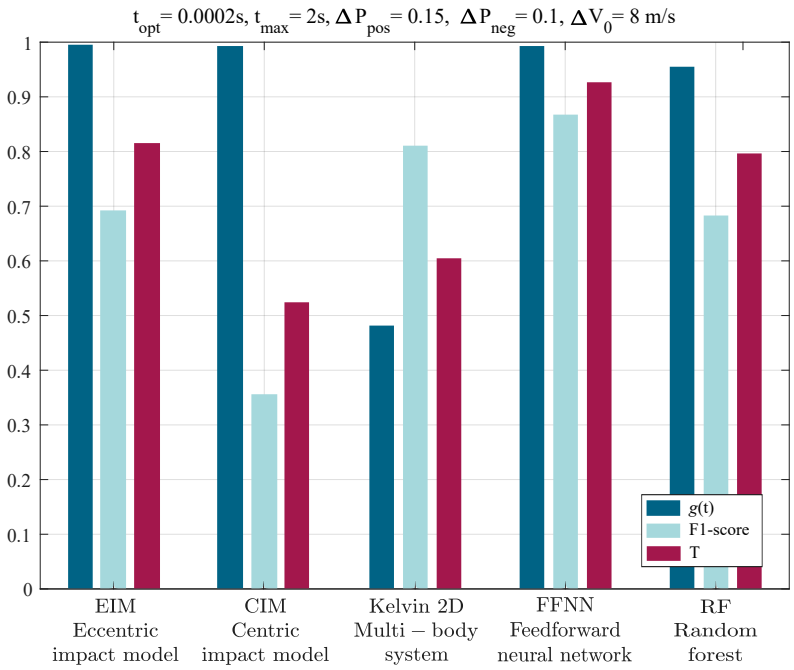

Figure 4.9: Comparison model accuracy and execution time - The figure contrasts the normed execution time $g(t)$, the F1-score, and T-value for the eccentric impact model (EIM), centric impact model (CIM), Multi-body system (Kelvin 2D), feedforward neural network (FFNN), and random forest (RF).

5 Risk based motion planning

5.1 Ego vehicle dynamic

The feasibility of trajectories constraints the ego vehicle transitions $T(s,a,s')$ between states s_{t_p} and $s_{t_{p+1}}$. That includes the vehicle dynamic $\tau_{\mathrm{E,dyn}}$ (equ. 5.1) as well as interaction between the vehicle's tire and the road surface (equ. 5.2 and 5.3) by the hard constraints $\boldsymbol{\lambda}$:

$$\lambda_{1,m}(\boldsymbol{z}_{\mathrm{E,dyn}},\boldsymbol{a}) = \boldsymbol{z}_{\mathrm{E,dyn},m+1} - \tau_{\mathrm{E,dyn,discrete}}(\boldsymbol{z}_{\mathrm{E,dyn},m},\boldsymbol{a}_m) \quad = \mathbf{0} \tag{5.1}$$

$$\lambda_{2,m}(\boldsymbol{z}_{\mathrm{E,dyn}},\boldsymbol{a}) = \frac{F_{\mathrm{long},f}^2 + F_{\mathrm{lat},f}^2}{\mu \cdot g \cdot m_f} \quad \leq 1 \tag{5.2}$$

$$\lambda_{3,m}(\boldsymbol{z}_{\mathrm{E,dyn}},\boldsymbol{a}) = \frac{F_{\mathrm{long},r}^2 + F_{\mathrm{lat},r}^2}{\mu \cdot g \cdot m_r} \quad \leq 1 \tag{5.3}$$

The literature provides different approaches to model a four wheel vehicle weighting accuracy, complexity, and necessary parameter identification. By way of example, [199, chap. 10, 11] presents several single-track and double-track models. In general, the application determines the necessary motion model. At one hand, the integral safety requires emergency manoeuvres up to the limits of dynamic and therefore the use of non-linear tire models. On the other hand, the dynamic model $\tau_{\mathrm{E,dyn}}$ should be as easy as possible to ensure fast calculations. Therefore, a non-linear single-track model is chosen as compromise to represent the ego vehicle dynamic:

$$\dot{\boldsymbol{z}}_{\mathrm{E,dyn}} = \tau_{\mathrm{E,dyn}}(\boldsymbol{z}_{\mathrm{E,dyn}}) \tag{5.4}$$

$$\dot{\boldsymbol{z}}_{\mathrm{E,dyn}} = \begin{pmatrix} \dot{x} \\ \dot{y} \\ \dot{v}_{\mathrm{long}} \\ \dot{v}_{\mathrm{lat}} \\ \dot{\varphi} \\ \dot{\omega} \end{pmatrix} = \begin{pmatrix} \cos(\varphi)\, v_{\mathrm{long}} - \sin(\varphi)\, v_{\mathrm{lat}} \\ \sin(\varphi)\, v_{\mathrm{long}} + \cos(\varphi)\, v_{\mathrm{lat}} \\ \frac{F_{\mathrm{long},f}+F_{\mathrm{long},r}-F_w}{m} + \omega\, v_{\mathrm{lat}} \\ \frac{F_{\mathrm{lat},f}+F_{\mathrm{lat},r}}{m} - \omega\, v_{\mathrm{long}} \\ \omega \\ \frac{F_{\mathrm{lat},r}\cdot l_r - F_{\mathrm{lat},f}\cdot l_f}{J_{zz}} \end{pmatrix} \tag{5.5}$$

$$\boldsymbol{a} = \begin{pmatrix} a_{\mathrm{in}} \\ \delta \end{pmatrix} \tag{5.6}$$

$$F_{\mathrm{long},f} = \cos\delta\ k_e\ a_{\mathrm{in}}\ m + \sin\delta\ F_{\mathrm{tire},f}(\alpha_f) \tag{5.7}$$

$$F_{\mathrm{long},r} = (1-k_e)\ a_{\mathrm{in}}\ m \tag{5.8}$$

$$F_{\mathrm{lat},f} = -\sin\delta\ k_e\ a_{\mathrm{in}}\ m + \cos\delta\ F_{\mathrm{tire},f}(\alpha_f) \tag{5.9}$$

$$F_{\text{lat},r} = F_{\text{tire},r}(\alpha_r) \tag{5.10}$$

$$F_w = k_{\text{air}} \cdot v_{\text{long}}^2 \tag{5.11}$$

$$F_{\text{tire},f/r}(\alpha_{f/r}) = D_{f/r} \cdot \sin\left(C_{f/r} \arctan_{f/r}\left(B_{f/r} \cdot \alpha_{f/r}\right)\right) \tag{5.12}$$

$$\alpha_f = \delta - \arctan\left(\frac{l_f \omega + v_{\text{lat}}}{v_{\text{long}}}\right) \tag{5.13}$$

$$\alpha_r = \arctan\left(\frac{l_r \omega - v_{\text{lat}}}{v_{\text{long}}}\right) \tag{5.14}$$

The composition and definition of the state $\boldsymbol{z}_{\text{E,dyn}}$ is already discussed in section 3.1. The input action $\boldsymbol{a}$ consists of the acceleration a_{in} and steering angle δ. Apart from the definition assignments, the dynamic model $\tau_{\text{E,dyn}}$ (equ. 5.5) comprise the longitudinal and lateral force balance as well as the principle of angular momentum around the center of gravity (COG). Thereby, it is distinguished between the front axle f and rear axle r with the dimensions $l_{f/r}$ related to the COG. The tire sideforces (equ. 5.12) are modelled by a simplification of Pacjeka's magic formula [225] with the slip angle $\alpha_{f/r}$. Furthermore, k_e splits the proportions of the engine to front and rear, and k_{air} constitutes a constant of the flow resistance. Figure 5.1 visualises the parameters of the differential equation 5.5.

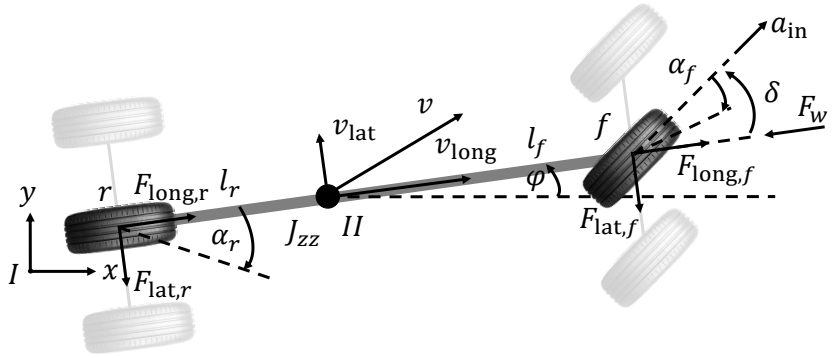

Figure 5.1: Non-linear single-track model - It depicts the parameters of equations 5.4 to 5.14.

The constraints 5.2 and 5.3 ensure the traction in general over all driving stages by the *circle of friction*. Additionally, a *dynamic window* restricts the available actions $\boldsymbol{a}$ in the current state s_{t_p}. The time continuous model $\tau_{\text{E,dyn}}$ (equ. 5.4) is integrated by the Runge-Kutta method third order (RK3) with a step size $\Delta t_{\tau_{\text{E,dyn}}} = t_{m+1} - t_m = 50\,\text{ms}$.

5.2 Reward function

The reward function $Re(s,a,s')$ constitutes the numerical basis for the trajectory optimisation problem according to section 2.2.2.2. Thereby, the reward $Re_{t_i}(s,a,s')$ relates to the

instantaneous time step t_i of the assigned transition $T_p(s,a,s')$. It weights the features $f_{t_i}(s,a,s')$ of the categories safety, comfort, and progress with the weights $\boldsymbol{\theta}$:

$$Re_p(s,a,s') = \sum_{i=1 \mid t_i \in [t_p, t_{p+1}]}^{N_{i,p}} Re_{t_i}(s,a,s')\,\Delta t_i \qquad \text{with} \tag{5.15}$$

$$\begin{aligned} Re_{t_i}(s,a,s') &= \sum_{n=1}^{N_f} -\theta_n f_n(s,a,s') \\ &= \left.\begin{aligned} &-\theta_1 (v_{d,t_i} - v_{\text{long},t_i})^2 - \theta_2\, d_{\text{lat},t_i}^2 - \theta_3\, d_{\varphi,t_i}^2 \end{aligned}\right\} \text{progress with } f_{\text{progress}}(s,a,s') \\ &\quad \left.\begin{aligned} &-\theta_4\, \dot{a}_{\text{long},t_i}^2 - \theta_5\, \dot{a}_{\text{lat},t_i}^2 - \theta_6\, a_{\text{long},t_i}^2 - \theta_7\, a_{\text{lat},t_i}^2 \end{aligned}\right\} \text{comfort with } f_{\text{comfort}}(s,a,s') \\ &\quad \left.\begin{aligned} &-\theta_8\, R_{f,t_i} \end{aligned}\right\} \text{safety with } f_{\text{crit}}(s,a,s') \end{aligned} \tag{5.16}$$

The deviation to the desired velocity $(v_d - v_{\text{long}})$ as well as the displacement to the road centerline d_{lat} and vehicle road alignment d_φ ensures progress and normal driving. The comfort depends on the longitudinal and lateral jerks $\dot{a}_{\text{long/lat}}$ and accelerations $a_{\text{long/lat}}$. The risk R_f is the safety feature avoiding accidents or at least mitigating the harm. When referring to the risk feature R_f, the label "f" is used as indicator and else, when referring to the risk in general, it is omitted.

The features $f(s,a,s')$ are derived from the environment model M (sec. 3.1) and belong to the groups of progress $f_{\text{progress}}(s,a,s')$, comfort $f_{\text{comfort}}(s,a,s')$, and safety $f_{\text{crit}}(s,a,s')$. Thereby, the number and types of features $f(s,a,s')$ comply with the requirements of the evaluation scenarios with focus on integral safety (sec. 6.2). In general, selecting the features $f(s,a,s')$ and afterwards accumulating and tuning the reward function $Re(s,a,s')$ is a major effort in automated driving. It is a basis to determine the vehicle behaviour and driving style. However, in this thesis the focus lies on the integral safety without special interest, e.g., on comfortable or fast driving. Thus, only a basic weighting of the competing features $f(s,a,s')$ of equation 5.15 is derived in section 5.3 as far as needed to illustrate the integral safety approach. However, further research may focus on optional, safety-independent advanced customer demands. Besides, the tuning is a major interface to implement ethical guidelines and administrative regulations. Since such standards are currently not available, the tuning can only be provisional in that point of view. In short, the final configuration needs to be prescribed by public authorities representing the expectations of the society.

The single features $f(s,a,s')$ work as *soft constraints*, i.e., the optimal solution π^* is affected by reward and penalties rather than strict rules. That is an important premise to uncertain environments and integral safety applications. It is not regarded suitable to guarantee behaviour, such as collision avoidance or complying a certain safety distance. By way of example, [77] uses the collision probability with an upper bound as *hard constraint* in the motion planning. As result, the optimisation procedure fails if the threshold is violated due to any cause whatsoever. That needs to be prevented, especially in critical scenarios.

Identifying the current appropriate vehicle behaviour leads to a general conflict of objectives. By way of example, taking as little risk as possible could be an prevalent demand. But

prioritising the safety over all would impede locomotion due to the inherent risk of participating in road traffic. It is essential to accept the amount of *residual risk*. However, facing an imminent collision the requirements change to maximal safety even if the locomotion is impeded. The ethical background to *consequentoalism*, referring to the reward function and its strict execution, and *deontological* ethics, referring to constraints and rule based behaviour, is discussed in [169, chap. 5]. In conclusion, there exists no overall reward function $Re(s,a,s')$ with static, situational independent weights $\boldsymbol{\theta}$ assuming a commitment to ethical responsibility (sec. 2.2.3).

Therefore, the presented integral driving adopts the approach of *graceful degradation*. Reference [169, sec. 23.6] provides a short introduction to that subject. In the original, *graceful degradation* means a reaction of the system on malfunctions or unexpected events with the goal to maintain the functionality as much as possible. As result, a total failure is avoided accepting temporary reduced performance. Transferring the idea to the integral approach, secondary objectives, such as comfort and progress, are neglected in critical scenarios by changing the belonging weights $\boldsymbol{\theta}$ of the reward function 5.15 to zero. That means the optimisation problem changes to prioritised safety objectives. In other words, a hybrid of consequentialism and deontological ethics is applied in this work. Additionally, the residual planning framework remains similar enabling a fast switching in a bidirectional manner. Besides, the engineering effort is reduced by maintaining only one driving architecture.

The implemented graceful degradation bases on two levels as shown in figure 2.8. The regular driving constitutes the first level. It needs a well-balanced reward function for the desired locomotion what means to consider the aspects of safety, progress, and comfort equally. The second level includes the emergency manoeuvres. Here, only the risk feature R_f with $\theta_8 \neq 0$ remains to solve the situation by maximising the safety. Thereby, with reference to section 2.1.3.1, the collision avoidance and mitigation by combined braking and swerving is not distinguished directly. That property is an essential part of the system design. The risk R as expected value chooses the appropriate vehicle behaviour for maximum benefit under uncertainties automatically. A more detailed graceful degradation is discussed in [226] and [169, sec. 23.6]. However, they mainly focus on aspects of functional safety and regular driving being out of scope to this thesis. In conclusion, also a manifold state machine with complex surveillance system could guide different driving stages at a superior level [169, sec. 23.6]. Giving one more example, driving with low velocities v_{long} would lead to a small potential accident severity $\psi \to 0$ and hence reduce the risk $R \to 0$ even if a collision is immanent with $P(C) \to 1$. Consequently, the driving with low velocity, e.g., due to parking or congestions, would require an own driving configuration. For example, the collision probability $P(C)$ could yield as direct feature in the reward function $Re(s,a,s')$.

The switching between preventative and emergency tuning is based on the risk R itself. Enhancing the safety, false positives (unnecessary safety manoeuvre) are preferred to false negatives (imminent collision not detected). Therefore, the risk threshold R_{thr} obtains an additional safety margin in the direction to preventative driving as shown in figure 2.8. In a sense, such system architecture is similar to ADAS, where the system intervention and emergency manoeuvre planning is based solely on safety features. What is more, the bidirectional switching is necessary to impede undesired driving behaviour in the case of col-

lision avoidance. By way of example, switching only once to the risk minimisation could lead to a road exit rather than a smooth avoidance manoeuvre. Alternatively, a subordinated counterpole could be used to find a compromise between the safety prioritising at first stage and the prevention of a subsequent critical scenario evolvement. For example, the deviation to the centerline d_{lat} impedes an arbitrary swerving and favours the return to the centerline after the critical incident.

Figure 5.2 shows an extract of the MDP with risk $R_{f,t}$ over time t. Due to the modelling of instantaneous substates and time steps t_i, the condition between single time steps is neglected. As result, time based modifications of the reward function $Re(s,a,s')$ are necessary for motion planning as experienced in the evaluation (chap. 6). In the following, it is discussed on the risk feature R_f since that is the essential part for integral safety. However, similar considerations are necessary for other features of the reward function (equ. 5.15) in advanced regular driving.

Giving a short recap to section 2.2.2.2, it should be noticed that three different time discretisation levels are used in the motion planning. The action sampling of the MDP, feature derivation $f(s,a,s')$ including the criticality estimation R_f, and the dynamic model τ are considered with independent step sizes $\Delta t_{p/i/m}$, respectively. They solely need to provide the information between the different levels periodically as shown in figure 2.14. Thereby, it needs to be satisfied that the sampling rates matches the current ego vehicle dynamic. For example, the time based planning could be referred to the x-y-space where potential collisions are assessed by the risk R_f and thus ensure that important incidents are not passed unnoticed due to the discretisation. That might be achieved by an appropriate overall fixed time interval Δt_{fix} or variable step size $\Delta t_{\text{variable}}$ according to the vehicle dynamic of the current driving.

In general, the time intervals $\Delta t_i = t_i - t_{i-1}$ as part of the prediction horizon TH (fig. 5.2(a)) have not a uniform length. Therefore the features $f(s,a,s')$ are scaled with the time interval Δt_i of the current time step as defined by equation 5.15.

Furthermore, the curve of instantaneous risks R_{f,t_i} indicates only potential collisions at specific moments t_i (fig. 5.2(b) trajectory II). Otherwise, the risk declines before and beyond to insignificance what leads to bad numerical conditions. For example, it is difficult to chose the appropriate trajectory when distinguishing between latent persistent risk (fig. 5.2(b) trajectory I) or temporary high risk peaks (fig. 5.2(b) trajectory II). Especially, if the areas under trajectory I and II are equally. The integral of the risk $R_{f,t}$ over time t would be the exact mathematical solution for the total risk if the time steps were stochastic independent, what they are not. In contrast, the maximum risk seems to be a promising approximation due to the conservative, safety-related construction. If a collision with high severity occurs (fig. 5.2(b) trajectory II), it does not matter what was predicted beyond that short moment. The accident happens anyway. Therefore, the maximum risk value is an important indicator for potential collisions even if the discontinuity complicates the trajectory optimisation. However, the risk accumulation (integral solution) enables to differentiate multiple trajectories on the risk amount. For example, it seems reasonable to prefer trajectory II instead of trajectory III in figure 5.2(b).

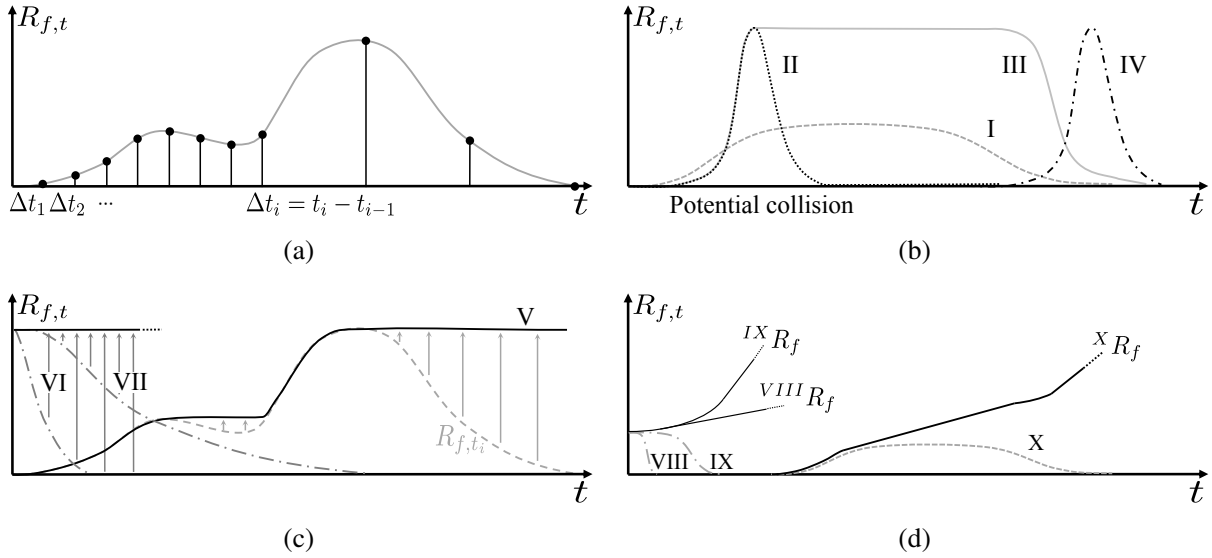

Figure 5.2: Characteristic risk curves - The figure illustrates important special cases of risk curves. The reward function $Re(s,a,s')$ needs to deal with all types of them: (a) multiple step sizes Δt_i, (b) risk accumulation by integrals and max-operators, (c) hybrid of integral and max-operator, and (d) final strategy for the risk features R_f.

Therefore, a hybrid approach is suggested where the reward function $Re(s,a,s')$ accumulates the previous maximum risk value as shown in figure 5.2(c) by trajectory V. Besides, it contributes to the discount factor γ of the MDP enabling a differentiation between trajectory II and IV in figure 5.2(b). In a sense, that accumulating max-operator matches the nature of collision events. If a collision is occurred, the binary indicator does not change back even if the collision objects remain in the rest position. Unfortunately, also that accumulation has disadvantages as shown by trajectories VI and VII in figure 5.2(c). It impedes the assessment or rather differentiation of trajectories when already yielding a high risk from the beginning.

Therefore, once again the risk feature R_f is manipulated. Finally, the accumulation of previous time steps is used as offset to the current risk value with $R_{f,t_i} := \sum_{n=1}^{i-1} R_{f,t_n} + R_{t_i} \cdot \Delta t_i$ (fig. 5.2(d)). Since the risk value increase rapidly dominating the reward function $Re(s,a,s')$, that accumulation is only chosen after switching to the emergency manoeuvres. Here, only little time remains to solve the dangerous situation preventing numerical overflows.

In regular driving, the risk feature R_f contains the unmodified risk value $R_{f,t_i} := \sum_{k=1}^{N_O} \sum_{j=1}^{N_H} p(h_k^j) \cdot R(\mathrm{EK}_{i,k}^j)$ according to equation 3.3. The competing features $f(s,a,s')$ interact with residual risks and thus low-risk trajectories are chosen according to the balance of the reward function $Re(s,a,s')$.

5.3 Tuning of the driving function

5.3.1 Tuning strategy

The tuning strategy of the reward function 5.15 follows a scenario based approach as discussed in section 2.2.1.2. Thereby, a tuning is mainly needed for the regular driving. Even if the focus lies on integral safety in this thesis, a basic regular driving capability is necessary for the scenario evolvement and hence demonstration of the integral approach. An other aspect constitutes the transition between single criticality levels and the feature interaction. That is analysed by a systematic parameter screening. At one hand, it is used to verify the weighting strategy for emergency manoeuvres as presented in section 5.2. On the other hand, it is used to show the weighted feature influences in general.

Section 5.2 discusses by deductive logic that one static weighting $\boldsymbol{\theta} = \text{const}$ is not suitable for integral approaches or, more general, when dealing with changing criticality. Similarly, the question arise if the weights $\boldsymbol{\theta}$ should be changed between different functional scenarios FS at the same criticality level or if static parameters $\boldsymbol{\theta}$ are sufficient in regular driving. The latter would reduce the engineering effort dramatically. It would avoid to generate different instances of the reward function 5.15 at every driving stage. In a sense, the changing instantiation of the reward function means to modify the optimisation problem situational dependent with additional challenges on the situation classification for parameter assignment. Therefore, multiple functional scenarios FS (sec. 5.3.2) are investigated separately deriving an optimal weighting set ${}^{\text{FS}n}\boldsymbol{\theta}^*$ for each instance FSn. Afterwards the results are compared and a recommendation on the general weighting $\boldsymbol{\theta}^*$ is derived for the evaluation in chapter 6. Figure 5.3 visualises the simulation study for the tuning process. What is more, the graceful degradation of section 5.2 is suspended for the tuning process to reduce disturbing interactions. Anyhow, the regular driving constitutes one remaining level with less criticality and the parameter screening on different criticality levels is supposed to verify this very approach of graceful degradation. As result, both cases do especially not need the graceful degradation.

The tuning of the weights ${}^{\text{FS}n}\boldsymbol{\theta}$ is formulated as an own optimisation problem apart from the planning procedure presented in section 2.2.2.2. The objective is to find the best tuning to comply the system requirements of an automated vehicle. Unfortunately, there exists currently no standardised approval or rating of automated driving competency (sec. 2.2.1.2). Consequently, the weighting $\boldsymbol{\theta}^*$ can only be provisional following at least ethical guidelines (sec. 2.2.3) and assuming common standards. By way of example, that includes safe, collision free, and comfortable driving to the destination. Besides, as mentioned earlier, the weighting $\boldsymbol{\theta}$ is only needed exemplary to illustrate the integral approach and might be adjusted on future demands anyway.

Similarly, related work defines arbitrary a ground truth to tune their driving function. For example, [197] tries to find the optimal weighting reproducing previously recorded human driving style. In point of fact, it focus on the development of the tuning procedure based on reinforcement learning rather than the final quantitative weights, here again, due to the lack

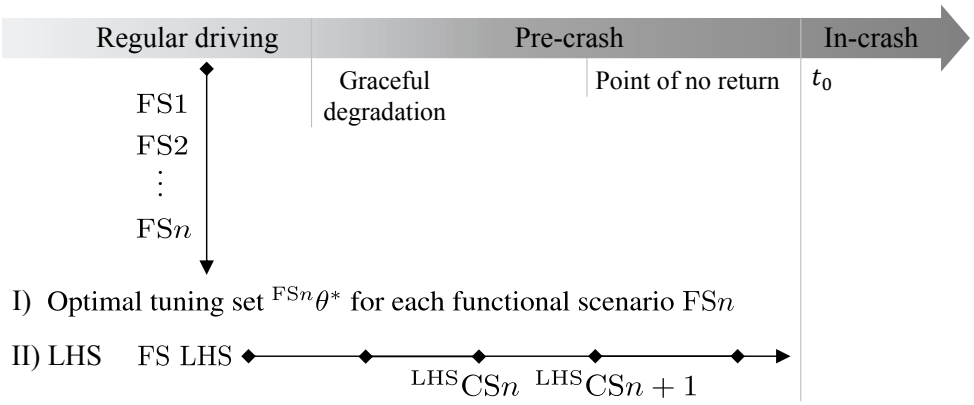

Figure 5.3: Course of tuning - Multiple functional scenarios FS in regular driving and multiple concrete scenarios CS with different criticality are analysed with the objective of a tuning set $\boldsymbol{\theta}^*$ for the evaluation in chap. 6.

of official directives. Furthermore, the approach of [197] bases on a reference trajectory to evaluate the driving performance. That enables a fast reward in every driving stage. Seeing that advantage, work such as [227] tries to find the optimal reference trajectory for single scenarios independent of a certain driving function. However, also that reference trajectory bases on a non-official or rather arbitrary objective function. In contrast, this thesis assess the driving performance without a reference trajectory at the end of the test drive. In other words, the full scenario evolvement is evaluated entirely (fig. 5.4). That approach bases on the integral character of the risk based planner. For example, if an accident occurs, it does not matter how the driving performance was previously. Here, only the accident severity rates the driving or rather mitigation performance. What is more, [197] and [227] focus solely on collision avoidance. An intelligent crash interaction is out of scope for both works. On top of that, this work tries especially not to copy human driving capabilities since an average human driver acts almost randomly in critical situations what opposes the presented integral approach.

Figure 5.4 shows the procedure of cost generation. The basis constitutes the driving architecture, visualised in figure 2.13. As special feature, the end of simulation is either obtained by reaching the destination in the functional scenario FSn or by the occurrence of an accident. Afterwards, the cost J is generated to assess the closed-loop driving process. Due to the posteriori examination, the data of the entire driving process are available. Besides, the usage of a simulation environment (sec. 6.3) provides ground truth data. At one hand, that enables an accurate cost calculation, e.g., due to the exact collision configuration without uncertainty of any observer's point of view. On the other hand, the perception module and its uncertainty as well as the vehicle dynamic need to be emulated.

In compliance with the previous publication [30], a hierarchical objective function J is suggested to tune the driving function or rather formulate an optimisation problem:

$$\boldsymbol{\theta}^* = \arg\min_{\boldsymbol{\theta}} J \tag{5.17}$$

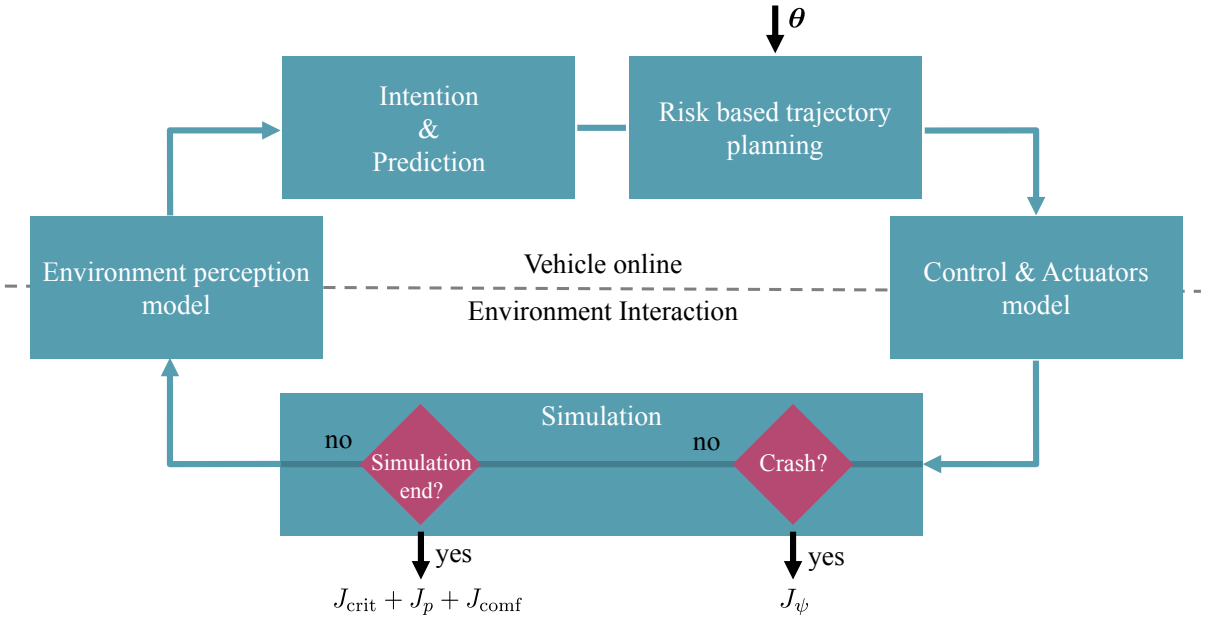

Figure 5.4: Tuning cost generation - The driving function is instantiated with the tuning parameters $\boldsymbol{\theta}$. The closed-loop environment interaction is simulated to gather the ground truth data of the driving process. Afterwards, the objective function J assess the total test drive depending on the scenario evolvement.

At the first level, if an accident occurs, labelled with the binary indicator $C = 1$, the accident outcome J_ψ dominates the entire scenario assessment J. Otherwise, if the drive has been collision free ($C = 0$), a simplified criticality measure J_{crit}, the progress J_p, and comfort J_{comf} form the cost J at the second level. Thereby, the collision outcome is set to zero with $J_\psi = 0$. As result, the total objective function J is expressed by:

$$J = \begin{cases} J_\psi & C = 1 \\ J_{\text{crit}} + J_p + J_{\text{comf}} & C = 0 \end{cases} \quad \text{with } {}^{\min}J_\psi > J_{\text{crit}} + J_p + J_{\text{comf}} \tag{5.18}$$

Each term of the objective function J is modelled with an own heuristic to differentiate multiple test drives. The detailed derivations are explained in the previous publication [30]. Here, only a short summary is presented in the following.

The accident severity $\psi_J = \Delta v$ is weighted with the shape of a P(MAIS2+)-sigmoid function (fig. 2.4(a)), accordingly to the GIDAS database [142], between the minimal costs ${}^{\min}J_\psi > J_{\text{crit}} + J_p + J_{\text{comf}}$ and maximal costs ${}^{\max}J_\psi$. The criticality J_{crit} in collision free driving bases on the number of conflicts (NOC). Related works, such as [228] and [33, sec. 33.6], indicate a TTC $< 1.75\,\text{s}$ as critical event. Therefore, that point is used to anchor a decreasing exponential function, beginning at the maximal costs ${}^{\max}J_{\text{crit}}$ with TTC = 0. The TTC is calculated along the planned trajectory with constant velocity (CV) and constant turn rate (CTR). The comfort bases on the longitudinal a_{long} and lateral acceleration a_{lat}. A sigmoid function is set symmetrically around average human comfort limits, e.g. according to [228], [229], [230, sec. 3], and [33, sec. 32.9, sec. 33.6]. Both, criticality cost J_{crit} and comfort cost J_{comf} are obtained iteratively for every planning step with $J_{\text{crit}} = \sum_n J_{\text{crit},n}$ and

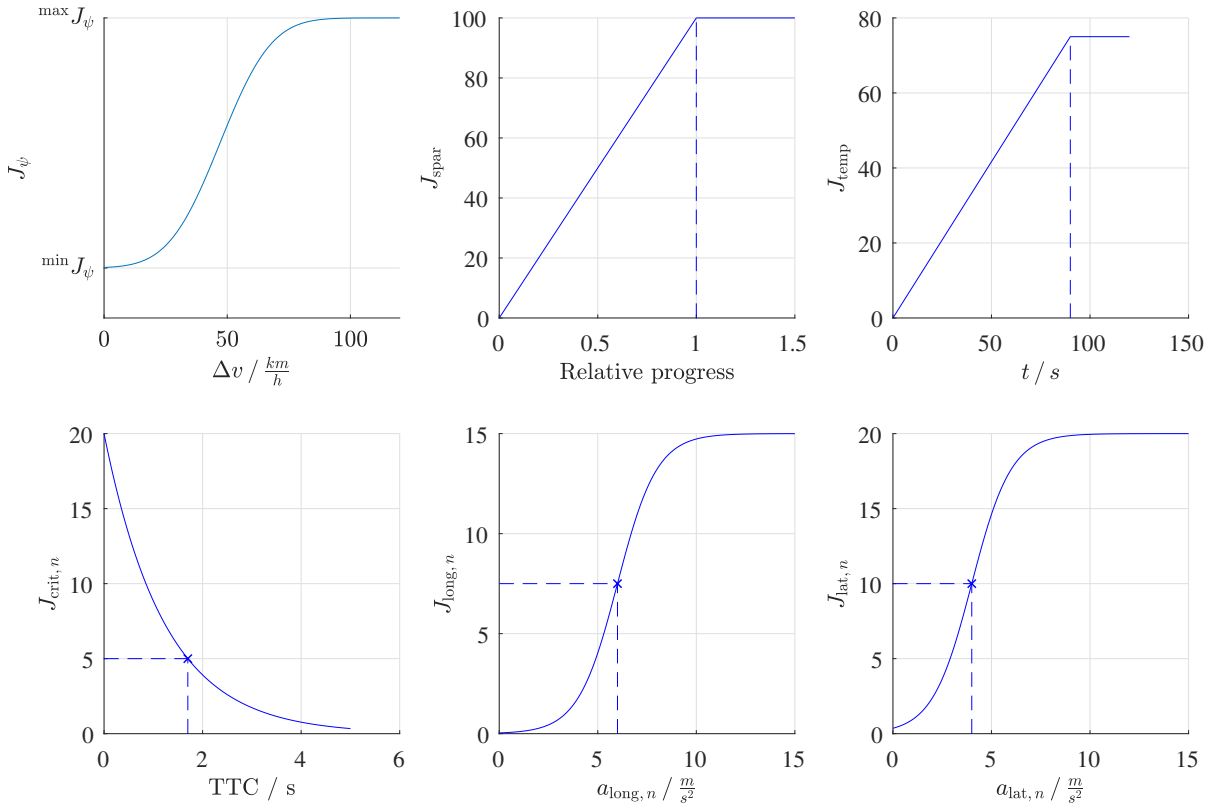

Figure 5.5: Heuristics tuning objective function - The objective function 5.18 combines different sub-objectives with dedicated heuristics. In general, they constitute a conflict of objectives.

$J_{comf} = \sum_n J_{long,n} + J_{lat,n}$, respectively. Contrary, the progress is evaluated spatially J_{spar} and temporally J_{temp} once at the end of the drive with $J_p = J_{spar} + J_{temp}$.

The systematic parameter screening on different criticality levels (fig. 5.3) bases on latin hypercube sampling (LHS) [231]. Thereby, samples ${}^{s}\boldsymbol{\theta} \in \Theta$ with count $|\Theta| = N_{LHS} = 50$ instantiate the reward function $Re(s,a,s')$ in multiple concrete scenarios ${}^{LHS}CS$ of the functional scenario FS LHS with ${}^{LHS}CSn \in$ FS LHS. Further details on the scenario description are presented in section 5.3.2. Verifying the deductive weighting strategy for increased criticality presented in section 5.2, the analyses of the LHS focus on the collision cost J_ψ in section 5.3.3.

Due to the non-linear structure of the objective function J, a *genetic algorithm* (GA, e.g., [232]) is used to optimise the parameters ${}^{FSn}\boldsymbol{\theta}$ for the functional scenarios FS (sec. 5.3.2) with focus on regular driving. Satisfying a local minima, the result of the GA is further developed by a local search based on *generalized pattern search algorithm* (GPSA, e.g., [233]). Further information on the settings of the algorithm are given by the previous publication [30].

5.3.2 Tuning scenarios

The goal of the integral approach is to enhance the road safety. Therefore, accident-pone functional scenarios are derived in the following. However, as mentioned in section 2.2.1.2, the unknown future accident occurrence impedes a clear choice or rather assessment of the significance. Therefore, systematic considerations and the experience of previous accident blackspots are used as a basis for the tuning process. Besides, the scenario catalogue could be further developed with increased number of automated vehicles in real traffic. Thus, further experience and feedback of the automated driving competencies could be used to improve the tuning of the next generation driving function. A full discussion on scenarios for the integral approach is presented in section 6.2.

The functional scenario selection for the tuning process focus on accidents with injury outcome according to the GIDAS database [142]. Here, the integral approach is seen with the highest potential to increase the road safety. Figure 5.6 shows a histogram of injured persons over GIDAS accident types (UTYP). The encoding of accident types follows the GIDAS description [234]. The GIDAS accident type (UTYP) refers to the initial incident which cause the crash scenario evolvement. It is independent of the actual accident constellation or crash configuration. The data refer to injuries of the time range with year 2000 to the middle of year 2018. The histogram shows that only few accident types dominate the accident outcome. Thereby, the accident types which cause 50 % of injuries are selected at the first stage (UTYP 211-341). Additionally, scenarios are chosen which resemble in the scenario evolvement even if they have minor frequencies, such as UTYP 243 and 223. Finally, 38 GIDAS accident types are selected (fig. 5.8). They constitute 12,5 % of all GIDAS accident types (fig. 5.7(a)) but two-thirds of all injuries (fig. 5.7(b)). Moreover, they gather two-thirds of all accidents independent of the injury outcome (fig. 5.7(b)) and spread more or less uniformly over the domains of highway, rural roads, and urban roads.

The 38 GIDAS accident types (fig. 5.8) are aggregated to 25 functional scenarios (fig. 5.9). By way of example, the street course is neglected for the tuning process in the UTYP 424, 454 and 473. In point of fact, the occluded pedestrian is the dominating element in that scenario and not the intersection before and after. Exemplary, one concrete scenario CS is derived of each functional scenario FS.

Independent of the accident blackspots, a critical scenario depends generally on relative poses and dynamics between the ego vehicle and other objects. That idea is developed further in section 6.2. Here, it is used to define the functional scenario FS LHS independent of any scenario emergence. That includes an ego vehicle which drives a straight line when suddenly an object vehicle appears in front of the ego vehicle in the same line at the point $\lambda_{\text{ego}} = 0$. Depending on the relative distance, the collision is physically avoidable or not. Thereby, five concrete scenarios ${}^{\text{LHS}}\text{CS}n$ are derived. They differ in the relative distance $d_n \in \{36\,\text{m}, 27\,\text{m}, 24\,\text{m}, 20\,\text{m}, 17\,\text{m}\}$ of the object appearance as shown in figure 5.10. Thereby, the criticality varies due to the chaning distance d_n. The ego vehicle starts with constant velocity $v_{\text{E}} = 50\,\text{km/h}$ while the object remains on the initial pose with $v_{k=1} = 0\,\text{km/h}$.

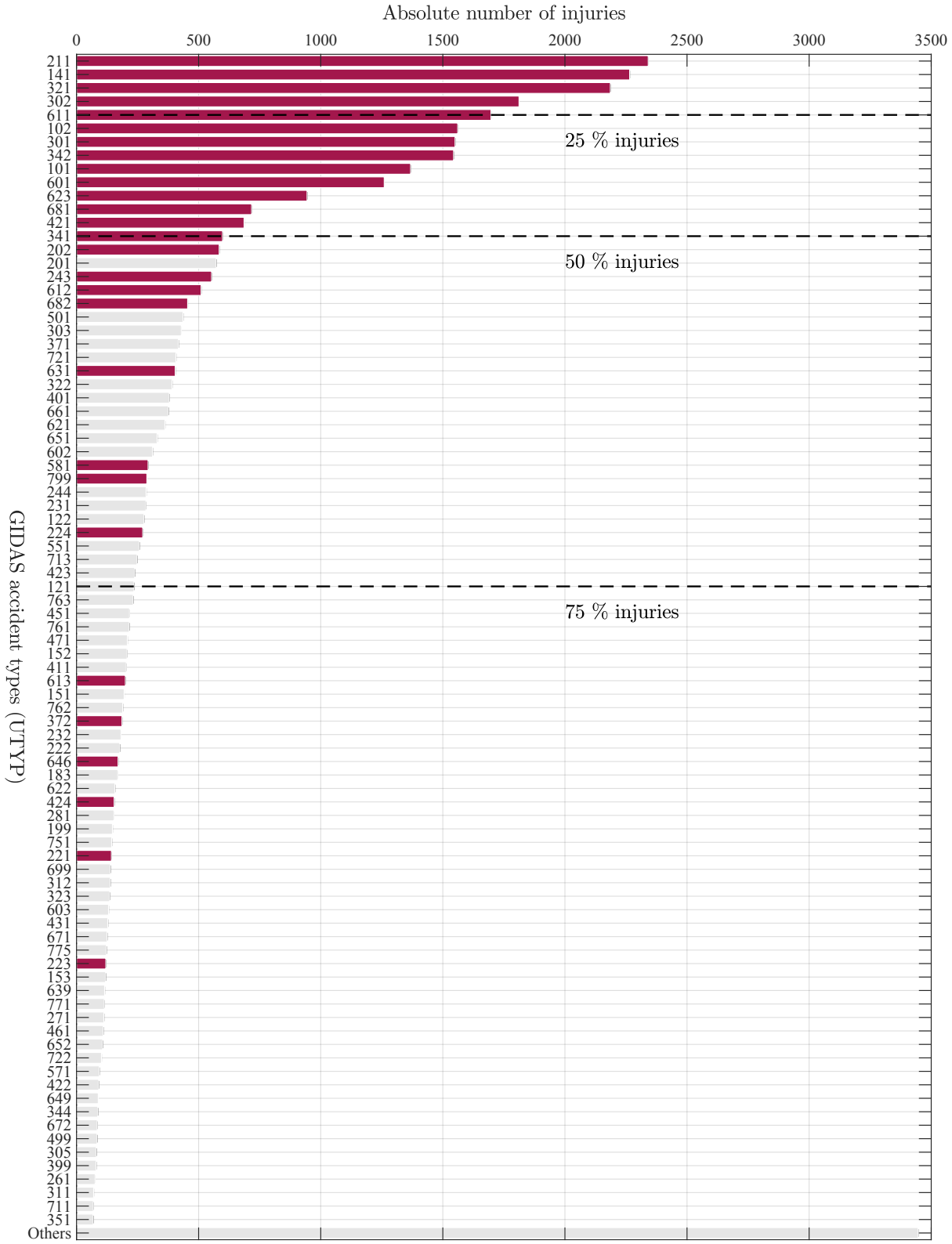

Figure 5.6: Scenario selection absolute injuries - The scenario selection (red) covers more than 50 % of the absolute numbers of injuries. The data base on [142].

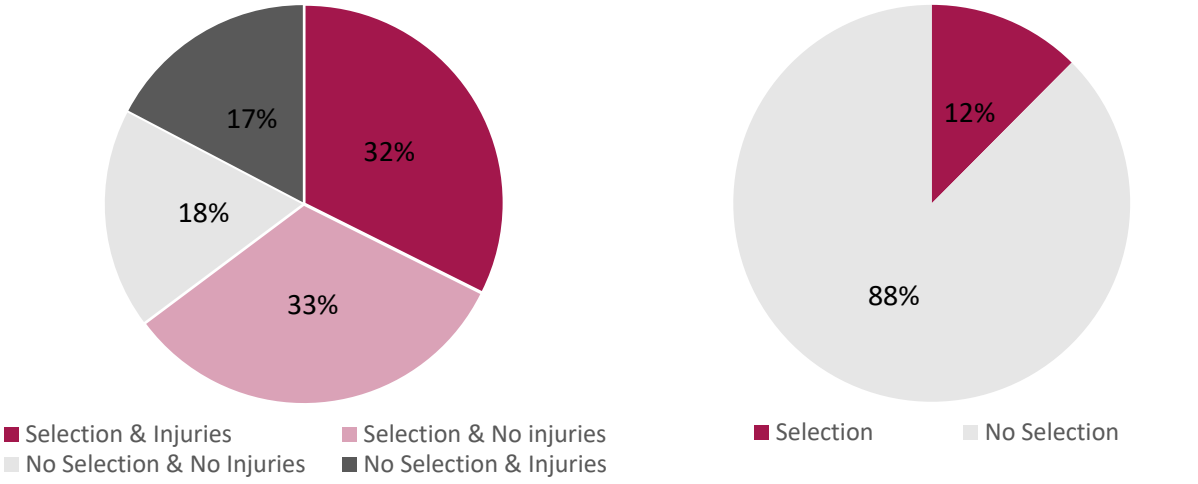

(a) All accidents with and without injuries (b) All GIDAS accident types (UTYP)

Figure 5.7: Scenario selection percentage - Relation of selected tuning scenarios to the population according to [142].

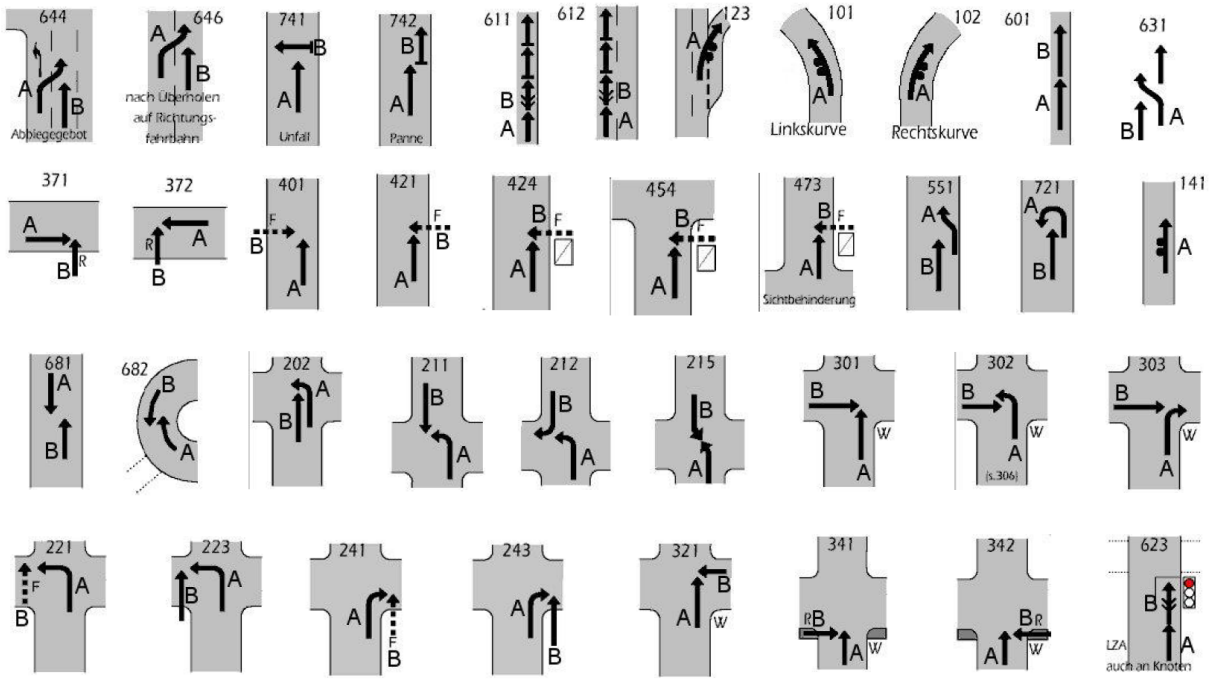

Figure 5.8: Scenario selection UTYP - It shows the scenario selection of the GIDAS accident types (UTYP) according to [234].

5.3.3 Tuning results

Figure 5.11 visualises the ego vehicle dynamic and criticality of a selection of test drives from the $N_{\text{LHS}} = 50$ samples with high diversity. The residual test drives range mainly between that selection (appendix A.1). Therefore, the full set of the test drives is not shown as it would make the figure illegible. The presented time variant values refer to the ini-

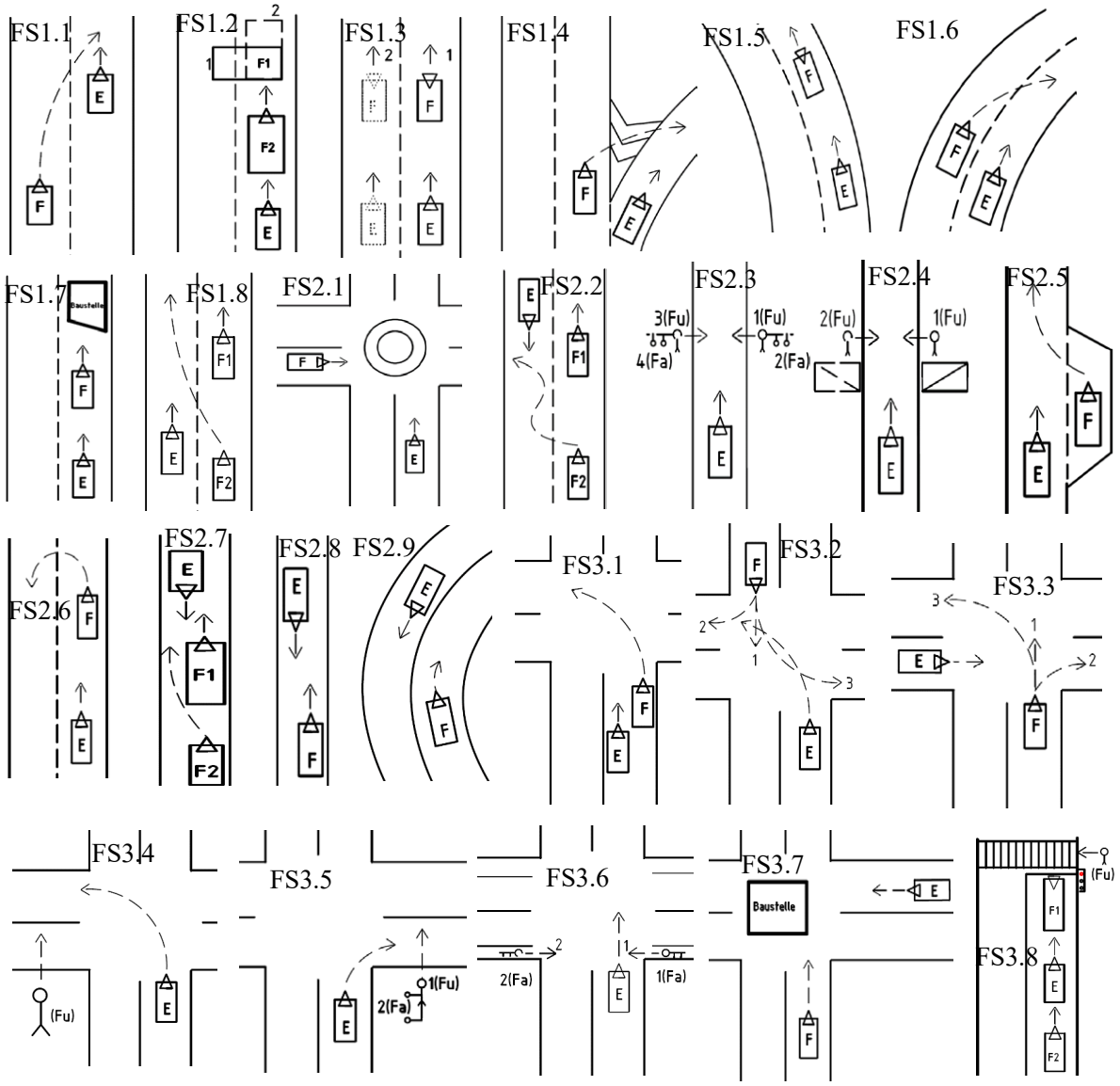

Figure 5.9: Extraction of functional scenarios FS - It shows the extraction of 25 functional scenarios FS based on the GIDAS accident types (UTYP) of figure 5.8. The labels mark the ego vehicle with E, a general object o_k with F, and specifies a pedestrian with Fu. The arrows depict the desired trajectories. The arrangement complies with the previous publication [30].

tial time step $t_i = t_0$ of the planning process. In other words, the real driven trajectory is shown without any values of the prediction horizon TH. The figures contrast the drives in the scenario ${}^{\text{LHS}}CS1$ (fig. 5.11(a)) with the drives in the scenario ${}^{\text{LHS}}$CS5 (fig. 5.11(b)) for the tunings ${}^{s}\boldsymbol{\theta}$. The time variant values are shown over the driven path λ_{ego} of the ego vehicle. The rows of the subplots constitute the driven velocity profile v_{ego}, the deviation from the centerline d_{ego}, and the criticality subfeatures of collision probability $P(C_{i=0})$, accident severity $\psi_{i=0}$, and risk $R_{i=0}$.

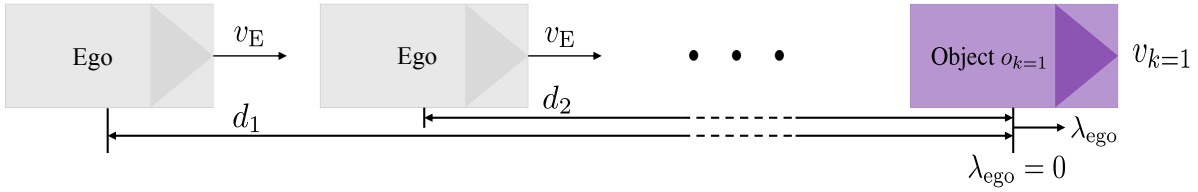

Figure 5.10: Sketch functional scenario FS LHS - Increasing criticality levels are induced by different appear distances d_n of the object vehicle o_k. Thereby, distance d_n refers to the concrete scenario ${}^{\text{LHS}}\text{CS}n$ of the functional scenario FS LHS.

Due to the LHS, the full spectrum of actions is scouted. Depending on the tuning ${}^{s}\boldsymbol{\theta}$, the ego vehicle decelerates strong (e.g., ${}^{s5}\boldsymbol{\theta}$), reduces the velocity slightly (e.g., ${}^{s4}\boldsymbol{\theta}$) or holds the velocity bluntly (e.g., ${}^{s2}\boldsymbol{\theta}$). Furthermore, the drive of weighting ${}^{s1}\boldsymbol{\theta}$ and ${}^{s3}\boldsymbol{\theta}$ ends abruptly in the subplot 1-1. That indicate a collision with the object $o_{k=1}$. Seeing that, the increased criticality in scenario ${}^{\text{LHS}}$CS5 (fig. 5.11(b)) leads to a collision in all cases. Accordingly to the collision occurrence, the collision probability rises to the maximum $P(C_{i=0}) \to 1$ (subplot 3-1 and 3-2). In other cases, the ego vehicle evades the object $o_{k=1}$. Therefore, the collision probability remains at a low level with $P(C_{i=0}) \to 0$ (subplot 3-1). Due to the closed-loop interaction with the environment, the ego vehicle reacts directly on emerging risk what results the low values. In other words, temporary high risk values in the planning process are reduced with the scenario evolvement immediately and thus increased risk values can not be seen apart from the critical incident. The subplot 2-1 shows that the collision is basically avoided by swerving. Depending on the maximum possible deceleration ${}^{\min}a_{\text{in}}$, a full brake would prevent the crash as well but with more inconvenience. For example, the reward function $Re(s,a,s')$ prefers to keep the velocity and penalises strong accelerations and jerks. On the other hand, the scenario description with the appearance distances d_n refers to the ground truth. However, the vehicle reaction is delayed by the update time and information processing due to other modules (fig. 2.2.2.1) as discussed in section 6.3. Besides, the last point to steer is reached later than the last point to brake at such velocities $v = 50\,\text{km/h}$ and object extensions $\vartheta(\cdot)$ (e.g., [67, sec. 2.2.4]). In scenario ${}^{\text{LHS}}$CS5 a collision is inevitable. Therefore, the ego vehicle tries to reduce the velocity, as shown in subplot 1-2, rather than to avoid a the collision by swerving, as shown by the low deviation d_{lat} from the centerline in subplot 2-2. The severity $\psi_{i=0}$ follows from the velocity profile (subplot 1-1 and 1-2) and object constellation. Here, the decline at the position of the object $o_{k=1}$ is conspicuous in subplot 2-1. Prior to the object appearance, the ego vehicle follows the lane with constant velocity v_E. Reacting on the object $o_{k=1}$, it decelerates temporary and then tries to continue the drive unchanged. Furthermore, the optimal tuning set $\boldsymbol{\theta}^*$ depends on the scenario ${}^{\text{LHS}}\text{CS}n$ or rather criticality level. By way of example, while the tuning ${}^{s2}\boldsymbol{\theta}$ performs well in regular driving (scenario ${}^{\text{LHS}}$CS1), it gains the highest impact severity ψ_{impact} in subplot 3-2. Conversely, the weighting ${}^{s5}\boldsymbol{\theta}$ performs very conservative in regular driving but has the lowest impact severity ψ_{impact} in scenario ${}^{\text{LHS}}$CS5. The final risk feature R_f is dominated by the collision probability $P(C_{i=0})$ in scenario ${}^{\text{LHS}}$CS1. Therefore, only the test drives with the weights ${}^{s1}\boldsymbol{\theta}$ and ${}^{s3}\boldsymbol{\theta}$ have an increased risk. In all other test drives,

the risk is reduced instantaneously with $R_f \to 0$. Contrary, subplot 5-2 shows an increased risk to all drives caused by the collisions.

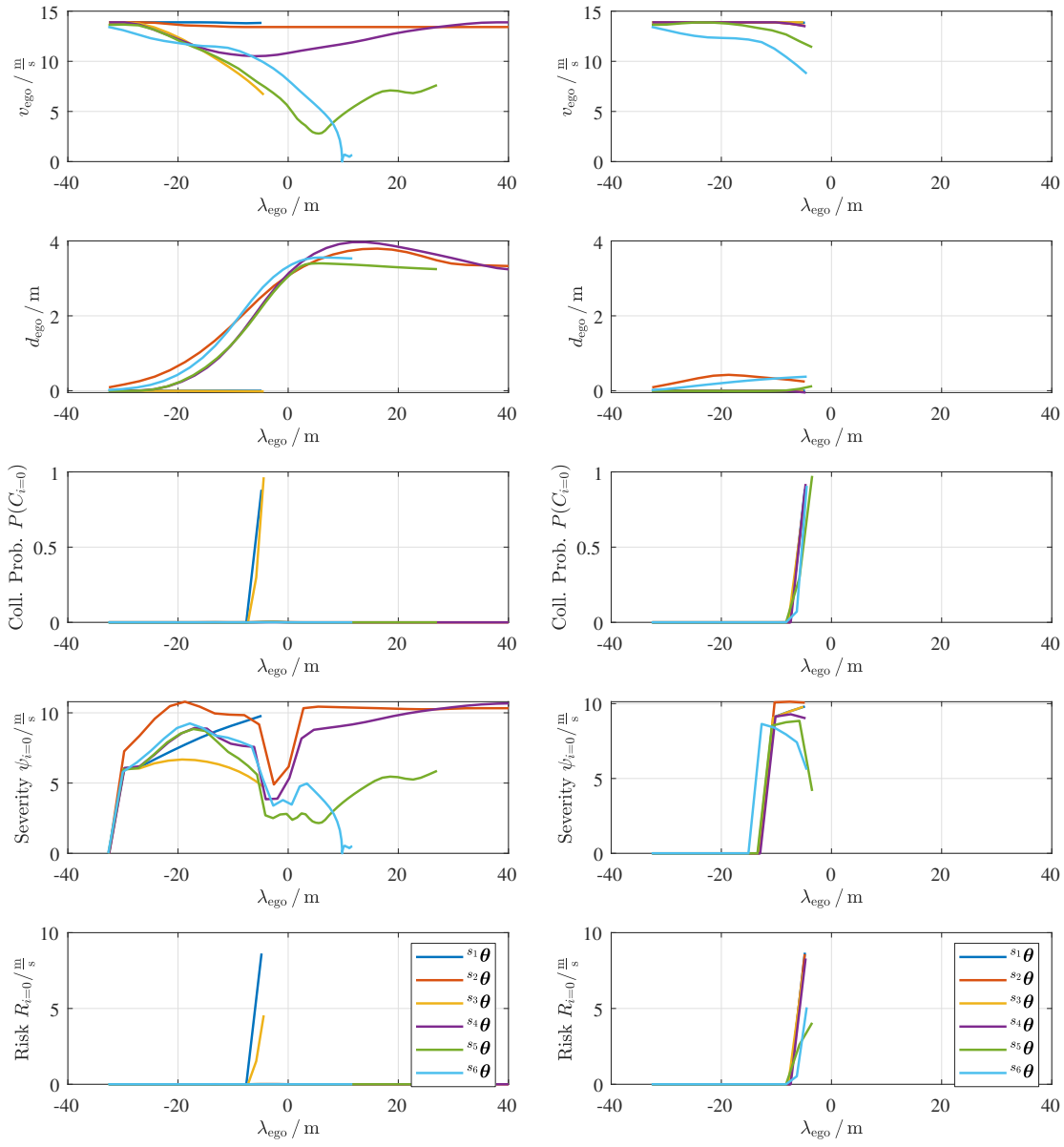

(a) Scenario $^{\text{LHS}}$CS1 (b) Scenario $^{\text{LHS}}$CS5

Figure 5.11: Test drives scenario FS LHS - It shows the dynamics and criticality subfeatures for a selection of the LHS tuning sample sets ${}^{s}\boldsymbol{\theta}$ in regular driving of scenario $^{\text{LHS}}$CS1 and emergency scenarios $^{\text{LHS}}$CS5. The subplots are referred by the row and column index. By way of example, the deviation in scenario $^{\text{LHS}}$CS5 is shown by subplot 2-2.

Summarising, the concrete scenarios CS include several criticality levels from regular driving $^{\text{LHS}}$CS1 to inevitable collisions $^{\text{LHS}}$CS5. Thereby, the tuning decides between collision avoidance or accident occurrence, both by swerving and braking, even in uncritical scenarios such as $^{\text{LHS}}$CS1. The weights $\boldsymbol{\theta}$ determines the optimisation problem and hence driving behaviour crucially, as discussed in section 5.3.1. Furthermore, the weights $\boldsymbol{\theta}$ which

produce the desired driving behaviour in regular driving (fig. 5.11(a)) are not necessarily the tuning set to reduce the impact severity in critical scenarios (fig. 5.11(b)).

Figure 5.12 shows the impact severity ψ_{impact} of all $N_{\text{LHS}} = 50$ samples over the most important feature weights $\boldsymbol{\theta}_n$ for all criticality levels CS. That includes the weights for the risk θ_8, lateral acceleration θ_7, centerline θ_2 and velocity θ_1, each presented in one column. They are selected to represent the categories of progress, comfort and safety according to equation 5.15. The direction has a minor impact in that longitudinal scenario FS LHS and thus is not imaged. Furthermore, pursuant to the ego vehicle behaviour as shown in figure 5.11, the lateral motion dominates the scenario FS LHS rather than the longitudinal deceleration. Therefore, the lateral acceleration is chosen as representative. Moreover, it effects stronger and longer than the lateral jerk. The full overview with all features is presented in appendix A.2. If a collision does not occur, the severity is set to zero by $\psi_{\text{impact}} = 0\,\text{m/s}$. The rows refer to the concrete scenarios CSn.

The impact severities $\boldsymbol{\psi}_{\text{impact}}$ have the same amount in every subplot, yet they are resorted to show the correlation to the feature weights θ_n. In the regular driving (scenario $^{\text{LHS}}$CS1) the most tuning sets ${}^{s}\boldsymbol{\theta}$ enable the vehicle to avoid a collision. That is shown by the majority of zero impact severities $\boldsymbol{\psi}_{\text{impact}} = 0$. The circumstance changes continuously with increasing criticality. Finally, in scenario $^{\text{LHS}}$CS5, all test drives ends in a collision. Additionally, a trend line indicates the correlation based on the least squares method.

The impact severity ψ_{impact} shows a strong correlation with the risk weight θ_8. The amount of collisions is very low in regular driving (scenario $^{\text{LHS}}$CS1). In that way, if a collision occurs nonetheless, the safety feature R_f is weighted very low (subplot 1-1). The declining trend line visualises that issue. However, due to the generous distance to the object o_k, the trend line decrease only moderately since multiple adjustments are able to avoid the collision. Contrary, more critical scenarios such as $^{\text{LHS}}$CS2 and $^{\text{LHS}}$CS3 react more sensitive on the risk weight θ_8 and hence the trend line declines stronger than in $^{\text{LHS}}$CS1. While the tuning in $^{\text{LHS}}$CS2 decides between collision avoidance and accident occurrence, the tuning in scenario $^{\text{LHS}}$CS3 is mainly necessary to reduce the impact severity ψ_{impact}. A collision becomes inevitable with increased criticality independent of the tuning $\boldsymbol{\theta}$. Therefore, the trend line flattens in subplot 4-1 again and remains almost constant in subplot 5-1.

Compared to the risk weight θ_8, the weight of the lateral acceleration θ_7 induces an inverse correlation to the impact severity ψ_{impact}. That confirms the conflict of objectives between safety, comfort, and progress in general. More detailed, collisions occur in subplot 1-2 mainly if the weighting θ_7 is very high. In other words, the feature of lateral acceleration a_{lat} impedes a swerving manoeuvre and hence in the scenario FS LHS the collision avoidance. Increasing the scenario criticality in scenario $^{\text{LHS}}$CS2 and $^{\text{LHS}}$CS3, the trend line levels off due to the increased occurrence of the collisions. Nevertheless, the tendency is shown further on. Finally, if a collision becomes inevitable in scenario $^{\text{LHS}}$CS4 and $^{\text{LHS}}$CS5, only small, if any, swerving is necessary for impact point localisation at one hand. That bases on the scenario design with the ego vehicle already driving in the direction of the optimal crash constellation. On the other hand, only few time remains due to the criticality and thus it is

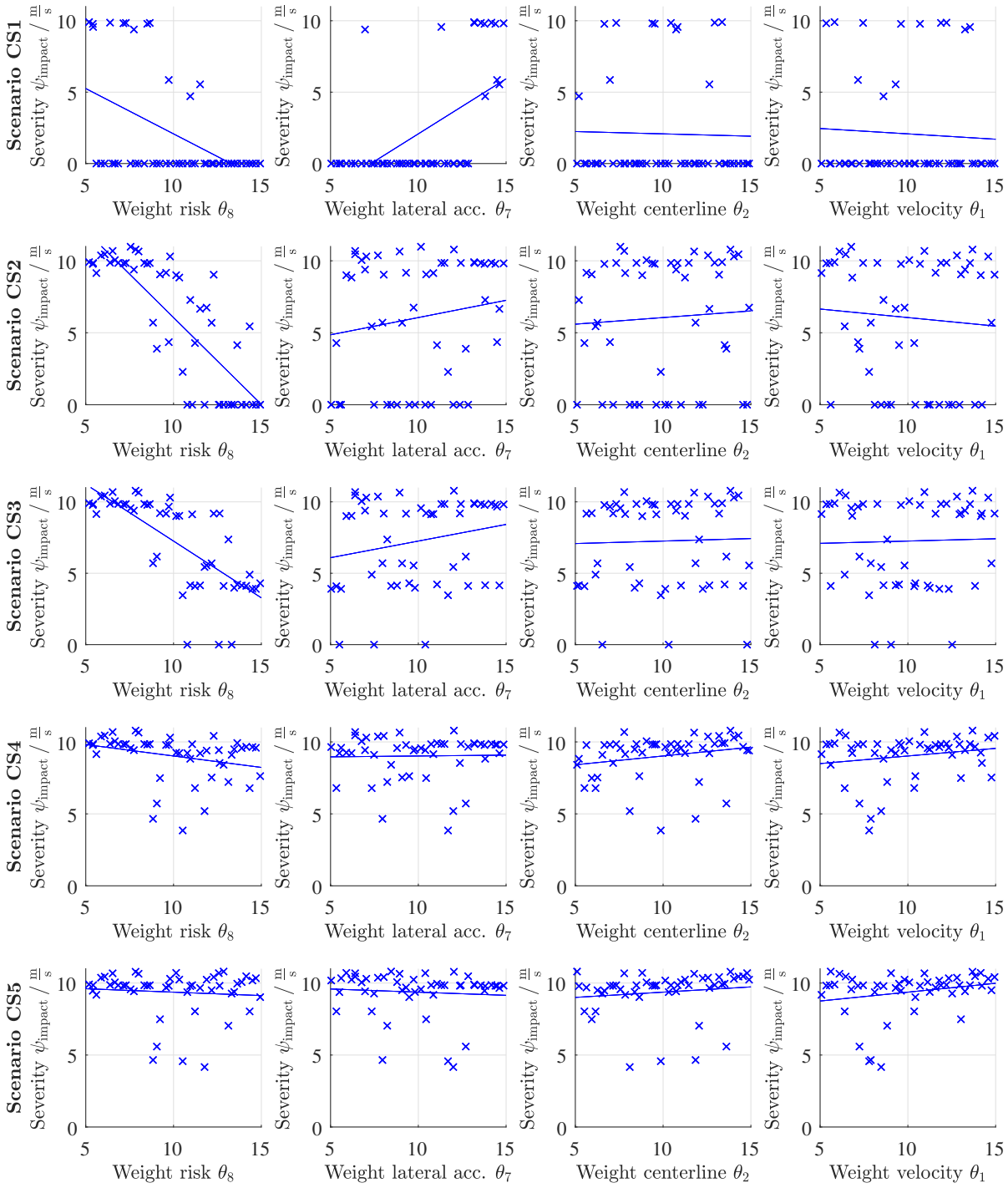

Figure 5.12: Correlation tuning parameter FS LHS - It shows the corrletation of tuning paramters to the accident severity ψ_{impact}. The subplots are referred by the row and column index.

very challenging to perform a mitigating manoeuvre. As result, the weighting θ_7 loses here the sensitivity and the trend line remains almost constant.

The weight of the centerline θ_2 and weight of the deviation to the desired velocity θ_1 have a minor impact in the scenario FS LHS. In regular driving, that bases on the connection

between longitudinal and lateral motion due to the circle of friction. In other words, the collision avoidance is dominated by swerving according to figure 5.11. Here, the velocity feature declines only moderate and hence it has a minor impact. In the other scenarios with increased criticality ($^{\mathrm{LHS}}$CS2 and $^{\mathrm{LHS}}$CS3), the risk dominates the driving process. Finally, if the collision is inevitable in scenario $^{\mathrm{LHS}}$CS4 and $^{\mathrm{LHS}}$CS5, the weightings θ_1 and θ_2 lose the significance anyway similar to the other weightings as described before. Moreover, even if the weighting θ_2 of the centerline is mainly dominated by the risk feature, it gains importance when leading the vehicle back to the centerline after the successful swerving manoeuvre.

Summarising, the screening with LHS shows exemplary the weighting influences with increasing criticality. In conclusion, the risk weighting θ_8 is an essential part for the vehicle safety. It is sensitive to the collision avoidance and collision mitigation in emergency manoeuvres. In regular driving, a well-balanced tuning $\boldsymbol{\theta}$ is enough for preventative driving. In contrast, an increased risk weight θ_8 is needed to maximise the safety in critical scenarios. In other words, it shows the requirements to the tuning in emergency scenarios. These include a risk prioritisation and a reduction of other influences due to the conflict of objectives. In a sense, it supports the deductive derived tuning strategy with graceful degradation (sec. 5.3.1) inductively. What is more, the amount of samples with $N_{\mathrm{LHS}} = 50$ enables only a basic screening. Crossinfluences of the features leads to outliers from the trend. However, they are neglected in the qualitative evaluation of the tendency due to the random compilations of weights $\boldsymbol{\theta}$.

Figure 5.13 visualises the tuning results $^{\mathrm{FS}n}\boldsymbol{\theta}^*$ of the functional scenarios FS of figure 5.9. Deep insights on the optimisation progress and the simulation outputs are discussed in the previous publication [30]. For each functional scenario FSn, the optimal weights $^{\mathrm{FS}n}\boldsymbol{\theta}^*$ are plotted and connected by a line to simplify the comparison. The results show plainly, that the optimal tunings $^{\mathrm{FS}n}\boldsymbol{\theta}^*$ change arbitrary between the driving domains as well as the functional scenarios FSn in one driving domain. Rather, the results spread over the full range of possible values. Seeing that, it seems not appropriate to formulate a global tendency or tendencies between certain subsets. Therefore, following conclusions are derived. Firstly, it seems not suitable to adjust the driving function with one global tuning set $\boldsymbol{\theta}^* = \mathrm{const}$. The feature needs rather to be adjusted situational dependent. Secondly, this final tuning sets $\boldsymbol{\theta}^*$ relate to the part of regular driving with less criticality of the accident-prone scenarios FSn. Besides, the discussion on the simulation results of the LHS (fig. 5.12) has already derived numerically that the tuning in regular driving is mainly required to optimises the progress and comfort. In other words, the safety weighting has a subordinated impact since the most tuning sets avoid collisions. The risk weight θ_8 is only used to adjust a conservative or rather preventative driving and thus to avoid inconvenient emergency manoeuvres. That is already ensured by small risk weights θ_8. The necessity of higher risk weights θ_8 emerges only in critical scenarios what is addressed with the graceful degradation in this work. Consequently, the tuning of the regular driving has a minor impact related to the contribution of this thesis. Therefore, the parameter ranges of the simulation results are used as indicator for the tuning sets in the evaluation (chap. 6). Even though, the final configuration is further adjusted manually to have one static tuning set $^{\mathrm{FS}n}\boldsymbol{\theta}$ in the current evaluation scenario FESn.

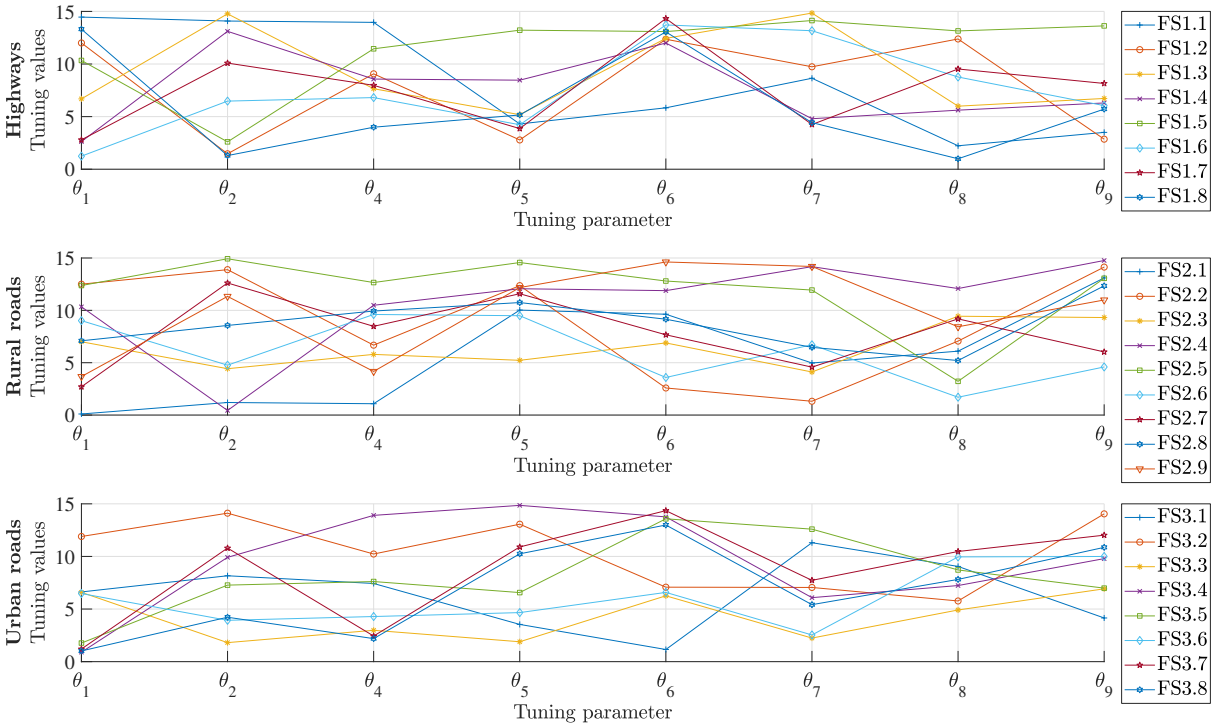

Figure 5.13: Tuning results regular driving - It depicts the tuning results of regular driving according to the functional scenarios FS of figure 5.9. The data base on the previous publication [30]. Hence, it should be noticed that the tuning θ_3 of the direction is exchanged by θ_9 of the collision probability. However, the conclusions are thereby not affected and thus it is referred to [30] for futher details.

What is more, eliminating crossinfluences, the integral driving function and the reference planner are adjusted with the same tuning set for the relative evaluation in chapter 6. In a sense, that reduces again the importance of the regular driving tuning set as long as a basic driving behaviour is enabled.

6 Evaluation of the risk based driving function

6.1 Evaluation strategy

The focus of this chapter lies on the evaluation of the integral driving function performance at the level of the full system integration. The safety benefit of the risk based driving function is investigated according to the research questions of section 1.2. More detailed, that includes the performance of the collision avoidance, collision mitigation with impact point localisation, uncertainty adaptation, and real time capabilities. Thereby, it is not appropriate to investigate all aspects at once due to crossinfluences and thus a test strategy is presented in the following. Additionally, showing the linkage between single evaluation steps presented in different chapters of this work, an overview of the evaluation aspects is given in this section at first. Thereby, pursuant to the V-model, unit tests and system integrations are listed.

Table 6.1 visualises the overview of the evaluation strategy. The rows constitute the evaluation aspects of the ascending branch of the V-model. They are grouped in four categories (A-D). These comprise an unit test on the level of normal distributed substate $\boldsymbol{Z}_{\mathrm{EK}}$ (A), the posteriori application of the risk assessment on recorded data (B), an evaluation of the full system integration what means closed-loop driving (C), and for the sake of completeness a statement to the risk measure itself (D). The main columns refer to the evaluation aspect, location, subject of evaluation, and available evaluation environments. The latter includes a reduced simulation environment, a software in the loop simulation for the driving function (sec. 6.3), test drives on the testing ground (sec. 6.3), fleet data of real road traffic, and an accident database. These evaluation environments are matched to the current evaluation aspect with the objective of maximum meaningfulness.

In the following, the selected tests are motivated with respect to the interaction of evaluation aspects and available environments. Besides, it is not appropriate to evaluate all contributions of the integral approach at once due to crossinfluences. Therefore, the categories (A-C) are split into several aspects to assess the driving function capabilities transparently, comprehensively and with minimal crossinfluences. The final results of the selected tests are presented in the subsequent sections.

The four categories (A-C) comprise following evaluation aspects:

A) At low level of the environment model (sec. 3.1), the risk based driving function combines the collision probability $P(C)$ and accident severity ψ of the normal distributed substate $\boldsymbol{Z}_{\mathrm{EK}}$. The final driving function depends on tremendous single executions and thus it is regarded as own category. Besides, the labelled reference data refer to that modelling level. Furthermore, this unit test is separated into tests of the computation time consumption (A1, A3) and function accuracy (A2, A4).

Table 6.1: Overview evaluation strategy - Single unit tests and integration tests are matched with appropriate evaluation environments. The turquoise cells summarise the evaluation aspects presented at different sections of this thesis. Additionally, the following system tests of chapter 6 are red marked.

	Aspect	Location	Description	Simulation (reduced environment)	Simulation (SIL - Full driving function)	Testing ground	Fleet data	Accident database
A	Basis functionality (criticality estimation on substate $\boldsymbol{Z}_{\mathrm{EK}} = \boldsymbol{Z}_{i,k}^{j}$)							
A1	Feasibility of collision probability at substate $\boldsymbol{Z}_{\mathrm{EK}}$	[207]	Execution time based on relative comparisons	Relative comparison due to lack of final platform	Relative comparison due to lack of final platform	Final platform and full driving function	-	-
A2	Accuracy of collision probability at substate $\boldsymbol{Z}_{\mathrm{EK}}$	[207]	Model accuracy based on statistical investigations	Monte Carlo simulation as ground truth	No additional benefit	No additional benefit	-	-
A3	Feasibility of accident severity prediction at substate $\boldsymbol{Z}_{\mathrm{EK}}$	Section 4.3	Execution time based on relative comparisons	Relative comparison due to lack of final platform	Relative comparison due to lack of final platform	Final platform and full driving function	-	-
A4	Accuracy of accident severity prediction η at substate $\boldsymbol{Z}_{\mathrm{EK}}$	Section 4.3	Model accuracy based on statistical investigations	FEM simulations as ground truth	No additional benefit	No additional benefit	-	-
B	Open-loop (post-process)							
B1	Executed drive at time step $t_i = t_0$	Section 6.4	Comparison between characteristic risk courses	Driving function not available	Full data available due to closed-loop driving $\rightarrow$ actually D	Full data available due to closed-loop driving $\rightarrow$ actually D	Hamburg data recordings	GIDAS
C	Closed-loop (Full system integration with reference to sec. 2.2.2.1)							
C1	Tuning strategy	Section 5.3	Tuning of the driving function based on the cost function J	Driving function not available	Accident occurrence allowed and automated execution of many test drives	Not appropriate due to the amount of test drives	-	-
C2	Feasibility of system integration	Section 6.3	Average execution time while driving	Not every module available	All modules available but no final platform	All modules available on test platform	-	-
C3	Uncertainty-adaptivity	Section 6.5	Comparison between vehicle reactions based on different uncertainty levels	Driving function not available	Possible but sensor model required	Real uncertain environment perception	-	-
C4	Mitigation application	Section 6.6	Comparison between risk based planner and reference planner based on impact severity ψ_{impact}	Driving function not available	Accident occurrence allowed and automated execution of many test drives	Both, testing with real physical equipment as well as virtual objects	-	-
D	Risk as a measure							
D1	Risk as a measure	Section 2.1.3.2 and 3.2	Conclusion derived by deductive logic Expected value demands for statistical evaluation approach	No further investigations needed				

The underlying calculations of the collision probability $P(C)$ (sec. 3.3) are already assessed in previous work [207]. Thereby, the reference uses their own simulation environment and hardware. Therefore, only the results related to the effectiveness are directly transferable to this thesis. The reference or rather ground truth for the collision probability is derived by Monte Carlo simulations with multiple binary collision checks. The study of the efficiency is used as performance indicator nonetheless, since the final platform of the automated vehicle is unknown. The investigation bases on a relative comparison to reference measurements, conducted by established Mote Carlo simulations with different sample numbers, and to the computation time of other approximating calculation methods.

The aspects pursuant to the accident severity ψ are already presented in section 4.3.3. Here again, a simplified simulation framework is used to assess the function effectiveness and the efficiency by relative comparisons. The accuracy of the severity prediction model η refers to FEM simulations which constitute the ground truth.

B) The next evolution step is seen in the posteriori, open-loop evaluation of the driving function (B1). Since it refers to previous measured data, a software in the loop simulation is not suitable. Fleet data of the Hamburg mobility partnership (sec. 6.4.2) and the GIDAS accident database (sec. 6.4.1) are used to address both, regular driving and critical incidents. Due to the safety driver as part of the Hamburg fleet, the data of the automated drives refer to regular driving. In critical scenarios, the driver takes over the vehicle control. Consequently, collisions have not occurred so far. Seeing that, the accident data supplements these recordings appropriately.

   Based on that data, characteristic risk courses over all criticality levels are obtained. The current state at the time step $t_i = t_0$ indicates the committed criticality of the driving function according to the risk modelling (B1). Thereby, the Hamburg data are biased by the safety driver's subjective risk awareness. In other words, the control remains automated in regular driving while the human driver reduces the criticality in all other cases. Therefore, in a sense, the driver's action can be used as indicator for critical situations. Contrary, the GIDAS accident data refer to average human driving style. Finally, the comparison of the yielded criticality is used to derive the threshold R_{thr} (sec. 5.2) for automated emergency manoeuvres.

   What is more, also the simulation results or test drives on the testing ground can be investigated posteriori. However, the criticality at the time step $t_i = t_0$ is already measured due to the closed-loop driving and thus no additional benefit is seen in this opportunity.

C) The full driving capability is evaluated closed-loop (C). It includes the feedback of the planned trajectory to the scenario evolvement. Necessarily, the full driving function (fig. 2.13) is involved and hence effects the evaluation data. Due to the level of development, the risk based driving function has currently no approval for the real road traffic what requires the testing ground or simulation as evaluation environment. The evaluation is conducted scenario based being the most promising testing strategy ac-

cording to section 2.2.1.2. The functional evaluation scenarios (FES) are presented in section 6.2.

The tuning of the automated driving function (C1) is already presented in section 5.3. Here, the SIL simulation is used to perform massive test drives automatically. The cost function J assess the entire scenario evolvement and ranks different configurations.

The final feasibility (C2) refers to the hardware of the product or rather, at the current development state, to the test vehicle. Therefore, the execution times of the full system integration are measured and presented in section 6.3. Furthermore, it needs to be mentioned that also the test vehicle has provisional hardware equipment. It is expected that the hardware differs to any final product but that is out of scope to this thesis.

The uncertainty-adaptivity (C3) is shown in real test drives on the testing ground to affect the drive with real obtained uncertain information. The characteristic risk courses and vehicle motion at the time step $t_i = t_0$ of different test drives in selected scenarios (sec. 6.2) are compared.

According to section 2.2.1.2, the mitigation performance (C4) is evaluated with relative comparisons to a reference planner which is already specified in section 2.2.2.3. Minimising crossinfluences, the reference planner is equipped with the same adjacent modules (fig. 2.13) and tuning parameters $\boldsymbol{\theta}$ (sec. 5.3.3). Both planners perform test drives in selected evaluation scenarios presented in section 6.2. These scenarios focus on a high criticality level to investigate the benefit of the integral approach with impact point localisation. Thereby, the entire scenario evolvement is assessed, once at the end, and hence the accident severity ψ_{impact} ranks the test drives. In the case of no collision, the accident severity is set to zero with $\psi_{\text{impact}} = 0\,\frac{\text{m}}{\text{s}}$. The evaluation takes place on the testing ground and in the simulation environment.

D) The risk measure (D) is established in well-known safety strategies (sec. 2.1.3.2). It refers to deductive logic or rather safety by design and thus requires no separate evaluation. The final system behaviour is adjusted by the demanded risk limits. What is more, according to section 3.2, the risk constitutes the expected values of the severity Ψ with reference to the planned trajectories. That way, a driving behaviour is derived which bases on a statistical approach. Consequently, also the evaluation requires statistical investigations. In other words, test drives for single evaluation aspects need to be repeated significantly. That concerns both, the risk based planner and the reference planner. Due to potential outliers, it is not possible to derive conclusions on single test drives. Therefore, the main part of the statistical evaluation is performed in simulation studies. Additionally, a reduced selection of scenarios is evaluated on the testing ground.

6.2 Evaluation scenarios

The evaluation of the final system integration (tab. 6.1 - D) uses a scenario-based approach as motivated in section 2.2.1.2. The underlying idea of the scenario selection bases on the assumption that if all possible critical scenarios are passed appropriately, the driving function is well-prepared to encounter the real world. Hence, the goal is to extract a finite number of significant scenarios. Accordingly, the generation of functional evaluation scenarios (FES) is explained in the following.

The integral approach of this thesis has its strength especially in critical scenarios (sec. 2.1.1). Here, the decision between collision avoidance and collision mitigation and thus the combined use of multiple safety measures gains the most importance. Therefore, it is focused on accident-prone functional scenarios in the following. Here lies the main difference to the scenarios of section 5.3.2. The tuning of section 5.3 contributes more or less to the risk assessment in regular driving (FS1.1 - FS3.8) and motivates the *graceful degradation* (FS LHS), while this section focus on the entire integral approach with an uncertainty-adaptive collision avoidance and mitigation strategy. Thereby, it should be noticed that both scenario sets base, at least partly, on the GIDAS accident database but derive different aspects according to the current focus. What is more, with reference to the safe system approach (sec. 1.1), implications on the use cases for mitigation strategies are discussed in the following. In other words, a vehicle able to perform mitigation trajectories has also a strong collision avoidance competency what needs to be considered in the scenario selection.

Finally, owing to the unknown future accident occurrences, promising testing scenarios are derived by systematical considerations and matched with the GIDAS accident database [142] as well as Shanghai's *A Nice City* scenario catalogue [191]. Figure 6.2 summaries the considerations.

Basically, an accident happens if two objects impact each other. Moreover, a collision becomes unavoidable earlier when the point of no return is exceeded, also referred by ICSs. In other words, relative poses $\Delta\tilde{\boldsymbol{g}} = (\Delta x, \Delta y, \Delta\varphi)^{\mathrm{T}}$ between the ego vehicle E and the object o_k with a DOF = 3 in relation to the current dynamics ($v_{\mathrm{E},k}$, $a_{\mathrm{E},k}$ etc.) determine the criticality level. Thereby, a systematic parameter variation can be used to derive arbitrary collision configurations or rather initial scenes from scratch as shown in figure 6.1(a). Thereby, the application determines the amount and type of further scenario features, such as the number of road users, object classifications, traffic participants behaviour, and road conditions. In this thesis, a scene with an object number $N_k \leq 2$ and object classification $x_c \in$ [vehicle, pedestrian] independent of detailed road conditions is seen sufficient to derive the conclusions on the integral approach. Besides, even if more than two objects encounter typical road traffic, collisions refer often to two opponents, the ego vehicle E and one object $o_{k=1}$ [142]. Furthermore, collisions between two vehicles and between a vehicle and a pedestrian constitute a major accident type. Nevertheless, the findings may be transferred to other, possibly more complex scenarios.

Figures 6.1(b) and 6.1(c) illustrate upper bounds to the initial scenes pursuant to German road traffic. Referring to highways, the roadways are separated and the traffic is straightened

(fig. 6.1(b)). In that case, assuming a recommended speed of $v = 130\,\frac{\mathrm{km}}{\mathrm{h}}$ and a maximum deceleration of ${}^{\min}a = -9\,\frac{m}{s^2}$, a vehicle needs $t_{\mathrm{brake}} \approx 4\,\mathrm{s}$ to brake into a full stop. Contrary, a swerving emergency lane change would require $t_{\mathrm{swerve}} \approx 1\,\mathrm{s}$ [235]. Thereby, the dynamic of adjacent traffic is neglected to deal with the worst case. In general, such full braking or hard swerving manoeuvres are not necessary due to the traffic flow what would increase the TTC. Nevertheless, exceptions might occur, such as encountering the end of a traffic jam behind a hilltop. On rural roads (fig. 6.1(c)), the relative velocities increase with $v_{\mathrm{rel}} = 200\,\frac{\mathrm{km}}{\mathrm{h}}$ due to the lack of constructional separations. However, assuming a cooperative driving behaviour, both vehicles need $t_{\mathrm{brake,rural}} \approx 3\,\mathrm{s}$ to stop even if the braking distance counts double. A lane change manoeuvre would require less time similar to the previous highway assumption. However, even if swerving seems to be the better option at high velocities, braking remains important to not involve third parties due to daring evasive manoeuvres and thus to not disregard the guidelines of the ethics commission [202]. In all other cases, including urban traffic, it is assumed that the velocities will be lower and thus the required time to avoid a collision. On top of that, the more the permitted speed decreases, the more crossing traffic emerge and thus gains importance. However, the extremum of orthogonal traffic is similar to sudden appearing objects in the longitudinal direction due to the absence of a velocity component in that very direction.

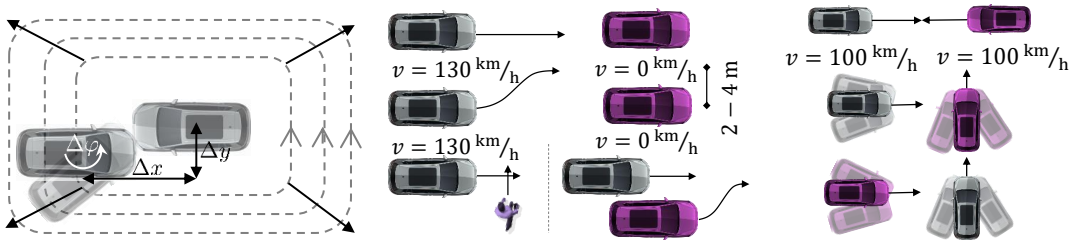

(a) Systematic (b) Highway (c) Rural and urban roads

Figure 6.1: Schematic scenario generation - The cases of possible collision scenarios are restricted by the traffic infrastructure and regulations.

Seeing the previous derived TTCs, and owing to a planning horizon of TH $> 4\,\mathrm{s}$, the question arises when collisions with automated vehicles will appear at all. Therefore, table 6.2 presents an overview where the driving criticality is *suddenly* recognised in different criticality phases. Thereby, it is separated between the ego vehicle and the object causing that criticality level. Each cell of the table body lists causes for that state and formulates a conclusion related to the expected reaction of the automated vehicle. In regular driving, it is assumed that potential incidents are eliminated immediately due to the preventative driving. Furthermore, it is expected that only driving functions will be released that follow the road traffic regulations and have an advanced driving competency. That way, increased criticality with the responsibility of the automated vehicle is seen mainly due to system failures. If they are serious, accidents will occur even with the best safety measure. However, that issue refers to functional safety out of scope to this thesis. One theoretical exception refers to temporary malfunctions. Here, the temporary malfunction causes a critical event but shortly thereafter the driving performance normalise and the automated vehicle reacts on

Table 6.2: Accident responsiblity - It relates the accident responsibility to the criticality phases and derives the reaction of the automated vehicle. Proper use cases for the integral approach are marked turquoise.

	Criticality recognition in...		
	...**regular driving**	...**pre-crash phase** but still **avoidable**	...**pre-crash phase** and **unavoidable**
Ego responsibility	Happens continuously due to various reasons Vehicle answer: • eliminate risk • preventative driving • avoid collissions	• Persistent system failure (functional safety, out of scope) • temporary system failure (e.g., unnoticed temporary bad perception, traffic rules violation) Vehicle answer: • It is expected that the **accident will occur unchanged**. • Theoretically, **CA** and **CM** are possible if the vehicle performance recovers in time.	• Persistent system failure (functional safety, out of scope) • temporary system failure (e.g., unnoticed temporary bad perception, traffic rules violation) Vehicle answer: • It is expected that the **accident will occur unchanged**. • Theoretically, **CM** is possible if the vehicle performance recovers in time.
Object responsibility		• Similar to current accident occurrence Vehicle answer: **CA**	• Similar to current accident occurrence • Very sudden object appearance Vehicle answer: **CM**

the self-inflicted incident. For example, it could refer to a mistake of situation interpretation leading to the violation of traffic rules and thus increased criticality. An other example constitutes unnoticed temporary perception failures, e.g., due to changing weather conditions. However, such issues are seen more or less as an theoretical idea to cause emergency manoeuvres. Rather, it is expected that system failures will induce accidents directly due to the short time horizons.

In contrast, the target object has less restrictions or rather is assumed to have a lower driving competency. For example, it might violate regulations, be overstrained, or just be careless. As result, accidents will occur independent of the automation level of the ego vehicle. Therefore, it is expected that these cases resemble the related subset of current accident data. Thereby, in the case of avoidable collisions, the automated vehicle will reduce the risk due to the preventative attitude. Consequently, mitigation is only provoked in very sudden incidents, such as appearing objects behind occlusions or target driving mistakes on rural roads. In conclusion, third-party responsibility is seen as main use case for the developed integral approach. Therefore, corresponding accident cases from the GIDAS accident database are considered in the following. A short statistical background on the injury frequency is presented in figure 5.6. Further details might be derived from the GIDAS database directly.

Shaghai has been the first city in China permitting automated vehicles to carry passengers [236]. Among others, a license bases on the passing of a scenario catalogue with general

traffic scenarios. The subset of safety related scenarios is used in this work as one example for administrative approval directives.

Finally, table 6.3 matches scenarios at the functional level from the three previous mentioned scenario sources to determine the final functional evaluation scenarios FES. Further details on the concrete instances as well as the evaluation results are presented in the dedicated subsections.

Summarising, figure 6.2 presents an overview of the used scenarios in this work. It shows the functional scenarios over the criticality levels. Thereby, also the tuning scenarios of section 5.3.2 are sorted. It illustrates the uniform distribution of the scenario selection over all criticality levels. While the tuning process also addresses regular driving, the functional evaluation scenarios (FES) focus mainly on the tipping point between CA and CM, and appropriate mitigation strategies in general.

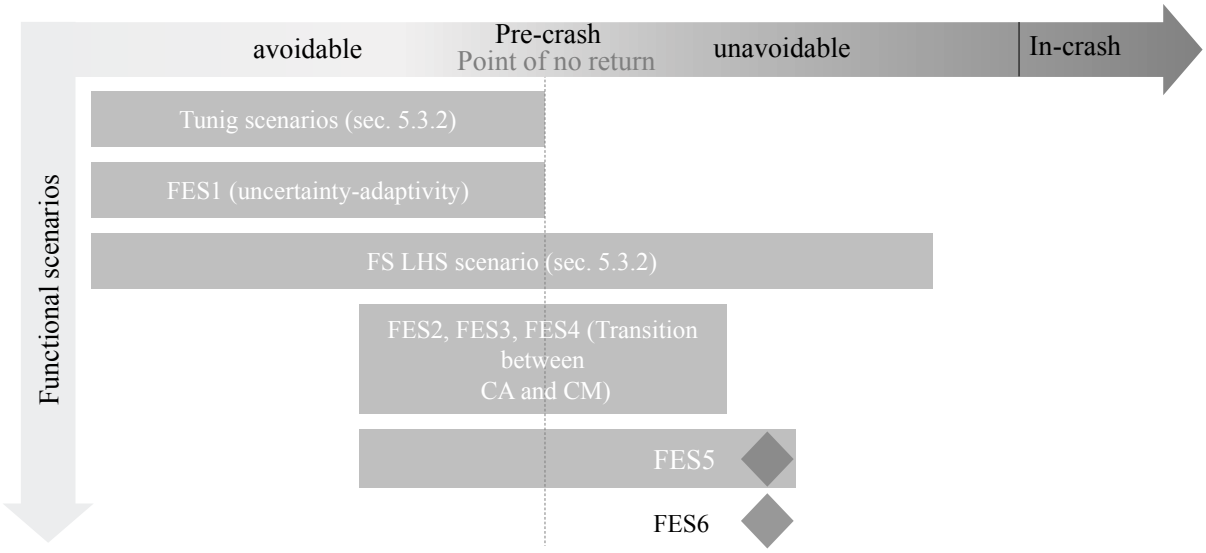

Figure 6.2: Functional scenarios on criticality level - The figure sorts the used functional scenarios (sec. 5.3 and 6.2) to the criticality level. It extends figure 5.3.

6.3 Test setup and simulation environment

A selection of the the evaluation scenarios is performed in real teat drives on the testing ground. Therefore, the test vehicle constitutes the reference for the feasibility of the developed risk based motion planning. Figure 6.3(a) shows a picture of one vehicle of the test fleet. A detailed architecture of the vehicle electronic is out of scope to this thesis. Nevertheless, important aspects are presented in the following.

The sensor equipment consist of several lidars and radars as well as one stereo camera. These are used to percept the environment. That includes the object detection as well as its uncertainty quantification for the risk assessment. More detailed, each sensor provides an object detection including the state $\boldsymbol{z}_k$, uncertainty $\boldsymbol{\Sigma}_k$ and classification $x_{c,k}$. Afterwards,

Table 6.3: Evaluation scenarios - Systematic considerations, the GIDAS accident database, and the Shanghai's scenario catalogue are used to derive the evaluation scenarios.

#	Description	GIDAS	A nice city (Shanghai)	Final evaluation scenario
FES1	A pedestrian is stepping in front of the vehicle. The scenario investigates the vehicle reaction on a changing uncertainty level which is manipulated due to the use of different sensor sets.	UTYP 4xx, such as: 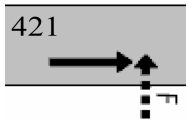	Autonomous emergency braking to pedestrians 	a) 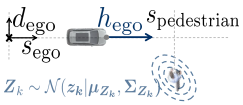 b) 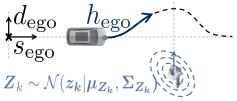
FES2	A low speed vehicle ahead impedes suddenly the onward journey while an additional vehicle drives in the adjacent lane with opposite direction. The point of no return is exceeded. The evaluation focus on the decision between potential CA by swerving or CM by braking, both under changing uncertainty.	Approximately UTYP 6xx, such as: 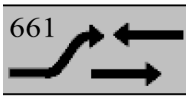	Overtaking 	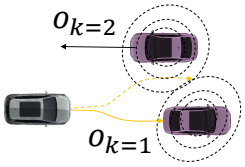
FES3	An object appears straight ahead of the ego vehicle, e.g., due to pulling out from an occluded parking lot. Only an emergency swerving manoeuvre may avoid the collision if the adjacent lane is free. If it is blocked by an other object, a collision is unavoidable but still time remains to mitigate the crash consequences. The focus lies on the appropriate CA and CM strategy in potential future accident hotspots.	Approximately UTYP 6xx, such as: 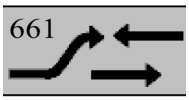	Overtaking 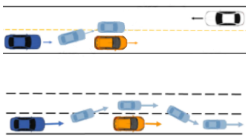	a) 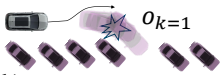 b) 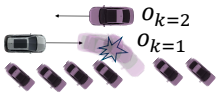
FES4	An object appears suddenly in front of the ego vehicle. Thereby, the lateral offset Δy and relative angle $\Delta\varphi$ are permuted to generate different concrete scenarios. Thus, the CA and CM strategy is evaluated theoretically but also more systematically compared to the other scenarios.	-	-	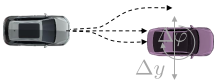
FES5	The ego object drives straight ahead when an object $o_{k=1}$ provokes a critical incident by swerving carelessly into the lane of the ego vehicle. The focus lies on the appropriate CA and CM strategy in potential future accident hotspots.	UTYP 3xx, 63x, 64x such as: 	Identification and response to forward vehicle lane change 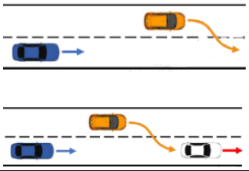	
FES6	An object $o_{k=1}$ overtakes the object $o_{k=2}$. Thereby, it overlooks the ego vehicle and thus both, the ego vehicle and the object $o_{k=1}$, are involved into an unavoidable crash. The focus lies on the appropriate CM strategy in potential future accident hotspots.	UTYP 661 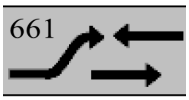	Overtaking 	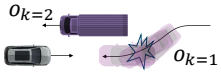

a Kalman filter based object fusion merges these single objects. Due to the characteristics of the lidar and radar sensors, the physical obstacle is moved slightly enabling the object

(a) (b)

Figure 6.3: Test equipment - It shows a) the test vehicle and b) the evaluation with virtual objects.

classification by each sensor solely. Alternatively to the sensor set, evaluating the impact point localisation, virtual objects are generated independent of the perception module to preserve the test equipment. Thereby, the object uncertainty is emulated similar to the evaluation in the simulation environment. Figure 6.3(b) illustrates the fusion of the real ego vehicle and the virtual objects. The reference data of the ego vehicle state is recorded by an Inertial Navigation System (INS) in combination with an differential Global Navigation Satellite System (GNSS).

The modules of figure 2.13 are splitted on several computing units. The planner bases the massive parallel computations of the trajectory optimisation on one GPU. The reaction time of the entire driving function cumulates about 40-100 ms of the perception, 100-200 ms of the environment prediction, 200 ms of the trajectory planning and several hundred milliseconds for the actuators. Thereby, the concrete time periods depend on the instantiation of the modules. Therefore, the final computation time of the risk based trajectory planning depends on several properties of the planner configuration. The main features constitute the planning horizon TH and its time intervals of the planning steps t_p, the reward time steps t_i and ego dynamic model time steps t_m. Furthermore, the amount of actions $\mathcal{A}_s$ in state s, the size of the pruning and number of objects N_k influence the computation time. The final instantiation changes on the evaluation scenarios. While the reserved time interval for the trajectory planning constitutes 200 ms ($f_{\text{update}} = 5\,\text{Hz}$), the average calculation time is about $\bar{t}_{\text{planner}} = 127\,\text{ms}$ for a scenario with one target object.

Alternatively to the test vehicle, a simulation environment is used to derive the various repetitions for the statistical evaluation. Thereby, the driving functions consists as far as possible of the same modules as the test vehicle. The only exception constitutes the interaction with the environment. These interfaces need to be emulated as shown in figure 6.5(a). The environment perception model projects the recorded uncertainties from the fleet data (sec. 6.4.2) on the ground truth data of the simulation. Thereby, simplifications are used since a detailed sensor model is out of scope of this thesis. Most sensitive, the object detection uncertainty depends on the relative distance between the ego vehicle and the object o_k. That relations

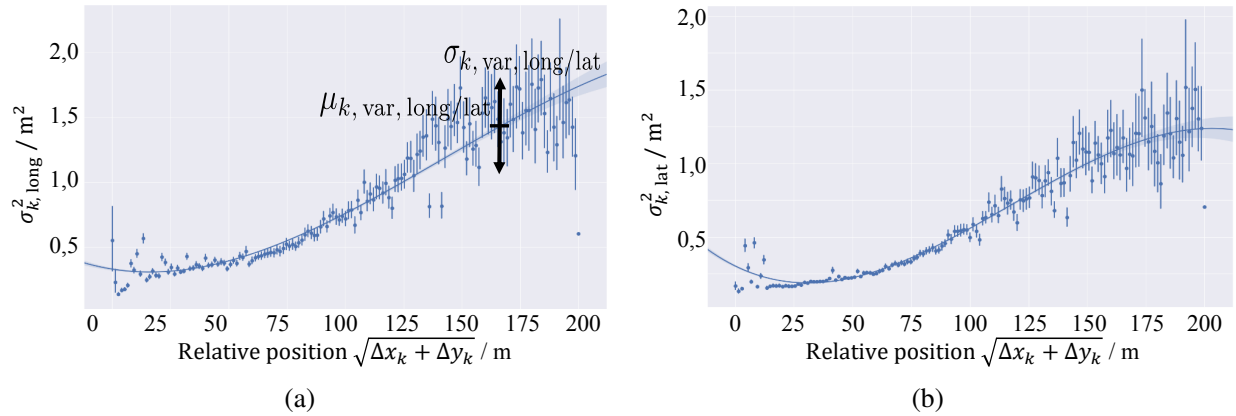

Figure 6.4: Sensor model - Regresseion of the a) longitudinal and b) lateral object position uncertainty $\sigma_{k,\text{long/lat}}$ pursuant to the relative distance.

are shown in figure 6.4. The expected value $\mu_{k,\text{var,long/lat}}$ of the variance $\sigma^2_{k,\text{long/lat}}$ as well as the uncertainty $\sigma_{k,\text{var,long/lat}}$ of the variance $\sigma^2_{k,\text{long/lat}}$ related to that expected value increase pursuant to the relative distance. Therefore, the final uncertainty is created by:

$$\mathbf{\Sigma}_{k,\text{long/lat}} = \begin{pmatrix} \sigma^2_{k,\text{long}} & 0 \\ 0 & \sigma^2_{k,\text{lat}} \end{pmatrix} \quad \text{with} \tag{6.1}$$

$$\sigma^2_{k,\text{long/lat}} = \sigma_{k,\text{var,long/lat}} \cdot n + \mu_{k,\text{var,long/lat}} \tag{6.2}$$

$$n \in N \sim \mathcal{N}(0,1)$$

$$\sigma_{k,\text{var,long/lat}} = f(\Delta x_k, \Delta y_k) \tag{6.3}$$

$$\mu_{k,\text{var,long/lat}} = f(\Delta x_k, \Delta y_k) \tag{6.4}$$

Afterwards the variance $\mathbf{\Sigma}_{k,\text{long/lat}}$ is aligned to the vehicle orientation φ_k and thus the final covariance $\mathbf{\Sigma}_{xy}$ results.

Exemplary, figure 6.5(b) shows a screenshot from the simulation environment. It shows the ego vehicle evading to a pedestrian stepping in front of the vehicle. Thereby, the planned trajectory is visualised by a white line above the vehicle. The underlying criticality subfeatures of the risk, collision probability, and accident severity are illustrated red, magenta and cyan, respectively.

6.4 Subsequent risk assessment of fleet data

6.4.1 GIDAS accident database

The German In-depth Accident Study (GIDAS) database [142] contains detailed accident information about selected accidents, collected in the region of the Germans cities Hannover and Dresden. It is the largest in-depth accident data collection project in Germany. An

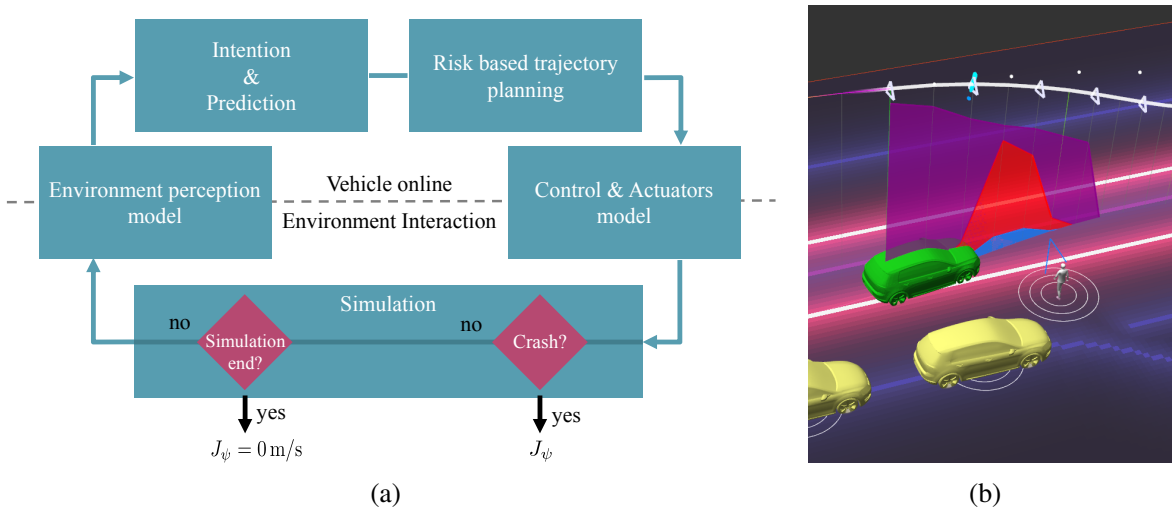

Figure 6.5: Simulation environment - a) shows the driving function architecture with specific modules for the simulation environment and b) displays a screenshot of the visualisation of the simulation environment.

interdisciplinary team gathers various accident aspects, such as accident kinematics and injuries, from the accident site directly. The project is a foundation of multiple stakeholders, such as vehicle original equipment manufactures (OEM) and research institutes, started in 1999.

Enhancing the data, the accident evolvements are reconstructed and these detailed information about the pre-crash phase are stored in the *Pre-Crash-Matrix* (PCM). It contains mainly information about the participants, motion characteristics and surroundings of the last five seconds before the first collision. These data constitute the basis to evaluate the characteristic risk course in real accidents in this thesis. However, the data need to be filtered to enable a consistency evaluation. By way of example, accidents with barriers, VRU, skidding, rollover, and in general accidents before the year 2000 are excluded. In other words, the data selection focus on vehicle-vehicle crashes and bases on plausibility checks. Even if mostly experienced accident investigators collect the data, the information are obtained post crash and superimpose with subjective assessments and error-prone assumptions. Nevertheless, the data are expected to have a higher quality than comparable data points of national accident recordings, e.g., contained in [3]. Finally, 4164 accident cases are used in the following for the evaluation of the risk assessment. What is more, the PCM contains only non-probabilistic data. A reconstruction of possible uncertainties related to the driver's or rather vehicle's point of view is not available. Therefore, the sensor model of the simulation environment (sec. 6.3) is applied.

Figure 6.6 shows the vehicle dynamic, uncertainty and criticality over the last five seconds related to the crashes of selected accident cases with maximum diversity. The velocity profiles show that the accidents occur without significant accident mitigation activities. Rather it indicates that the majority of human drivers does not react at all. Only in the last few hundred milliseconds they decelerate negligibly. Due to the instantaneous risk evaluation, the

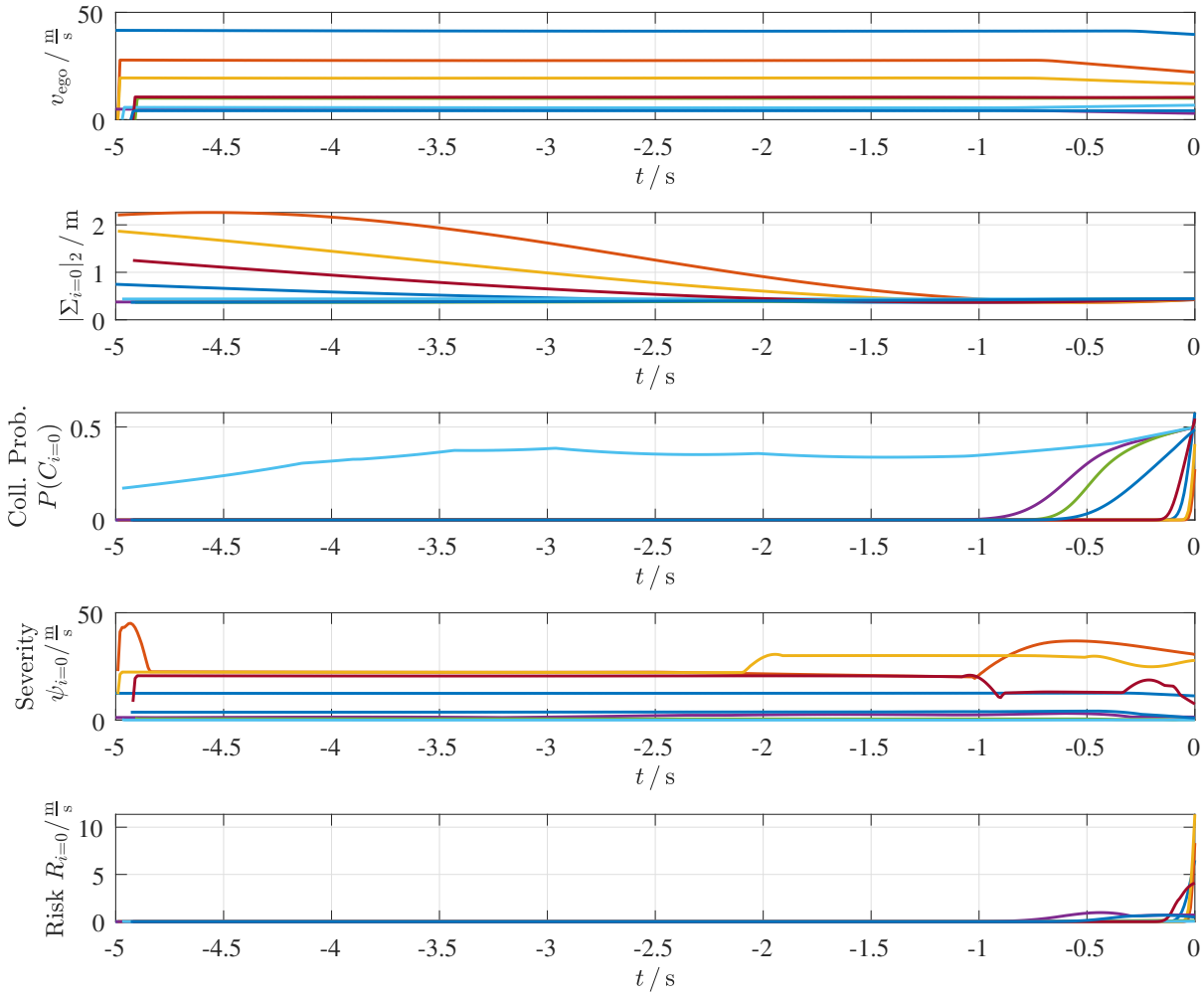

Figure 6.6: Criticality of GIDAS accident cases - It shows the velocity profiles and criticalities of a selection of GIDAS accident cases.

collision probability $P(C_{i=0})$ of the most cases remains zero for a long time period and then increase suddenly before the collision. In contrast, the severity $\psi_{i=0}$ is estimated for the most probable collision configuration $\omega_{\text{coll}}^{\text{Pmax}}$ and hence is distinctive all the time. Thereby, it follows the initial velocity profile in general. The risk $R_{i=0}$ combines these two criticality subfeatures and hence increase only with the collision probability $P(C_{i=0})$ shortly before the collision occurs. An exception is visualised by the cyan accident case. Here, the accident opponents approach over the full five seconds continuously with increased collision probability $P(C_{i=0})$. However, the underlying velocities of that scenario are very low and thus the risk follows at low level. Transferred to the risk based motion planning, the automated vehicle would not react on such incidents caused by no recognition of any dangerous situation. As mentioned in section 5.2, such incident is solved more focused with a state machine for low velocities. Here, a collision would be simply avoidable at any stage according to the collision probability.

Figure 6.7 visualises statistics to all accident cases. Subfigure 6.7(a) shows a histogram of the criticality subfeatures at the impact. Most noticeable, the average impact collision probability is given by $\overline{P}(C_{i=0}) \approx 50\,\%$. At one hand, it could be expected that a collision is indicated by $P(C_{i=0}) = 100\,\%$. On the other hand, the maximum collision probability $P(C_{i=0}) = 100\,\%$ is only possible if a collision occurs with zero uncertainty. Therefore, the remaining uncertainty due to the sensor model (e.g., fig. 6.6 with $|\Sigma_{i=0,\text{impact}}|_2 \approx 0.4\,\text{m}$) as well as the heuristics of the probability estimation (sec. 3.3) produce that reduced value. All in all, the values spread between 25 % and 75 %. The shape of the risk histogram follows the shape of the accident severity. Thereby, it is damped by the collision probability and hence the average value decrease from $\overline{\psi}_{i=0} \approx 8.6\,\frac{\text{m}}{\text{s}}$ to $\overline{R}_{i=0} \approx 4.2\,\frac{\text{m}}{\text{s}}$.

In general, the initial velocity bias the final accident severity. Therefore, subfigure 6.7(b) shows the percentiles pursuant to four velocity intervals of the initial dynamic. Thereby, the amount of data points decrease with higher velocities. The percentiles of the collision probability remain approximately between 45 % and 55 % independent of the velocity range. In contrast, the severity $\psi_{i=0}$ increase according to the velocity profile and thus the risk $R_{i=0}$.

Summarising, the risk based criticality indicates accidents with increased risk values appropriately. Thereby, due to the heuristics and remaining uncertainties the values of the criticality feature follow a characteristic range. The lowest values to indicate a collision with the collision probability is about $P(C_{i=0}) \approx 20\,\%$. A collision probability of 50 % indicates that it is more probable to collide than to have a collision free drive, while 70 % indicates a certain crash. Similar to the course of the collision probability, the risk remains at zero and increases solely if a collision is imminent, a few hundred milliseconds before a crash. In conclusion, already low risk values $R_{\text{thr}} \approx 3\,\frac{m}{s}$ seem suitable to activate the graceful degradation. A more detailed system configuration would adjust the risk threshold R_{thr} on the certain velocity. Alternatively, the collision probability could switch entire system states as well.

6.4.2 Fleet data Hamburg

The Volkswagen Group and the city Hamburg entered into a strategic mobility partnership to foster the launch of automated vehicles (e.g., [237] and [238]). For that purpose, the city Hamburg invests in intelligent infrastructure, such as traffic lights for vehicle-to-infrastructure (V2I) communication. The goal is a test route for automated vehicles to establish Hamburg as an innovative city for new intelligent mobility solutions. One key milestone constitute the Intelligent Transportation System World Congress in the year 2021 in Hamburg to present and debate about new mobility solutions and trends. On the other hand, Volkswagen tests the automated driving with a fleet of e-Golfs. The vehicles are equipped with lidar, radar and cameras similar to the test vehicle described in section 6.3.

The obtained data are used to improve the automated systems further on. Accordingly, this thesis uses available data to evaluate the risk based criticality open-loop. Even if the test area is extended continuously, the current available data for this thesis are limited to the

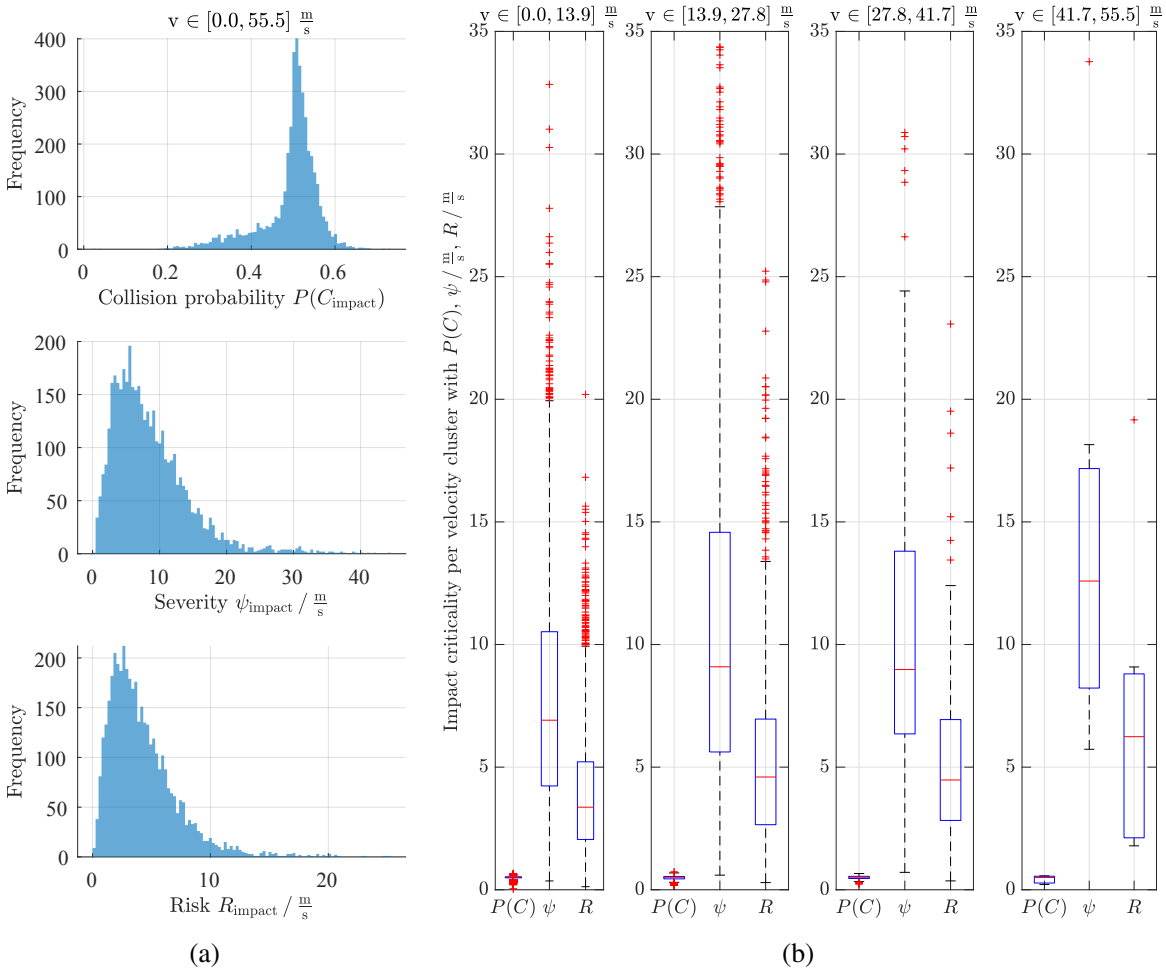

Figure 6.7: Criticality of GIDAS accident statistics - a) shows a histrogram of the impact collision probability $P(C_{\text{impact}})$, impact severity ψ_{impact}, and impact risk R_{impact}. Due to the bias of the underlying velocity profile, b) visualises the same data in four different clusters.

test route shown by figure 6.8(c). Basically, the tests drives are supposed to take place in Hamburg's city between the exhibition grounds and the Elbphilharmonie.

Figure 6.9 concatenates multiple test drives. It presents about 30 minutes of mixed automated and manual driving. The moderate velocity profile follows the speed limits of German cities and the stop and go of inner city traffic. Contrary to the accident cases of section 6.4.1, the histogram 6.9(a) shows that almost all detected collision probabilities $P(C_{i=0})$ remains below 20 %. Only few exceptions occur for single instantanous time steps as shown by figure 6.9(b). That bases on an error-prone object perception and prediction rather than the occurrence of real crashes. More detailed, only 43 data points have a collision probability greater than 20 % and only 7 data points exceed 30 %. The point numbers relate to an update frequency of $f_{\text{update}} = 5\,\text{Hz}$ according to section 6.3. In fact, as expected, the majority of collision probabilities remain near zero or rather below 10 %. The distribution of the accident severity $\psi_{i=0}$ follows the inner city velocity profile. Due to the low collision probabilities, also the final risk values remain at low level. Besides, the few higher collision

(a) Picture: [239]

(b) Picture: [239]

(c) Picture bases on [240]

Figure 6.8: Hamburg mobility partnership - a) and b) show vehicles of the Hamburg fleet on the street and c) visualises the test route of the available data with the magenta dashed line.

probabilities are concatenated with low accident severity and thus produce low risk values as well. All in all, the maximum risk value $R_{i=0}$ falls below $2\,\frac{\mathrm{m}}{\mathrm{s}}$.

Additionally to the criticality, figure 6.9(b) distinguishes automated and assisted driving. Unfortunately, the dataset available for this thesis contains only few automated driving time periods. Nevertheless, a characteristic risk course of real traffic interaction is shown. Thereby, the low criticality values enable a clear differentiation to critical incidents which require only a threshold $R_{\mathrm{thr}} \approx 3\,\frac{\mathrm{m}}{\mathrm{s}}$, as shown in section 6.4.1. Finally, providing an additional safety margin, a risk threshold $R_{\mathrm{thr}} = 2\,\frac{\mathrm{m}}{\mathrm{s}}$ is suggested for the following scenario based evaluations. Thereby, it should be noticed that the risk value depends on the underlying velocity profile. Therefore, that threshold should be adjusted for higher velocities, such as on highways. Alternatively, a collision probability of $P(C) = 20\,\%$ could indicate a collision as well.

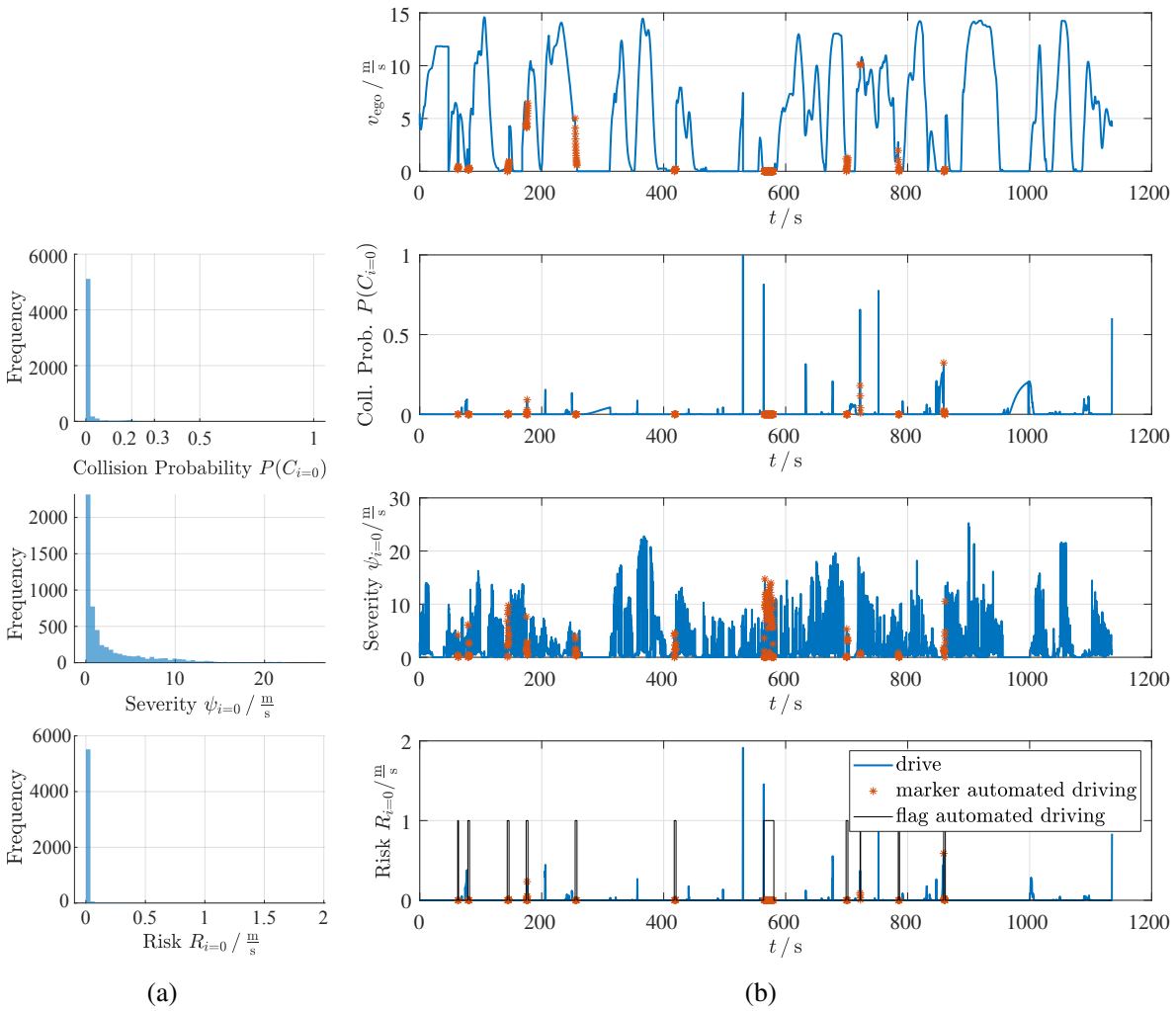

Figure 6.9: Criticality of Hamburg test drives - a) shows a histogram of the criticality subfeatures at the initial planning time step $t_i = t_0$. b) visualises the same criticality data over the time.

6.5 Uncertainty-adaptive driving

The uncertainty-adaptivity is shown by two example evaluations. At first, it is referred to the scenario FES1 with similar discussion in the previous publication [28]. Secondly, an vehicle swerving manoeuvre with oncoming traffic (FES2) is investigated.

The experimental setup of scenario FES1 is shown in table 6.3. The automated vehicle drives straight ahead with constant velocity $v_{ego}(\lambda_{ego}) = 30\,\frac{km}{h}$ and percepts a pedestrian crossing the street at $\lambda_{ped} = 87.5\,m$. Due to the obstacle, the vehicle needs to avoids a collision either by braking or swerving. Thereby, the vehicle is restricted by a wheel angle $\delta = 0°$ (FES1a) and input acceleration $a_{in} = 0\,\frac{m}{s^2}$ (FES1b), respectively. At one hand, these constraints increase the reproducibility of multiple test runs. On the other hand, they enable to derive conclusions without crossinfluences. Besides, further disturbances are eliminated

Table 6.4: Sensor configurations - The table assigns the sensor set to the instances of the the object fusions.

	Camera object	Camera classification	Lidar 1	Lidar 2	Radar
Object fusion 1			x		
Object fusion 2	x				
Object fusion 3	x		x		
Object fusion 4	x		x	x	x
Object fusion 5		x		x	
Object fusion 6		x			x
Object fusion 7		x	x	x	x

by neglecting the graceful degradation. Therefore, this scenario constitute an exception to the mitigation applications of table 6.3. The driving is performed with the tuning set $\boldsymbol{\theta} = [1e10, 1e9.5, 1e14, 1e13, 1e3, 1e7, 1e3, 1e14]$. Due to the pedestrian, the used severity measure follows section 4.1.2.

The object perception represents exemplary multiple uncertainty sources, as presented in section 2.1.3.1. Thereby, the perception uncertainty varies due to the used sensor equipment. Among others, that emulates temporary malfunction, changing weather conditions, or different uncertainty levels in general. The sensor configurations are a combination of lidar, radar, and stereo camera devices as shown by table 6.4. Thereby, each sensor device provide an environment perception including the object extraction with information on poses, uncertainties, as well as classifications. Afterwards, these single sensor information are merged by a Kalman filter based object fusion. Among others, the object classification is enabled by the characteristic movement of the pedestrian. Thereby, the stereo camera is used in two ways. At one hand, it solely provides the object classification (fusion 5-7) in addition to the pose detection of other sensors. On the other hand, it also generates an object for the subsequent fusion (fusion 2-4). The quantitative, time variant uncertainties of each object fusion or rather uncertainty level is aggregated by the Schatten-2-norm. In general, the scenario refers to regular driving and thus the vehicle is able to avoid the potential collisions with all sensor configurations. Moreover, the vehicle reaction is investigated by 3-11 repetitions for the braking as well as swerving scenario. However, enhancing the legibility, the following figures present only the average values of the drives. One exception constitute figure 6.10. Here, also the the one-sigma bound is shown.

Figures 6.10 to 6.12 show the results of the braking scenario FES1a. They present the driven dynamic and criticality for the initial time step $t_i = t_0$. Thereby, figure 6.10 visualises the ego vehicle's velocity profile v_{ego} over the driven path λ_{ego}. Due to the changing sensor equipments, the perception performance varies and thus the form of the collision avoidance by braking differs. In general, higher uncertainties lead to a more conservative driving beha-

viour compared to a drive with lower uncertainties. It is shown by an early deceleration as well as an additional safety margin to the pedestrian. These characteristics are emphasised by the two smaller subfigures. Furthermore, it should be noticed that the divergence of the test drives have its maximum during the deceleration rather than on the stopping point. That relates to the numerical issue of the risk measure. If the velocity decrease by $v \to 0$ the severity decrease as well $\psi \to 0$ and thus the risk $R \to 0$. As result, the different drives merge at lower velocity. If necessary, such aspects could be filtered by an enhanced graceful degradation. As mentioned earlier, the collision probability $P(C)$ could be used at low velocities to indicate the criticality solely. In conclusion, the automated vehicle shows an intelligent, uncertainty-adaptive collision avoidance behaviour. The same planning function adapts inherently to changing conditions.

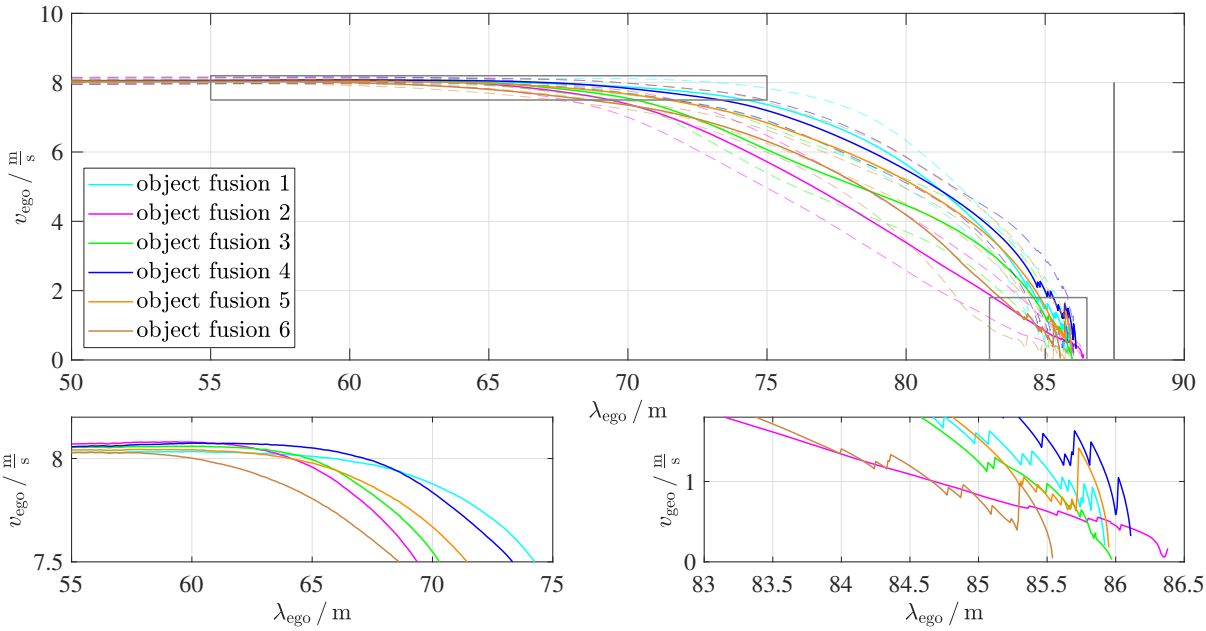

Figure 6.10: Sensor-adaptive collision avoidance by braking - The velocity v_{ego} of the ego vehicle is visualised over the progress λ_{ego}. The vehicle brakes to a pedestrian at distance $\lambda_{\text{pedestrian}} = 87.5\,\text{m}$ which is indicated by a grey line. The velocity profile changes depending on the uncertainty level due to the object fusion. The upper subfigure indicates the average (solid line) and the one-sigma-bound (dashed line) of multiple test drives. The other subfigures emphasise areas of interest according to the uncertainty-adaptive driving. The saw shape results of a different ending of the test drives. Moreover, the vehicle with object fusion 2 approaches the pedestrian continuously due to the bad depth information. The figure follows the previous publication [28].

More detailed, figure 6.11 highlights the difference between the maximum (object fusion 2) and minimum induced uncertainty level (object fusion 1). Similar to figure 6.10, it shows the vehicle approach to the pedestrian but here the uncertainty course is emphasised. The object fusion 2 leads to a very conservative deceleration while the object fusion 1 leads to a very late but strong braking. Combining both sensors (object fusion 3), the vehicle shows first an conservative deceleration due to the early object detection by the camera. Later on, the lidar

contributes to the object perception as well. Thus, if the lidar provides information to the object perception, the uncertainty decreases suddenly and hence the vehicle reconsiders its driving behaviour. That results in the switching to the more aggressive pedestrian approach similar to the behaviour with object fusion 1. Thereby, crossinfluences due to any correction of the vehicle pose are excluded as shown by the third subfigure. The pose correction of the object fusion amounts $\Delta\mu_{x,y} < 0.5\,\mathrm{m}$ at the progress range of $\lambda_{\mathrm{ego}} \in [70, 75]\,\mathrm{m}$ while the total change of the behaviour accumulates approximately to $\Delta\lambda_{\mathrm{ego}} = 5\mathrm{m}$. Thereby, the distance r_{obj} indicates the expected euclidean distance between the ego vehicle and the pedestrian. It changes imperceptible with the object fusion.

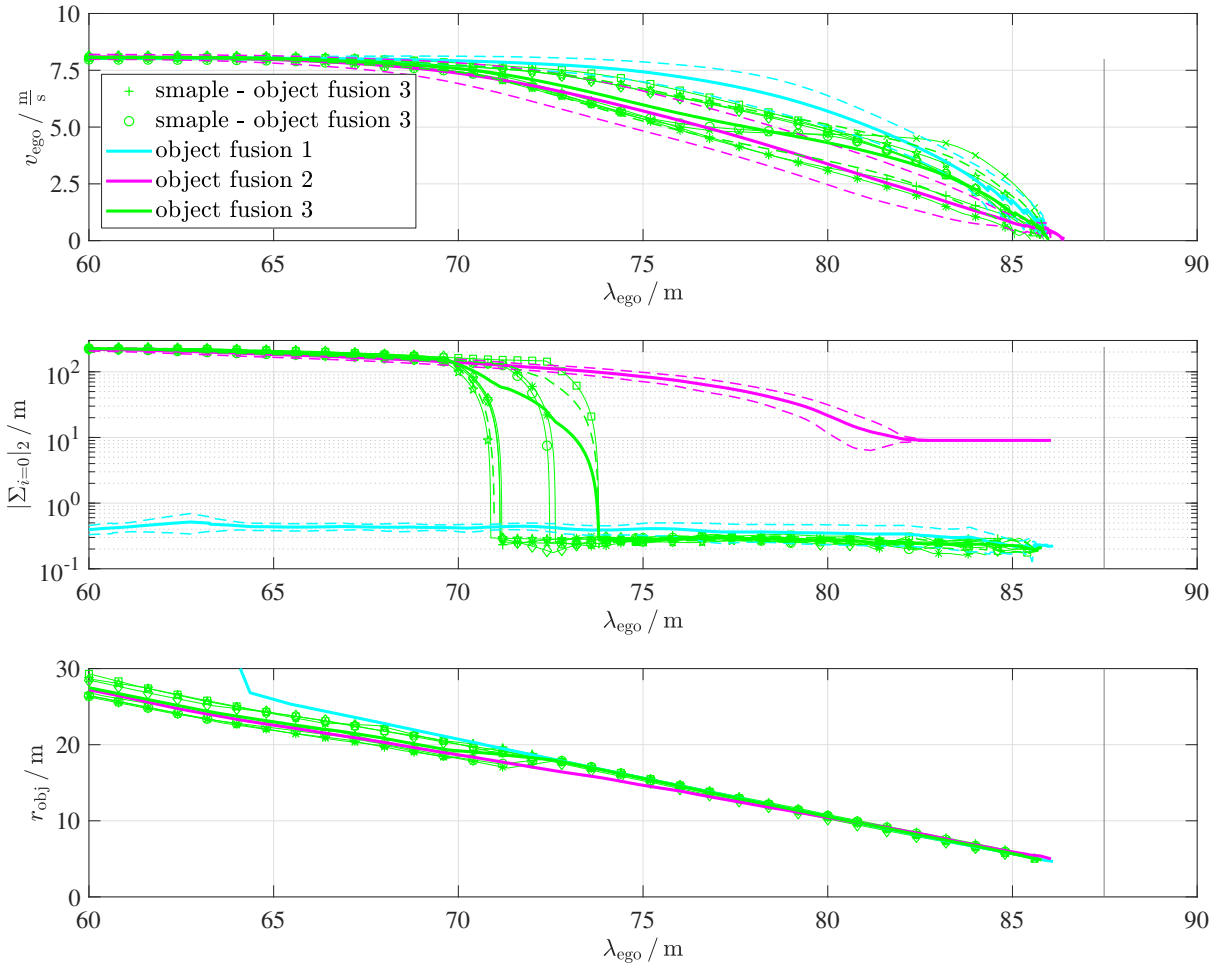

Figure 6.11: Uncertainty interaction - The selection of object fusions emphasise the uncertainty-adaptivity. The figure shows the vehicle drives for the object fusions with camera, lidar, and combination of both. The latter shows an early object perception and precise obstacle approach based on the changing uncertainty level. The figure follows the previous publication [28].

Details of the criticality are presented in figure 6.12. The velocity profile and uncertainty course is the same as in figure 6.10 and 6.11 to show the relationship. The vehicle drives with constant velocity v_{ego} as long as the object is not detected. Accordingly the collision

probability $P(C_{i=0})$ and thus the risk remains at zero. Then, starting at the distance of $\lambda_{\text{ego}} \approx 40\,\text{m}$, both values increase having the maximum in front of the pedestrian. Only the radar (object fusion 6) constitutes an exception which has lost the static object. The severity $\psi_{i=0}$ follows the velocity profile. At first, it seems to have an diffuse course, but that is based on the nature of the average calculation. Each test drive detects the pedestrian at a different distance λ_{ego} and thus the average amounts between zero and the full velocity. Finally, at the progress $\lambda_{\text{ego}} \approx 65\,\text{m}$, the severity $\psi_{i=0}$ decreases accordingly to the vehicle deceleration. The risk $R_{i=0}$, starts at zero pursuant to the collision probability, then it increases due to the object detection, and afterwards, due to the vehicle reaction and related velocity reduction, it decreases again in front of the pedestrian. Here once more, the uncertainty-adaptivity can be seen as discussed with figure 6.11. At the beginning, the risk of object fusion 3 follows the characteristics of object fusion 2. Afterwards, according to the additional information of the lidar, the uncertainty decrease suddenly and thus the risk declines to zero what leads to the more aggressive vehicle approach similar to object fusion 1.

Figure 6.13 shows the criticality according to the swerving manoeuvre FES1b. Here, the vehicle is allowed to steer but the braking is restricted by $a_{\text{in}} = 0\,\frac{\text{m}}{\text{s}^2}$. Consequently, the collision with the pedestrian is avoided by swerving. Therefore, figure 6.13 shows the deviation from the centerline d_{ego} instead of the velocity profile v_{ego}. Thereby, two data clusters can be seen. At one hand, object fusions [2-4] show an early object generation and thus an early adaptation of the current drive. Here, the lane change is triggered mainly by the contribution of the camera to the object fusion. On the other hand, the camera is solely used for object classification in the object fusions [1, 5-7] and thus the swerving manoeuvre is executed later on. Thereby, the late swerving leads to an increased overshooting of the manoeuvre. The collision probability $P(C_{i=0})$ and risk $R_{i=0}$ imply the two clusters as well. Due to the early reaction of the drive with object fusions [2-4] the collision probability $P(C_{i=0})$ has its maximum approximately at 10 %. Contrary, the collision probability for the object fusions [1, 5-7] raises up to 30 %. The accident severity $\psi_{i=0}$ remains unchanged due to the forbidden braking. Only, if the object is lost, the severity $\psi_{i=0}$ declines to zero. The combination, the risk $R_{i=0}$, follows accordingly. Besides, here again, the particularity of object fusion 3 can be seen. While the risk of object fusion 3 increases pursuant to object fusion 2 at the beginning, it changes to the course of the object fusion 1 later on. However, that aspect has a minor impact to the vehicle behaviour in that scenario.

The experimental setup of scenario FES2 is shown in table 6.3. The ego vehicle drives straight ahead when suddenly two objects $o_{k=1,2}$ appear. One vehicle $o_{k=1}$ stays in the same lane as the ego vehicle and thus obstructs the onward journey. Thereby, the last point to brake is already passed. Nevertheless, the collision with object $o_{k=1}$ could be evaded by swerving. Unfortunately, the oncoming traffic $o_{k=2}$ impedes a clear or rather safe evasive manoeuvre. The test drive is repeated with changing but predefined uncertainty level related to the appearing objects $o_{k=1,2}$. All in all, a collision free driving is not guaranteed and therefore the object in front as well as the oncoming traffic are virtual objects. Further details on the scenario emergence are out of scope for the conclusion of that experiment. What is more, due to the vehicle scenario, the severity measure refers to section 4.1.3.

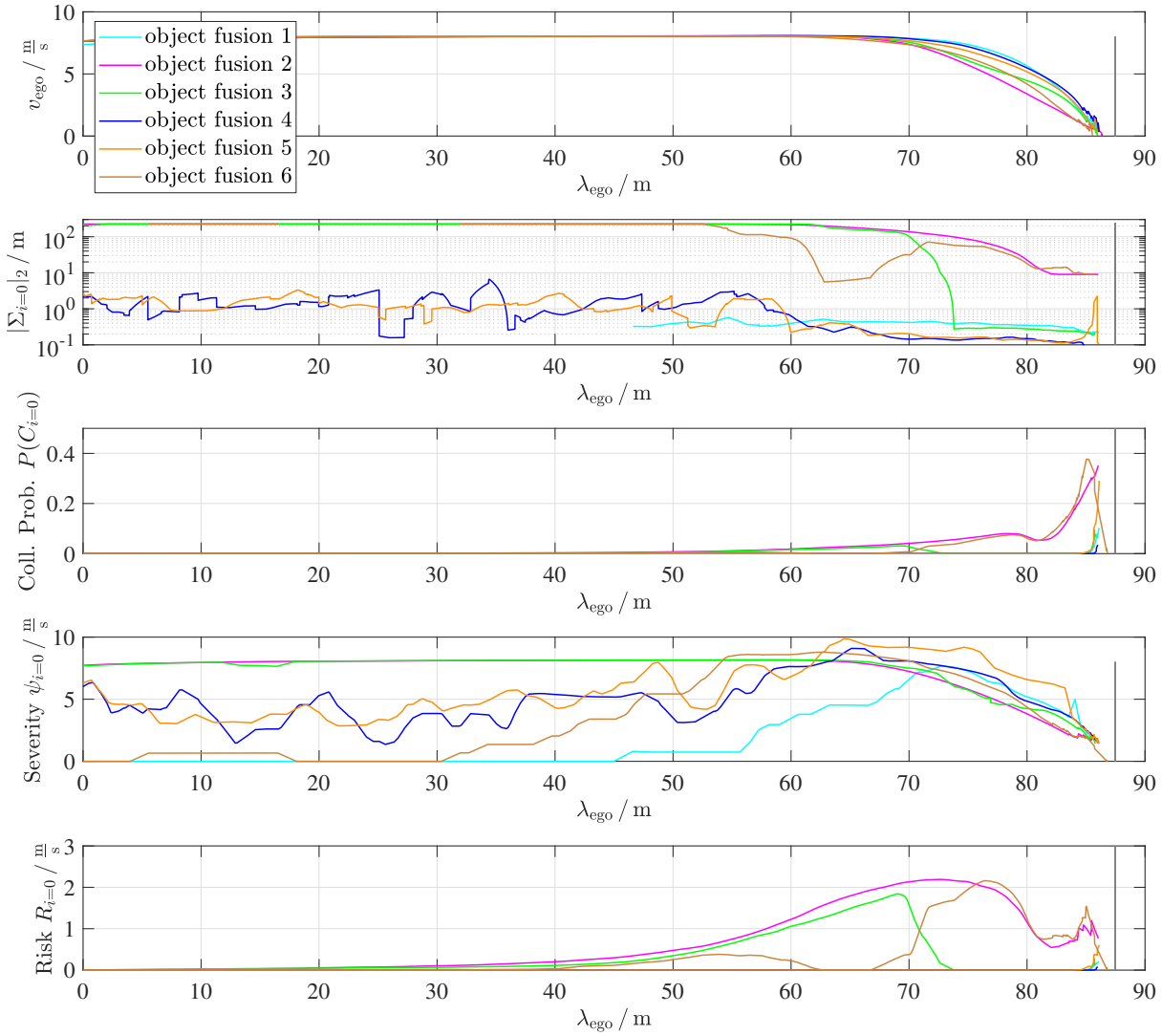

Figure 6.12: Criticality of collision avoidance by braking - The risk based subfeatures ($R_{i=0}$, $P(C_{i=0})$, $\psi_{i=0}$) of the initial time step $t_i = t_0$ are presented for the braking scenario FSE1. The figure follows the previous publication [28].

The scenario requires a choice between two disadvantageous opportunities. At one hand, braking would mitigate the collision with object $o_{k=1}$ but also commit a certain crash. On the other hand, swerving provides the chance of collision avoidance with both objects $o_{k=1,2}$ but if it fails, the collision occurs with even higher severity due to the high relative velocity related to the oncoming traffic $o_{k=2}$. In other words, if it is possible to predict a safe evasive manoeuvre, it is preferred to the collision mitigation. Vice versa, if the collision avoidance is not possible, the mitigation is preferred. Figure 6.14 visualises the safety benefit of these ranked opportunities. Thereby, the decision depends on the potential accident severity and its uncertainty, namely the risk R. In other words, a low uncertainty allows an informed decision on the evasive manoeuvre. However, if the uncertainty increase too high, the collision mitigation is chosen.

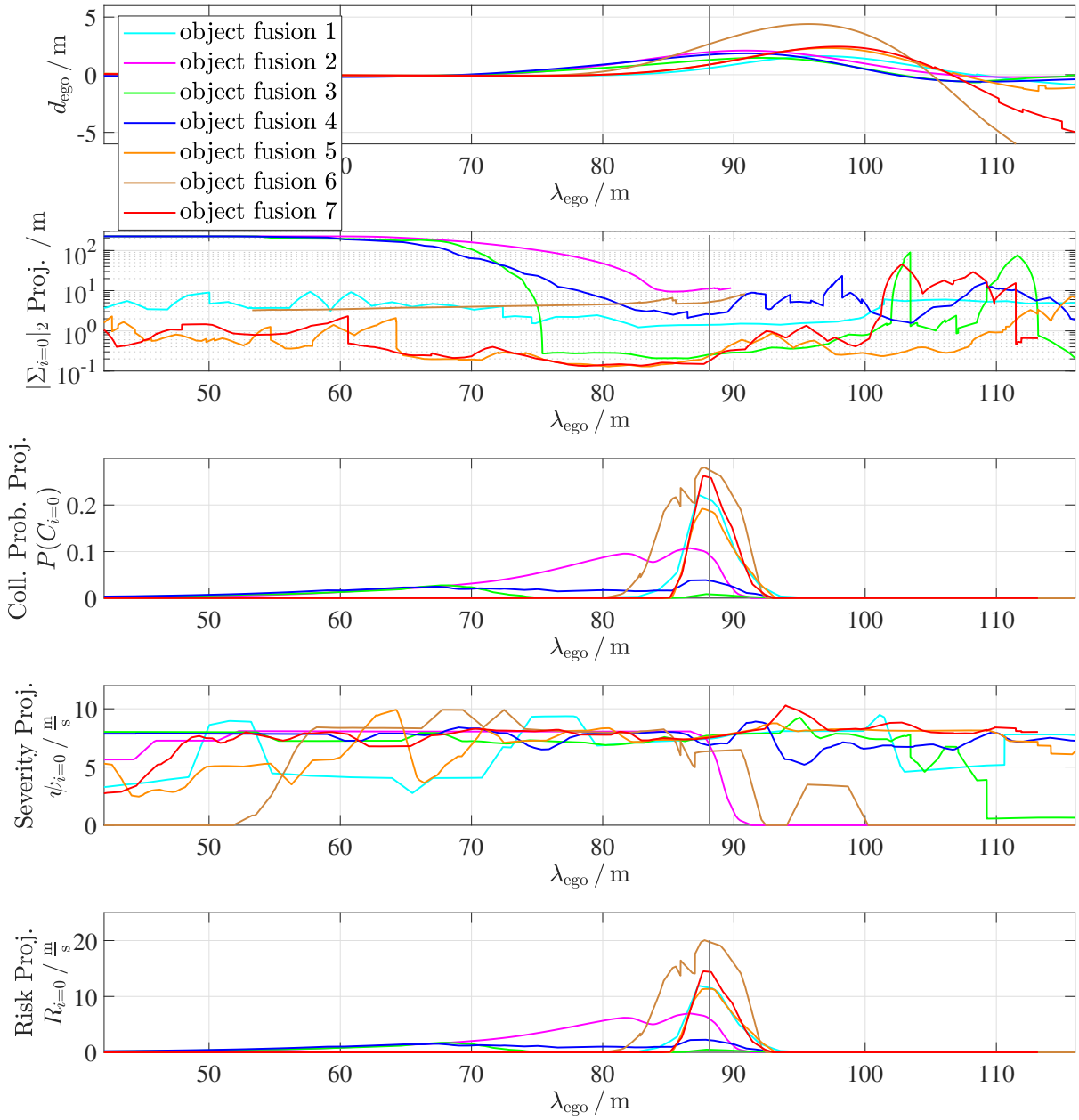

Figure 6.13: Criticality of collision avoidance by swerving - The ego vehicle follows a straight line λ_{ego} and swerves to avoid a collision with a pedestrian at distance $\lambda_{pedestrian} = 87.5\,m$ which is indicated by a grey line. Due to different sensor equipments, the maximal deviation varies depending on the uncertainty level. The figure follows the previous publication [28].

Apart from the theoretical expectations, figure 6.14 shows the impact severity ψ_{impact} of test drives at several uncertainty levels σ. The decision between steering and braking bases solely on the risk assessment. A previous selection between these two opportunities is especially not made. Besides, the driving is performed with the tuning set $\boldsymbol{\theta} = [3e11, 1e13, 1e16, 1e13, 1e15, 1e10, 1e10, 1e14]$ and the graceful degradation ensures

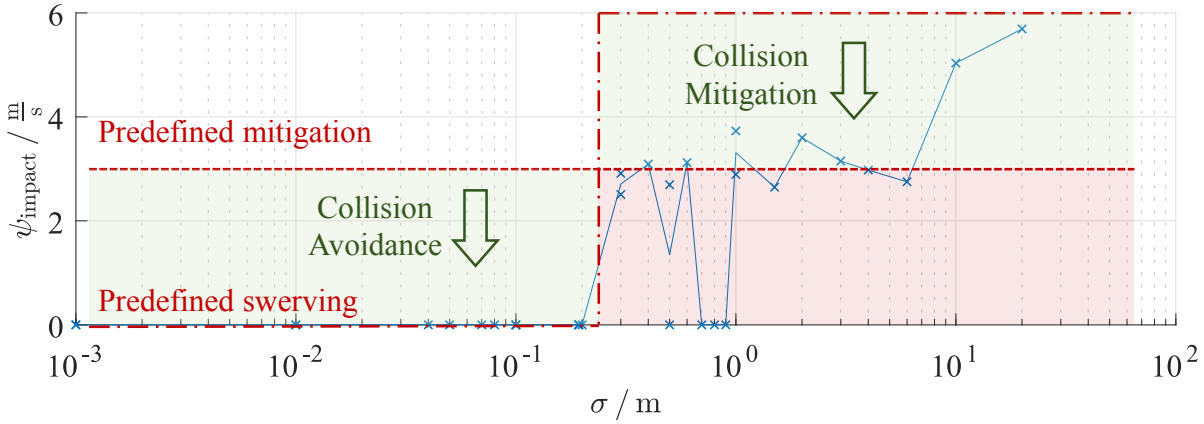

Figure 6.14: Safety benefit due to uncertainty considerations - The figure shows the scenario outcome ψ_{impact} depending on the uncertainty level. Furthermore, it indicates the theoretical and real measured safety benefit.

the most possible safety. Due to the predefined, constant velocity profiles of the objects $o_{k=1,2}$, the uncertainty σ is the only changing factor and thus has a major responsibility for the scenario outcome. An uncertainty below $\sigma \leq 0.2\,\text{m}$ allows a collision avoidance by swerving while a collision mitigation is preferred between $1\,\text{m} < \sigma < 10\,\text{m}$. In the middle, a transit phase exist where the vehicle is only able to avoid the collision in some cases. Otherwise, a collision mitigation is obtained. Among others, that is caused on the statistical nature of the risk R as well as slight different scenario evolvement between single test drives. If the uncertainty σ increase even higher, such as $\sigma > 10\,\text{m}$, the vehicle has no basis for the decision making and hence continues the drive unchanged. At one hand, that might seem peculiar. But on the other hand, such high uncertainty values σ raise the question if the system has already malfunctions and thus the subject refers rather to functional safety than to the driving capability. In a sense, this poor perception indicates that objects are most probably ahead but further information are missing. Hence, a *safe stop* would resolve the situation. Alternatively, that high uncertainty σ could be temporary and the ego vehicle might wait a short moment or rather update cycles to derive an informed decision then.

Figure 6.15 visualises the dynamic and criticality over the driven path λ_{ego} for different uncertainty levels σ whereby the selection is based on maximum diversity. It gives further information about the previous discussion of the uncertainty-adaptivity pursuant to figure 6.14. The deviation d_{ego} shows clearly the separation in swerving emergency manoeuvres, and mitigation trajectories ending with the crash. Accordingly, the velocity profiles v_{ego} comply with collision avoidance by braking and swerving, or with the mitigating deceleration, respectively. Thereby, the lowest velocity is obtained near the objects $o_{k=1,2}$ what is also shown by the severity course $\psi_{i=0}$. The risk R remains almost at zero if the collision is evaded caused by the collision probability $P(C_{i=0})$ near zero. Contrary, if a crash occurs, the collision probability $P(C_{i=0})$ raise and hence the risk R.

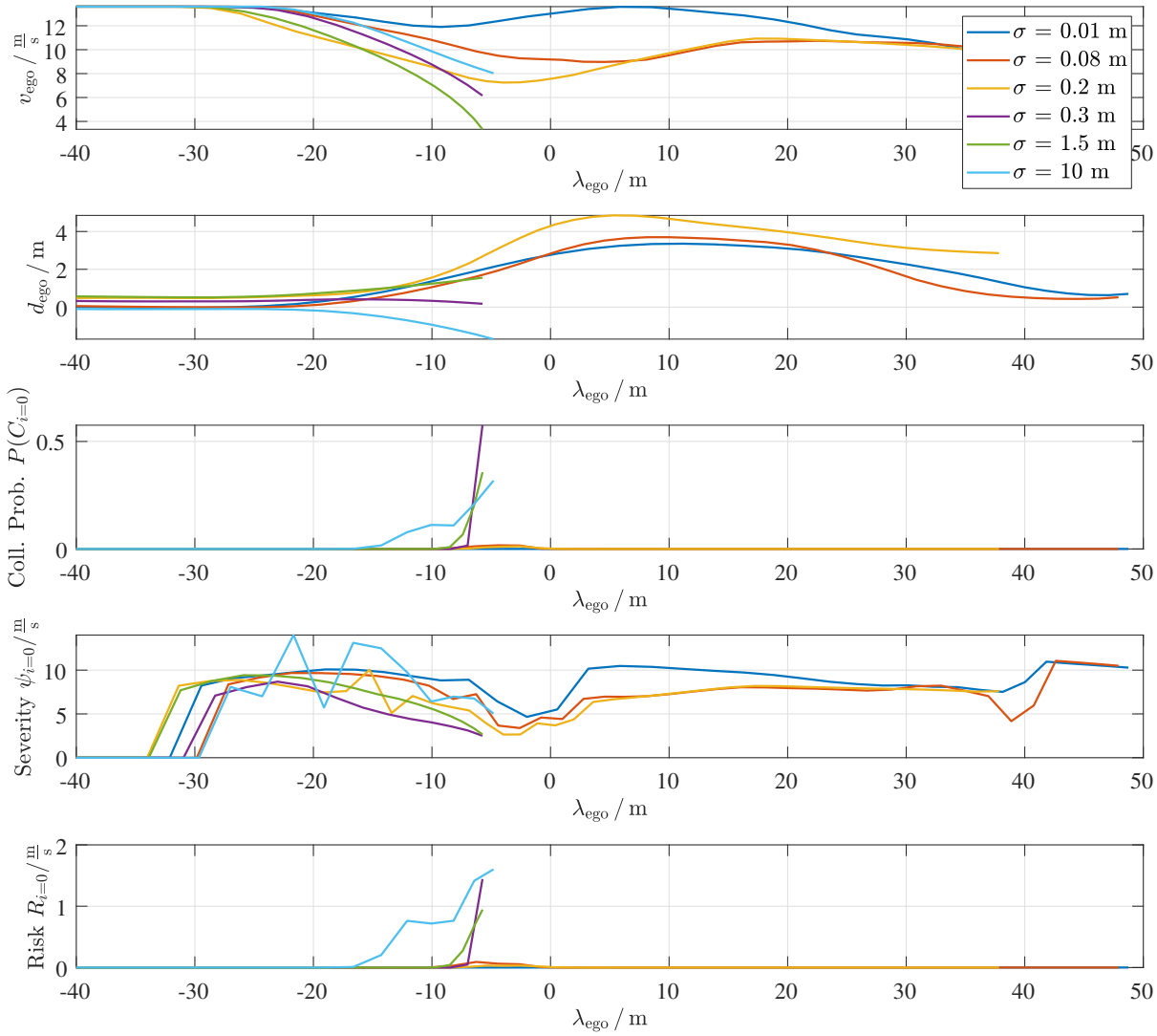

Figure 6.15: Criticality of scenario FES2 - The Figure shows the dynamic and criticality at the initial time step $t_i = t_0$. It shows a selection of test drives according to figure 6.14 with maximum diversity.

6.6 Mitigation application

6.6.1 Real test drives on proving ground

The scenario FES3, accordingly to table 6.3, is designed to investigate the mitigation performance of the risk based planner. The basis version FES3a contains the ego vehicle which drives straight ahead when suddenly a potential collision object $o_{k=1}$ occurs. Consequently, the ego vehicle needs to perform an emergency manoeuvre. Thereby, different opportunities are available depending on the object appearance distance λ_{appear} as illustrated by figure 6.16. The underlying velocities effect that the last point to brake (LPTB) is exceeded before the last point to steer (LPTS). If the distance λ_{appear} is large enough, the ego vehicle is free to choose an appropriate collision avoidance manoeuvre based on the risk assess-

ment. Decreasing the distance λ_{appear}, a collision is only avoidable by steering. If the collision object $o_{k=1}$ appears very suddenly, avoidance is no longer possible but an emergency collision mitigation manoeuvre may still reduce the impact severity ψ_{impact}. Beyond, scenario FES3b constitutes an modification of the scenario FES3a. Here, two objects $o_{k=1,2}$ appear in front of the vehicle. Thereby, the object $o_{k=2}$ impedes a collision free emergency swerving manoeuvre. In other words, a collision becomes unavoidable earlier than in the scenario version before. However, here again, the ego vehicle has the only remaining opportunity of mitigating the crash severity ψ_{impact} to ensure the maximum safety. One example of the scenario emergence is shown in table 6.3. While object $o_{k=2}$ is allowed to drive on the adjacent lane regularly, the object $o_{k=1}$ neglects the right of way and pulls out behind the occluding parked cars. Besides, these parked cars impede a collision avoidance manoeuvre to the right side. The driving is performed with the tuning set $\boldsymbol{\theta} = [3e11, 1e13, 1e16, 1e13, 1e15, 1e10, 1e10, 1e14]$ and the graceful degradation ensures the most possible safety. What is more, virtual objects are used due to the potential collisions and the severity measure refers to section 4.1.3.

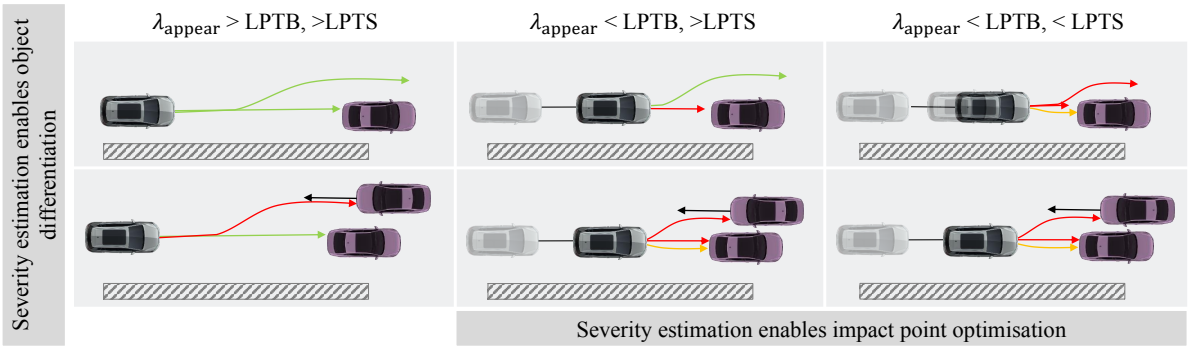

Figure 6.16: Emergency manoeuvres opportunities - It shows the opportunities for collision avoidance and mitigation based on the appearance distance λ_{appear}, LPTB, and LPTS.

The impact of the ranked safety strategies are illustrated in figure 6.17. Additionally, apart from the theoretical expectations, it shows the impact severity ψ_{impact} obtained by real test drives. Thereby, the accident outcome changes due to the appearance distance λ_{appear}. The safety benefit is derived relatively to the reference planner. The results show a similar qualitative shape for both planners according to the theoretical background. A collision is avoided at high appearance distances λ_{appear}. If the remaining distance decrease, a collision becomes inevitable and thus the impact severity ψ_{impact} raises. Besides, a longer distance λ_{appear} gives more time to react compared to a shorter one and thus to chose the appropriate mitigation strategy, such as mitigation by strategy. Therefore, the impact severity ψ_{impact} increase steadily by reducing the spacing. As expected, the second scenario FES3b reaches the point of no return earlier than scenario FES3a due to the second object $o_{k=2}$ blocking the adjacent lane. Unfortunately, only few data points are available in the transit phase and for the reference planner. However, in accordance with the few data, the risk based planner performs a little better in both scenarios compared to the reference. Based on the tendency, the safety benefit accumulates approximately to $\Delta\psi_{\text{impact}} \approx 1 - 2\,\frac{\text{m}}{\text{s}}$ what accumulates to a benefit of 20-40 %. A more detailed one-to-one comparison is unfortunately not possible due the divergence in the scenario emergence, e.g., due to the appearance distance λ_{appear}.

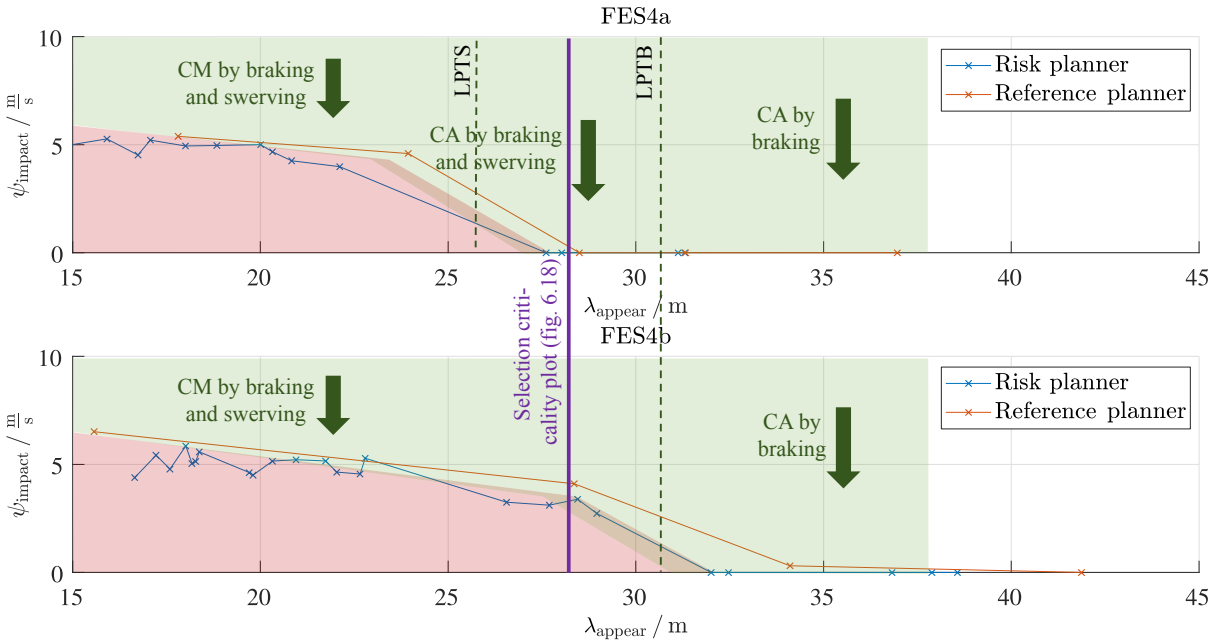

Figure 6.17: Safety benefit due to mitigation capabilities - The figure shows the scenario outcome ψ_{impact} for scenario FES3a and FES3b for the risk based planner and the reference planner. Additionally, the theoretical safety margin is marked.

Figure 6.18 shows the criticality as marked in figure 6.17 exemplary. The selection bases approximately on the same appearance distance $\lambda_{\text{appear}} = 28\,\text{m}$ to enhance the comparability. In the first scenario FES3a both planners are able to avoid the collision. However, due to the small difference in the object appearance distances λ_{appear} and the different lateral positions d_{ego} at $\lambda_{\text{ego}} \approx -30\,\text{m}$, the risk based planner needs both, braking and swerving, to avoid a crash while the reference is able to evade the collision solely by swerving. Contrary, if the object $o_{k=2}$ blocks the adjacent line, both planners commit a crash. Thereby, they mitigate the crash consequences ψ_{impact} by braking. Additionally, the risk based planner uses the remaining time to steer in the direction of a full overlap to reduce the crash severity ψ_{impact} further on. In contrast, the reference planner decelerates solely based on the TTC trigger. The collision probability $P(C_{i=0})$ follows accordingly. If an crash occurs, it raises over 50 % and otherwise it remains below 20 %. The severity $\psi_{i=0}$ follows the deceleration of the velocity profile in general. Similarly, the risk is minimised in the collision avoidance scenario while it raises shortly before the collisions otherwise.

Supplementary to the previous scenarios, figure 6.19 presents data of a more systematic evaluation. Independent of any scenario evolvement, scenario FES4 varies the lateral offset Δy and relative angle $\Delta\varphi = \varphi_k - \varphi_{\text{E}}$. Thereby, the obstacle $o_{k=1}$ is virtual and appears suddenly when the ego vehicle reaches a point with distance $d = 27\,\text{m}$ to the following object pose. The lateral offset is chosen from the interval $\Delta y \in \{0, 1, 2\}\,\text{m}$. The angle changes between $\varphi_k \in \{-150 : 30 : 0, -15, 15\}^\circ$. All in all, the data include 67 test drives with the risk based planner and 17 reference values. The number of test drives with the risk based planner includes three repetitions for the same input factors. Nevertheless, some datapoints are lost due to malfunction in the data recordings. For the reference values, only

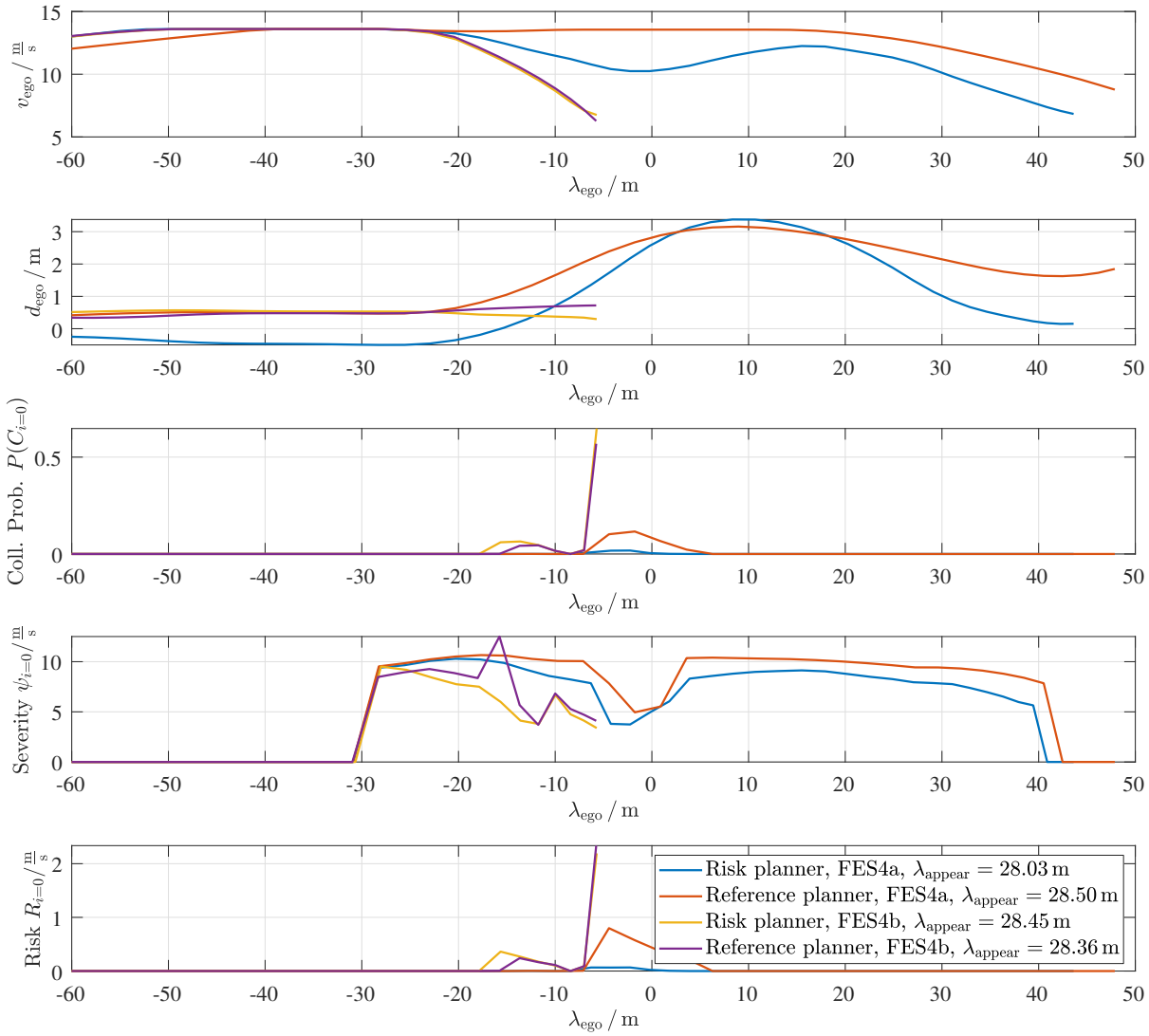

Figure 6.18: Criticality of scenario FES3 - The figure shows the dynamic and criticality for a selection of test drives at the initial time step $t_i = t_0$, as marked in figure 6.17.

single data points are available for each input set. Besides, a few datapoints are lost similar to the risk based planner. The planners have the similar settings as in scenario FES3.

Subfigure 6.19(a) shows the histogram of the deviation $\Delta\psi_{\text{impact}} = \psi_{\text{risk planner}} - \psi_{\text{ref. planner}}$ and subfigure 6.19(b) shows the connected data points. Thereby, multiple datapoints at one input set are aggregated by the average. Based on the few available data, the safety benefit implies an average of $\overline{\Delta\psi}_{\text{impact}} \approx -0.2\,\frac{\text{m}}{\text{s}}$ and empirical standard deviation of $s_{\Delta\psi} = 2.1\,\frac{\text{m}}{\text{s}}$. That means a little benefit by the risk based planner. Nevertheless, it also occurs that the reference beats the risk based planner. As mentioned earlier, that bases on the statistical nature of the risk and is also shown by the distribution of the deviation. Furthermore, due to the real test drives, crossinfluences superimpose the conclusions. By way of example, even if the object $o_{k=1}$ is triggered in all test drives at the same distance $\lambda = 27\,\text{m}$, the final appearance distance λ_{appear} varies slightly related to the vehicle's point of view. Among

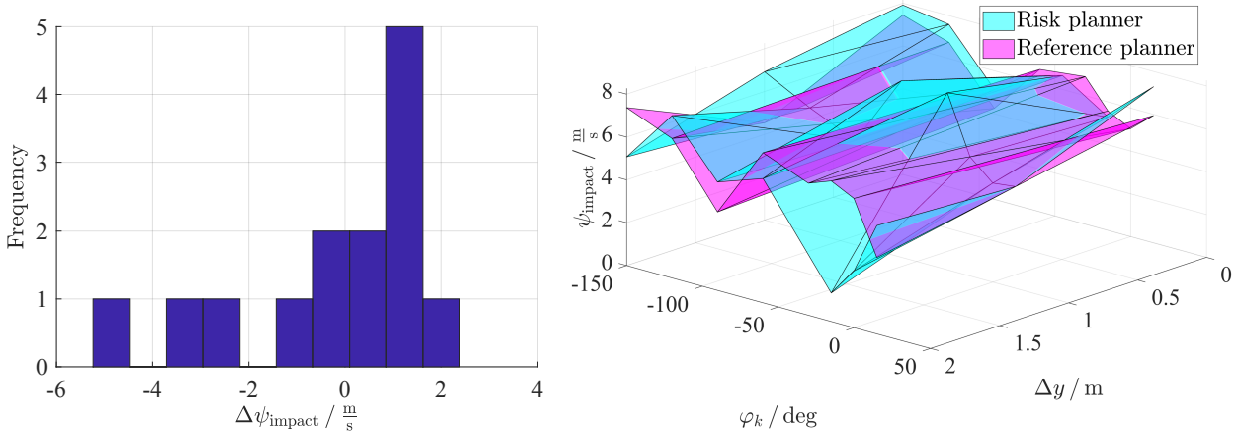

(a) (b)

Figure 6.19: Systematic data evaluation FES4 in real test drives - The figure displays the impact severities ψ_{impact} for the risk based planner and reference planner for multiple test drives depending on changing vehicle offset Δy, and relative angle $\Delta\varphi$. A histogram aggregates the relative criticality $\Delta\psi_{\text{impact}}$ in subfigure a) while the data points are shown directly in subfigure b).

others, it depends on the current driving stage, such as update cycle time and computation load of other modules. That makes it difficult to compare the datasets of the risk based planner and the reference due to the deviation of the theoretical independent input factors. At one hand, it is tried to reduce the impact by up to three repetitions per case of the risk based planner. On the other hand, a lot more test drives would be necessary. Furthermore, seeing the scatter of the measured data, the reference would need repetitions, too.

Therefore, the same evaluation scenario FES4 is conducted in simulation in section 6.6.2. Advantageously, in the simulation the previous mentioned crossinfluences do not exist or at least remain constant over all test drives and therefore have no impact on the conclusions.

6.6.2 Driving performance in simulation

The systematic evaluation of section 6.6.1 is repeated in simulation with similar planner settings. It refers to scenario FES4. At one hand, that enables the execution of various test drives. On the other hand, crossinfluences are reduced. In total, 400 test drives are conducted for both, the risk based planner and the reference. Thereby, the offset is varied between $\Delta y \in \{0, 0.7, 1.4, 2.1\}$ m and the relative angle changes by $\Delta\varphi \in \{0 : 20 : 180\}$ deg. Furthermore, each concrete scenario is repeated 10 times due to the requirement on the statistical evaluation. The sensor model of section 6.3 emulates the uncertainty. The underlying criticality of the scenario is near the point of no return. In that transit phase, a major impact of the integral approach is expected. If the collision avoidance would be too easy, both planners would yield no crash severity. Similarly, if the scenario is too abrupt, both planners would yield the maximum severity without any distinction. Due to the simulation, the scenario

evolvement is equal in every test drive. Therefore, contrary to the real test drives of section 6.6.1, crossinfluences are significantly reduced.

Figure 6.20 presents the results in a histogram and 3D plan plot. The accumulated frequency of the histogram 6.20(a) bases on the 40 different scenario variations. The 10 repetitions are recognised by the average value and thus the safety benefit $\Delta\psi_{\text{impact}}$ is obtained. The mean benefit amounts to $\overline{\Delta\psi} \approx -3.2\,\frac{\text{m}}{\text{s}}$ with an empirical standard derivation $s_{\Delta\psi} \approx 2.7\,\frac{\text{m}}{\text{s}}$. That shows quantitatively the improvement of the integral approach. In accordance to an underlying velocity profile of $v_{\text{ego}} \approx 13.9\frac{\text{m}}{\text{s}}$, and pursuant to the injury risk function P(MAIS2+) of figure 2.4(a), the safety benefit $\Delta\psi_{\text{impact}}$ is equivalent to a reduction of approximately 30 % injury probability. However, these values focus on the specific scenario FES4. Other settings and especially velocity profiles may result in different quantitative values. The concrete scenarios, contributing to the safety benefit $\Delta\psi_{\text{impact}}$, are shown by subfigure 6.20(b). Due to the underlying criticality near to the point of no return, the risk based planner is able to avoid a collision approximately at $\Delta y \geq 2\,\text{m}$. Contrary, the reference commits a crash based on the average in every presented concrete scenario. Nevertheless, if the offset Δy decrease, both planners commit a crash. Thereby, the improvement of the risk based planner decreases with raising criticality of the scenario. In a sense, it confirms the deductive considerations that the most safety benefit is obtained near the transit phase between collision avoidance and collision mitigation. Furthermore, it should be noticed, that the risk based planner improves the safety on average. In other words, the reference will also beat the risk based planner in single test drives as shown by figure 6.20(a).

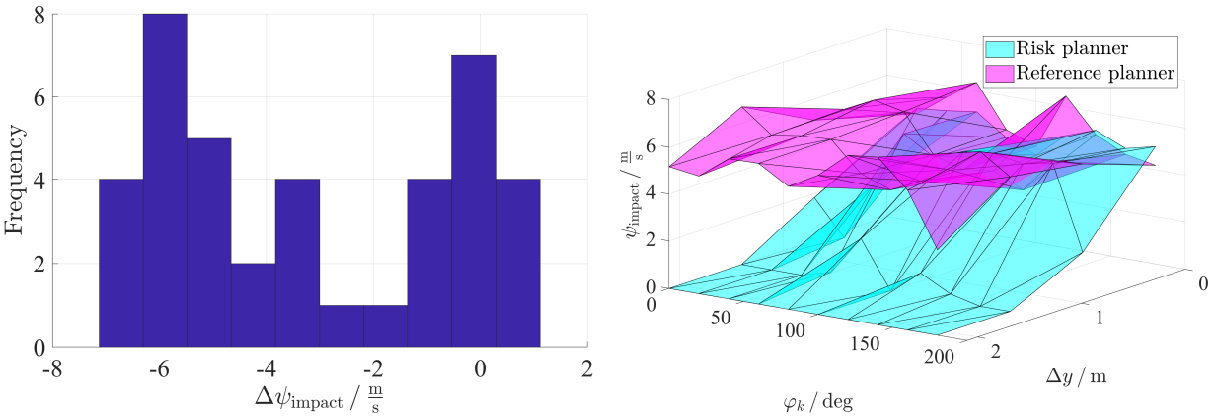

(a) (b)

Figure 6.20: Systematic data evaluation FES4 in simulation - The figure presents the impact severity for the risk based planner and reference planner in scenario FES4. Thereby, the input factor Δy and $\Delta\varphi$ are varied. Furthermore, each concrete scenario is repeated 10 times and therefore the average value is shown per case. a) shows a histogram of the safety benefit $\Delta\psi_{\text{impact}}$ and b) visualises the average value per concrete scenario directly.

Figure 6.21 presents the results of the evaluation scenarios FES5 and FES6. Pursuant to section 6.2, they constitute frequent GIDAS accident scenarios which potentially require an intelligent mitigation strategy. Based on the third-party responsibility, the scenario evolve-

ment is independent of the automation level of the ego vehicle and thus concerns also automated vehicles. Moreover, the focus lies here on the scenario emergence rather than on theoretical or systematic evaluations. Therefore, only one possible instance of a concrete scenarios is derived and investigated. The uncertainty is emulated by the sensor model of section 6.3 and 10 repetitions ensure the statistical significance. The driving is performed with the tuning set $\boldsymbol{\theta} = [3e11, 1e13, 1e16, 1e13, 1e15, 1e10, 1e10, 1e14]$ and the graceful degradation ensures the most possible safety.

Scenario FES5 describes an object $o_{k=1}$ reeving suddenly into the lane of the ego vehicle and thus provokes a critical incident. The results are visualised in subfigure 6.21(a). The example show that the risk based driving function does not always outperform the reference. Here, the reference has a mean benefit of $\overline{\Delta\psi}_{\text{impact}} \approx 0.58\,\frac{\text{m}}{\text{s}}$. Besides, the underlying velocity profile with $v_{\text{ego}} = 13.9\frac{\text{m}}{\text{s}}$ is not directly forwarded to the crash severity. Due to the reeving of the object $o_{k=1}$, the crash is limited to a slight touching and thus both vehicles retain mostly their initial velocity. Therefore, pursuant to the injury risk functions of figure 2.4, it is expected that these crash severities ψ_{impact} have a minor impact on the injury severity. That refers to both, the absolute values as well as the difference between the planners. In other words, the reference performs statistically better than the risk based planner but the obtained injury severity does not change significantly and may be neglected anyway. At least that refers to the primary crash, most probably followed by further incidents. However, secondary crashes may be managed by other safety systems, such as a multi collision brake (MKB). What is more, investigating the cause of the driving performance, it is referred mainly to error-prone functionality of the prediction module. When the other vehicle reeves into the lane of the ego vehicle, the prediction presumes constantly a regular driving. That includes to predict the return to the original lane and thus no necessity for reactions. Even if that might be most likely in normal driving, it impedes the current evaluation of the mitigation performance. Consequently, the reference planner which triggers an emergency braking by critical incidents becomes independent of the prediction and thus outperforms the risk planner.

Scenario FES6 describes a GIDAS hotspot on rural roads. A careless driver of an object $o_{k=1}$ tries to overtake a truck $o_{k=2}$. Thereby, it misjudges the space remaining for a safe manoeuvre and thus it involves the ego vehicle in an unavoidable accident. Due to the ethical guidelines of the ethics commission [202], it is an incident between the ego vehicle and object $o_{k=1}$ what means that the truck $o_{k=2}$ is out of scope for the mitigation. Besides, the bigger mass of the truck compared to the ego vehicle would induce an higher crash severity and thus is not the best choice for a mitigation manoeuvre anyway. The quantiles of the scenario outcome are presented in figure 6.21. The mean safety benefit amounts to $\overline{\Delta\psi}_{\text{impact}} \approx -0.5\,\frac{\text{m}}{\text{s}}$. In general, it can be seen, that the reference values spread wider compared to the risk based planner. While the risk planner tries to mitigate the crash by braking and swerving into a full overlap, the reference obtains the crash severity passive based on the object uncertainty.

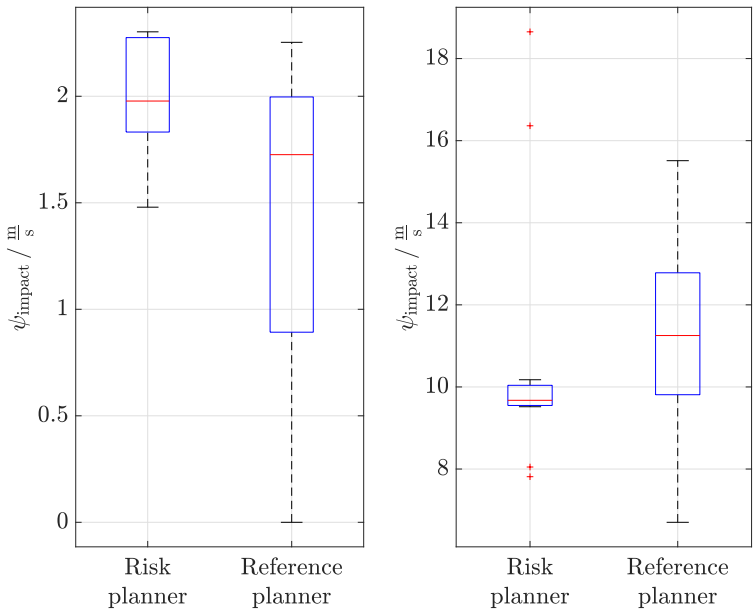

(a) Scenario FES5 (b) Scenario FES6

Figure 6.21: Driving performance in mitigation scenarios FES5 and FES6 - It shows the quantiles of the scenario outcome ψ_{impact} for the risk based planner and the reference planner.

7 Conclusion and Prospects

The objective of this work has been to illustrate an approach for integral vehicle safety as part of the "Safe System Approach". It bases on the assumption that when every related safety domain feels responsible for the road safety in general, it will gain the most benefit as well as will have an optimal cost-benefit relationship. The underlying technical idea bases on a risk criticality measure which compares the combined use of different safety systems under uncertainties of the driving process.

Exemplary for integral vehicle safety, this work takes the combined consequences due to the usage of the throttle, steering, and the protection of the crumple zone in all driving stages on one unified scale into account. In other words, in the trajectory planning of automated vehicles a potential crash consequence is assigned to each trajectory. Thus, not only a collision free driving is favoured but more general a reduced harmful behaviour. If a collision is evitable, an avoidance manoeuvre is conducted. On the other hand, if a collision is inevitable, the impact point of vehicle-vehicle crashes is optimised. Thereby, the pre-crash predicted velocity change during a potential crash Δv is used as severity measure. Accordingly, the evaluation of the presented approach shows an severity reduction of about 20-30 % related to an reference system based on AEB in selected critical scenarios what corresponds to one-third less injury probability based on MAIS injury risk functions. Thereby, the AEB mitigates the crash consequences already reasonable and thus constitutes a high baseline to quantify the benefit. Furthermore, it should be noticed that the quantitative values base on the arrangement of the underlying evaluation scenarios. Even if promising scenarios are derived systematically in use case analyses, the final benefit varies on multiple scenario parameters, such as the velocity profiles, involved vehicle types, and geometric constellations. Therefore, the improvements show the potential of the presented approach exemplary rather than being a statistical representation. Moreover, the latter is hard to derive due to the lack of standardised approval procedures. Future work could focus on such evaluation strategies to assess the benefit of the integral approach or in general the capabilities of automated driving functions statistically. Here, it is seen promising to follow the example of California what means to accompany the release of automated vehicles with an advanced reporting system to gain short-term feedback of the real world safety impact. What is more, a huge safety potential is seen by including further reversible and irreversible restraint systems, such as belt tensioner, seat backrest levelling, and airbags, to the integral approach. Thereby, the generalised integral approach constitutes a basis for further developments. Most important, it should be noticed that the application determines the severity measure which in turn is key to decide upon appropriate safety function deployments. Thereby, if injury severities are required the measure may change in relation to this work and thus the severity prediction functions need most probably to be adapted. However, a human related severity measure could be an enabler for new activities of the occupants while driving, such as sitting out of position. Thereby, the meaningfulness of the chosen measure needs to be investigated itself. Furthermore, it should be noticed that pre-crash activations of irreversible restraint

systems might constitute a binary state transition. Once triggered, the system needs to deal with the deployment. Mathematically, it might be seen as additional constraint restricting the solution space in subsequent optimisations.

Uncertainties in the driving process are considered by a risk measure. That refers to the expected value of the severity measure and thus to established safety strategies. In addition to the severity measure, the collision probability considers geometrical environment uncertainties, such as the pose of other objects as well as their shape. That supports especially the decision between potential collision avoidance or concious collision mitigation in critical scenarios. The expected accident severity for each accident configuration is represented by the most likely collision configuration. Further uncertainties on internal parameters, such as the mass of other vehicles, are neglected in the current development state. Nevertheless, future work could focus on such considerations to increase the reliability of the calculations. For example, dealing with normal distributions, it seems promising to linearise the chosen severity prediction function and thus to derive a distribution on the severity measure. As result, further statistical parameters, such as the variance, could improve the driving decision. Nevertheless, arbitrary distributions or an estimation of characteristic values based on statistical approaches are conceivable. Besides, existence and classification uncertainties are neither regarded but interesting for future work. What is more, the evaluation shows not only the founded decision between collision avoidance and collision mitigation in dedicated multi object scenarios, but also an inherent adaptation of the driving function to the uncertainties. In other words, the evaluation shows the direct adaptation of the vehicle behaviour to the availability of the sensor set, e.g., due to temporary malfunctions or hardware updates, and changing perception quality, e.g., due to changing weather conditions. Furthermore, due to the statistical driving approach it might occur, that single activities increase the harm of collision. However, the evaluation shows a safety benefit in average what complies to the requirements of the ethics commission to a positive risk balance.

The real time capabilities of the presented integral approach are shown by real test drives on the testing ground. A planning step in total is allowed to take 200 ms in total while an instantaneous risk calculation takes about several micro seconds. The fast, instantaneous risk assessment is enabled by approximating calculations with the final set of an eccentric impact model and a 3D Minkowski Difference estimating the severity measure and the collision probability, respectively. The average execution time for one planning step amounts 127 ms. The trajectory optimisation bases on dynamic programming with multiple adjustment possibilities, such as the length of the prediction horizon, the resolution of the trajectory, and and the width of search. While the properties in this thesis are adjusted with expert knowledge, further work could investigate these settings according to the integral approach more systematically. As result, the minimal possible execution time and thus the final hardware requirements could be indicated more detailed.

All in all, the integral safety and thus this thesis focus on an interdisciplinary linkage between several research fields. Thereby each subfield constitutes an own field of research and thus a certain level of abstraction is necessarily chosen for the scope of this thesis. Nevertheless, the investigations enable to state system requirements well-founded. In the following, subordinate findings and prospects are summarised.

Accident severity prediction is used in various research areas. In this work, the challenge was to find a compromise between the prediction accuracy and execution time while the available input parameters are limited. Two impact models, a multi-body system, a feed-forward neural network, and random forest are investigated and finally an eccentric impact model is applied to demonstrate the integral approach. Even if a hyper parametrisation is used to identify the most promising representatives in accordance with the state of the art, it is shown that much more investigations and model instances are imaginable based on the desired use case and its requirements. In other words, the final instances depend directly on constraints, such as available input parameters, execution times, or output measures. Furthermore, non-measureable parameters are determined statistically on the basis of more than 6000 FEM simulations. Even if that number seems huge, it actually is a sparse representation due to the various input parameters. Thus, it is recommended to improve the reference database for future work. At one hand, that could mean to conduct much more FEM simulations, also including vehicles out of the Volkswagen Group. On the other hand, a hierarchical prediction approach seems conceivable. Here, an accurate prediction model, which is most probably unable for real time applications but faster than FEM simulations, could be parametrised based on the FEM database. Afterwards it could be used to generate massive references for much more approximating prediction models. What is more, the classification of measureable and non-measureable parameters depends directly on the used sensor set. The availability could be improved by emerging technologies such as V2X-communication. Beyond, this thesis focus on vehicle-vehicle crashes. Further investigations could also focus on other collision types.

This thesis bases the optimisation of the trajectory planning on dynamic programming. It has been a prerequisite of this work to be compatible to other functionalities and thus to demonstrate the integral approach cost-beneficial. Nevertheless, it should be mentioned that also other planning approaches could be applied. Besides, the current approach is very resource consuming. Improvements are seen in a hybrid optimisation between global optimisations to generate an initial, best guess solution for fast local optimisation. Additionally, the question arise which solution is sufficient and how the stop criterion of the optimisation should be designed. Further investigations could avoid efforts of the exhaustive search.

Furthermore, a hierarchical planning concept seems promising. At one hand, it is already state of the art by *strategic*, *tactical*, and *operational* motion planning. On the other hand, it is a very rough classification. Related to the the levels of tactical and operational planning, the optimisation problem including the reward function needs to be configured according to the situational conditions. That is discussed by the results of the tuning process where an overall configuration of the reward function could not be found. Besides, that issue can also be addressed by deductive logic. By way of example, due to ethical guidelines, it might be appropriate to apply a collision mitigation manoeuvre or contrary forbid such manoeuvres if third-parties are involved. An other example constitutes the switching between self and target protection. In a sense, it refers to the objective of conflicts between deontology and consequentialism. In other words, it seems promising to map certain rules by a state machine while in all other cases, the system should be free to chose an appropriate vehicle behaviour without too restrictive pre-selections. In short, further research should improve the

tuning of the reward function and thus the preventative driving function with the objective of an overall strategy to all scenarios. Thereby, cross-influences of single tuning parameters among each other and the settings of the optimisation problem should be regarded.

Ethical issues are excluded as far as possible from the technical background of this thesis. If necessary, assumptions or rather definitions are made to proceed with the integral safety investigations and not to stagnate due to the lack of final regulations. By way of example, that include the ego vehicle protection in vehicle-vehicle crashes as well as the choice of the reference point *tunnel middle*. However, as mentioned earlier, ethical guidelines can be directly applied by the adjustment of the reward function or by a hierarchical planning concept. Nevertheless, it is important that the society and responsible representatives are encouraged to make progress on that area. Otherwise, it could impede a market launch of such products.

The main results of the evaluation are derived by systematic test drives on the testing ground as well as in simulation. Future work could investigate the integral approach on real road traffic. Unfortunately, the risk based driving function lacks of administrative approval and thus it is not possible to investigate the function behaviour directly. However, it could be tested passively without activation. Similarly, the driving function could be evaded on massive recorded fleet data. As result, a real perception without modelling would be used and the scenario selections would follow the real world. Moreover, realistic risk thresholds could be derived data driven. What is more, the evaluation bases on a full driving integration. Improvements on other modules, such as the perception or traffic prediction, could enhance the overall driving capability directly without further adjustments in the risk based trajectory planner.

While the risk measure is usable in regular driving as well as in the pre-crash phase, the most benefit is gained in critical scenarios, e.g., by advanced emergency manoeuvres with impact point localisation. Thereby, the focus of this thesis lies on the automated driving and thus use cases are obtained which mainly focus on third-party negligence. In general, it is assumed that such integral safety approaches encourage the emerging technology due to fail safe opportunities. Furthermore, the developed mitigation strategies can easily be transferred to assisted driving. In addition to the current approach, only an ego driver behaviour prediction and appropriate triggering strategy is required. Here, since no automated system ensures preventative driving, the use cases increase matching most probably the current accident occurrence. Furthermore, cooperative collision mitigation could constitute an use case in future times. Even if third-parties should not be involved due to ethical guidelines, the circumstances change if the involved objects approve the emergency manoeuvre. What is more, the risk measure could be used to give feedback on the manual driving style and thus, e.g., improve the personal driving capabilities, or individualise insurances offerings. Thereby, a detailed driver model is a prerequisite.

As final statement, vehicles able to deal with all levels of criticality are well prepared to encounter the real world. Predicting the risk preventively increase the safety for future mobility and thus takes the “Vision Zero“ one step further.

References

[1] World Health Organization, *Global status report on road safety 2018*, Geneva, 2018.

[2] World Health Organisation, *Top 10 global causes of death*, 2016, URL: https://www.who.int/en/news-room/fact-sheets/detail/the-top-10-causes-of-death (visited on 01/08/2020).

[3] German Federal Statistical Office, *GENESIS-Online*, Wiesbaden, 2020, URL: https://www-genesis.destatis.de/genesis/online (visited on 14/04/2020).

[4] European Commission, *Europe on the move, Sustainable Mobility for Europe: safe, connected, and clean*, Brussels, 2018.

[5] Swedish, Parlament, & Committee on Transport and Communications, *Committee report 1997/ 98:TU4, Protcol 1997/98:13*. Decision on Vision Zero for road traffic safety, 1997.

[6] Deutscher Verkehrssicherheitsrat, 'Vision Zero, Grundlage & Strategien', In: *Schriftenreihe Verkehrssicherheit*, vol. 16 (2012).

[7] Ann-Catrin Kristianssen, Ragnar Andersson, Matts-Ake Belin et al., 'Swedish Vision Zero policies for safety – A comparative policy content analysis', In: *Safety science*, vol. 103 (2018), pp. 260–269, DOI: 10.1016/j.ssci.2017.11.005, Elsevier.

[8] European Commission, *Towards a European road safety area: policy orientations on road safety 2011-2020*, Brussels, 2010.

[9] Adminaité-Fodor, D., Heilpern, C. and Jost, G., 'Ranking EU Progress on Road Safety, 13th Road safety performance index report', In: *Road Safety Performance Index Report*, vol. 13 (2019), European Transport Safety Council.

[10] Sabine Radke, *Verkehr in Zahlen 2019/2020*, ed. by Bundesministerium für Verkehr und digitale Infrastruktur, 2020.

[11] European Commission, *EU Road Safety Policy Framework 2021-2030 - Next steps towards "Vision Zero"*, Brussels, 2019.

[12] Gonter, M. and Seiffert, U., *Integrated Automotive Safety Handbook*, SAE International, 2014, ISBN: 978-0-7680-6437-7.

[13] Braess, H.-H. and Seiffert, U., *Vieweg-Handbuch Kraftfahrzeugtechnik*, 7th edition, ATZ/MTZ-Fachbuch, Braess, Hans-Hermann (ed.) and Seiffert, Ulrich (ed.), Wiesbaden: Vieweg & Teubner, 2013, ISBN: 978-3-322-93874-9, DOI: 10.1007/978-3-322-93873-2.

[14] DEKRA, 'Verkehrssicherheitsreport 2019, Kinder im Straßenverkehr', In: *Schritte zur Realisierung der Vision Zero* (2019).

[15] DEKRA, 'Verkehrssicherheitsreport 2017, Bewährte Maßnahmen', In: *Schritte zur Realisierung der Vision Zero* (2017).

[16] DEKRA, 'Verkehrssicherheitsreport 2018, Güterverkehr', In: *Schritte zur Realisierung der Vision Zero* (2018).

[17] German Federal Statistical Office, 'Verkehr, Verkehrsunfälle', In: *Special series 8 Series 7* (2017).

[18] National Transportation Safety Board, *Collision Between Vehicle Controlled by Developmental Automated Driving System and Pedestrian, Accident No: HWY18MH0 10*, 2018, URL: https://ntsb.gov/investigations/Pages/HWY18FH010.aspx (visited on 01/08/2020).

[19] The Tesla Team, *A Tragic Loss*, 2016, URL: https://www.tesla.com/blog/tragic-loss (visited on 01/08/2020).

[20] The Tesla Team, *An Update on Last Week's Accident*, 2018, URL: https://www.tesla.com/blog/update-last-week%E2%80%99s-accident (visited on 01/08/2020).

[21] National Transportation Safety Board, *Preliminary Report Issued for Investigation of Fatal, Mountain View, California, Tesla Crash*, 2018, URL: https://www.ntsb.gov/news/press-releases/pages/nr20180607.aspx (visited on 14/04/2020).

[22] Johansson, R., 'Vision Zero - Implementing a policy for traffic safety', In: *Safety science*, vol. 47 iss. 6 (2009), pp. 826–831, DOI: 10.1016/j.ssci.2008.10.023, Elsevier.

[23] Belin, M.-Å., Tillgren, P. and Vedung, E., 'Vision Zero – a road safety policy innovation', In: *International Journal of Injury Control and Safety Promotion*, vol. 19 iss. 2 (2012), pp. 171–179, DOI: 10.1080/17457300.2011.635213.

[24] Kim. Ellen, Muennig, P. and Rosen, Z., 'Vision zero: a toolkit for road safety in the modern era', In: *Injury Epidemiology*, vol. 4 iss. 1 (2017), DOI: 10.1186/s40621-016-0098-z, SpringerOpen.

[25] Society of Automotive Engineers, 'Taxonomy and Definitions for Terms Related to On-Road Motor Vehicle Automated Driving Systems', In: *Surface vehicle information report* (2014), SAE International.

[26] Hruschka, C. M., Töpfer, D. and Zug, S., 'Risk assessment for integral safety in automated driving', In: *IEEE International Conference on Intelligent Autonomous Systems (ICoIAS)* (2019), pp. 102–109, DOI: 10.1109/ICoIAS.2019.00025, IEEE.

[27] Gerhardus, M., Hruschka, C. M., Schmidt, M. et al., 'Verhaltensentscheidung auf der Grundlage einer kontinuierlichen Risikobewertung als ein Schlüssel zum sicheren automatisierten Fahren', In: *Assistenzsysteme, Automatisierungssysteme und eingebettete Systeme (AAET)* (2018).

[28] Hruschka, C. M., Schmidt, M. and Zug, S., 'Uncertainty-adaptive risk based motion planning in automated driving', In: *IEEE International Conference on Vehicular Electronics and Safety (ICVES)* (2019), DOI: 10.1109/ICVES.2019.8906305, IEEE.

[29] Dezelak, N., 'Untersuchung von Methoden zur Vorhersage der technischen Unfallschwere von Fahrzeugkollisionen für die Risikobewertung bei automatisierten Fahrzeugen', Institut für Regelungstechnik, Master thesis, Braunschweig: Technische University Braunschweig, 2019.

[30] Liu, Q., 'Parametrierung einer automatisierten Fahrfunktion in unfallgeneigten Verkehrssituationen', Institute for Automation and Applied Informatics, Master thesis, Karlsruhe: Karlsruhe Institute of Technology, 2019.

[31] International Organisation for Standardisation, ed., *Road vehicles - Traffic accident analysis - Part 1: Vocabulary*, ISO 12353-1:2020 (ISO), 2020.

[32] Eskandarian, A., *Handbook of Intelligent Vehicles*, 2nd edition, Eskandarian, Azim (ed.), London: Springer-Verlag, 2012, ISBN: 978-0-85729-084-7, DOI: 10.1007/978-0-85729-085-4.

[33] Winner, H., Hakuli, S. and Wolf, G., *Handbuch Fahrerassistenzsysteme, Grundlagen, Komponenten und Systeme für aktive Sicherheit und Komfort*, 1st edition, A TZ/MTZ-Fachbuch, Winner, Hermann (ed.); Hakuli (ed.), Stephan; Wolf, Gabriele (ed.), Wiesbaden: Vieweg+Teubner GWV Fachverlage GmbH, 2009, ISBN: 978-3-8348-0287-3.

[34] Schnieder, E. and Schnieder, L., *Verkehrssicherheit, Maße und Modelle, Methoden und Maßnahmen für den Straßen- und Schienenverkehr*, VDI, Berlin u.a.: Springer Vieweg, 2013, ISBN: 978-3-540-71032-5, DOI: 10.1007/978-3-540-71033-2.

[35] Amditis, A., Bertolazzi, E., Bimpas, M. et al., 'A Holistic Approach to the Integration of Safety Applications: The INSAFES Subproject Within the European Framework Programme 6 Integrating Project PReVENT', In: *IEEE Transactions on intelligent Transportation systems*, vol. 11 iss. 3 (2010), DOI: 10.1109/TITS.2009.2036736, IEEE.

[36] Kusano, K. D. and Gabler, H. C., 'Safety Benefits of Forward Collision Warning, Brake Assist, and Autonomous Braking Systems in Rear-End Collisions', In: *IEEE Transactions on Intelligent Transportation Systems (T-ITS)*, vol. 13 iss. 4 (2012), pp. 1546–1555, DOI: 10.1109/TITS.2012.2191542, IEEE.

[37] Dahl, J., Campos, G. R. de, Olsson, C. et al., 'Collision Avoidance: A Literature Review on Threat-Assessment Techniques, A Literature Review on Threat-Assessment Techniques', In: *IEEE Transaction on Intelligent Vehicles (T-IV)*, vol. 4 iss. 1 (2019), pp. 101–113, DOI: 10.1109/TIV.2018.2886682, IEEE.

[38] Lefèvre, S., Vasquez, D. and Laugier, C., 'A survey on motion prediction and risk assessment for intelligent vehicles', In: *ROBOMECH Journal*, vol. 1 iss. 1 (2014), DOI: 10.1186/s40648-014-0001-z, SpringerOpen.

[39] Gonzalez, D., Perez, J., Milanes, V. et al., 'A Review of Motion Planning Techniques for Automated Vehicles', In: *IEEE Transaction on Intelligent Transportation Systems (T-ITS)*, vol. 17 iss. 4 (2016), pp. 1135–1145, DOI: 10.1109/TITS.2015.2498841, IEEE.

[40] Paden, B., Cap, M., Yong, S. Z. et al., 'A Survey of Motion Planning and Control Techniques for Self-Driving Urban Vehicles', In: *IEEE Transaction on Intelligent Vehicles (T-IV)*, vol. 1 iss. 1 (2016), pp. 33–55, DOI: 10.1109/TIV.2016.2578706, IEEE.

[41] Elbanhawi, M. and Simic, M., 'Sampling-Based Robot Motion Planning: A Review', In: *IEEE Access*, vol. 2 (2014), pp. 56–77, DOI: 10.1109/ACCESS.2014.2302442, IEEE.

[42] Yu, R. and Abdel-Aty, M., 'Utilizing support vector machine in real-time crash risk evaluation', In: *Accident Analysis and prevention*, vol. 51 (2013), pp. 252–259, DOI: 10.1016/j.aap.2012.11.027, Elsevier.

[43] Hossain, M., Abdel-Aty, M., Quddus, M. A. et al., 'Real-time crash prediction models: State-of-the-art, design pathways and ubiquitous requirements', In: *Accident Analysis and prevention*, vol. 124 (2019), pp. 66–84, DOI: 10.1016/j.aap.2018.12.022, Elsevier.

[44] Chen, Z. and Qin, X., 'A novel method for imminent crash prediction and prevention', In: *Accident Analysis and prevention*, vol. 125 (2019), pp. 320–329, DOI: 10.1016/j.aap.2018.07.011.

[45] Xu, C., Tarko, A. P., Wang, W. et al., 'Predicting crash likelihood and severity on freeways with real-time loop detector data', In: *Accident Analysis and prevention*, vol. 57 (2013), pp. 30–39, DOI: 10.1016/j.aap.2013.03.035.

[46] Li, Z., Kolmanovsky, I., Atkins, E. et al., 'Road Risk Modeling and Cloud-Aided Safety-Based Route Planning', In: *IEEE transactions on cybernetics*, vol. 11 (2016), pp. 2473–2483, DOI: 10.1109/TCYB.2015.2478698.

[47] Dijkstra, A. and Drolenga, H., *Safety effects of route choice in a road network: Simulation of changing route choice*, ed. by SWOV Institute for Road Safety Research, Leidschendam, 2008.

[48] Xiupeng, S., 'Accident risk assessment and prediction using surrogate indicators and machine learning', School of Civil and Environmental Engineering, Phd thesis, Singapore: Nanyang Technological University, 2019.

[49] Hayward, J., *Near-miss determination through use of a scale of danger*, ed. by Transportation and Traffic Safety Center, Pennsylvania, 1972.

[50] Zhang, Y., Antonsson, E. K. and Grote, K., 'A new threat assessment measure for collision avoidance systems', In: *IEEE Intelligent Transportation Systems Conference (ITSC)* (2006), pp. 968–975, DOI: 10.1109/ITSC.2006.1706870.

[51] Hillenbrand, J., Spieker, A. M. and Kroschel, K., 'A Multilevel Collision Mitigation Approach - Its Situation Assessment, Decision Making, and Performance Tradeoffs', In: *IEEE Transaction on Intelligent Transportation Systems*, vol. 7 iss. 4 (2006), pp. 528–540, DOI: 10.1109/TITS.2006.883115, IEEE.

[52] Hillenbrand, J., Kroschel, K. and Schmidt, V., 'Situation Assessment Algorithm for a Collision Prevention Assistant', In: *IEEE Intelligent Vehicles Symposium (IV)* (2005), DOI: 10.1109/IVS.2005.1505146, IEEE.

[53] Andreas Tamke, Thao Dang and Gabi Breuel, 'A flexible method for criticality assessment in driver assistance systems', In: *IEEE Intelligent Vehicles Symposium (IV)* (2011), DOI: 10.1109/IVS.2011.5940482.

[54] Sebastian Sontges, Markus Koschi and Matthias Althoff, 'Worst-case Analysis of the Time-To-React Using Reachable Sets', In: *IEEE Intelligent Vehicles Symposium (IV)* (2018), DOI: 10.1109/IVS.2018.8500709.

[55] Svensson, A. and Hydén, C., 'Estimating the severity of safety related behaviour', eng, In: *Accident Analysis and prevention*, vol. 38 (2006), pp. 379–385, DOI: 10.1016/j.aap.2005.10.009, Elsevier.

[56] Berthelot, A., Tamke, A., Dang, T. et al., 'A novel approach for the probabilistic computation of Time-To-Collision', In: *Intelligent Vehicles Symposium (IV)* (2012), DOI: 10.1109/IVS.2012.6232221, IEEE.

[57] Adam Berthelot, Andreas Tamke, Thao Dang, Gabi Breuel, 'Handling Uncertainties in Criticality Assessment', In: *IEEE Intelligent Vehicles Symposium (IV)* (2011), DOI: 10.1109/IVS.2011.5940483.

[58] Stellet, J. E., Schumacher, J., Branz, W. et al., 'Uncertainty propagation in criticality measures for driver assistance', In: *IEEE Intelligent Vehicles Symposium (IV)* (2015), pp. 1187–1194, DOI: 10.1109/IVS.2015.7225844.

[59] Schreier, M., Willert, V. and Adamy, J., 'An Integrated Approach to Maneuver-Based Trajectory Prediction and Criticality Assessment in Arbitrary Road Environments', In: *IEEE Transaction on Intelligent Transportation Systems (T-ITS)*, vol. 17 iss. 10 (2016), pp. 2751–2766, DOI: 10.1109/TITS.2016.2522507, 2016.

[60] Schreier, M., 'Bayesian Environment Representation, Prediction, and Criticality Assessment for Driver Assistance Systems', Electrical Engineering and Information Technology, Dissertation, Darmstadt: Technical University of Darmstadt, 2015.

[61] Campos, G. R. de, Runarsson, A. H., Granum, F. et al., 'Collision avoidance at intersections: A probabilistic threat-assessment and decision-making system for safety interventions', In: *IEEE International Conference on Intelligent Transportation Systems (ITSC)* (2014), pp. 649–654, DOI: 10.1109/ITSC.2014.6957763, IEEE.

[62] Brannstrom, M., Coelingh, E. and Sjoberg, J., 'Model-Based Threat Assessment for Avoiding Arbitrary Vehicle Collisions', In: *IEEE Transaction on Intelligent Transportation Systems (T-ITS)*, vol. 11 iss. 3 (2010), pp. 658–669, DOI: 10.1109/TITS.2010.2048314, IEEE.

[63] Lee, D., Han, K. and Huh, K., 'Collision detection system design using a multilayer laser scanner for collision mitigation', In: *Proceedings of the Institution of Mechanical Engineers, Journal of Automobile Engineering*, vol. 226 iss. 7 (2012), pp. 905–914, DOI: 10.1177/0954407011430920.

[64] Ammoun, S. and Nashashibi, F., 'Real time trajectory prediction for collision risk estimation between vehiclesProcessing second', In: *International Conference on Intelligent Computer Communication and Processing* (2009), DOI: 10.1109/ICCP.2009.5284727, IEEE.

[65] Li, M., Straub, F., Kunert, M. et al., 'A Novel Cost Function for Decision-Making Strategies in Automotive Collision Avoidance Systems', In: *IEEE International Conference on Vehicular Electronics and Safety (ICVES)* (2018), pp. 1–8, DOI: 10.1109/ICVES.2018.8519591.

[66] Kim, B., Park, K. and Yi, K., 'Probabilistic Threat Assessment with Environment Description and Rule-based Multi-Traffic Prediction for Integrated Risk Management System', In: *Special Section on the IEEE Intelligent Vehicles'15 Symposium (IV)*, vol. 9 iss. 3 (2017), pp. 8–22, DOI: 10.1109/MITS.2017.2709807, IEEE.

[67] Jansson, J., 'Collision Avoidance Theory with Application to Automotive Collision Mitigation', Department of Electrical Engineering, Division ofAutomatic Control, Dissertation, Linköping: Linköping University, 2005.

[68] Käfer, E., 'Situationsklassifikation und Bewegungsprognose in Verkehrssituationen mit mehreren Fahrzeugen', Technischen Fakultät, Dissertation, Bielefeld: Universität Bielefeld, 2013.

[69] Werling, M., 'Ein neues Konzept für die Trajektoriengenerierung und -stabilisierung in zeitkritischen Verkehrsszenarien', Angewandte Informatik / Automatisierungstechnik, Dissertation, Karlsruhe: Karlsruher Institut für Technologie, 2012, DOI: 10.1524/auto.2012.0970.

[70] Werling, M. and Liccardo, D., 'Automatic collision avoidance using model-predictive online optimization', In: *IEEE 51st Conference on Decision and Control (CDC)* (2012), pp. 6309–6314, DOI: 10.1109/CDC.2012.6426612, IEEE.

[71] Werling, M., Ziegler, J., Kammel, S. et al., 'Optimal trajectory generation for dynamic street scenarios in a Frenét Frame', In: *IEEE International Conference on Robotics and Automation (ICRA)* (2010), pp. 987–993, DOI: 10.1109/ROBOT.2010.5509799, IEEE.

[72] Reichardt, D., 'Kontinuierliche Verhaltenssteuerung eines autonomen Fahrzeugs in dynamischer Umgebung', Fachbereich Informatik, Dissertation, Kaiserslautern: Universität Kaiserslautern, 1996.

[73] Reichardt, S., 'Collision Avoidance in dynamic environments applied to autonomous vehicle guidance on the motorway - Intelligent Vehicles '94 Symposium, Proceedings of the', In: *Proceedings of the Intelligent Vehicles '94 Symposium* (1994), DOI: 10.1109/IVS.1994.639475, IEEE.

[74] Althoff, M., Stursberg, O. and Buss, M., 'Model-Based Probabilistic Collision Detection in Autonomous Driving', In: *IEEE Transaction on Intelligent Transportation Systems (T-ITS)*, vol. 10 iss. 2 (2009), pp. 299–310, DOI: 10.1109/TITS.2009.2018966, IEEE.

[75] Althoff, D., Wollherr, D. and Buss, M., 'Safety Assessment of Trajectories for Navigation in Uncertain and Dynamic Environments', In: *IEEE International Conference on Robotics and Automation (ICRA)* (2011), DOI: 10.1109/ICRA.2011.5980115, IEEE.

[76] Lambert, A., Pierre, Gruyer, Dominique and Guillaume Saint, 'A Fast Monte Carlo Algorithm for Collision Probability Estimation', In: *International Conference on Control, Automation, Robotics and Vision* (2008), DOI: 10.1109/ICARCV.2008.4795553, IEEE.

[77] Hardy, J. and Campbell, M., 'Contingency Planning Over Probabilistic Obstacle Predictions for Autonomous Road Vehicles', In: *IEEE Transactions on Robotics*, vol. 29 iss. 4 (2013), pp. 913–929, DOI: 10.1109/TRO.2013.2254033, IEEE.

[78] Wang, H., Huang, Y., Khajepour, A. et al., 'Crash Mitigation in Motion Planning for Autonomous Vehicles', In: *IEEE Transaction on Intelligent Transportation Systems (T-ITS)*, vol. 20 iss. 9 (2019), pp. 3313–3323, DOI: 10.1109/TITS.2018.2873921, IEEE.

[79] Wang, H., Huang, Y., Khajepour, A. et al., 'Local Path Planning for Autonomous Vehicles: Crash Mitigation', In: *IEEE Intelligent Vehicles Symposium (IV)* (2018), DOI: 10.1109/IVS.2018.8500662, IEEE.

[80] Rasekhipour, Y., Khajepour, A., Chen, S.-K. et al., 'A Potential Field-Based Model Predictive Path-Planning Controller for Autonomous Road Vehicles', In: *IEEE Transaction on Intelligent Transportation Systems (T-ITS)*, vol. 18 iss. 5 (2017), pp. 1255–1267, DOI: 10.1109/TITS.2016.2604240, IEEE.

[81] Shimizu, T. and Raksincharoensak, P., 'Motion planning via optimization of risk quantified by collision velocity accompanied with AEB activation', In: *IEEE International Conference on Vehicular Electronics and Safety (ICVES)* (2017), pp. 19–25, DOI: 10.1109/ICVES.2017.7991895, IEEE.

[82] Lambert, A., Gruyer, D., Pierre, G. S. et al., 'Collision Probability Assessment for Speed Control', In: *Conference on Intelligent Transportation Systems (ITSC)* (2008), pp. 1043–1048, DOI: 10.1109/ITSC.2008.4732692, IEEE.

[83] Ruf, M. and Ziehn, J., 'Situation Prediction And Reaction Control (SPARC)', In: *Workshop Fahrerassistenzsysteme (FAS)* (2014), Fraunhofer Verlag.

[84] Ruf, M., Ziehn, J., Willersinn, D. et al., 'A Continuous Approach to Autonomous Driving', In: *Proceedings of the Conference on Vehicle and Infrastructure Safety improvement in Adverse Conditions and Night Driving (VISION)* (2014).

[85] Stellet, J. E., Vogt, P., Schumacher, J. et al., 'Analytical derivation of performance bounds of autonomous emergency brake systems', In: *IEEE Intelligent Vehicles Symposium (IV)* (2016), pp. 220–226, DOI: 10.1109/IVS.2016.7535389, IEEE.

[86] Gilbert, A., Petrovic, D., Warwick, K. et al., 'Autonomous Vehicle Simulation Model to Assess Potential Collisions to Reduce Severity of Impacts', In: *Proceedings of the 4th International Conference on Vehicle Technology and Intelligent Transport Systems (VEHITS)*, vol. 1 (2018), pp. 243–250, DOI: 10.5220/0006663102430250, SciTePress.

[87] Xie, G., Zhang, X., Gao, H. et al., 'Situational Assessments Based on Uncertainty-Risk Awareness in Complex Traffic Scenarios', In: *Sustainability*, vol. 9 iss. 9 (2017), DOI: 10.3390/su9091582, MDPI.

[88] Althoff, D., Kuffner, J., Wollherr, D. et al., 'Safety assessment of robot trajectories for navigation in uncertain and dynamic environments', In: *Autonomous Robots*, vol. 32 iss. 3 (2012), pp. 285–302, DOI: 10.1007/s10514-011-9257-9, SpringerLink.

[89] Damerow, F. and Eggert, J., 'Balancing risk against utility: Behavior planning using predictive risk maps', In: *IEEE Intelligent Vehicles Symposium (IV)* (2015), pp. 857–864, DOI: 10.1109/IVS.2015.7225792, IEEE.

[90] Damerow, F. and Eggert, J., 'Risk-Aversive Behavior Planning under Multiple Situations with Uncertainty', In: *IEEE 18th International Conference on Intelligent Transportation Systems (ITSC)* (2015), pp. 656–663, DOI: 10.1109/ITSC.2015.113, IEEE.

[91] Damerow, F. and Eggert, J., 'Predictive Risk Maps', In: *IEEE 17th International Conference on Intelligent Transportation Systems (ITSC)* (2014), DOI: 10.1109/ITSC.2014.6957772, IEEE.

[92] Horia Porav, P. N., 'Imminent Collision Mitigation with Reinforcement Learning and Vision', In: *IEEE 21st International Conference on Intelligent Transportation Systems (ITSC)* (2018), DOI: 10.1109/ITSC.2018.8569222, IEEE.

[93] Braeuchle, C., Flehmig, F., Rosenstiel, W. et al., 'Maneuver decision for active pedestrian protection under uncertainty', In: *IEEE 16th International IEEE Annual Conference on Intelligent Transportation Systems (ITSC)* (2013), DOI: 10.1109/ITSC.2013.6728304, IEEE.

[94] Themann, P., Kotte, J., Raudszus, D. et al., 'Impact of positioning uncertainty of vulnerable road users on risk minimization in collision avoidance systems', In: *IEEE Intelligent Vehicles Symposium (IV)* (2015), DOI: 10.1109/IVS.2015.7225846, IEEE.

[95] Simon, B., Franke, F., Riegl, P. et al., 'Motion Planning for Collision Mitigation via FEM–Based Crash Severity Maps', In: *IEEE Intelligent Vehicles Symposium (IV)* (2019), DOI: 10.1109/IVS.2019.8813832, IEEE.

[96] Heck, P., Bellin, J., Matousek, M. et al., 'Collision mitigation for crossing traffic in urban scenarios', In: *IEEE Intelligent Vehicles Symposium (IV)* (2013), pp. 559–566, DOI: 10.1109/IVS.2013.6629526, IEEE.

[97] Heck, P., 'Grundlagen für ein bordautonomes Handlungskonzept zur Unfallfolgenminderung im Querverkehr', Fakultät für Elektrotechnik, Informationstechnik, Physik, Dissertation, Brunswick: Technische Universität Braunschweig, 2014.

[98] Parseh, M., Asplund, F., Nybacka, M. et al., 'Pre-Crash Vehicle Control and Manoeuvre Planning: A Step Towards Minimizing Collision Severity for Highly Automated Vehicles', In: *IEEE International Conference on Vehicular Electronics and Safety (ICVES)* (2019), DOI: 10.1109/ICVES.2019.8906431, IEEE.

[99] Vangi, D., Virga, A. and Gulino, M.-S., 'Combined activation of braking and steering for automated driving systems, Adaptive intervention by injury risk-based criteria', In: *Procedia Structural Integrity - AIAS 2019 International Conference on Stress Analysis*, vol. 24 (2019), pp. 423–436, DOI: 10.1016/j.prostr.2020.02.039, Elsevier.

[100] Böhmländer, D., Dirndorfer, T., Al-Bayatti, A. H. et al., 'Context-aware system for pre-triggering irreversible vehicle safety actuators', In: *Accident Analysis and prevention*, vol. 103 (2017), pp. 72–84, DOI: 10.1016/j.aap.2017.02.015, Elsevier.

[101] Böhmländer, D., Yano, V., Brandmeier, T. et al., 'A Novel Approach for Intelligent Pre-Crash Threat Assessment Systems', In: *IEEE 17th International Conference on Intelligent Transportation Systems (ITSC)* (2014), DOI: 10.1109/ITSC.2014.6957812, IEEE.

[102] Böhmländer, D. C. B., 'Innovative Crash-sensing Architectures - A new approach in contact-less vehicle crash detection', Software Technology Research Laboratory, Phd thesis, Leicester: De Montfort University.

[103] Marcus Müller, Parthasarathy Nadarajan, Michael Botsch et al., 'A Statistical Learning Approach for Estimating the Reliability of Crash Severity Predictions', In: *Inf. Conf. on Intelligent Transportation Systems*, vol. Int. Conf. on Intelligent Transportations Systems (2016), 2016.

[104] Müller, M., Botsch, M., Böhmländer, D. et al., 'Machine Learning Based Prediction of Crash Severity Distributions for Mitigation Strategies', In: *Journal of Advances in Information Technology (JAIT)*, vol. 9 (2018), DOI: 10.12720/jait.9.1.15-24.

[105] Müller, M., Long, X., Botsch, M. et al., 'Real-Time Crash Severity Estimation with Machine Learning and 2D Mass-Spring-Damper Model', In: *IEEE 21st International Conference on Intelligent Transportation Systems (ITSC)* (2018), pp. 2036–2043, DOI: 10.1109/ITSC.2018.8569471, IEEE.

[106] Rao, M. K., Cuddihy, M. and Yopp, W., 'Method for operating a pre-crash sensing system to deploy airbags using confidence factors prior to collision', US 9663052 B2 (United States Patent), Ford Global Technologies LLC, 2007.

[107] Rao, M. K., Strumoto, G. S., Parakah-Asante, K. O. et al., 'Method for operating a pre-crash sensing system in a vehicle having external airbags', US 6950014B2 (United States Patent), Ford Global Technologies LLC, 2005.

[108] Meinecke, M.-M., Raimond, H., Mark, G. et al., 'Side-Pre-Crash Sensing System for Automatic Vehicle Height Level Adaptation', In: *3rd International Workshop on Intelligent Transportation (WIT)* (2006).

[109] Ashtikar, O., Basangar, A., Kendurkar, C. et al., 'Smart Collision Mitigation System for Automobiles Using Shear Thickening Fluids', In: *International Conference on Sustainable Computing in Science, Technology & Management (SUSCOM-2019)* (2019), DOI: 10.2139/ssrn.3356673, SSRN.

[110] Muehlfeld, F., Doric, I., Ertlmeier, R. et al., 'Statistical Behavior Modeling for Driver-Adaptive Precrash Systems', In: *IEEE Transactions on Intelligent Transportation Systems (T-ITS)*, vol. 14 iss. 4 (2013), pp. 1764–1772, DOI: 10.1109/TITS.2013.2267799, IEEE.

[111] Meier, A., 'Verfahren zur vorkollisionären Prognose der zu erwartenden Unfallschwere von Fahrzeugfrontalkollisionen', Faculty of Computer Science, Dissertation, Magdeburg: Otto-von-Guericke-Universität Magdeburg, 2015.

[112] Meier, A., Gonter, M. and Kruse, R., 'Artificial intelligence for developing an accident severity prediction function', In: *ATZ worldwide*, vol. 5 (2017), pp. 64–69, DOI: 10.1007/s38311-017-0026-z.

[113] Meier, A., Gonter, M. and Kruse, R., 'Precrash Classification of Car Accidents for Improved Occupant Safety Systems', In: *Procedia Technology*, vol. 15 (2014), pp. 198–207, DOI: 10.1016/j.protcy.2014.09.072.

[114] Meier, A., Gonter, M. and Kruse, R., ' Symbolic Regression for Precrash Accident Severity Prediction', In: *Hybrid Artificial Intelligence Systems (HAIS)* (2014), pp. 133–144, Springer International Publishing.

[115] Cho, K., Choi, S. B. and Lee, H., 'Design of an Airbag Deployment Algorithm Based on Precrash Information', In: *IEEE Transactions on Vehicular Technology (T-VT)*, vol. 60 iss. 4 (2011), pp. 1438–1452, DOI: 10.1109/TVT.2011.2126614, IEEE.

[116] Cho, K., Choi, S. B., Shin, K. et al., 'A pre-crash discrimination system for an airbag deployment algorithm', In: *American Control Conference* (2010), pp. 6949–6954, DOI: 10.1109/ACC.2010.5531329, IEEE.

[117] Wallner, D., Eichberger, A. and Hrischberg, W., 'A novel control algorithm for integration of active and passive vehicle safety systems in frontal collisions', In: *Journal of systemics, cybernetics and informatics*, vol. 8 iss. 5 (2009).

[118] Eichberger, A., 'Contributions to Primary, Secondary and Integrated Traffic Safety', Automotive Engineering, Habilitation thesis, Graz: Graz University of Technology, 2010.

[119] Wallner, D., 'Physikalische Modellbildung von integrierten Fahrzeugsicherheitssystemen, Theoretische Untersuchungen hinsichtlich Integration und Optimierung aktiver und passiver Sicherheitssysteme', Institute of Automotive Engineering, Diploma thesis, Graz: Graz University of Technology, 2008.

[120] Kramer, F., *Integrale Sicherheit von Kraftfahrzeugen, Biomechanik - Simulation - Sicherheit im Entwicklungsprozess*, 4th edition, ATZ/MTZ-Fachbuch, Kramer, Florian (ed.), Wiesbaden: Springer Fachmedien Wiesbaden, 2013, ISBN: 978-3-8348-2607-7.

[121] Lau, M. and Alstadt, C., 'Motor vehicle with multi-collision brake', US10053072B2 (United States Patent), Volkswagen AG (assignee), 2018.

[122] Yang, D., Jacobson, B., Jonasson, M. et al., 'Minimizing vehicle post impact path lateral deviation using optimized braking and steering sequences', In: *International Journal of Automotive Technology,* vol. 15 iss. 1 (2014), pp. 7–17, DOI: 10.1007/s12239âĹŠ014âĹŠ0002âĹŠ1.

[123] Official Journal of the European Union, *Regulation (EU) 2015/758 of the European parliament and of the council*, 2015.

[124] Official Journal of the European Union, *Commission Delegated Regulation (EU) 2017/79*, 2017.

[125] State of Minnesota - Department of public safety, *Emergency 911 communications systems*, 2009.

[126] Kononen, D. W., Flannagan, C. A. C. and Wang, S. C., 'Identification and validation of a logistic regression model for predicting serious injuries associated with motor vehicle crashes', In: *Accident Analysis and prevention*, vol. 43 (2011), pp. 112–122, DOI: 10.1016/j.aap.2010.07.018, Elsevier.

[127] Bahouth, G., Digges, K. and Schulman, C., 'Influence of Injury Risk Thresholds on the Performance of an Algorithm to Predict Crashes with Serious Injuries', In: *56th Annual Conference Annals of Advances in Automotive Medicine (AAAM)*, vol. 56 (2012), pp. 223–230.

[128] Buendia, R., Candefjord, S., Fagerlind, H. et al., 'On scene injury severity prediction (OSISP) algorithm for car occupants', eng, In: *Accident; analysis and prevention*, vol. 81 (2015), pp. 211–217, DOI: 10.1016/j.aap.2015.04.032.

[129] Nishimoto, T., Mukaigawa, K., Tominaga, S. et al., 'Serious injury prediction algorithm based on large-scale data and under-triage control', eng, In: *Accident Analysis and prevention*, vol. 98 (2017), pp. 266–276, DOI: 10.1016/j.aap.2016.09.028, Elsevier.

[130] Shalev-Shwartz, S., Shammah, S. and Shashua, A., *On a Formal Model of Safe and Scalable Self-driving Cars*, ed. by Mobileye, 2017.

[131] Bellman Richard, *Dynamic Programming*, ed. by Princeton University Press, 1957.

[132] Köppen, M., 'The curse of dimensionality', In: *5th Online World Conference on Soft Computing in Industrial Applications (WSC5)*, vol. 1 (2000), pp. 4–8.

[133] Johannsen, H., *Unfallmechanik und Unfallrekonstruktion, Grundlagen der Unfallaufklärung*, 3th edition, ATZ/MTZ-Fachbuch, Wiesbaden: Springer Vieweg, 2013, ISBN: 978-3-658-01593-0, DOI: 10.1007/978-3-658-01594-7.

[134] Niederer P., Walz F., Muser M et al., 'Was ist ein «schwerer», was ist ein «leichter» Verkehrsunfall?', In: *Schweizerische Ärztezeitung*, vol. 82 iss. 28 (2001), pp. 1535–1539, DOI: 10.4414/saez.2001.08299, ETH Zürich.

[135] Croft, A. C. and Freeman, M. D., 'Correlating crash severity with injury risk, injury severity, and long-term symptoms in low velocity motor vehicle collisions', In: *Medical science monitor* (2005).

[136] Schindler, V., Kühn, M. and Siegler, H., *Intelligente Rückhaltesysteme, Berichte der Bundesanstalt für Straßenwesen (bast)*, Berichte der Bundesanstalt für Straßenwesen, Bundesanstalt für Straßenwesen (ed.), Bremerhaven: Wirtschaftsverlag NW, 2004, ISBN: 3-86509-192-X.

[137] Ivan, J. N. and Konduri, K. C., 'Safe Mobility: Challenges, Methodology and Solutions', In: *Safe Mobility: Challenges, Methodology and Solutions (Transport and Sustainability)*, vol. 11 (2018), pp. 325–350, DOI: 10.1108/S2044-99412018000001-1017, Emerald Publishing Limited.

[138] Burg, H. and Moser, A., *Handbuch Verkehrsunfallrekonstruktion, Unfallaufnahme, Fahrdynamik, Simulation*, 3th edition, ATZ/MTZ-Fachbuch, Burg, Heinz (ed.) and Moser, Andreas (ed.), Wiesbaden: Springer Vieweg, 2017, ISBN: 978-3-658-16142-2, DOI: 10.1007/978-3-658-16143-9.

[139] Shelby, S. G., 'Delta-V as a measure of traffic conflict severity', In: *3rd International Conference on Road Safety and Simulation* (2011).

[140] Husted, D. C., Biss, D. J. and Heverly, D. E., 'The Appropriate Use of "Delta-V" in Describing Accident Severity', In: *SAE Technical Paper Series*, 1999-01-1295 (1999), DOI: 10.4271/1999-01-1295, SAE Technical Paper.

[141] Gabauer, D. J. and Gabler, H. C., 'Comparison of roadside crash injury metrics using event data recorders', In: *Accident; analysis and prevention*, vol. 40 iss. 2 (2008), pp. 548–558, DOI: 10.1016/j.aap.2007.08.011, Elsevier.

[142] GIDAS, *GIDAS database*, 2020, URL: https://www.gidas.org/willkommen/ (visited on 10/05/2020).

[143] Volkswagen AG, *Der neue Volkswagen Golf*, 2020, URL: https://www.volkswagen-newsroom.com/de/storys/car2x-im-neuen-golf-ein-technischer-meilenstein-5919 (visited on 20/01/2021).

[144] Volkswagen AG, *Produkte, Forschung, Sicherheit, Technik: Golf (1997)*, 1997, URL: https://www.volkswagen-newsroom.com/de/suche?query=Crashtests&type=image&utf8=%E2%9C%93 (visited on 20/01/2021).

[145] NHTSA, *National Automotive Sampling System (NASS) - Crashworthiness Data System (CDS)*, 2020, URL: https://www.nhtsa.gov/research-data/national-automotive-sampling-system-nass (visited on 10/05/2020).

[146] MDGO, *Save Drivers. Drive Savings.* 2020, URL: https://www.mdgo.io/ (visited on 20/01/2021).

[147] Vangi, D., 'Coherence assessment of accident database kinematic data', In: *Accident Analysis and prevention*, vol. 123 (2019), pp. 356–364, DOI: 10.1016/j.aap.2018.12.004, Elsevier.

[148] Chidester, A., Hinch, J., Mercer, T. et al., *Recording Automotive Crash Event Data*, ed. by National Highway Traffic Safety Administration, 2001.

[149] Prasad, P. and Belwafa, J. E., *Vehicle Crashworthiness and Occupant Protection*, ed. by American Iron and Steel Institute, Prasad, Priya (ed.) and Belwafa, Jamel E. (ed.), 2004.

[150] Marzougui, D., Samaha, R. R., Cui, C. et al., *Extended Validation of the Finite Element Model for the 2010 Toyota Yaris Passenger Sedan*, ed. by The national crash analysis center, 2010, (visited on 20/01/2021).

[151] Brach, R. and Brach Matthew, 'A Review of Impact Models for Vehicle Collision', In: *SAE transactions* (1987), pp. 175–190.

[152] Dankert, J. and Dankert, H., *Technische Mechanik, Statik, Festigkeitslehre, Kinematik/Kinetik*, 7th edition, Wiesbaden: Springer Vieweg, 2013, ISBN: 978-3-8348-1809-6, DOI: 10.1007/978-3-8348-2235-2.

[153] Brach, R. and Brach Matthew, 'Analysis of collisions - Point Mass Mechanics and Planar Impact Mechanics', In: *Collision: the international compendium for crash research*, vol. 2 iss. 1 (2007), pp. 38–50.

[154] Antonetti, V. W., 'Estimating the Coefficient of Restitution of Vehicle-to-Vehicle Bumper Impacts', In: *SAE Technical Paper*, 980552 (1998).

[155] Cipriani, Bayan, Woodhouse et al., 'Low Speed Collinear Impact Severity: A Comparison between Full Scale Testing and Analytical Prediction Tools with Restitution Analysis', In: *SAE Technical Paper* (2002).

[156] Harmati, I., Rovid, A. and Varlaki, P., 'Approximation of Force and Energy in Vehicle Crash Using LPV Type Description', In: *WSEAS Transactions on Systems*, vol. 9 iss. 7 (2010), pp. 734–743.

[157] Pawlus, W., Karimi, H. R. and Robbersmyr, K. G., 'Development of lumped-parame ter mathematical models for a vehicle localized impact', In: *Journal of Mechanical Science and Technology*, vol. 25 iss. 7 (2011), pp. 1737–1747, DOI: 10.1007/s12206-011-0505-x, SpringerLink.

[158] Pawlus, W., Nielsen, J. E., Karimi, H. R. et al., 'Development of Mathematical Models for Analysis of a Vehicle Crash', In: *Transaction on applied and theoretical mechanics (WSEAS)*, vol. 5 iss. 2 (2010), pp. 156–165.

[159] Pawlus, W., Karimi, H. R. and Robbersmyr, K. G., 'Investigation of vehicle crash modeling techniques, Theory and application', In: *The International Journal of Advanced Manufacturing Technology*, vol. 70 (2014), pp. 965–993, DOI: 10.1007/s00170-013-5320-3, SpringerLink.

[160] Munyazikwiye, B. B., Karimi, H. R. and Robbersmyr, K. G., 'Optimization of Ve hicle-to-Vehicle Frontal Crash Model Based on Measured Data Using Genetic Algorithm', In: *IEEE Access*, vol. 5 (2017), pp. 3131–3138, DOI: 10.1109/ACCESS.2017.2671357, IEEE.

[161] Brückner, S., 'Ein ähnlichkeitsmechanisches System zur Prognose des Crashpulses beim Pkw-Frontalaufprall', Aerospace Engineering and Geodesy, Dissertation, Stuttgart: University of Stuttgart, 2005.

[162] Gandhi, U. N. and Hu, S. J., 'Data-based approach in modeling automobile crash', In: *International journal of impact engineering*, vol. 16 iss. 1 (1995), DOI: 10.1016/0734-743X(94)E0029-U, Elsevier.

[163] Mounir M. Kamal and Kuang-Huei Lin, *Modern automotive structural analysis, Collision Simulation*, Kamal, Mounir M. (ed.) Wolf, Joseph Albert (ed.), New York: van Nostrand Reinhold, 1982, ISBN: 0-44 2-24 83 9-3.

[164] Pawlus, W., Robbersmyr, K. G. and Karimi, H. R., 'Performance evaluation of feedforward neural networks for modeling a vehicle to pole central collision', In: *4th WSEAS International Conference on Energy and Development (GEMESED)* (2011), pp. 14–16.

[165] Pawlus, W., Karimi, H. R. and Robbersmyr, K. G., 'Data-based modeling of vehicle collisions by nonlinear autoregressive model and feedforward neural network', In: *Information Sciences*, vol. 235 (2013), pp. 65–79, DOI: 10.1016/j.ins.2012.03.013.

[166] Omar, T., Eskandarian, A. and Bedewi, N., 'Vehicle Crash Modelling Using Recurrent Neural Networks', In: *Mathematical and computer Modelling*, vol. 28 iss. 9 (1998), pp. 31–42.

[167] Thrun, S., Burgard, W. and Fox, D., *Probabilitstic Robotics*, London: The MIT Press, 2006, ISBN: 978-0-262-20162-9.

[168] Thrun, S., 'Probabilistic Algorithms in Robotics', In: *AI Magazine*, vol. 21 iss. 4 (2000), DOI: 10.1609/aimag.v21i4.1534.

[169] Maurer, M., Lenz, B., Winner, H. et al., *Autonomes Fahren, Technische, rechtliche und gesellschaftliche Aspekte*, Maurer, Markus (ed.), Lenz, Barbara (ed.), Winner, Hermann (ed.), Gerdes, Christian (ed.), Springer Vieweg, 2015, ISBN: 978-3-662-45853-2, DOI: 10.1007/978-3-662-45854-9.

[170] Schmidt, M., Töpfer, D. and Schmidt, S., 'Predicting vehicle control errors in emergency swerving maneuvers', In: *12th International Workshop on Robot Motion and Control (RoMoCo)* (2019), pp. 92–97, DOI: 10.1109/RoMoCo.2019.8787383, IEEE.

[171] Tuan Tran Nguyen, 'A Reliability-Aware Fusion Concept Toward Robust Ego-Lane Estimation Incorporating Multiple Sources', Faculty of Computer Science, Dissertation, Magdeburg: Otto-von-Guericke-Universität Magdeburg, 2018.

[172] Niehaus, A. and Stengel, R. F., 'Probability-based decision making for automated highway driving', In: *IEEE Transactions on Vehicular Technology (T-VT)*, vol. 43 iss. 3 (1994), pp. 626–634, DOI: 10.1109/25.312814, IEEE.

[173] Keller, C. G., Dang, T., Fritz, H. et al., 'Active Pedestrian Safety by Automatic Braking and Evasive Steering', In: *IEEE Transactions on Intelligent Transportation Systems (T-ITS)*, vol. 12 iss. 4 (2011), pp. 1292–1304, DOI: 10.1109/TITS.2011.2158424, IEEE.

[174] Sontges, S. and Althoff, M., 'Determining the Nonexistence of Evasive Trajectories for Collision Avoidance Systems', In: *IEEE 18th International Conference on Intelligent Transportation Systems (ITS)* (2015), pp. 956–961, DOI: 10.1109/ITSC.2015.160, IEEE.

[175] International Organisation for Standardisation, ed., *Risk management — Guidelines*, ISO 31000, 2018.

[176] Deutsche Institut für Normung e.V., ed., *Funktionale Sicherheit - Sicherheitstechnische Systeme für die Prozessindustrie*, DIN EN 61511, 2019.

[177] International Atomic Energy Agency, *Safety of Nuclear Power Plants: Design*, Wien, Österreich, 2012.

[178] International Standardisation Organisation, ed., *Road vehicles - Functional safety - Part1: Vocabulary*, ISO 26262-1, 2011.

[179] Deutsche Institut für Normung e.V., ed., *Funktionale Sicherheit sicherheitsbezogener elektrischer/elektronischer/programmierbarer elektronischer Systeme*, DIN E N 61508-1, 2011.

[180] Arora, S., Choudhury, S., Althoff, D. et al., 'Emergency maneuver library - ensuring safe navigation in partially known environments', In: *IEEE International Conference on Robotics and Automation (ICRA)* (2015), pp. 6431–6438, DOI: 10.1109/ICRA.2015.7140102, IEEE.

[181] Surakitbanharn, C. A., 'Designing a Proactive Risk Mitigation Environment for Integrated Autonomous Vehicle and Human Infrastructure, Integrating People and Intelligent Systems', In: *Conference on Intelligent Human Systems Integration (IHSI)* (2017), DOI: 10.1007/978-3-319-73888-8_5, Springer International Publishing.

[182] Fraichard, T. and Asama, H., 'Inevitable collision states - a step towards safer robots?', In: *Advanced Robotics,* vol. 18 iss. 10 (2012), pp. 1001–1024, DOI: 10.1163/1568553042674662, 2012.

[183] Fraichard, T., 'A Short Paper about Motion Safety', In: *IEEE International Conference on Robotics and Automation (ICRA)* (2007), DOI: 10.1109/ROBOT.2007.363138, IEEE.

[184] Ulbrich, S., Menzel, T., Reschka, A. et al., 'Defining and Substantiating the Terms Scene, Situation, and Scenario for Automated Driving', In: *IEEE 18th International Conference on Intelligent Transportation Systems (ITS)* (2015), pp. 982–988, DOI: 10.1109/ITSC.2015.164, IEEE.

[185] Bagschik, G., Menzel, T., Reschka, A. et al., 'Szenarien für Entwicklung, Absicherung und Test von automatisierten Fahrzeugen', In: *11. Workshop Fahrerassistenzsysteme und automatisiertes Fahren* (2017), pp. 125–135, Uni-DAS e. V.

[186] Shladover, S. E. and Nowakowski, C., 'Regulatory challenges for road vehicle automation, Regulatory challenges for road vehicle automation: Lessons from the California experience', In: *Transportation Research Part A: Policy and Practice*, vol. 122 (2019), pp. 125–133, DOI: 10.1016/j.tra.2017.10.006, Elsevier.

[187] Hydén, C., *The development of a method for traffic safety evaluation: The Swedish Traffic Conflicts Technique.* Ed. by Bulletin Lund Institute of Technology, Department 70, Lund, Sweden: Lund University, 1987.

[188] Krajewski, R., Moers, T., Nerger, D. et al., 'Data-Driven Maneuver Modeling using Generative Adversarial Networks and Variational Autoencoders for Safety Validation of Highly Automated Vehicles', In: *21st International Conference on Intelligent Transportation Systems (ITSC)* (2018), DOI: 10.1109/ITSC.2018.8569971, IEEE.

[189] Watanabe, H., Tobisch, L., Rost, J. et al., 'Scenario Mining for Development of Predictive Safety Functions', In: *2019 IEEE International Conference on Vehicular Electronics and Safety (ICVES)* (2019), DOI: 10.1109/ICVES.2019.8906293.

[190] Junietz, P., Schneider, J. and Winner, H., 'Metrik zur Bewertung der Kritikalität von Verkehrssituationen und -szenarien', In: *11. Workshop Fahrerassistenzsysteme* (2017).

[191] Lu, A., *Autonomous connected cars on their way*, ed. by ShanghaiDaily, 2016, URL: https://archive.shine.cn/business/biz-special/Autonomous-connected-cars-on-their-way/shdaily.shtml (visited on 20/01/2021).

[192] Donges, E., 'A Conceptual Framework for Active Safety in Road Traffic', In: *Vehicle System Dynamics*, vol. 32 iss. 2-3 (1999), pp. 113–128, DOI: 10.1076/vesd.32.2.113.2089.

[193] Ulbrich, S. and Maurer, M., 'Probabilistic Online POMDP Decision Making for Lane Changes in Fully Automated Driving', In: *16th International IEEE Annual Conference on Intelligent Transportation Systems (ITSC)* (2013), DOI: 10.1109/ITSC.2013.6728533, IEEE.

[194] Tas, Ö. S., Kuhnt, F., Zöllner, J. M. et al., 'Functional System Architectures towards Fully Automated Driving', In: *IEEE Intelligent Vehicles Symposium (IV)* (2016), DOI: 10.1109/IVS.2016.7535402.

[195] Heinrich, S., Stubbemann, J. and Rojas, R., 'Optimizing a driving strategy by its sensor coverage of relevant environment information', In: *IEEE Intelligent Vehicles Symposium (IV)* (2016), DOI: 10.1109/IVS.2016.7535423.

[196] Heinrich, S., 'Planning Universal On-Road Driving Strategies for Automated Vehi cles', Institute of Computer Science, Phd thesis, Berlin: Freie Universität Berlin, 2018, DOI: 10.1007/978-3-658-21954-3.

[197] Rosbach, S., James, V., Großjohann, S. et al., 'Driving with Style: Inverse Reinforcement Learning in General-Purpose Planning for Automated Driving', In: *arXiv preprint arXiv*, vol. 2019 iss. 1905.00229 (2019).

[198] Bauer, K.-L., 'Echtzeit-Strategieplanung für vorausschauendes automatisiertes Fahren', Department of Mechanical Engineering, Dissertation, Karlsruhe: Karlsruhe Institute of Technology, 2019.

[199] Schramm, D., Hiller, M. and Bardini, R., *Modellbildung und Simulation der Dynamik von Kraftfahrzeugen*, Berlin, Heidelberg: Springer, 2010, ISBN: 978-3-540-89313-4, DOI: 10.1007/978-3-540-89315-8.

[200] Dreyfus, S., 'Richard Bellman on the Birth of Dynamic Programming', In: *Operations Research*, vol. 50 iss. 1 (2002), pp. 48–51, DOI: 10.1287/opre.50.1.48.17791.

[201] Awad, E., Dsouza, S., Kim, R. et al., 'The Moral Machine experiment', In: *Nature*, vol. 563 iss. 7729 (2018), pp. 59–64, DOI: 10.1038/s41586-018-0637-6.

[202] Ethik-Kommission, *Automatisiertes und vernetztes Fahren, Bericht Juni 2017*, ed. by Bundesministerium für Verkehr und digitale Infrastruktur, 2017.

[203] Perdomo López, D., 'Scenario interpretation for automated driving at urban intersections', Department of Mathematics and Computer Science, Dissertation, Berlin: Freie Universität Berlin, 2018.

[204] Perdemo Lopez, D., Waldmann, R., Joerdens, C. et al., 'Scenario Interpretation Based on Primary Situations for Automatic Turning at Urban Intersections', In: *International Conference on Vehicle Technology and Intelligent Transport Systems*, vol. 2 (2017), pp. 15–23, DOI: 10.1007/978-1-137-31426-0_1, SCITEPRESS.

[205] Perdemo Lopez, D., Waldmann, R., Joerdens, C. et al., 'Scenario Interpretation for Automated Driving at Intersections', In: *Smart Cities, Green Technologies, and Intelligent Transport Systems* (2014), pp. 171–189, DOI: 10.1007/978-1-137-31426-0_1, Springer International Publishing.

[206] Gerhardus, M. and Schmidt, M., 'Verfahren und Vorrichtung zum Bestimmen einer Kollisionswahrscheinlichkeit eines Fahrzeugs mit einem Objekt', DE 10 2016 218 080 B3, 2017, DOI: 10.1109/IROS.2010.5652763.

[207] Hruschka, C. M., 'Effiziente Berechnung von Kollisionswahrscheinlichkeiten zur Risikoabschätzung im automatischen Fahren', Diploma thesis, Dresden: Dresden University of Technology, 2017.

[208] Ericson, C., *The Gilbert-Johnson-Keerthi algorithm*, 2005, URL: http://realtimecollisiondetection . net / pubs / SIGGRAPH04 _ Ericson _ GJK _ notes . pdf (visited on 20/01/2021).

[209] Tomiczkova, S., 'Algorithms for the computation of the Minkowski difference', In: *Proceedings of the 26th Conference on Geometry and Computer Designers* (2006), pp. 37–42.

[210] Petersen, K. B. and Pedersen, M. S., *The Matrix Cookbook*, 2012, URL: http://matrixcookbook.com (visited on 20/01/2021).

[211] Hadavand-Siri, M. and Deutsch, Clayton, V., 'Some Thoughts on Understanding Correlation Matrices', In: *CCG Annual Report 14*, 408 (2012).

[212] Nawri, N., *Berechnung von Kovarianzellipsen*, 1996, URL: http://hacol13.physik.uni-freiburg.de/fp/origin/covariance_ellipses.pdf (visited on 20/01/2021).

[213] Didonato, A. R., Jarnagin M.P. and Hageman R. K., *Computation of the Bivariate Normal Distribution over convex Polygons*, ed. by Naval Surface Weapons Center, Dahlgren, Virginia, 1978.

[214] Burg, H., 'Approximation von trägheitsmomenten bei Personenkraftwagen', In: *Verkehrsunfall*, vol. 20 iss. 3 (1982), Information Verlag, Bundesanstalt für Straßenwesen (BASt).

[215] Maclnnis, D. D. and Cliff, William E.: lsing, Kurt W., 'A Comparison of Moment of Inertia Estimation Techniques for Vehicle Dynamics Simulation', In: *SAE transactions* (1997), pp. 1557–1575, SAE Technical Paper.

[216] Bertram, A. and Glüge, R., *Solid Mechanics: Theory, modeling, and problems*, Cham: Springer International Publishing, 2015, ISBN: 978-3-319-19565-0, DOI: 10.1007/978-3-319-19566-7.

[217] Hornik, K., 'Approximation Capabilities of Muitilayer Feedforward Networks', In: *Neural networks*, vol. 4 iss. 2 (1991), pp. 251–257, DOI: 10.1016/0893-6080(91)90009-T, Elsevier.

[218] Probst, P., Wright, M. N. and Boulesteix, A.-.-L., 'Hyperparameters and tuning strategies for random forest', In: *Wiley Interdisciplinary Reviews: Data Mining and Knowledge Discovery (WIRE)*, vol. 9 iss. 3 (2018), p. 281, DOI: 10.1002/widm.1301.

[219] Oshiro, T. M., Perez, P. S. and Baranauskas, J. A., 'How Many Trees in a Random Forest?', In: *International workshop on machine learning and data mining in pattern recognition* (2012), Springer.

[220] MathWorks, *Constrained Nonlinear Optimization Algorithms*, 2020, URL: https://de.mathworks.com/help/optim/ug/constrained-nonlinear-optimization-algorithms.html (visited on 22/08/2020).

[221] MathWorks, *Surrogate Optimization*, 2020, URL: https://www.mathworks.com/help/gads/surrogate-optimization.html (visited on 22/08/2020).

[222] MathWorks, *Deep Learning Toolbox*, 2020, URL: https://de.mathworks.com/help/deeplearning/index.html?s_tid=CRUX_lftnav (visited on 22/08/2020).

[223] MathWorks, *Statistics and Machine Learning Toolbox*, 2020, URL: https://www.mathworks.com/products/statistics.html (visited on 22/08/2020).

[224] Torgo, L. and Ribeiro, R., 'Precision and Recall for Regression', In: *International Conference on Discovery Science* (2009), Springer.

[225] Pacejka, H. B. and Bakker, E., 'The magic formula tyre model', In: *Vehicle System Dynamics*, vol. 21 iss. sup001 (1992), pp. 1–18, DOI: 10.1080/00423119208969994.

[226] Reschka, A., Böhmer, J. R., Nothdurft, T. et al., 'A surveillance and safety system based on performance criteria and functional degradation for an autonomous vehicle', In: *15th International IEEE Conference on Intelligent Transportation Systems (ITS)* (2012), pp. 237–242, DOI: 10.1109/ITSC.2012.6338682, IEEE.

[227] Herrmann, S. and Utschick, W., 'Availability and Interpretability of Optimal Control for Criticality Estimation in Vehicle Active Safety', In: *Design, Automation & Test in Europe Conference & Exhibition (DATE)* (2016), pp. 415–420, IEEE.

[228] Benmimoun, M., Fahrenkrog, F., Zlocki, A. et al., 'Erkennung und Klassifizierung kritischer Fahrsituationen mittels fahrzeugdaten', In: *ATZ-Automobiltechnische Zeitschrift*, vol. 114 iss. 10 (2012), pp. 820–826.

[229] Shamir, T., 'How Should an Autonomous Vehicle Overtake a Slower Moving Vehicle, Design and Analysis of an Optimal Trajectory', In: *IEEE Transactions on Automatic Control*, vol. 49 iss. 4 (2004), pp. 607–610, DOI: 10.1109/TAC.2004.825632, IEEE.

[230] Gartner, N. H., Messer, C. J. and A. Rathi, *Traffic flow theory, A state-of-the-art report*, 2001, URL: https://www.researchgate.net/publication/248146380_Traffic_Flow_Theory_A_State-of-the-Art_Report (visited on 20/01/2021).

[231] McKay, M. D., Beckman, R. J. and Conover, W. J., 'Comparison of Three Methods for Selecting Values of Input Variables in the Analysis of Output from a Computer Code', In: *Technometrics*, vol. 21 iss. 2 (1979), pp. 239–245, DOI: 10.1080/00401706.1979.10489755.

[232] Weicker, K., *Evolutionäre Algorithmen*, 3rd edition, Wiesbaden: Springer Vieweg, 2015, ISBN: 978-3-658-09957-2, DOI: 10.1007/978-3-658-09958-9.

[233] Kolda, T. G., Lewis, R. M. and Torczon, V., 'Optimization by Direct Search: New Perspectives on Some Classical and Modern Methods', In: *SIAM review*, vol. 45 iss. 3 (2003), pp. 385–482, DOI: 10.1137/S0036144502428893.

[234] GIDAS, *GIDAS Codebook*, 2018.

[235] Meyer, H., 'Echtzeitoptimierung für Ausweichtrajektorien mittels der Sensitivitätsanalyse eines parametergestörten nichtlinearen Optimierungsproblems', Dissertation, University Bremen, 2016.

[236] Daws, R., *Shanghai becomes the first Chinese city to license self-driving cars to carry passengers*, ed. by IoTnews, 2019, URL: https://iottechnews.com/news/2019/sep/19/shanghai-first-chinese-city-license-self-driving-cars-passengers/ (visited on 20/01/2021).

[237] Volkswagen Group, *Volkswagen fährt vollautomatisiert in Hamburg*, 2019, URL: https://www.volkswagen-newsroom.com/de/pressemitteilungen/volkswagen-faehrt-vollautomatisiert-in-hamburg-4797 (visited on 15/07/2020).

[238] Volkswagen Group, *Laser, Radar, Ultrasound: Autonomous Driving in Hamburg*, 2019, URL: https://www.volkswagenag.com/en/news/stories/2019/04/laser-radar-ultrasound-autonomous-driving-in-hamburg.html (visited on 15/07/2020).

[239] Volkswagen AG, *Volkswagen tests highly-automated driving in Hamburg*, 2019, URL: https://www.volkswagen-newsroom.com/en/press-releases/volkswagen-tests-highly-automated-driving-in-hamburg-4797 (visited on 20/01/2021).

[240] Open Street Map, *Screenshot Hamburg*, 2020, URL: https://www.openstreetmap.de/karte.html (visited on 20/01/2021).

List of Tables

List of Figures

Appendix A:

Extension to the tuning process

Extensive simulation results of the tuning process (sec. 5.3.3). Additional information are presented in the figure captions shortly.

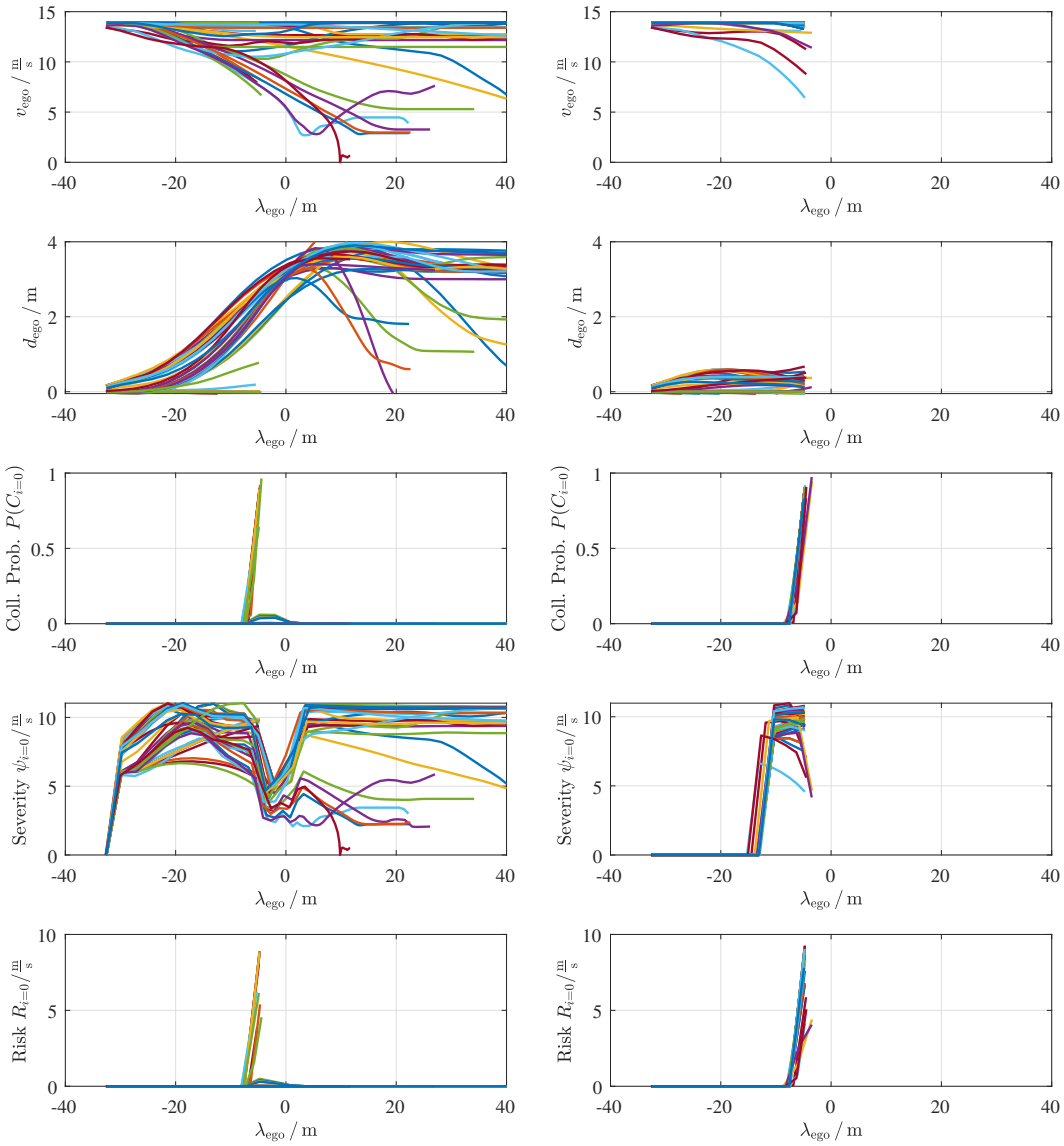

(a) Scenario ^{LHS}CS1 (b) Scenario ^{LHS}CS5

Figure A.1: All test drives scenario FS LHS - It shows the dynamics and criticality subfeatures for all LHS tuning sample sets ${}^{s}\boldsymbol{\theta}$ in regular driving of scenario ^{LHS}CS1 and emergency scenarios ^{LHS}CS5.

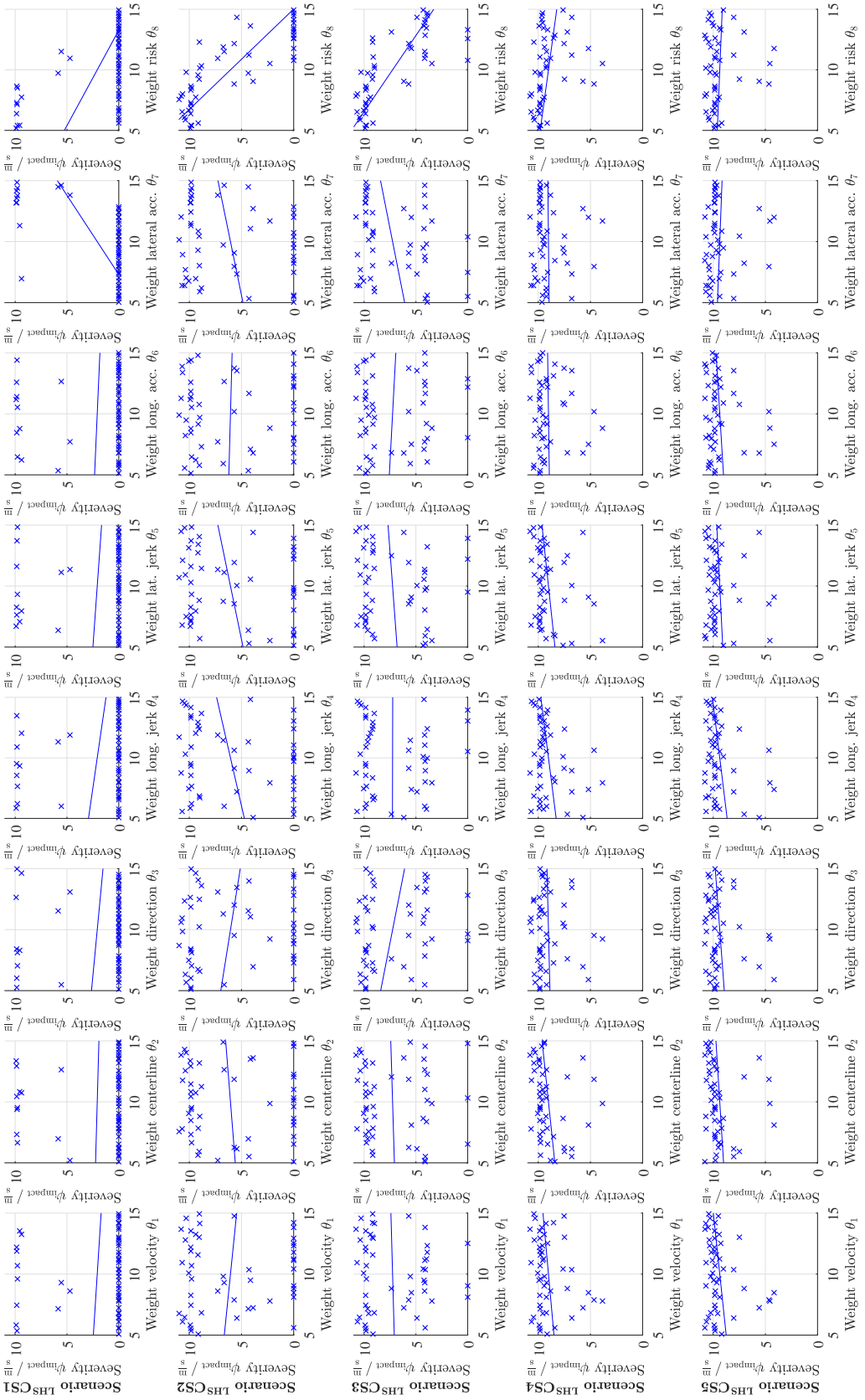

Figure A.2: Correlation of all tuning parameters - The explanation follows figure 5.12. The additional tuning parameters have a minor impact to the safety in the scenario FS LHS.